University of Minnesota
St. Anthony Falls Hydraulic Laboratory

Project Report No. 195

MATHEMATICAL MODELING FOR CROSS-IRONDEQUOIT TUNNEL AND ASSOCIATED FACILITY

by

Charles C. S. Song

and

Kim Sau Leung

Prepared for

MONROE COUNTY DIVISION OF PURE WATER
IRONDEQUOIT BAY PURE WATERS DISTRICT

July, 1980
Minneapolis, Minnesota

TABLE OF CONTENTS

Page

LIST OF FIGURES

Figure Nr.

Figure Nr.

Figure Nr.

Figure Nr.

LIST OF TABLES

MATHEMATICAL MODELING FOR CROSS-IRONDEQUOIT TUNNEL AND ASSOCIATED FACILITIES

I. INTRODUCTION AND GENERAL SYSTEM DESCRIPTION

The Cross-Irondequoit tunnel was originally designed as a trunk sewer whose main function was to convey the combined flow to a pumping station. This system (Fig. I-1) is located in a developing section of Rochester, New York. It is currently underutilized, and it is not expected to reach capacity for another 50 years. The system studied consists of a 7 ft diameter, 3 mile long, portion of the Irondequoit Creek interceptor, which ends at the Browncroft junction chamber, followed by a short 12 ft diameter section joining the junction chamber to the transition chamber and a 16 ft diameter, 6 mile long, tunnel connecting the transition chamber and the pumping station. From there the flow is pumped through pressurized conduits to a waste water treatment plant. Eventually,another tunnel will also drain into the wet well.

Because of its current underutilization, Monroe County officials have proposed to use the tunnel for storage in order to minimize the combined sewer overflow in this area. Combined sewer overflow currently empties into a bay of Lake Ontario, causing a pollution problem.

If the Cross-Irondequoit system were to be used for storm water collection, major inflows would occur at Thomas Creek, at Densmore Creek, and from the Culver-Goodman system at a point close to the Densmore Creek overflow. These inflows can be modified by control structures at these points in order to safeguard the Cross-Irondequoit tunnel.

The Densmore Creek control structure and the Thomas Creek control structure both allow a certain portion of the flow to be let into the tunnel by adjusting sluice gates. The remaining flow is then bypassed down a creek through an adjustable roller gate and will eventually flow into the lake.

The Culver-Goodman system is a Y shaped system (Fig. I-2) with storm-water inflow at various points. An extensive study of this system has been

carried out at the St. Anthony Falls Hydraulic Laboratory [1]*. The downstream end of this system consists of a small reservoir with six adjustable ports in the side from which flow can be let into the Cross-Irondequoit tunnel in a regulated manner.

In order to capture the maximum amount of runoff, it is proposed to allow the tunnel to operate in a "mixed flow" condition. In this mode, the Cross-Irondequoit tunnel is allowed to fill so that the flow in part of the tunnel is fully pressurized. Since the system was originally designed solely for an open channel flow condition, this modified operation could present some problems due to water hammer pressures and surges.

The purpose of the Cross-Irondequoit tunnel model study, then, is threefold. The first part of the study is to determine the limiting hydraulic capacity of the existing tunnel. The goal of the second part of this study is to determine a procedure for operation of the inflow controls at Culver-Goodman and Densmore Creek in order to maximize the quantity of storm water stored, and, at the same time, ensure that the tunnel is operating within its limits of safety. It is especially desirous to capture as much of the first few minutes of runoff, the first flush, as possible, as this contains the highest pollution load. The third major objective is to determine a safe operating procedure and surge relief method to protect the pumps and force main against energency conditions.

The dynamic mixed flow transient model recently developed at the St. Anthony Falls Hydraulic Laboratory was used to carry out the study. The model is unique in that the complete kinematic and dynamic equations of motion for both open channel flow and pressurized flow phases are represented. Simultaneous occurrence of the open channel condition and the pressurized condition in any segment of a sewer system can be accurately simulated. Two versions of this model, both of which were used during the course of this study, are presented in Appendix A.

The mixed flow model was used to model the Cross-Irondequoit system. Separate flow models were developed for the control structures at Thomas Creek and Densmore Creek and the pump station-force main system. Hydrographs generated by O'Brien & Gere Engineers, using the SWMM model, were used as the input to these control structure models which then produce inflow hydrographs

---

*Numbers in brackets indicate references on page 165.

to the Cross-Irondequoit tunnel and overflows discharging down nearby creeks for various control manipulations. After separate study, these control structure models were added to the mixed flow model, thus,enabling the interaction between the inflow controls and the tunnel to be simulated.

Inflows at Culver-Goodman were produced by running a corresponding storm through the Culver-Goodman model, a similar dynamic mixed flow model previously developed for Lozier Engineers, Inc. and Monroe County, New York. In order to determine the exact relationship between these two systems, it was necessary to iterate between the two models.

The pump station design calls for nine pumps having a maximum pumping capacity of 425 cfs and providing a lift of 165 feet. Of the nine pumps, four are two-speed 16 in. pumps whose discharge sides are all connected to a 42 in. force main. The remaining five are single speed 24 in. pumps connected to a 60 in. force main. At the valve chamber the two lines are joined by a 30 in. cross connection and a surge relief manifold. Each force main is about 1400 ft long, ending at the Irondequoit diversion structure. Major concerns are (1) that the normal operating procedures of pumps and valves are compatible with various pumping requirements without causing excessive water hammer pressure, and (2) the adequacy of the pressure relief system during emergency conditions such as power failure.

A hydraulic transient model of the force main system was developed. (This model is described in Appendix C.) Various types of flow control devices such as pumps, ball valves, anticipation relief valves, and surge relief valves are included in the model. The transient characteristics of the force main system were analyzed in detail and the results included in the report.

II. HYDRAULIC PERFORMANCE OF EXISTING CROSS-IRONDEQUOIT TUNNEL

The purpose of this part of the study was to determine the operating limits for the safe utilization of the Cross-Irondequoit tunnel and the pump station prior to the construction of the Culver-Goodman tunnel and the proposed automatic control system.

The major inflow points are at Thomas Creek and Densmore Creek. Synthetic storm runoff hydrographs at these and other inflow points, plus the dry weather flow, were provided by O'Brien & Gere Engineers. The storm runoff hydrographs were for a typical storm, the one year, one hour storm; the 25 year, one hour storm; and the 100 year, one hour storm. The intake structures at Thomas Creek and Densmore Creek were not included in this model. Instead, the hydrographs were used as the inputs to the Cross-Irondequoit Tunnel model in the original unmodified form. A version of the dynamic mixed flow hydraulic transient model called Model II was used to perform all the simulations in this phase of the study.

A total of 20 successful runs, as listed in Table II-1, were completed. As indicated in this table, various combinations of storm events (column 2), initial storage conditions (column 3), and maximum pumping rates (column 4) were chosen. The number shown in column 3 represents the initial water surface elevation in the wet well measured from the invert of the tunnel. The pumping rates for all of these runs were determined in the manner described below. Denoting

y_s = depth in the wet well
Q_p = pumping rate
Q_i = inflow rate to the wet well
Q_m = maximum pumping capacity

then,

(1) No pumping if $y_s \leq 1$ ft
(2) $Q_p = |Q_i|$, if 20 ft > y_s > 1 ft. and $|Q_i| \leq Q_m$
(3) $Q_p = Q_m$, if 20 ft > y_s > 1 ft. and $|Q_i| > Q_m$
(4) $Q_p = Q_m$, if y_s > 20 ft.

The results of Run II-1 indicated that the typical storm generated such a small quantity of runoff that the conditions in the tunnel were not significantly changed even when the tunnel was initially filled to a depth of 24 ft at the downstream end. The system can store all the flow from a typical storm without any hydraulic problems.

TABLE II-1. LIST OF SIMULATION RUNS FOR EXISTING CROSS-IRONDEQUOIT TUNNEL

Run No.	Storm	Starting Downstream Depth (ft)	Maximum Pumping Rate (cfs)	Remarks
II-1	typical	24	0	Weir El. 39 ft
II-2	1 year	1	465	Weir El. 39 ft
II-3	1 year	12	0	Weir El. 39 ft
II-4	1 year	12	465	Weir El. 39 ft
II-5	1 year	24	0	Weir El. 39 ft
II-6	25 year	1	0	Weir El. 39 ft
II-7	25 year	1	465	Weir El. 39 ft
II-8	25 year	12	0	Weir El. 39 ft
II-9	25 year	23	465	Weir El. 39 ft
II-10	25 year	24	0	Weir El. 39 ft
II-11	25 year	24	465	Weir El. 39 ft
II-12	100 year	1	0	Weir El. 39 ft
II-13	100 year	1	465	Weir El. 39 ft
II-14	100 year	12	0	Weir El. 39 ft
II-15	100 year	12	465	Weir El. 39 ft
II-16	100 year	24	0	Weir El. 39 ft
II-17	100 year	24	465	Weir El. 39 ft
II-18	100 year	1	0	Weir El. 90 ft
II-19	100 year	1	465	Weir El. 90 ft
II-20	100 year	1	124	Weir El. 51 ft Flap gate removed

The results of Run II-2 were also favorable. The change in the flow depth with time in the wet well and at Thomas Creek is plotted in Fig. II-1. This clearly shows that the flow in the entire system remained in the open channel condition. No severe surges were observed. That is, if the tunnel is initially empty, and if the pumping capacity is large (465 cfs), then the existing system is safe for the one year, one hour storm.

Runs II-3 and II-4 were also for the one year storm, but with the depth at the wet well initially at 12 ft. Run II-3 was for no pumping and Run II-4 was for Q_m = 465 cfs. The resulting variations of water depths are compared in Fig. II-2. The computed depth at the wet well indicates that part of the tunnel will be pressurized for both cases. The maximum heads occurring in the system were 43 ft and 21 ft, respectively. These two maximum heads were generated by different mechanisms. In the case of Run II-3 for no pumping, the pressurization of the tunnel started at the downstream end which eventually spread to the Browncroft Junction chamber. A maximum water hammer pressure of 43 ft was generated as the result of the collision of the interface (the point of separation between open channel flow and the pressurized flow) with the flap gate at the junction chamber. Figure II-3 shows the head distribution at three different times. Curve 1 and Curve 2 are immediately before and after the collision, respectively. The maximum head of 43.25 ft occurred at the time of collision. No such collision occurred for Run II-4, and the maximum head was substantially lower. The depth at the wet well was limited to slightly greater than 39 ft by an overflow weir at an elevation of 39 ft. The amount of overflow in this case was negligible.

Run II-5 corresponds to the worst condition that may occur during a one year storm event. The water surface elevation at the wet well was assumed to be initially at 24 ft, and no pumping was used. The tunnel quickly pressurized, and a fairly large water hammer pressure occurred when the interface collided with the flap gate. Figure II-4 shows the pressure distribution shortly before and shortly after the interface collision with the flap gate. In this case, the maximum head generated by the collision was 131 ft at 38.4 minutes. Note that the reflected negative pressure wave traveled downstream and temporarily lowered the head as it passed through the system. A substantial amount of overflow occurred at the overflow weir, as can be judged from Fig. II-5, which shows the variation of depth at the wet well and at the Thomas Creek input point.

The head variations produced by Runs II-6 and II-7 are compared in Fig. II-6. These curves show the effect of the pumping rate on the water hammer pressure during a 25 year storm with the tunnel initially empty. The maximum pressures were again generated by the collision of the interface with the flap gate. These are 17 ft without pumping and 82.3 ft with pumping. Both runs produced substantial overflow at the overflow weir near the pumping station and at the weir located at the junction chamber. The overflow hydrographs for Run II-7 are plotted in Fig. II-7.

Runs II-8 and II-9 are similar to Runs II-6 and II-7 except that the tunnel was assumed to be initially half full. The resulting changes in head for Runs II-8 and II-9 are compared in Fig. II-8. The maximum heads produced were 153 ft with no pumping and 87 ft with pumping. Again, pumping reduced the maximum pressure by reducing the speed at which the interface struck the flap gate. A slight reduction in the maximum head from Run II-6 of 173 ft to Run II-8 of 153 ft can be noted. This reduction may be caused by the fact that when the tunnel started from a half filled condition, the complete pressurization occurred when the inflow rate was still relatively low. Because the tunnel was being filled less rapidly, the interface velocity was lower and the collision of the interface with the flap gate produced a smaller pressure shock. Thus, the transient pressures generated depend not only upon the initial conditions, but also upon the rate of filling of the tunnel. For this reason, it is not possible to formulate a general relationship between the initial conditions in the tunnel and the maximum hydraulic pressure produced without considering other factors such as the inflow rate and the pumping rate.

For Runs II-10 and II-11, the initial depth of water at the wet well was increased to 24 ft. Again, a comparison was made between the effect of no pumping and maximum pumping. The variations of the pressure heads are shown in Fig. II-9. As might be expected, the tunnel pressurized much sooner, and the impact pressures were somewhat reduced. Overflows increased considerably as the initial storage in the tunnel was increased. Figure II-10 shows the overflow hydrographs at the Diversion Structure and the Junction Chamber. This figure should be compared with Fig. II-7.

The next series of runs, from Run II-12 to Run II-17, were a repetition of the series from Run II-6 to Run II-11 using the 100 year, one hour storm. The

variations of the head with time for Runs II-12 and II-13 are compared in Fig. II-11. The corresponding overflows for Run II-12 are shown in Fig. II-12. The variations of head with time for Runs II-14 and II-15 are shown in Fig. II-13. Similar plots for Runs II-16 and II-17 are shown in Fig. II-14.

The effect of preventing overflow at the Diversion Structure was studied by raising the weir height to 90 ft in Runs II-18 and II-19. The variations of the head with time are shown in Fig. II-15. It is interesting to note that, while the maximum depths at the wet well have substantially increased (compare with Fig. II-11) due to raising the overflow weir elevation, the maximum water hammer pressure generated by the collision of the interface with the flap gate did not change substantially. Although the overflow at the Diversion Structure has been prevented, a corresponding increase in the overflow at the Junction Chamber occurred. The overflows for Runs II-18 and II-19 are shown in Fig. II-16.

Finally, in Run II-20, the effect of removal of the flap gate at the Junction Chamber was examined. It was determined that the maximum pressure in the previous runs was caused by the collision of the interface with the flap gate. Therefore, the removal of the gate should reduce the maximum pressure. Figure II-17 shows the variation of the head with time at the wet well and at the Thomas Creek flow point. For this run, the weir height at the Diversion Structure was changed to 51 ft. Consequently, the maximum depth at the wet well was about 52.8 ft, but the maximum head in the system was 90.79 ft. This is a significant reduction when compared with Runs II-18 and II-19. Figure II-18 shows typical hydraulic grade lines (measured from the tunnel invert) due to surges and water hammer pressure. The removal of the slap gate also increased the overall storage capacity of the system and somewhat reduced the overflow rate.

Conclusions

1. The typical storm is so small that it can be totally captured without causing any harm to the tunnel even if a downstream portion of the tunnel is filled at the beginning of the storm.

2. The one year, one hour storm can also be captured by the tunnel if the tunnel is initially empty and the pumping capacity is large.

3. The 25 year, one hour storm and the 100 year, one hour storm, if entirely taken into the tunnel, would cause severe hydraulic problems. Therefore,

some type of control is necessary to protect the tunnel during a large storm event.

4. Removal of the flap gate at the Browncroft Junction Chamber would lessen the hydraulic pressures produced in the event that the tunnel is filled. This would also increase the storage capacity of the system.

5. Increasing the overflow weir height at the downstream end of the tunnel has no effect on the hydraulic transient pressure generated by the tunnel closure.

6. Any change in pumping rate can change the hydraulic pressure produced and also affect the ability of the system to handle the one year, one hour storm.

7. Overflows will occur for large storm events at the pump station and possibly at the Browncroft Junction chamber. Raising the height of one of these structures would simply shift the point of overflow to some other part of the system and would not change the total amount of overflow.

III. CONTROL STRUCTURE MODELING

The control structures at Thomas Creek and at Densmore Creek are quite similar in design and can be represented by the sketch shown in Fig. III-1. A roller gate installed across the original creek creates a small reservoir and regulates the head. A pair of sluice gates control the amount of flow diverted to the Cross-Irondequoit tunnel. Inflow to each of these reservoirs is assumed to be the outflow from the runoff model and is considered given. The flow rate to the Cross-Irondequoit tunnel will be regulated by the sluice gates according to the hydraulic conditions in the tunnel and the pumping rate. The flow rate to the tunnel is also limited by the hydraulic capacities of the conduits from the control structures to the tunnel. These hydraulic capacities were analyzed and found to be 1000 cfs at Thomas Creek and 600 cfs at Densmore Creek. The excess flow is spilled into the downstream side of the creek and eventually into the lake. A description of the mathematical model is given in Appendix B.

Two series of simulation runs were carried out. The first series, Runs III-1 to III-8, were made for the purpose of determining the operating limitations of the sluice gates from the viewpoint of preventing excessive hydraulic transients in the reservoir and gate instability. The second series, Runs III-9 to III-15, were made to determine the roller gate operation requirements in order to prevent excessive head in the reservoir during emergency conditions.

Runs III-1 through III-8 are listed in Table III-1. The 100 year, one hour storm hydrograph without the Culver-Goodman tunnel in operation was used for these runs. The roller gate was assumed to be at its lowest position so that overflow could occur only when the water surface elevation exceeded the top of the roller gate. In Run III-1, the sluice gates, initially 1/2 ft open, were opened instantaneously in two steps (2.5 ft and 5 ft) when the inflow rate reached certain points. The resulting gate opening, pool depth, discharge through sluice gate, and the overflow rate are plotted in Fig. III-2. Because of the rapid and large gate movements, large amplitude pool depth oscillations or surges occurred. Clearly, this is not a desirable operating procedure.

The operating procedure for Run III-2 was the same as that of Run III-1 except that the gate opening was based on the pool depth, which is a more easily measurable quantity than inflow rate. The results of Run III-2 are shown in Fig. III-3. Here, both the pool depth and the gate opening became very unstable.

TABLE III-1. CONTROL STRUCTURE SIMULATIONS WITH ROLLER GATE CLOSED

Run No.	Structure	Description
III-1	Thomas Creek	Control based on inflow rate, gates moved in steps
III-2	Thomas Creek	Control based on pool depth, gate moved in steps
III-3	Thomas Creek	Continuous control based on pool depth
III-4	Thomas Creek	As above at lower speed
III-5	Densmore Creek	Continuous control in flow limited to 600 cfs
III-6	Densmore Creek	Gates fixed at 3-1/2 ft
III-7	Thomas Creek	Gates fixed at 6 ft
III-8	Densmore Creek	Sudden gate closure at peak inflow

For the next two runs, Runs III-3 and III-4, the gate opening was continuously adjusted according to the pool depth. Gate opening speeds of 3 fps and 0.5 fps, respectively, were used. The results are shown in Figs. III-4 and III-5. The results of Run III-3 indicate that the gate tends to vibrate at a frequency of 5 HZ and an amplitude of 0.3 ft when the gates are continuously modulated according to the current value of the pool depth at a speed of 3 fps. This kind of gate vibration is hardly noticeable when the gate speed was cut to 0.5 fps.

A separate analysis of the Densmore Control Structure and the downshaft indicated a limiting hydraulic capacity of 600 cfs due to the restricted flow condition in the downshaft. For this reason, the maximum allowable opening of the sluice gates was determined to be 3.5 ft.

In Run III-5, the Densmore Control Structure was operated in the same manner as that of Run III-4. The results of this run are shown in Fig. III-6. The model performed satisfactorily.

Run III-6 was conducted for the purpose of determining the consequence of leaving the sluice gates open 3.5 ft for the entire storm period. The results, as shown in Fig. III-7, were very satisfactory. The flow to the Cross-Irondequoit Tunnel gradually increased to a maximum of 600 cfs, while the depth in the pool reached a maximum of 10 ft. Thus, the roller gate in the closed position offers adequate protection to the structure as long as the sluice gates are open during the peak inflow period.

The effect of leaving the Thomas Creek sluice gates open all the time at 6 ft while the roller gate is in a closed condition, was simulated in Run III-7 and the results plotted in Fig. III-8. Again, the results are very satisfactory.

Finally, the Densmore Control Structure model was used to simulate the effect of a sudden sluice gate closure during the peak inflow condition in Run III-8. At t = 40 min., when the pool depth was at 10 ft, both sluice gates were closed at the rate of 3 fpm while maintaining the roller gate at the closed position. Figure III-9 shows that the pool depth very quickly increased to 14.1 ft without oscillation.

The last run, Run III-8, indicates that the spilling capacity of the roller gate is not adequate if the sluice gates are closed during the peak period of

the 100 year storm. This means that there is a need to modulate the roller gate opening to allow some underflow as well as overflow. Since the Thomas Creek structure is nearly identical to the Densmore Creek structure, the study on roller gate movement was carried out using the Densmore model only. A total of seven runs, Runs III-9 - III-15, as listed in Table III-2, were conducted. The runoff hydrograph due to the 10 year storm was used as the input.

TABLE III-2. Roller Gate Operation at Densmore Creek.

Run No.	UpCL	LOCL	OTS	SGM	GSZ	SGS
B9	9.43	8.0	1.0	1.0	0.5	Closed T > 0
B10	9.43	8.0	1.0	1.0	0.3	Closed T > 0
B11	9.43	8.0	0.5	1.0	0.3	Closed T > 0
B12	9.43	8.0	1.0	1.0	0.3	Open T > 80 Closed T > 80
B13	9.43	8.0	1.0	1.0	0.3	Closed Open T > 100
B14	9.43	8.0	1.0	1.0	0.3	Closed Open T > 105
B15	9.43	8.0	1.0	1.0	0.3	Open all time

Notes:

UpCL = upper control level (ft)
LOCL = lower control level (ft)
OTS = operating step (min.)
SGM = speed of gate movement (fpm)
GSZ = gate step size (ft)
SGS = sluice gate status

Previous experience with the sluice gate control simulation has shown that the speed and the step size of the gate movement should not be too large in order to prevent instability. It was also found to be undesirable to relate the gate opening directly to the instantaneous water level. These factors were taken into account in this series of simulation runs. The maximum allowable depth was given as 11.5 ft. Two control levels, UpCL and LOCL, were established. The pool level is checked at constant time intervals, OTS. The gate is

programmed to open at a specific speed, SGM, for a specified amount, GSZ, if the pool level exceeds UpCL. Conversely, the gate is programmed to close at the same speed and the same amount if the pool level is less than LOCL.

Runs III-9 - III-11 were made based on the assumption that the sluice gates are kept closed all the time and all the runoff must either remain in the reservoir or pass through the roller gate. The results of Run III-9 are shown in Fig. III-10. Some roller gate oscillations during the peak flow period make this control algorism undesirable. This roller gate oscillation was eliminated in Run III-10, as shown in Fig. III-11. Table III-2 indicates that the only difference between these two runs is the gate movement step size. While the 0.5 ft step caused a gate oscillation, the 0.3 ft step resulted in smooth operation of the gate. For the next run, the operating time step was reduced to 0.5 min. The results, as shown in Fig. III-12, are almost identical to those in Fig. III-11, indicating that there is no need for an operating time step of less than one minute.

Now that the algorism in Run III-10 has been determined to be satisfactory when the sluice gates are closed, it is necessary to check the performance under the most severe conditions. Run III-12 simulates the case when the sluice gates are opened to 3-1/2 ft until t = 80 min. but set to close at the rate of 1 fpm and kept fully closed thereafter. The results, shown in Fig. III-13, are very satisfactory. Note that the inflow hydrograph is just beginning to rise sharply at the time of closure. Run III-13 is an attempt to simulate the worst condition, the sluice gates closing at the time of peak inflow. The results shown in Fig. III-14 indicate the pool level overshooting to 11 ft, which is still 0.5 ft under the allowable maximum elevation.

Run III-14 and Fig. III-15 are for the case when the sluice gate closure occurs shortly after the peak inflow. The results are again satisfactory.

Finally, this series is concluded with Run III-15 and Fig. III-16 for the case when the sluice gate remains 3-1/2 ft open at all times. Notice that the roller gate was opened 0.3 ft during the high inflow period because the upper control level was set at 9.43 ft, which is about 2 ft below the maximum allowable value.

Conclusions

1. The sluice gate control can be based entirely on the requirements at the Cross-Irondequoit tunnel and the pumping station. As far as the control structure safety requirement is concerned, the sluice gate can be fixed at any opening without causing problems.

2. The roller gate needs to be opened at high inflow conditions coupled with restricted outflow to the Cross-Irondequoit tunnel.

3. Among the five parameters used, the system is most sensitive to the gate step size, GSZ.

4. The gate control algorithm should be adequate under emergency conditions for a 10 year storm. Since the inflow rate for a storm greater than the 10 year storm is likely to be limited by the existing carrying capacity of the network, the recommended algorithm should also work for larger storms under existing conditions.

5. Under the worst conditions, the discharge downstream of the roller gate may increase from zero to 800 cfs within 7 minutes.

Recommendations

1. The sluice gates should be controlled according to the algorithm developed in the next chapter, which is based on the Cross-Irondequoit tunnel requirements.

2. The speed of the sluice gates should not exceed 1 fpm.

3. The recommended roller gate control algorithm is that of Run III-10. The recommended values for the control parameters are, UpCL = 9.43 ft, LOCL = 8.0 ft, OTS = 1.0 min., SGM = 1 fpm, and GSZ = 0.3 ft.

4. It is suggested that the roller gate control mechanism may be improved before final implementation. The suggested improvement is to determine the value of GSZ based on the rate of rise of the pool level rather than using the constant value of 0.3 ft per step.

IV. EFFECT OF INFLOW FROM CULVER-GOODMAN TUNNEL

A. Maximum Inflow from Culver-Goodman Tunnel

The purpose of this part of the study was to examine the effect of the proposed Culver-Goodman tunnel inflows on the performance of the Cross-Irondequoit tunnel. The system was simulated using Model II. The input hydrographs were the runoff hydrographs due to the one hour, 5 year and one hour, 10 year storms.

The Culver-Goodman model was first run with the given hydrographs as inputs. The resulting discharge hydrographs from the Culver-Goodman tunnel are shown in Fig. IV-1. Note that the gate openings were set in such a way that the outflows never exceeded 1000 cfs. The output from the Culver-Goodman model was used as one of the inputs for the Cross-Irondequoit model and 11 runs were made as described below.

In Run IV-1, the inflow was the 5 year storm and was not modified by any control. The tunnel was initially empty and the following pumping rate was used:

1. The pumping rate is equal to the flow into the wet well if it is less than 124 cfs and the depth is less than 20 ft.
2. The pumping rate is equal to 124 cfs if the inflow exceeds 124 cfs or the depth exceeds 20 ft.

The resulting variation of the water depth at the pump station is shown in Fig. IV-2. It appears that the inflow rates were not large enough to cause severe surges. The maximum head for the entire run was 24.8 ft.

Run IV-2 was made using the unmodified inflow from the 10 year storm. All other conditions were the same as those of Run No. IV-1. The variation of the water depth at the pump station for this run is shown in Fig. IV-2, Curve 1. Because of the continuous inflow that was greater than the maximum pumping rate, the water surface level continued to rise after 160 min. Mild surges were also formed in the tunnel. The maximum head for the entire run (up to 190 min.) was 26.4 ft.

The inflow in Run IV-3 was also due to the 10 year storm. The inflow from the Culver-Goodman tunnel was limited to 124 cfs when the depth at the

pumping station reached 16 ft. Other conditions were the same as those of Run IV-1. The depth at the pump station is plotted as Curve 2 in Fig. IV-3. The depth stabilized at about 19.2 ft. The maximum head was 31.8 ft.

Again in Run IV-4, the inflow was from the 10 year storm. The inflow from the Culver-Goodman tunnel was limited to 100 cfs when the depth at the pumping station reached 16 ft. Other conditions were the same as those of Run No. IV-1. The depth at the pump station is plotted as Curve 3 in Fig. IV-3. The maximum head was equal to 27.8 ft.

In Run IV-5, the conditions were the same as Run IV-4 except that the inflow limit at the Culver-Goodman tunnel was set to 150 cfs. The depth at the pump station is plotted as Curve 4 in Fig. IV-3. The maximum head was equal to 26.4 ft.

The inflow in Run IV-6 was from the 10 year storm and was unmodified. The tunnel was initially empty. The pumping rate, Q_p , was determined by the depth at the pumping station, y_p , as follows:

1.	if	$y_p < 4.0$ ft	$Q_p = 0$
2.	if	$4.0 \text{ ft} \leq y_p < 8.0$ ft	$Q_p = 40$ cfs
3.	if	$8.0 \text{ ft} \leq y_p < 12.0$ ft	$Q_p = 80$ cfs
4.	if	$12.0 \text{ ft} \leq y_p$	$Q_p = 124$ cfs

Because it is difficult to measure the inflow rate to the pump station, the method for determining the pumping rate used for Run IV-1 through Run IV-5 may not be practical. For this reason, the pumping rate for this run is based on a more readily measurable quantity. The resulting variation in the depth at the pump station is shown as Curve 1 in Fig. IV-4. A slightly increased surge can be noted. Maximum head was 25.3 ft.

Run IV-7 used the inflow from the 10 year storm. The inflow at the Culver-Goodman tunnel was limited to 124 cfs when the depth at the pump station reached 16 ft. All other conditions were the same as those of Run IV-6. The depth at the pump station is shown as Curve 2 in Fig. IV-4. The maximum head was 26.8 ft.

The inflow in Run IV-8 was from the unlimited 10 year storm. The tunnel was initially empty. The pumping rate was increased as follows:

1. if $y_p < 4.0$ ft $Q_p = 0$
2. if $4.0 \text{ ft} \leq y_p < 8.0$ ft $Q_p = 140$ cfs
3. if $8.0 \text{ ft} \leq y_p < 12.0$ ft $Q_p = 280$ cfs
4. if $12.0 \text{ ft} \leq y_p$ $Q_p = 425.5$ cfs

The depth at the pump station is shown as Curve 1 in Fig. IV-5. A reduction in the water depth due to the increased pumping rate is noticeable. The maximum head occurring during the run was 22.3 ft.

For Run IV-9, the inflow was from the 10 year storm. The inflow from the Culver-Goodman tunnel was reduced to 124 cfs at a time of 140 min. All the other conditions were the same as those of Run IV-8. The depth at the pumping station is shown as Curve 2 in Fig. IV-5. It is interesting to note that the tunnel remained open at all times during this run, and the maximum head of 15.8 ft occurred at the pumping station.

Run IV-19 used the inflow from the unlimited 10 year storm. The tunnel was initially empty. The pumping rate was further increased to the following:

1. if $y_p < 4.0$ ft $Q_p = 0$
2. if $4.0 \text{ ft} \leq y_p < 8.0$ ft $Q_p = 200$ cfs
3. if $8.0 \text{ ft} \leq y_p < 12.0$ ft $Q_p = 400$ cfs
4. if $12.0 \text{ ft} \leq y_p$ $Q_p = 619$ cfs

The depth at the pump station is shown as Curve 1 in Fig. IV-6. With this high pumping rate, the tunnel filled much slower than in all of the previous runs. The depth, although still rising at the end of the computation time ($t = 190$ min.), should start to decrease shortly after $t = 190$ min.

Finally, in Run IV-11, the inflow was due to the 10 year storm. The inflow from the Culver-Goodman tunnel was reduced to 124 cfs at $t = 140$ min. All the other conditions were the same as those of Run IV-10. The depth at the pump station is shown as Curve 2 in Fig. IV-6. The tunnel would not fill up in this case.

B. Angle of Incidence Effect

There exist two unused stubs on the Cross-Irondequoit tunnel near the Densmore Creek inflow point. These stubs are potential inflow points for the Culver-Goodman tunnel. Because these two stubs make different

angles of incidence with the Cross-Irondequoit tunnel, it was felt necessary to study the effect of the incident angle on the flow conditions in the tunnel. For this purpose a new junction condition, taking into consideration the momentun input and output, was added to the Cross-Irondequoit model. Four runs, Runs IV-12 ~ IV-15, each for different angles of incidence, were made.

Figure IV-7 shows four hydraulic gradelines when the Culver-Goodman inflow was in a favorable direction, $\theta = 30^{\circ}$. In general, there was a slight increase in the depth of the flow from the upstream side to the downstream side of the connection. The maximum increase in the depth was about 1.1 ft in this case. Figure IV-8 shows similar plots for the case when there was an adverse angle of incidence, $\theta = 150^{\circ}$. There was a substantial amount of water surface drop from the upstream side to the downstream side of the connection. The maximum drop in this case was about three feet. The momentum of the inflow directed in the upstream direction retards the flow in the main tunnel, thereby causing the buildup on the upstream side. Naturally, there will be more water stored in the tunnel and less flow discharged into the wet well during the initial stage of the filling process when the inflow is directed in the upstream direction.

Figure IV-9 shows the hydrographs at the downstream end of the tunnel for the two cases, $\theta = 30^{\circ}$ and $\theta = 150^{\circ}$. This figure clearly shows the retardation effect and the consequent reduction in the peak discharge due to the adverse angle of incidence.

There is always a velocity discontinuity at the connection because of the point input. Since the inflow from Culver-Goodman is large in comparison with the original flow in the Cross-Irondequoit tunnel, a negative velocity may exist on the upstream side of the connection. When $\theta = 150^{\circ}$, the negative velocity is more pronounced than the case when $\theta = 30^{\circ}$. The change in the velocities across the connection for the $\theta = 30^{\circ}$ and the $\theta = 150^{\circ}$ cases are plotted in Figs. IV-10 and IV-11, respectively.

Finally, the maximum head drops across the connection are plotted as the function of θ in Fig. IV-12. Although there are only four data points in this graph, it appears that the head drop is linearly related with the angle of incidence.

In conclusion, it can be said that when the inflow is directed towards the upstream direction, it causes the water surface build-up on the upstream side and reduces the hydraulic efficiency. It would also cause more turbulence and energy loss near the inflow point. These are some of the disadvantages. However, it may have the slight advantage of increasing the utilization of the upstream storage capacity of the tunnel.

C. Intermittent Inflow

The effect of intermittent gate operation at the Culver-Goodman control on the hydraulic conditions in the Cross-Irondequoit tunnel was also examined.

The main concerns were that the intermittent input would cause the tunnel to fluctuate between open and pressurized flow, or that undesirable resonance conditions would be produced.

These computer simulations were carried out in order to test the validity of these concerns.

Run IV-16: The Cross-Irondequoit tunnel was nearly filled in a holding condition.

Initial condition: downstream portion (about 1000 ft) of the tunnel filled

Dry weather flow = 46.4 cfs

Culver-Goodman inflow = 350 cfs for 10 min. and 0 for 20 min

Pumping rate = 100 cfs

The pumping rate was slightly less than the average inflow rate and the tunnel was slowly filling. The inflow hydrograph and the predicted depths are plotted in Fig. IV-13. A quite regular oscillation of the water surface at the Culver-Goodman input point should be noted. The oscillation at the sump was less regular. The predicted wave height of 1.5 ft is too small to cause any problem. Typical hydraulic grade lines are shown in Fig. IV-14.

Run IV-7: The Cross-Irondequoit tunnel was full and in the dewatering condition.

Initial condition: tunnel was filled up to a short distance upstream of the Culver-Goodman input point

Dry weather flow = 46.6 cfs

Culver-Goodman inflow = 350 cfs for 10 min. and 0 for 20 min

Pumping rate = 200 cfs

Because the pumping rate was slightly greater than the average inflow rate, the tunnel was in a gradual dewatering phase. The interface oscillated and gradually moved downstream. Figure IV-15 shows the inflow hydrograph, the depth at the sump, and the head at the Culver-Goodman input point. The head and depth fluctuations were significantly greater in this case than in the previous case. This is due to the interference of the inflow with the interface which oscillates around the inflow point. Figure IV-16 shows two typical hydraulic grade lines. The maximum amount of depth osciallation in the sump was about 9 ft. This much water level oscillation at the sump is undesirable in terms of pump operation and should be avoided.

Run IV-18: The Cross-Irondequoit tunnel was nearly empty.

Initial condition: tunnel was nearly empty and carrying only dry weather flow

Dry weather flow = 46.4 cfs

Culver-Goodman inflow = 350 cfs for 10 min. and 0 for 20 min

Pumping rate = 100 cfs

The pumping rate was slightly less than the average inflow rate, hence, the tunnel was slowly filling. The depths of flow at the sump and at the Culver-Goodman inflow point are shown in Fig. IV-17. There was a small amplitude oscillation of water depth at the Culver-Goodman inflow point. This oscillation was almost completely damped out at the sump. Typical hydraulic gradelines are shown in Fig. IV-18. Because the wave speed and the wave length are relatively small in this case, the surface wave is more readily observable.

Conclusions and Recommendations

1. The allowable inflow rate from Culver-Goodman tunnel to Cross-Irondequoit tunnel depends on the depth in the sump, the inflow rate from other sources, and the pumping rate. Among these three variables, the depth in the sump is most important. Inflow from Culver-Goodman must be restricted to 125 cfs or less when the water level in the sump approaches the crown of the tunnel.

2. The oscillatory head and depth are small if the flow at the Culver-Goodman inflow point is open channel.

3. A significant amount of depth oscillation exists at the sump when the tunnel is filled just up to the Culver-Goodman inflow point. The predicted 9 ft depth oscillation may cause some difficulty in pump operation.

4. No run has been made when the Culver-Goodman input point is completely pressurized. Thus, the magnitude of head oscillation in this case is not known and could be significant.

5. It is recommended that the intermittent inflow from the Culver-Goodman tunnel be avoided if the tunnel is filled up to or beyond the Culver-Goodman input point. Intermittent inflow is allowable if the flow at the input point is of the open channel type.

V. TRANSIENT CONTROL STUDY FOR CROSS-IRONDEQUOIT TUNNEL

A. Gate Control Algorithm for 10 Year Design Storm

The purpose of this part of the study was to establish an algorithm for controlling the inflow into the Cross-Irondequoit tunnel in a manner that would maximize the utilization of the storage capacity without jeopardizing the structural safety of the tunnel. The goal was to fill the tunnel so that the depth in the wet well would increase gradually to some predetermined level and then be maintained at this level during the remainder of the storm. Large surges in the wet well and in the tunnel were to be avoided as these may generate large waterhammer pressures. This was found to occur in the preliminary study discussed in Chapter 1. Surges in the wet well would also adversely affect the pumps and cause transient conditions in the force main system. The hydrographs used were those generated by the 5 year and 10 year storms, assuming the Culver-Goodman tunnel was in place and operational.

A total of 23 runs, as listed in Table V-1, were carried out. Because of the previous findings, the sluice gates at Densmore Creek were assumed to move at a speed of 1 fpm, except for the first run in which 3 fpm was used. Various pumping rates between 0 and 280 cfs were used in combination with nine different control algorithms and three different control levels. The nine control algorithms are described as follows:

Definitions:

y_m = control level at wet well

y = measured water level at wet well

T = lag time, minutes

G_m = maximum gate opening

$\Delta_1 = (y_m - y)/T$ = allowable rate of rise, ft/min.

Δ_2 = measured rate of rise, ft/min.

Q_D = inflow from Densmore structure

Q_C = inflow from Culver-Goodman structure

Q_m = allowable total inflow

TABLE V-1. SIMULATION RUNS FOR THE PURPOSE OF DETERMINING THE INFLOW CONTROL ALGORITHM

Run No.	Storm	Gate Speed (fpm)	Pumping Rate (cfs)	Maximum Allowable Depth (ft)	Initial Condition	Algorithm #
V-1	10	3	100	15	empty	1
V-2	10	1	100	15	empty	2
V-3	10	1	0	15	empty	3
V-4	10	1	0	16	empty	4
V-5	10	1	124	16	empty	4
V-6	10	1	124	20	empty	5
V-7	10	1	124	20	empty	6
V-8	10	1	124	20	part full	6
V-9	10	1	124	20	empty	7
V-10	10	1	280	20	empty	7
V-11	10	1	280	20	empty	7
V-12	5	1	124	20	empty	7
V-13	10	1	124	20	empty	8
V-14	10	1	124	20	empty	8
V-15	10	1	124	20	empty	9
V-16	10	1	280	20	empty	9
V-17	10	1	0	20	empty	9
V-18	5	1	124	20	empty	9
V-19	1	1	124	20	part full*	9
V-20	1	1	0	20	part full*	9
V-21	2	1	124	20	part full**	9
V-22	2	1	124	20	part full†	9
V-23	10	1	124	20	empty††	9

* 13' at Wet Well

** 8' at Wet Well

† 8' + West Side interceptor

†† + West Side interceptor

Alogrithm No. 1

1. set y_m = 15 ft, T = 5 min.
2. if $\Delta_1 \leq \Delta_2$, gates close at 3 fpm
3. if $0.9\Delta_1 > \Delta_2$, gates open at 3 fpm

Algorithm No. 2

1. set y_m = 15 ft , T = 10 min.
2. if $\Delta_1 \leq \Delta_2$, close gates to G

   $G = 1/2\ G_m$, if $y \leq 2/3\ y_m$

   $G = 1/4\ G_m$, if $2/3\ y_m \leq y < 4/5\ y_m$

   $G = 0$, if $4/5\ y_m < y$
3. if $0.9\ \Delta_1 > \Delta_2$, open gates to G

   $G = 1/4\ G_m$, if $4/5\ y_m \leq y < y_m$

   $G = 1/2\ G_m$, if $2/3\ y_m \leq y < 4/5\ y_m$

   $G = G_m$, if $y < 2/3\ y_m$

Algorithm No. 3

1. set y_m = 15 ft , T = 10 min.
2. if $\Delta_1 \leq \Delta_2$, close gates to G_1
3. if $0.9\ \Delta_1 > \Delta_2$, open gates to G_2

range of y	G_1/G_m	G_2/G_m
0 - 7'	1	.75
7' - 10'	.75	.50
10' - 12'	.50	.25
12' - 13.5'	.25	.125
13.5' - 15'	.125	0

Algorithm No. 4

1. set y_m = 16 ft , T = 10 min.
2. if $\Delta_1 \leq \Delta_2$, close gates to G_1

3. if $0.9\ \Delta_1 > \Delta_2$, open gates to G_2

4. Gates can open only once for one storm event

range of y	G_1/G_m	G_2/G_m
0 - 7	1.0	.75
7 - 10.5	.75	.50
10.5 - 12.8	.50	.30
12.8 - 14	.30	.20
14 - 16	.20	.20
> 16	0	0

Algorithm No. 5 - Steps 1 - 4, see algorithm No. 4

range of y	G/G_m	G_2/G_m
0 - 7	1.0	.75
7 - 10.5	.75	.50
10.5 - 12.8	.50	.30
12.8 - 14	.30	.20
14 - 20	.20	.20
> 20	0	0

Algorithm No. 6 - Steps 1 - 4, see algorithm No. 4

range of y	G/G_m	G_2/G_m
0 - 7	1.0	.75
7 - 10.5	.75	.50
10.5 - 12.8	.50	.30
12.8 - 20	.30	.30
> 20	0	0

Note: For algorithms Nos. 1 through 6 the gate opening refers to the sluice gate opening at the Densmore control structure. Inflow from the Culver-Goodman tunnel is assumed to be controlled by sluice gates similar to those in the Densmore control structure.

Algorithm No. 7

1. set y_m = 16 ft, T = 10 min.
2. determine the allowable total inflow according to the rate of rise and the current level at the wet well.

2.1. If $\Delta_1 \leq \Delta_2$, then water level is rising too fast and the allowable inflow must be reduced to $Q_m = Q$, depending on y as specified in the table below.

3. determine the inflow rate at the Densmore Creek structure.

3.1. if $Q_m \geq 600$ cfs, the sluice gates at the Densmore Creek structure are opened to the maximum allowable opening (the opening that links the maximum flow to the tunnel to less than or equal to 600 cfs).

3.2. if $Q_m < 600$ cfs, the sluice gates are adjusted to produce inflow from Densmore structure equal to Q_m.

4. determine the inflow rate at the Culver-Goodman tunnel. The inflow from the Culver-Goodman tunnel is set equal to Q_m minus the inflow from the Densmore structure.

5. Table for Q_1 and Q_2

y, ft	Q_1, cfs	Q_2, cfs
0 - 7	1260	1020
7 - 10.5	1020	660
10.5 - 12.8	660	410
12.8 - 20	410	410
20 -	90	90

Algorithm No. 8

1. same as Algorithm No. 7.

2. same as Algorithm No. 7.

3. determine the gate opening for the condition $\Delta_1 \leq \Delta_2$.

3.1. determine the gate opening at the Culver-Goodman structure.

(i) if the current inflow from the Culver-Goodman structure is not zero, then calculate the inflow Q_c assuming the gates are closed by 0.5 ft. If $Q_D + Q_c \geq Q_1$ then the gates at the Culver-Goodman structure are closed by 0.5 ft. If $Q_D + Q_c < Q_1$, then no change is made.

(ii) if there is no inflow from the Culver-Goodman structure, then go to 3.2.

3.2. determine the gate opening at the Densmore structure.

(i) if the current inflow is not zero, then calculate Q_D assuming the gates are closed by 0.5 ft. If $Q_D \geq Q_1$, then close the gate by 0.5 ft. If $Q_D < Q_1$, then no change is made.

(ii) if current inflow is zero, then no change is made.

4. determine the gate opening under the condition $\Delta_1 > \Delta_2$.

4.1. determine the gate opening at the Densmore structure.

(i) if the current gate opening is less than 3.5 ft, then calculate Q_D assuming the gates are opened by 0.5 ft. If $Q_D + Q_c \leq Q_2$, then the gates are opened by 0.5 ft. If $Q_D + Q_c > Q_2$, then no change is made.

(ii) if the current gate opening is equal to or greater than 3.0 ft, then go to 4.2.

4.2. determine the gate opening at the Culver-Goodman structure

(i) if the gates are not fully open, then calculate Q_c assuming the gates are opened an additional 0.5 ft. If $Q_D + Q_c \leq Q_2$, then open the gates by 0.5 ft. If $Q_D + Q_c > Q_2$, then no change is made.

(ii) If gates are fully opened, then no change is made.

5. Table for Q_1 and Q_2 same as Algorithm No. 7.

Algorithm No. 9

Same as Algorithm No. 8 except Q_1 and Q_2 are changed to the following values.

y	Q_1	Q_2
0 - 12	1400	1000
12 - 15	1000	650
15 - 18	650	400
18 - 20	400	400
20 -	90	90

Note: In Algorithms 7 through 9, Q_m is only reduced from Q_1 to Q_2 and is never allowed to increase back to Q_1. This prevents instabilities in the controls from developing due to fluctuations in the flow conditions in the wet well. It may be possible to further refine these algorithms to allow Q_m to increase back to Q_1 by basing the decision on a running average of the conditions in the wet well and/or the conditions at the major inflow points.

B. Results of Computer Simulations

Some of the results from Run V-1, which uses Algorithm No. 1, are plotted in Fig. V-1. This method of control was unsatisfactory because the gates oscillate between the fully open condition and the fully closed condition. There was a 5 ft surge in the wet well water surface elevation, which was also undesirable.

The results of Run V-2, which used Algorithm No. 2, are plotted in Fig. V-2. In this simulation, the control gates were moved in steps. This produced a significant improvement. The amplitude and frequency of the gate oscillations, as well as the surge height in the wet well, were significantly reduced compared to Run V-1.

The gate step sizes were further reduced in Run V-3. The results are shown in Fig. V-3. Some residual gate oscillation still remained.

Noting that the gate oscillations of previous runs occurred only during the closing phase after the tunnel was nearly filled, the operating strategy was altered to prevent reopening after the gates entered the closing phase. This is Algorithm No. 4. Run V-4 used Algorithm No. 4 without pumping, and Run V-5 used the same algorithm with a pumping rate equal to 124 cfs. The results are plotted in Fig. V-4 and Fig. V-5, respectively. Both cases were quite satisfactory; no gate oscillations and no surges or water hammer occurred.

For all previous runs, the gates were completely closed when the depth reached the maximum specified value. Because of pumping, the storage decreased after it reached the maximum value. Run V-6 was an attempt to maintain maximum storage in the tunnel by leaving the gates open slightly so that the inflow matched the pumping rate. Also, inflow was permitted until $y = 20$ ft rather than $y = 16$ ft as in the previous run. The results are plotted in Fig. V-6. Very little change occurred. Run V-7 used Algorithm No. 6 in an attempt to increase the final storage by increasing the final gate opening. The results are shown in Fig. V-7. Note that the depth in the wet well exceeded 16 ft, but no severe transient occurred.

For all of the previous runs, the tunnel was assumed to be initially empty. To test the adequacy of the control algorithm, Run V-8 was carried out using Algorithm No. 6 and assuming that the tunnel was initially half full. The results are plotted in Fig. V-8. This figure shows that the final phase of the

tunnel behavior remained nearly the same when the initial storage was increased. This implies that Algorithm No. 6 is sufficient to avoid undesirable transient conditions regardless of the initial tunnel condition.

The utilization of the tunnel storage for the previous four runs is shown in Fig. V-9. As expected, Run V-5 resulted in the smallest storage because of premature gate closure. It is interesting to compare Runs V-7 and V-8 and observe that Run V-8 began with a greater amount of storage than Run V-7 and ended with less storage. The loss of storage in this case was roughly 0.15 million cubic feet. It is thus very important to keep the tunnel empty in order to maximize the amount of storm runoff captured.

The total inflow from Densmore Creek and the Culver Goodman tunnel for Run V-5 is shown in Fig. V-10 along with the gate opening. A smoother hydrograph could be generated by reducing the gate step size if it is desirable to do so.

The Culver-Goodman tunnel and the control structure were designed by assuming the maximum allowable flow to the Cross-Irondequoit tunnel to be 1,000 cfs. It is, therefore, desirable to study the effect of limiting the flow to the Cross-Irondequoit tunnel on the hydraulics of the Culver-Goodman tunnel. For this reason, the Culver-Goodman model was rerun in order to simulate the effect of the operation of the automatic control system. The resulting water depths in the Culver-Goodman tunnel control structure are plotted in Fig. V-11. Some surges were produced in the Culver-Goodman control structure due to the flow restrictions as indicated by curves b, c, and d. However, these surges did not cause unacceptable pressure in the Culver-Goodman tunnel. It is also interesting to note that, since the weir crest is at 32 ft, there was no overflow from the Culver-Goodman tunnel in Runs V-5 and V-7. A very small amount of overflow occurred in Run V-8.

In all previous runs, the control gates at Densmore Creek and the Culver-Goodman Tunnel were assumed to move in tandem, resulting in roughly equal inflows from the two sources and large overflows at Densmore Creek. Fig. V-11 clearly shows that ample storage capacity remained in the Culver-Goodman tunnel. In order to minimize the total overflow, especially for the smaller and more frequent storms, it was desirable to modify the control strategy further and give priority to the inflow from Densmore Creek. Algorithms No. 7 to No. 9 were developed for this purpose. Basically, an allowable total inflow

rate was determined by the rate of rise and the depth in the wet well. This allowable inflow rate was first allocated to Densmore Creek to the extent flow was available at Densmore Creek. After a maximum amount of inflow was taken from Densmore Creek, the remaining demand was taken from the Culver-Goodman tunnel. The gate opening at each structure was determined based on the allowable flow and the current water level behind the gates. The control gates were moved in steps of 0.5 ft, although a smaller value might be preferable.

Run V-9 was carried out using Algorithm No. 7 and a pumping rate of 125 cfs. Figure V-12 shows the resulting change in the wet well water depth and the gate opening at the Densmore control structure. The desired smooth increase in water level without large pressures was obtained. It is noteworthy that the sluice gate at Densmore Creek made only one adjustment after reaching the maximum opening, indicating minimum overflow at Densmore Creek. This point is more clearly demonstrated by Fig. V-13 in which hydrographs at both control structures are plotted. Because of the Densmore capacity limitation, there was some overflow at the Densmore control structure during the high runoff period. At about t=135 min. and thereafter, the inflow to the Cross-Irondequoit tunnel matched the runoff, and thereafter overflow was prevented. The inflow from the Culver-Goodman tunnel shows a large reduction during the period t=127 min. to t=136 min. dictated by the decrease in allowable inflow rate as the tunnel approached the critical stage. The inflow from the Culver-Goodman tunnel began to increase again at about t=136 min. when inflow from Densmore Creek started to decrease.

The effect of giving priority to the Densmore inflow and, thus, reducing the inflow from the Culver-Goodman tunnel at an earlier time on the performance of the Culver-Goodman tunnel model using the controlled hydrograph as shown in Fig. V-13 as the predetermined outflow from the Culver-Goodman tunnel was analyzed. The resulting change in the depth at the Culver-Goodman control structure is plotted and compared with that of Run V-5 in Fig. V-14. A slightly earlier and higher peak is noticeable but the resulting overflow and water hammer pressure were negligible.

The effect of increasing the pumping rate to 280 cfs on Algorithm No. 7 was tested in Run V-10. The resulting inflow hydrographs and the depth at the wet well are shown in Fig. V-15. Compared with the last run, the increased pumping rate caused the beginning of the water level rise to be delayed

about 10 min., but increased the rate of rise slightly. Also, a noticeable increase in the inflow rate from the Culver-Goodman tunnel is indicated.

A critical test on the control algorithm was furnished by simulating the condition of power failure occurring at the time of peak runoff. Run V-11 is similar to Run V-10 except that the pumping rate was changed from 280 cfs to 0 to t=120 min. The resulting depth at the wet well and the inflow hydrographs are shown in Fig. V-16. At the time of the pump failure, there was a noticeable increase in the rate of rise of the water level in the wet well. Otherwise, the pump failure caused no appreciable adverse effect and the control algorithm worked satisfactorily. Control Algorithm No. 7 was also applied to a 5 year storm in Run V-12. The results are plotted in Fig. V-17; it worked satisfactorily for this smaller storm.

The previous three runs assumed that the required inflow from the Culver-Goodman tunnel could be obtained regardless of the conditions at the Culver-Goodman tunnel and the control structure. This may not be realistic during a relatively low flow period. Runs V-13 and V-14 are attempts to correct this situation by using Algorithm No. 8, and also by coupling the Cross-Irondequoit tunnel model and the Culver-Goodman tunnel model through an iterative process. It should be recalled that in Run V-9 the two models were iterated once. This was done by first running the Culver-Goodman model by assuming no interference from the Cross-Irondequoit tunnel. The Culver-Goodman control gates were all opened at fixed positions. The resulting water level in the Culver-Goodman control structure is shown in Fig. V-18 as line a. Run V-9 of the Cross-Irondequoit model was performed using the water level indicated by curve a of Fig. V-18 as the input. The results of this run are shown in Fig. V-13. The controlled inflow obtained from this run was then used as the given outflow at the Culver-Goodman control structure, and the Culver-Goodman model was run a second time. The revised water surface level at the Culver-Goodman control structure is plotted as curve b in Fig. V-18. Note the sharp peak produced near t=122 min. by the gate closure. The first iteration for the Cross-Irondequoit model was then performed as Run V-13 using the water level given by curve b of Fig. V-18 as the input and using Algorithm No. 8 as the control. The results of this run are plotted in Fig. V-19. Some of the differences between Fig. V-19 and Fig. V-13 are due to the different control algorithms used. The control inflow obtained by Run V-13 was used as the input to the Culver-Goodman model and a revised water surface level was obtained at the Culver-

Goodman structure. This is plotted in Fig. V-18 as curve c. The final iteration was Run V-14 which used curve c as the input. The results are plotted in Fig. V-20. Comparison of Fig. V-20 with Fig. V-19 indicates that the desired convergence of the Cross-Irondequoit tunnel model was achieved. The next and final iteration for the Culver-Goodman model resulted in curve d of Fig. V-18. Because of the existence of a sharp peak at the time of gate closure, the Culver-Goodman model converged more slowly than the Cross-Irondequoit model. The true simulation solution for the Cross-Irondequoit model should lie somewhere between curve c and curve d.

The results of Runs V-13 and V-14 indicate that control Algorithm No. 8 is somewhat too conservative in that a significant amount of storage capacity would remain unused after the storm. Run V-15 used Algorithm No. 9 in an attempt to let more flow in at the end of the storm. This is allowable because no severe water hammer pressure will result from the relatively small inflow allowed by the small gate openings. For this and all subsequent runs, the condition at the Culver-Goodman control structure was assumed to be that given by curve a of Fig. V-18. The results of Run V-15 are plotted in Fig. V-21. Notice the increased inflow from the Culver-Goodman tunnel when compared with Fig. V-20. No change occurred for the inflow at Densmore Creek because this inflow has already been maximized. Increased inflow from the Culver-Goodman tunnel should have a beneficial effect on the Culver-Goodman structure by reducing the surge. Run V-16 is a repeat of Run V-15 with the pumping rate increased from 124 cfs to 280 cfs. The allowable total inflow rate was also increased by the corresponding amount. Figure V-22 shows that with this high pumping rate, no gate closure was necessary, at least until t=180 min. Undoubtedly, the inflow from the Culver-Goodman structure will have to be reduced some time after 180 min. when the tunnel is filled. Clearly, increasing the pumping rate will increase the amount of storm runoff captured. In Run V-17 the same control algorithm was tested for the case of no pumping. The results are plotted in Fig. V-23. As might be expected, the inflow from the Culver-Goodman structure was further restricted from that of Run V-15, but the Densmore inflow was not affected. Finally, the control algorithm was tested with the 5 year storm and a pumping rate equal to 124 cfs. The results are shown in Fig. V-24.

C. Application to Small Storms

There was some concern about the performance of the system for small storms because, in this case, the inflow hydrographs exhibited double peaks due to the shape of the watershed. For this reason control Algorithm No. 9 was tested for the 1 year and the 2 year storms. Run V-19 represents the simulation of the 1 year storm occurring at a time when the Culver-Goodman tunnel is half filled, and with a pumping rate of 124 cfs. The results, plotted in Fig. V-25, indicate complete capturing of the Densmore flow and the Culver-Goodman flow. Next, in Run V-20, the same hydrographs and initial conditions were used, except that the pumping rate was reduced to zero. Figure V-26 shows the results. Again, all of the Densmore flow was captured without causing adverse transient pressures or surges, even though the downstream end of the tunnel became pressurized.

Run V-21 simulated the control actions for the 2 year storm with an initial depth at the wet well of 8 ft and a pumping rate of 124 cfs. Figure V-27 shows again that no control action was taken and that all of the Densmore flow was captured.

D. Effect of West Side Addition

The mathematical model of the Culver-Goodman system was modified to take into account the possible future addition of a 12 ft tunnel connecting the wet well with the proposed West Side sewer system. Inflow from the West Side sewer was assumed not to exceed 77 cfs. A schematic drawing of the West Side sewer connection is shown in Fig. V-28. In order to avoid pressurizing the West Side tunnel before the Cross-Irondequoit tunnel, it is recommended that the crown of the West Side tunnel not be below that of the Cross-Irondequoit tunnel, as shown in Fig. V-28. This is because the control algorithms have been designed to avoid severe transient conditions in the Cross-Irondequoit tunnel. It is evident that, by restricting the flow rate in the West Side interceptor to 77 cfs or less, the dynamic aspect of the West Side interceptor is made insignificant. Under such conditions, it is possible to regard the West Side tunnel only as additional storage capacity. In the model, the wet well surface area was increased to account for the additional storage created by this tunnel.

Control Algorithm No. 9 was used in testing the effect of the addition of the West Side interceptor. Run V-22 uses the 2-year storm with an initial depth at the wet well of 8 ft and a pumping rate of 124 cfs. Figure V-29 shows the results of this run and should be compared with Fig. V-27, which is for the Cross-Irondequoit tunnel without the West Side interceptor. Very little difference between the two figures can be noted. Finally, in Run V-23 the modified model was tested with the 10 year storm and the results shown in Fig. V-30. Comparison of this figure with Fig. V-21 shows a slightly increased inflow from the Culver-Goodman structure due to the increased storage capacity.

Conclusions

1. Control Algorithm No. 9 works well for all cases tested enabling the minimization of overflow without adverse transient pressures and surges. Therefore, this algorithm is recommended for adoption.

2. The tunnel system has a large enough capacity to capture all runoff in most cases from storms equal to or less than the 2 year design storm.

3. The proposed West Side interceptor will increase the storage capacity and reduce the possibility of overflow and large transient pressures.

3. The 5 and 10 year storms, although two large to be completely captured, can be largely captured if the tunnel is initially empty and the automatic control system is adopted.

VI. TRANSIENT CONTROL STUDY FOR THE FORCE MAIN PUMP SYSTEM

A. Introduction

The pump station design calls for nine pumps having the maximum pumping capacity of 425 cfs against a head of 165 ft. Of the nine pumps, four are 16 in. pumps with discharge sides all connected to a 42 in. main. The other five are 24 in. pumps connected to a 60 in. main. At the valve chamber, the two mains are joined by a 30 in. cross connected to a 16 in. surge manifold. The lines end at the Irondequoit Diversion Structure, which is about 1400 ft from the pump station.

Undesirable transient pressures could be generated in the system by normal start-up or stoppage of pumps or by the related opening or closing of valves if such procedures are not properly designed. More severe transient pressures could occur during emergency conditions such as power failure or possible mechanical failure. A mathematical model was constructed for the purpose of studying the adequacy of the safety provisions and the best operating policies during normal and emergency conditions.

The model developed for the simulation of the Force Main was based on the method of characteristics as described in Appendix C. This model uses the complete one-dimensional equations of motion and continuity. Various types of flow control devices, such as pumps, ball valves, anticipation valves, and surge relief valves are included in the model. Velocity, discharge, and head of the flow at any time and any location can be computed. This model provides an excellent tool for the design and analysis of this system. Information such as the location of surges, reverse speed of pumps, effectiveness of relief valves, and the required pipe sizing etc., can all be generated by this mathematical model.

B. Model Construction

Figure VI-1 shows the area included in the model. Major components included are the wet well, pumps, ball valves at each pump, the 42 in. and 60 in. force mains, the valve chamber, the pressure relief lines, and the surge relief and anticipation valves. The original pipe network was divided into 50 ft long segments as shown in Figs. VI-2, VI-3, and VI-4. Pumps and valves were placed at nodal points. The only difference between these three configuration is the arrangement of the relief lines. System configuration B most closely

resembles the original design. Configuration A was used first because it simulated each force main operating separately or jointly in a simple manner. Configuration C was used later because it was found necessary to shorten the relief line in order to increase its effectiveness.

The rated quantities pertinent to the two types of pumps used here are listed below.

TABLE VI-1. PUMP RATINGS

Pump	N	Q	H	T	EFF.	Max. Reverse	I
16 NC	880	33.4	168	4610	86%	-1084	2540
24 NC	585	53.4	172.5	12748	86%	-721	10900

Where N = rotational speed, rpm.
Q = pumping rate, cfs.
H total dynamic head, ft.
T = torque, ft-lb.
I = moment of inertia, lb-ft^2.

The pump characteristic curves given by the manufacturer covered only the normal operating zone, a zone in which both the direction of pump rotation and the flow are in the intended direction. Complete characteristic curves, including reverse rotation and reverse flow, are needed to study the power failure condition. The characteristic curves in the normal zone are extended to cover the complete zones by assuming that the curves in dimensionless variables would be similar to that of Donsky's [2] test results conducted for a similar type of pump. These synthetic complete pump characteristic curves are shown in Fig. VI-5. The dimensionless variables found in Fig. VI-5 are defined as follows.

$$v = \frac{Q}{Q_r}$$

$$h = \frac{H}{H_r}$$

$$a = \frac{N}{N_r}$$

$$b = \frac{T}{T_r}$$

in which the subscript r indicates the rated value.

The data on the ball valves supplied by the manufacturer included the stoke-plug angle relationship and the head loss coefficient-plug angle relationship during steady flow. From this data it was possible to develop a quasi-steady ball valve operating characteristic curve as shown in Fig. VI-6. In this graph the variables are defined as

τ = time measured from the beginning of valve closure

t_c = time required for complete closure

τ = per cent opening

C. Results of the Simulation of Normal Operation

The first phase of this simulation study was to determine a safe operating procedure for normal start-up and shut-down conditions. Any operating procedure considered normal and satisfactory should not generate a high enough pressure in the system to trigger the opening of any pressure relief valve. It is also desirable to avoid pressure low enough to induce cavitation or column separation. Since the flow after a relief valve opening or the occurrence of cavitation was of no interest, model configuration A was used in this series of simulations.

Four of the simulation runs performed for normal operating conditions are listed in Table VI-2.

TABLE VI-2. SUMMARY OF SIMULATION RUNS FOR NORMAL OPERATION, CONFIGURATION A

Run No.	Force Main	Pump Schedule	No. of Relief Valves
VI-1	42"	All at the same time	2
VI-2	42"	Table VI-3, 16 NC	2
VI-3	60"	Table VI-3, 24 NC	2
VI-4	Combined	Table VI-3, combined	4

Note: All relief valves are set at 80 psi.

Run VI-1 was for the case when all of the pumps in the 42 in. force main were turned on simultaneously while all of the ball valves were initially closed. This was followed by a gradual opening of all of the ball valves, completing the

valve opening in 15 seconds. After the flow stabilized to a steady flow condition, all ball valves were closed simultaneously in 15 seconds with the pumps still running. Finally, all of the pumps were stopped. Simultaneous opening and closing of the ball valves produced a large enough water hammer pressure shortly after both the opening and the closing to open the pressure relief valves. Figure VI-7 shows the variation of piezometric head at pump No. 4 during the pump shutdown phase of the operation. The dotted line represents the head between the pump and ball valve, indicating that the head gradually increased to the shut-off head. The solid line represents the head immediately downstream of the ball valve. The curve shows that the head initially dropped to a low value (undoubtedly causing cavitation) followed by severe vibration. The negative head of less then -100 ft is potentially damaging and unacceptable. Since this negative head occurred before the relief valve opened, relief valves are not an effective preventative. The maximum head of 340 ft which occurred must have received some moderation from the relief valves. The variation of discharge at pump No. 4 is plotted as a dotted line, and the total discharge at the end of the 42 in. force main plotted as a solid line in Fig. VI-8. Reverse flow occurred because the relief valves were not reset after they were opened.

For Run VI-2, the pumps were started one at a time according to the schedule shown in Table VI-3. The ball valves downstream of the pumps were

TABLE VI-3. PUMP SCHEDULE

Time Sec	Pump 16 NC		Pump 24 NC	
	Start up	Shut down	Start up	Shut down
0-3	1L	1-4H	5	5,6,7,8,9
3-6	1H	1H,2H,3H	5,6	5,6,7,8
6-9	1H, 2L	1H, 2H	5,6,7	5,6,7
9-12	1H, 2H	1H	5,6,7,8	5,6
12-15	1H,2H,3L	None	5,6,7,8,9	5
15-18	1H,2H,3H	None	5,6,7,8,9	None
18-21	1-3H, 4L	None	5,6,7,8,9	None
21-	1-4H	None	5,6,7,8,9	None

opened immediately after the corresponding pumps were turned on. The intervals between each change were set at 3 seconds. Figure VI-9 shows the variation of the head at pump No. 4. The dotted line clearly indicates that pump No. 4 was the last to be started (at 18 sec) and that the pump was started in two steps (double peak). The solid line indicates that the head downstream of the ball valve received the effect of the other 3 pumps very early. The head remained within acceptable limits everywhere and the relief valves remained closed. Figure VI-10 shows the flow rate at pump No. 4 and at the force main outlet during the start-up process. No severe pressure surge is indicated. The system also behaved well during the step by step shutdown process.

In Run VI-3, the 60 in. force main was tested with a step by step start-up and shutdown schedule as listed in the last two columns of Table VI-3. The resulting change in the piezometric head at pump No. 5 predicted by the model for the entire operating period is shown in Fig. VI-11. Graph (a) in Fig. VI-11 shows a typical response of the pump head to valve opening and valve closure. Graph (b) of this same figure is the response of the force main to the operation. It shows an initial rapid increase in head followed by a period of steady conditions and, finally, the transients due to valve closure. The transient pressure remained below the maximum steady operating pressure and the relief valve remained closed. The minimum head of 82 ft due to the valve closure is safely above the cavitation level. The pumping rate at pump No. 5 and the total discharge at the end of the 60 in. force main predicted by Run VI-3 are shown in Fig. VI-12.

Finally, in Run VI-4, the two interconnected force mains were operated jointly using the same pump schedule as Run VI-2 and Run VI-3. The predicted piezometric heads at pump No. 4 and pump No. 5 are plotted in Fig. VI-13 and Fig. VI-14, respectively. Again, the system performed satisfactorily. In summary, safe operation was found to require a staggered pump schedule with a minimum 3 second interval between each pump or valve operation. Normal operation would require several minutes between pump starts.

D. Results of the Simulation of Power Failure

A total of 14 runs as listed in Table VI-4 were conducted to study the requirements for the protection of the system against possible hydraulic transients resulting from power failure. To be conservative, power failure was always assumed to occur while one or both force mains were carrying maximum flow.

TABLE VI-4. SUMMARY OF SIMULATION RUNS FOR POWER FAILURE

Run No.	Model Configuration	Force Main	Valve Closure Time	No. of Relief Valves
		(in.)	(sec.)	
VI-5	A	42	∞	2S
VI-6	A	42	5	2S
VI-7	A	42	5	2S
VI-8	A	42	10	2S
VI-9	A	42	15	2S
VI-10	A	42, 60	5	2S
VI-11	A	42	11	2A
VI-12	A	42	11	8A
VI-13	A	42	11	8S
VI-14	B	42, 60	11	2A, 2S
VI-15	B	42, 60	11	4A
VI-16	B	42, 60	11	10A
VI-17	C	42, 60	11	4A, 2S
VI-18	C	42, 60	11	6A, 2S

Notes:
1. S indicates surge relief valve
2. A indicates surge anticipation valve
3. wave speed = 4000 fps for Run VI-7
   wave speed = 3000 fps for all other runs

For the purpose of establishing a base for comparison, Run VI-5 was made for the 42 inch force main assuming no protective action is taken, i.e., all valves remained open after power failure. Fig. VI-15 shows the response of pump No. 1 to the power failure. It is interesting to note that both the flow (Q/Q_r) and the pump rotation (N/N_r) reverse directions a few seconds after the power failure. Corresponding piezometric heads at 4 representative points in the system are shown in Fig. VI-16. No severe transient heads are indicated.

To prevent the reverse flow and pump rotation, Run VI-6 was made assuming that the ball valves close in 5 seconds after the power failure. The resulting conditions at pump No. 1 and the 4 representative points are plotted in Fig. VI-17 and Fig. VI-18, respectively. These figures clearly show that the pump is now well protected at the expense of generating a large transient head, especially the cavitation causing negative head, in the force main. The relief valves were triggered and limited to maximum head of 302 ft. It appears that a compromise between the requirements for the pumps and the force main is needed. Run VI-7 was conducted to test the sensitivity of the transient characteristics to the pressure wave speed. A wave speed of 4,000 fps was used for this run, but the value, 3,000 fps, was used for all other runs. No significant difference was found between the results of this run and Run VI-6 and, therefore, the question of wave speed effect was dropped.

The conditions for Run VI-8 are identical to those of Run VI-6 except that the ball valve closure time was increased to 10 seconds. Fig. VI-19 shows that there was a reverse flow of 13 cfs but no reverse pump rotation. Fig. VI-20 shows that there existed a slightly higher positive head but less negative head in this case as compared with Run VI-6. It is interesting to observe that the head downstream of the ball valve (indicated by triangles) first dropped to a negative value before increasing to a peak, as shown in Fig. VI-18, when the valve was closed in 5 seconds. On the other hand, when the valve was closed in 10 seconds, the pressure increased to a higher peak without first dropping to a negative value.

In Run VI-9, the valve closure time was further increased to 15 seconds. Fig. VI-21 shows that there was a maximum reverse rotation of 900 rpm and a substantial amount of reverse flow. This is undesirable. Fig. VI-22 shows, however, that the transient conditions in the force main are within tolerable limits. Run VI-10 was conducted to study the effect of interconnecting the two force mains. With a valve closure time of 5 seconds, the predicted maximum

and minimum head were 352 ft and -122 ft. These are unsatisfactory values. The existing surge relief valves are not sufficient to protect the force main without sending the pumps into reverse rotation. It appears that the valve closure time should be less than 15 seconds to protect the pumps, and more relief valves are needed to protect the force main. In Run VI-11, the valve closure time was set at 11 seconds, and the two surge relief valves were replaced by two 12-inch anticipation valves. An anticipation valve is set to open immediately at power failure without waiting for the surge to develop. The resulting piezometric heads in the system are plotted in Fig. VI-23. This system performed quite satisfactorily in that no reverse rotation or excessive water hammer pressure occurred.

In Run VI-12, the number of anticipation valves was increased from 2 to 8, without changing the size of the relief lines. The results indicated only a marginal drop in maximum head (a drop of 20 ft). In Run VI-13 the eight anticipation valves were replaced by eight surge relief valves using the same size relief lines. The resulting heads, as plotted in Fig. VI-24, are even worse than those of Run VI-11. These results indicate the existing 12-in. relief lines are too small and, thus, additional relief valves without enlarging the line would not be effective.

It should be noted that the actual relief line configuration is equivalent to that of configuration B (see Fig. VI-1), rather than configuration A (see Fig. VI-3). Configuration A was used for its relative simplicity over that of configuration B. Run VI-14 simulates the joint operation of both force mains using two anticipation valves and two surge relief valves based on configuration B and using one 24-in. relief line. The predicted heads in the 42 in. main are plotted in Fig. VI-25 and the heads in the 60 inch main are plotted in Fig. VI-26. A maximum head of 411 ft was predicted. In Run VI-15 configuration B was simulated using four anticipation valves. The resulting heads are plotted in Fig. VI-27 and Fig. VI-28. The maximum head decreased slightly to 366 ft. Finally, Run VI-16 was made with the same configuration using 10 anticipation valves. The results are shown in Fig. VI-29 and Fig. VI-30. The maximum head in this run was 272 ft.

The results of the simulations so far indicate that shortening the relief lines would be of value. For this reason configuration C, as shown in Fig. VI-4, is proposed. In this configuration a new 50 ft long 24 in. relief line is attached to the 60 in. main. This new line is also interconnected to the existing 24 in. line. Run VI-17 was made using configuration C with four

anticipation valves and two surge relief valves. The resulting piezometric heads are shown in Fig. VI-31 and Fig. VI-32. The maximum head generated was 332 ft. Run VI-18 was then made with the same configuration and six anticipation valves and two surge relief valves. The results, plotted in Fig. VI-33 and Fig. VI-34, show a maximum head of 270 ft. An advantage of having a shorter relief line is the rapid damping of transients after the first peak.

Conclusions

1. Pumps and valves in each force main should not be opened or closed simultaneously. A minimum of 3 seconds should be allowed between each operation.
2. It is allowable to start or stop a pump or a valve in the two force mains simultaneously.
3. In order to protect pumps from runaway reverse rotation, it is necessary to close the valves in less than 11 seconds after power failure.
4. The existing surge relief valves and the relief lines are not sufficient to protect the force main from surges due to power failure.
5. Surge anticipation valves are more effective than the pressure activated relief valve partly because the relief lines are too long.
6. It is recommended that a short 24 in. relief line be added to the system. Two of the existing four relief valves should be replaced by two anticipation valves. In addition, four anticipation valves should be added to a shorter relief line.

VII. OTHER CONSIDERATIONS

A. Densmore Creek and Thomas Creek Downshaft Capacity

The hydraulic capacities of the connections between the control structures at Thomas Creek and Densmore Creek and the Cross Irondequit tunnel were examined in order to determine the effect of these capacities on the operation of the control structure.

Hand computation showed that the flow in the Thomas Creek connection would remain open at least up to 1000 cfs. This is greater than the flow rate predicted for the 100 year storm. The lateral force at the bend for this flow rate was found to be 20,000 lb. A similar computation showed that the Densmore Creek connection could convey 600 cfs at full pipe flow with no surcharge, or a flow of 800 cfs with a 5 ft surcharge. Simulation of the flow in the conduit using an implicit finite difference technique [3] showed that the flow in the conduit is supercritical, that open channel flow would be maintained up to an inflow rate of 600 cfs, and that due to the existence of supercritical flow, large pressures would be produced if the transition from open channel to closed conduit flow was allowed to occur. In order to avail these large water hammer pressures and the need for surcharge in the control structure, it is recommended that the flow from the control structure to the Cross Irondequoit tunnel be limited to a maximum of 600 cfs.

B. Ventilation Requirements

The greatest ventilation requirement occurs at the time of maximum inflow into the Cross-Irondequoit tunnel. In addition to the volume of air that must be evacuated to create room for inflowing water, the air entrained by the turbulent inflow should also be removed. The control algorithm has been designed to limit the inflow rate to the maximum of 1400 cfs. Therefore, assuming the adoption of this control algorithm, the maximum rate of air withdrawal is 1400 cfs. The dropshaft at the Culver Goodman inflow point has been designed to provide good ventilation for inflow rates up to 1000 cfs. For this reason additional ventilation requirements due to air entrainment at the Culver Goodman tunnel should be small. A similar provision is not provided for at the Densmore Creek or the Thomas Creek intake.

It is rather difficult to estimate the amount of air entrainment due to inflowing water. For the air entrainment by the flow over a spillway, a task committee set up by the American Society of Civil Engineers [4] recommended the

following equation based on Straub and Anderson's experiments [5].

$$\bar{C} = 0.743 \log_{10} \left(S\, q^{-0.2}\right) + 0.876 \qquad \text{(VII-1)}$$

In the above equation,

$\bar{C}$ = mean air concentration in volume,

S = slope of the channel, and

q = discharge per unit with, cfs/ft.

According to this equation, the air concentrations at Densmore Creek and Thomas Creek are very unlikely to exceed 0.876. Taking into account the inflows from the Culver Goodman tunnel and other sources, it appears conservative to estimate the total maximum ventilation requirement to be 2,000 cfs.

Ideally, the locations of the required ventilation should be as dispersed as possible. A minimum of four locations, the Browncroft Diversion Structure, the pump station, a point shortly upstream of the Densmore downshaft, and a point shortly downstream of the Culver-Goodman junction at 500 cfs capacity each are required. The reason why these two intermediate points are needed is because, under a high inflow rate and a large storage condition, the tunnel may be blocked at the Culver-Goodman junction.

The ventilation requirements stated above are based on the maximum inflow due to storm runoffs. There is another ventilation requirement which is to prevent odor during dry weather conditions. For this requirement, air should be let in as far upstream as possible, and let out at the pump station. Dispersed ventilation points in this case would not be desirable.

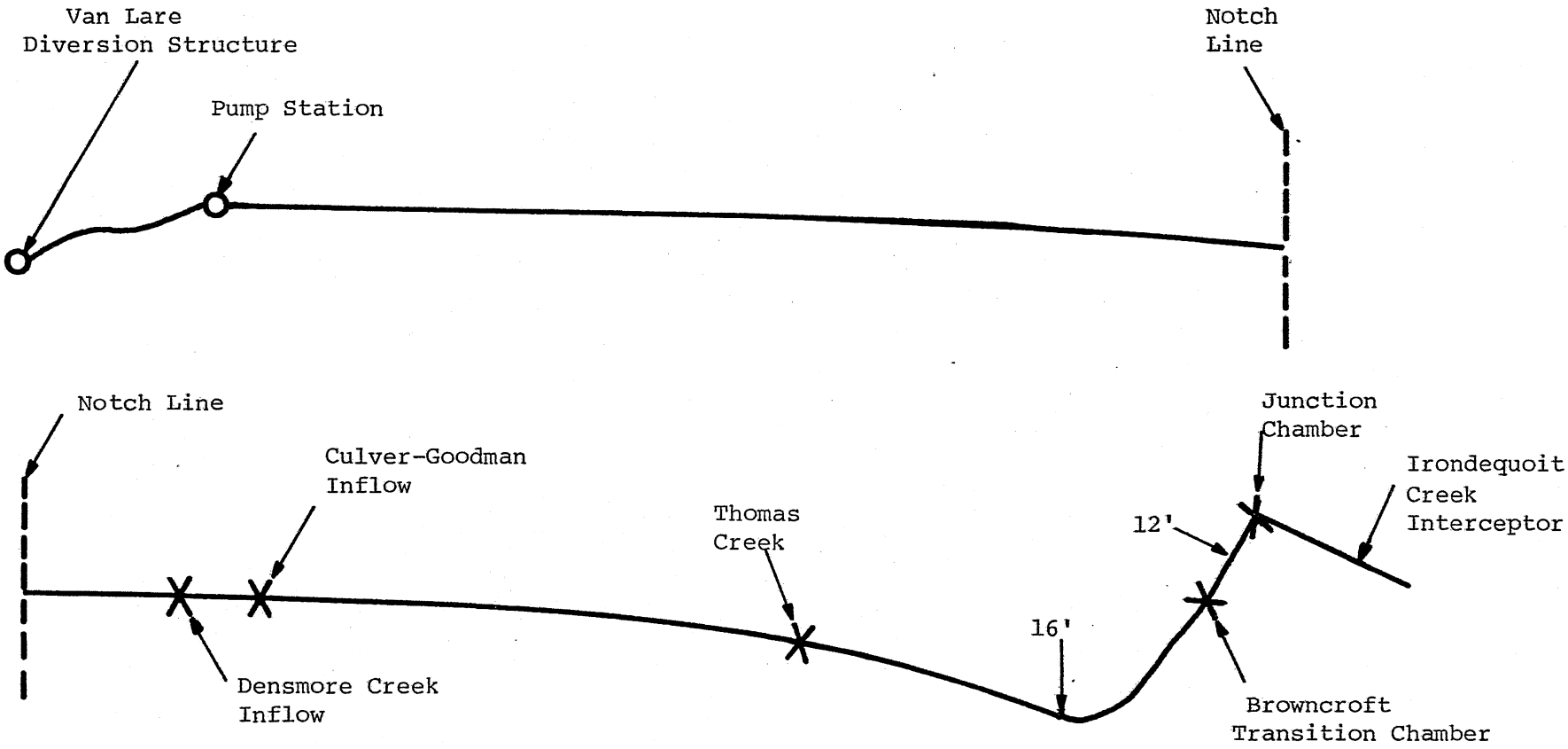

Fig. I-1. The General Layout of the Cross-Irondequoit Tunnel

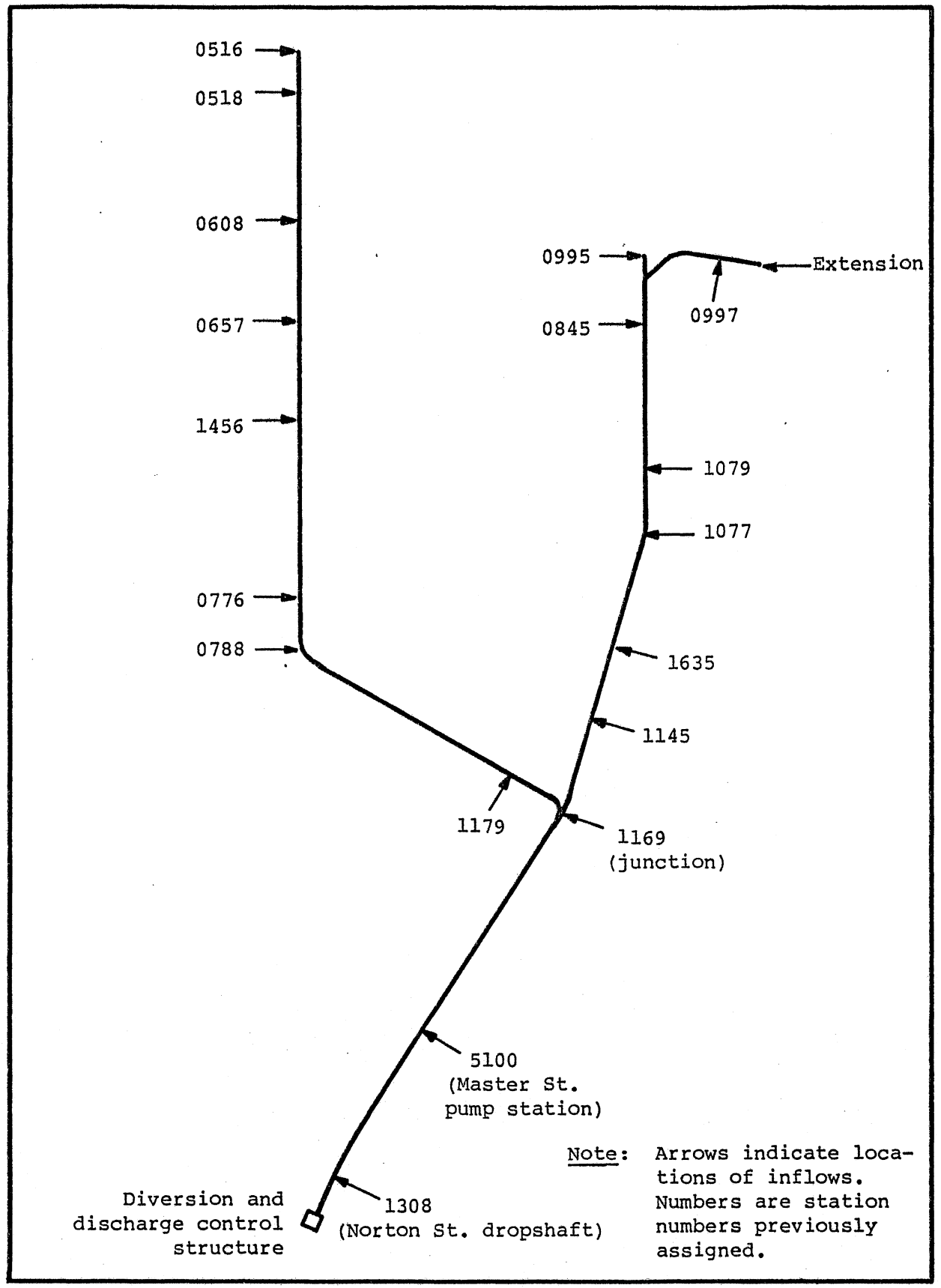

Fig. I-2. General Layout of the Culver-Goodman Tunnel.

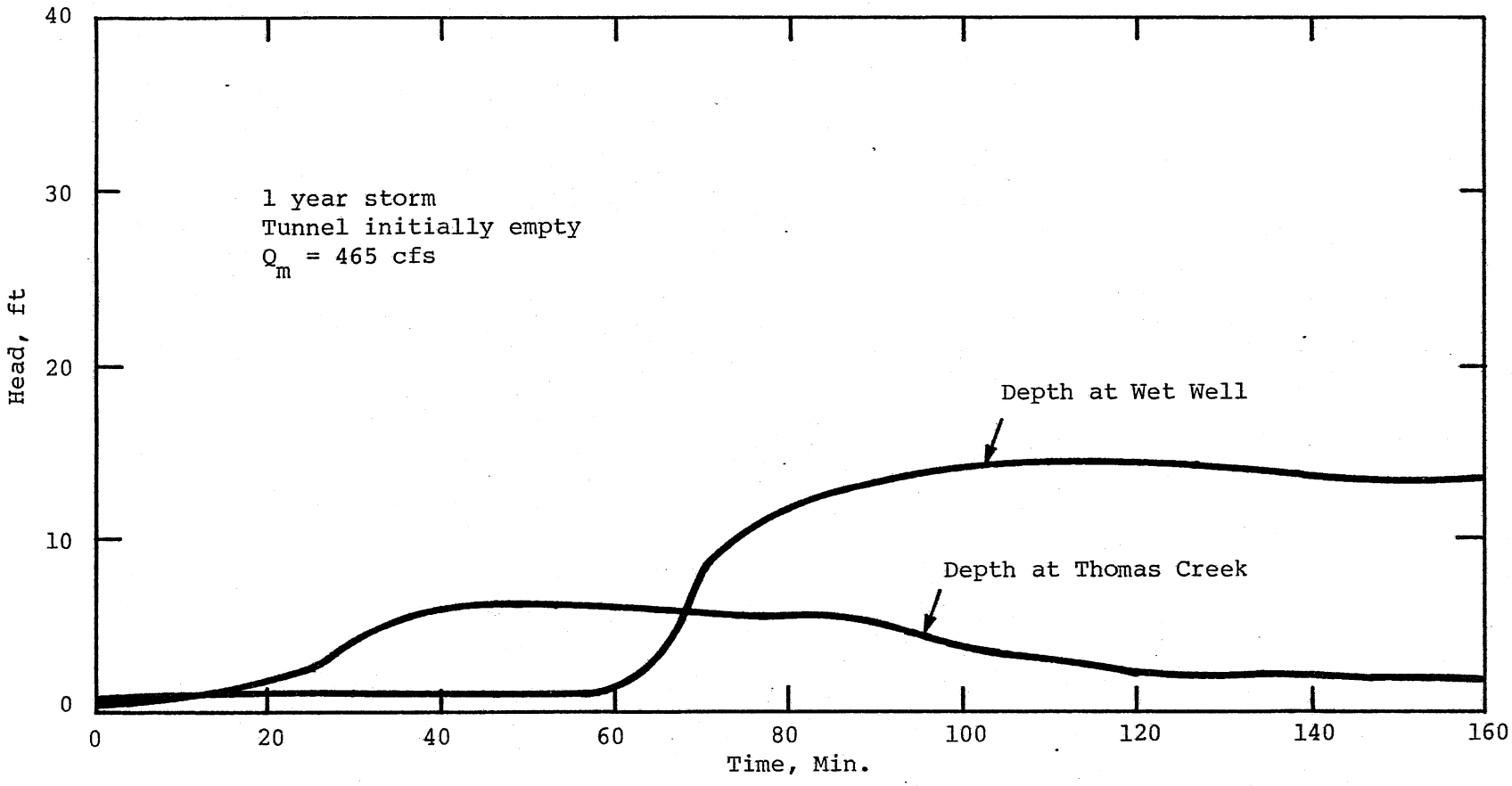

Fig. II-1. Change in Depth, Run II-1.

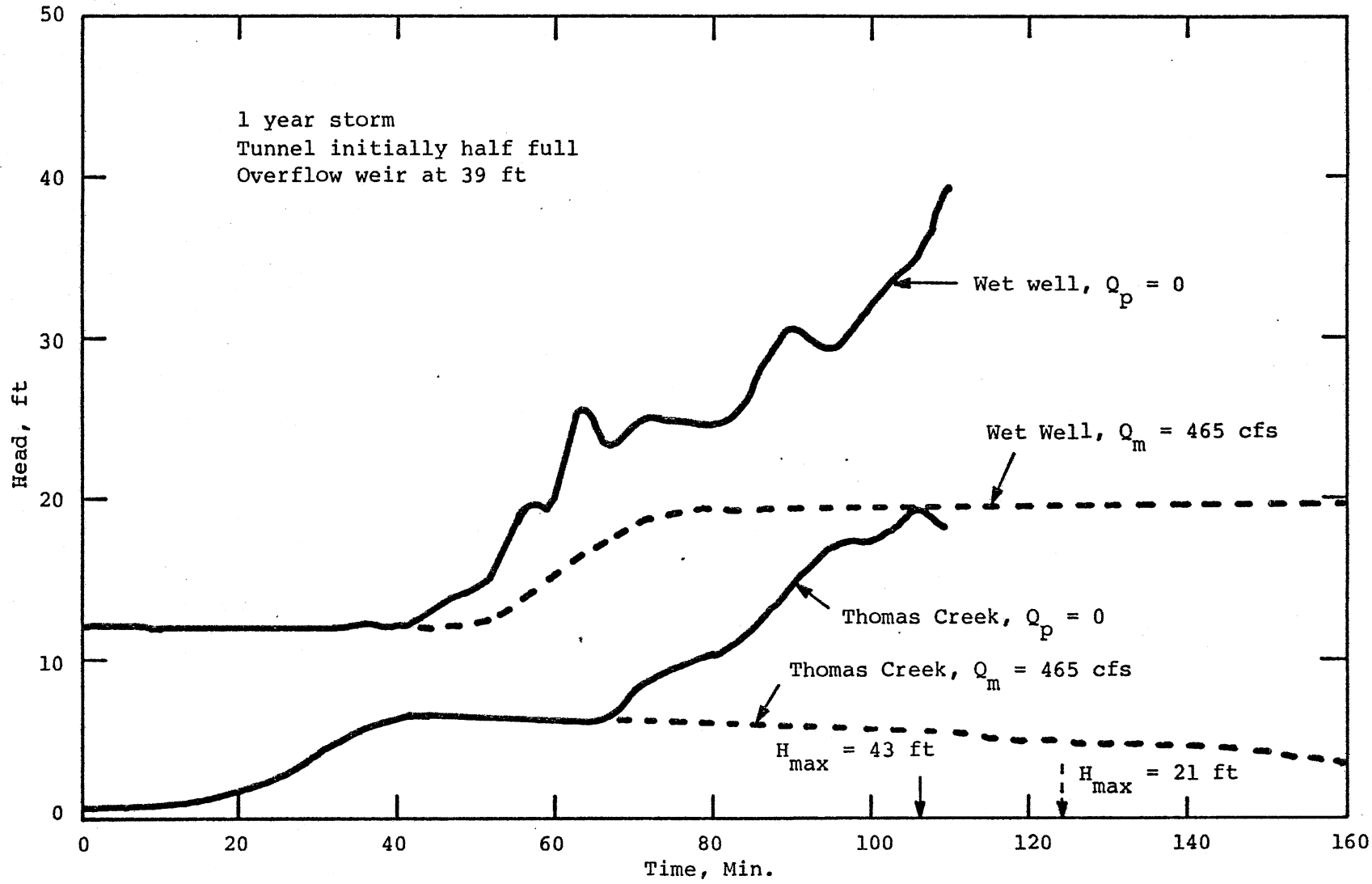

Fig. II-2. Change in Depths Compared, Runs II-3 and II-4.

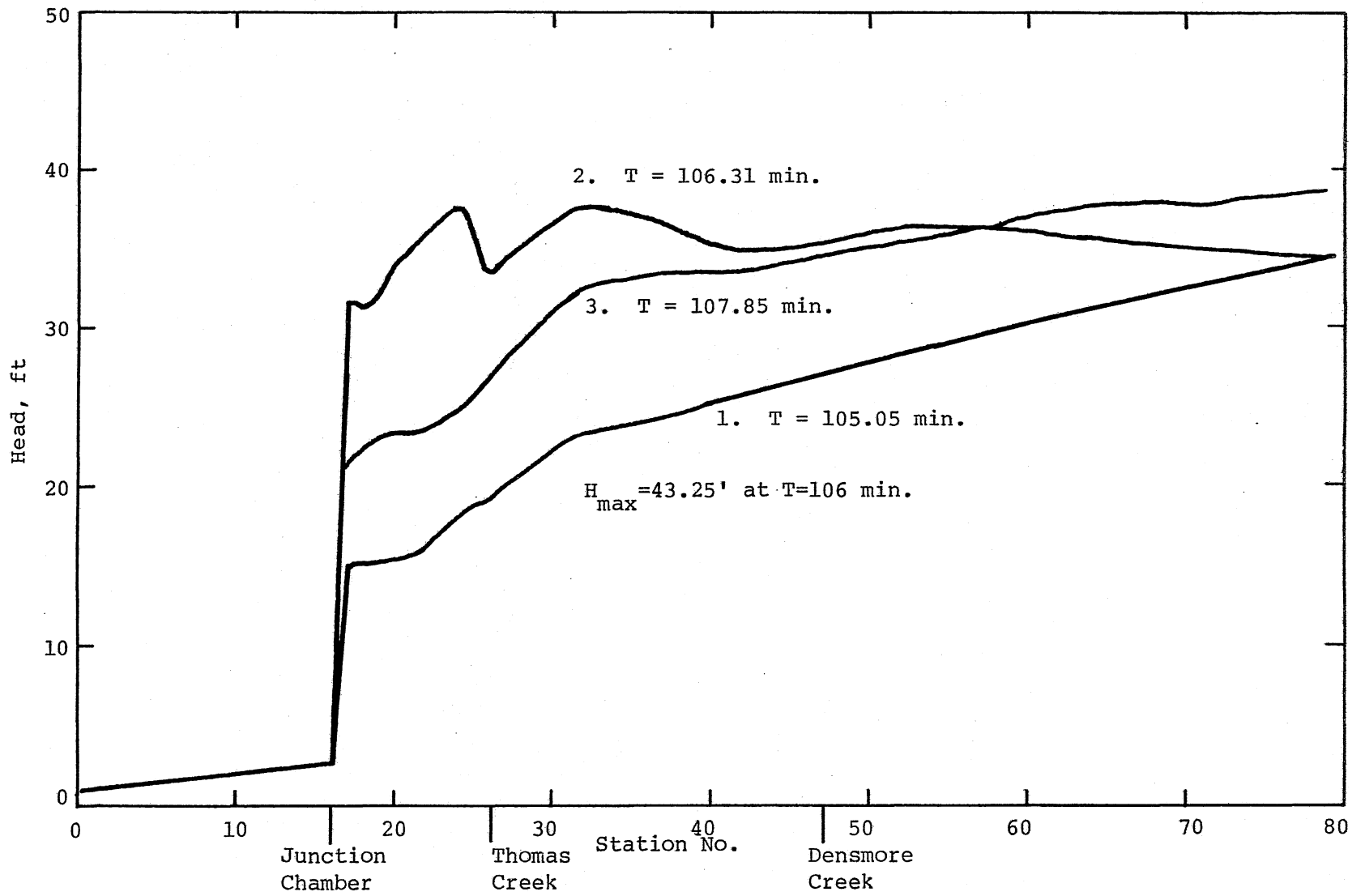

Fig. II-3. Head Distribution Before and After Complete Pressurization, Run II-3.

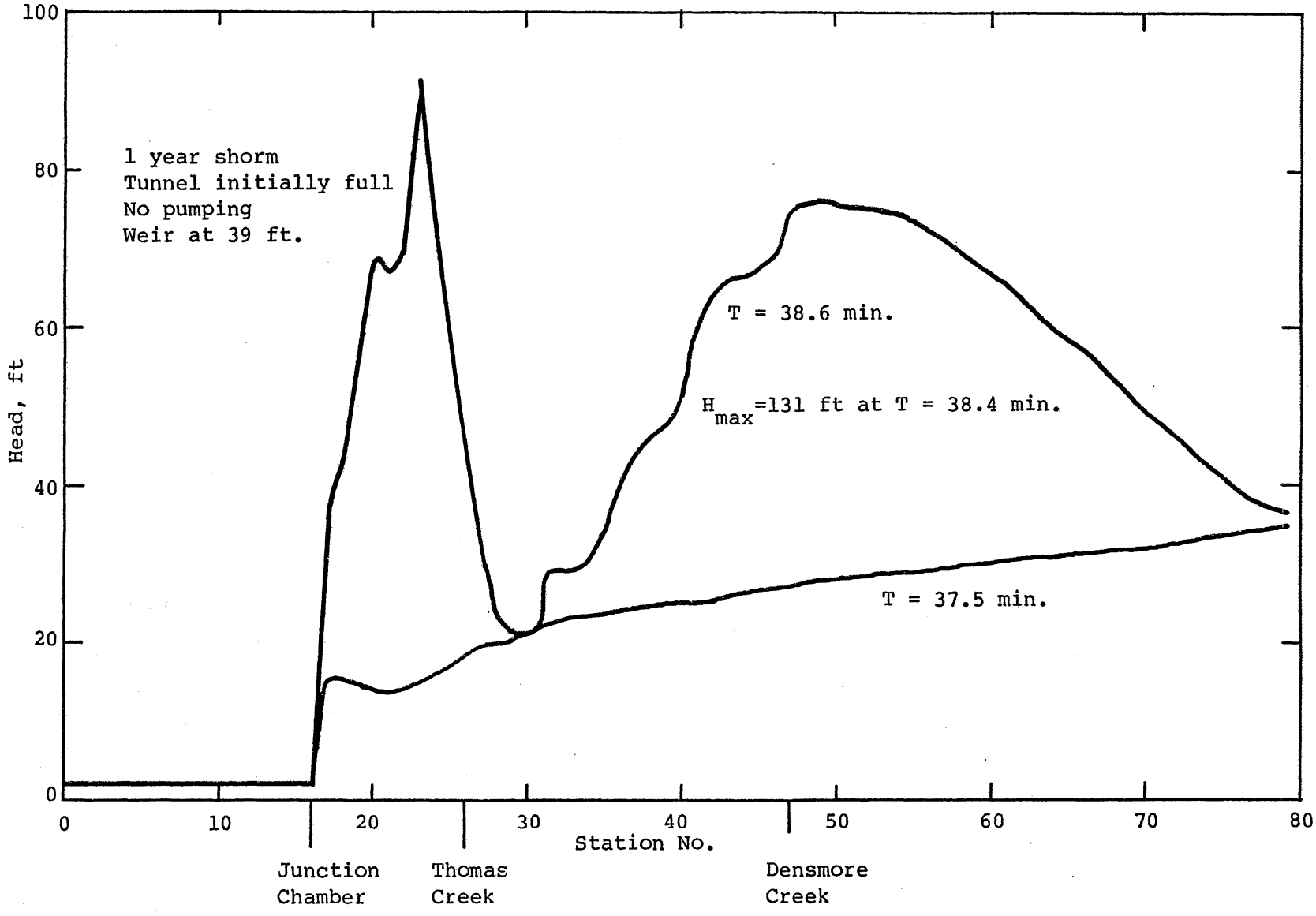

Fig. II-4. Head Distribution Shortly Before and After Complete Pressurization, Run II-5.

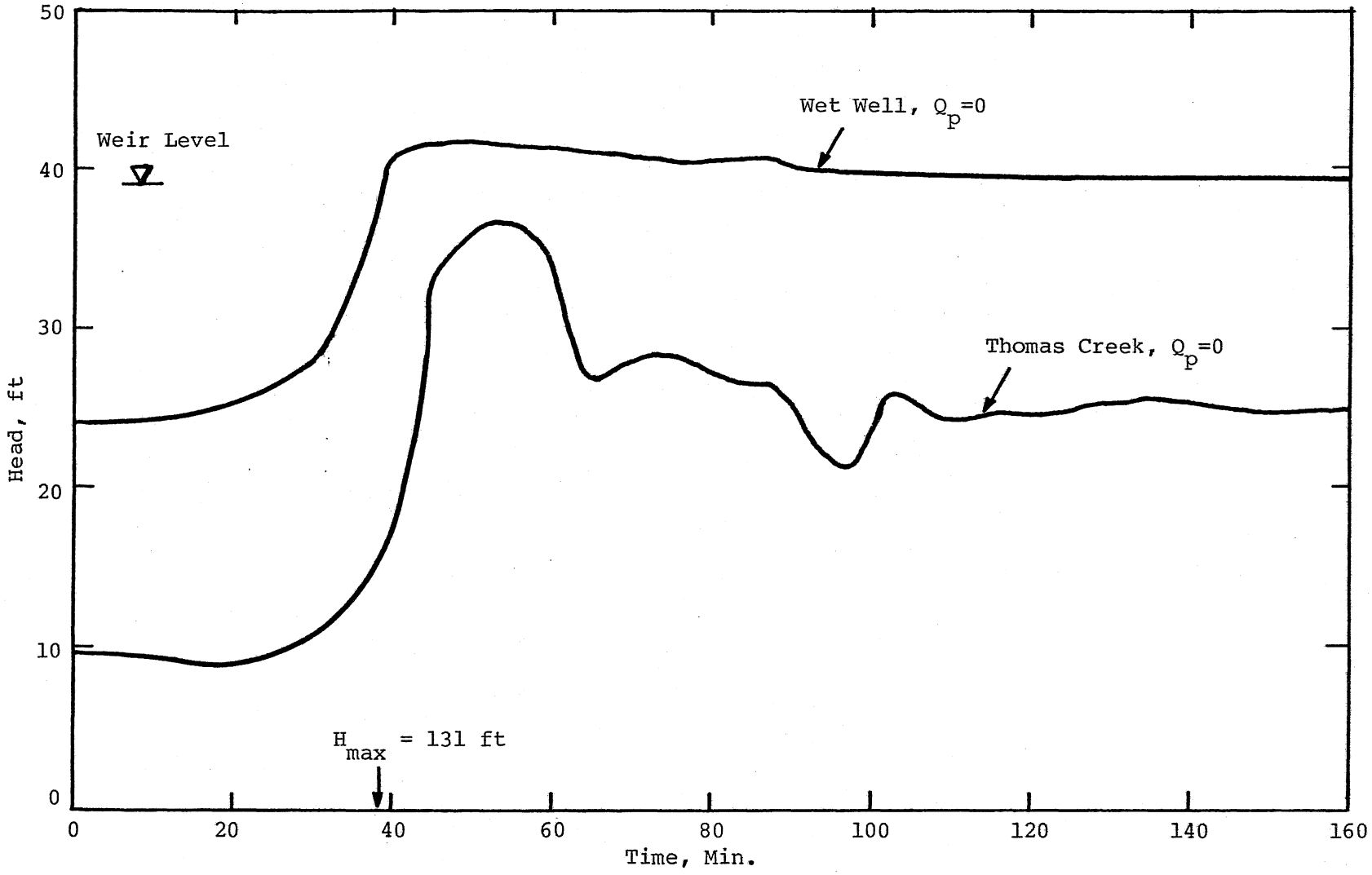

Fig. II-5. Change in Head Due to 1 year Storm, Tunnel Initially Full, Overflow Weir at 39 ft, Run II-5.

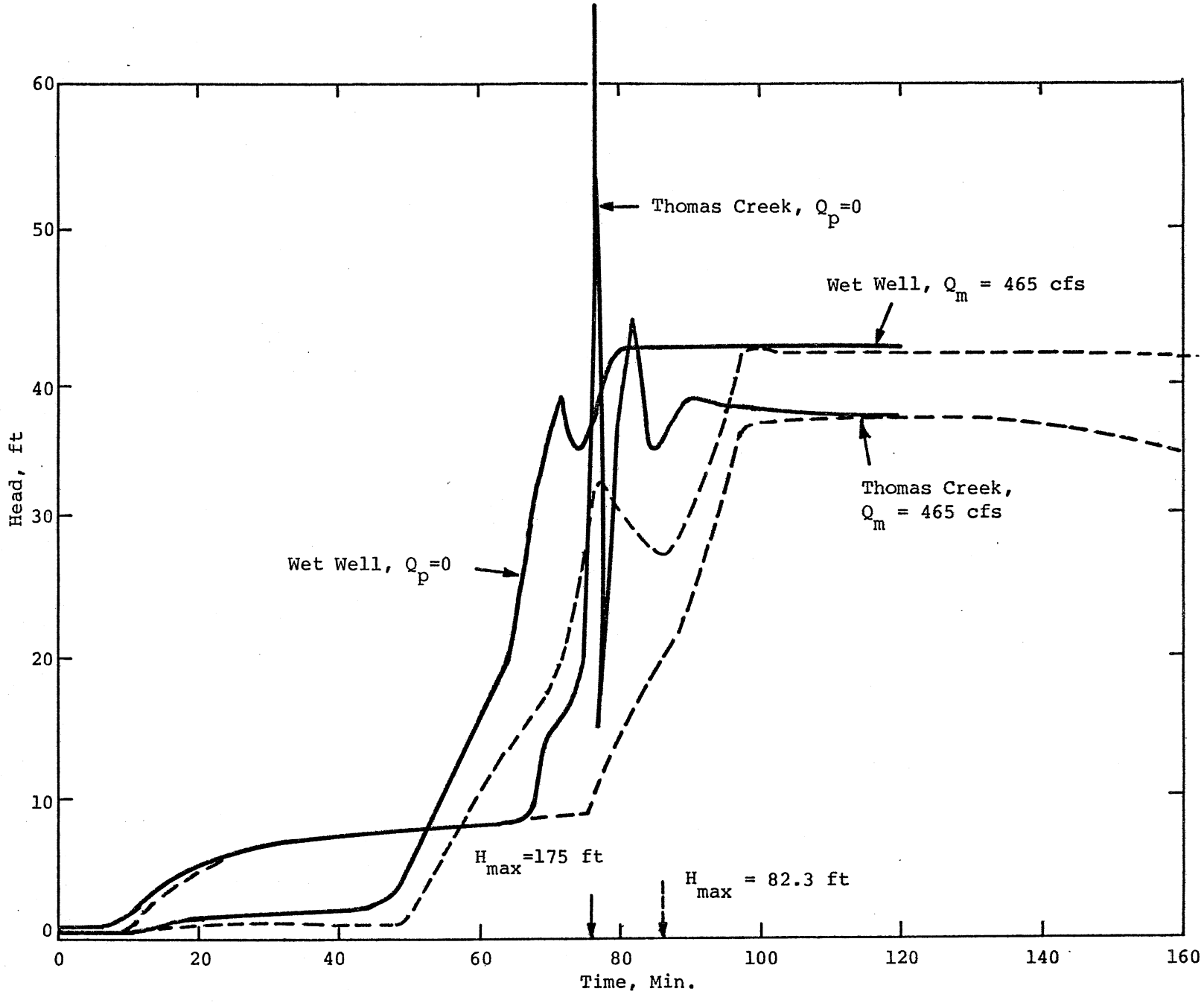

Fig. II-6. Change in Head Due to 25 Year Storm, Tunnel Initially Empty, Overflow Weir at 39 ft, Runs II-6 and II-7.

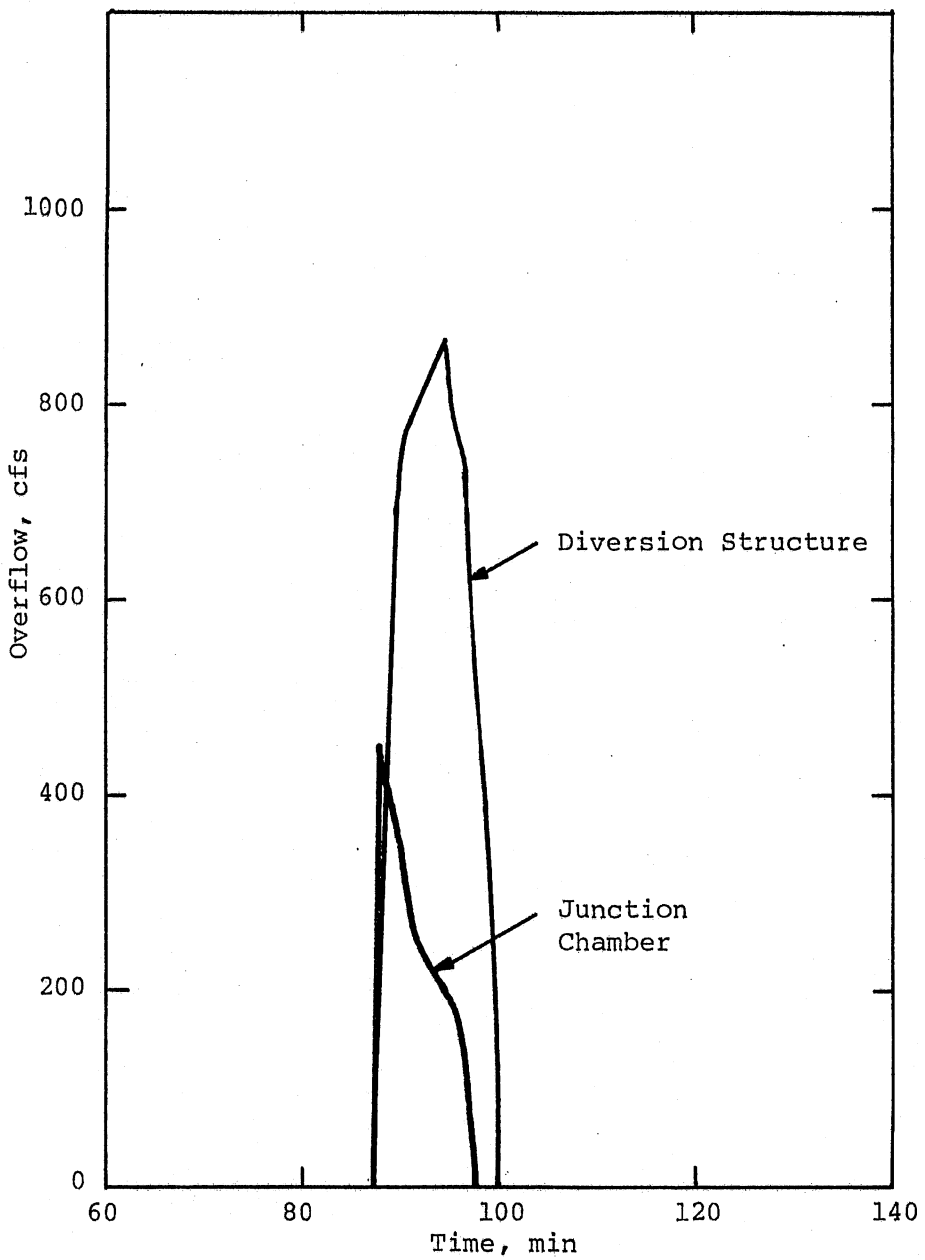

Fig. II-7. Overflow Hydrographs, 25 Year Storm, Tunnel Initially Empty, Q_m = 465 cfs, Run II-7.

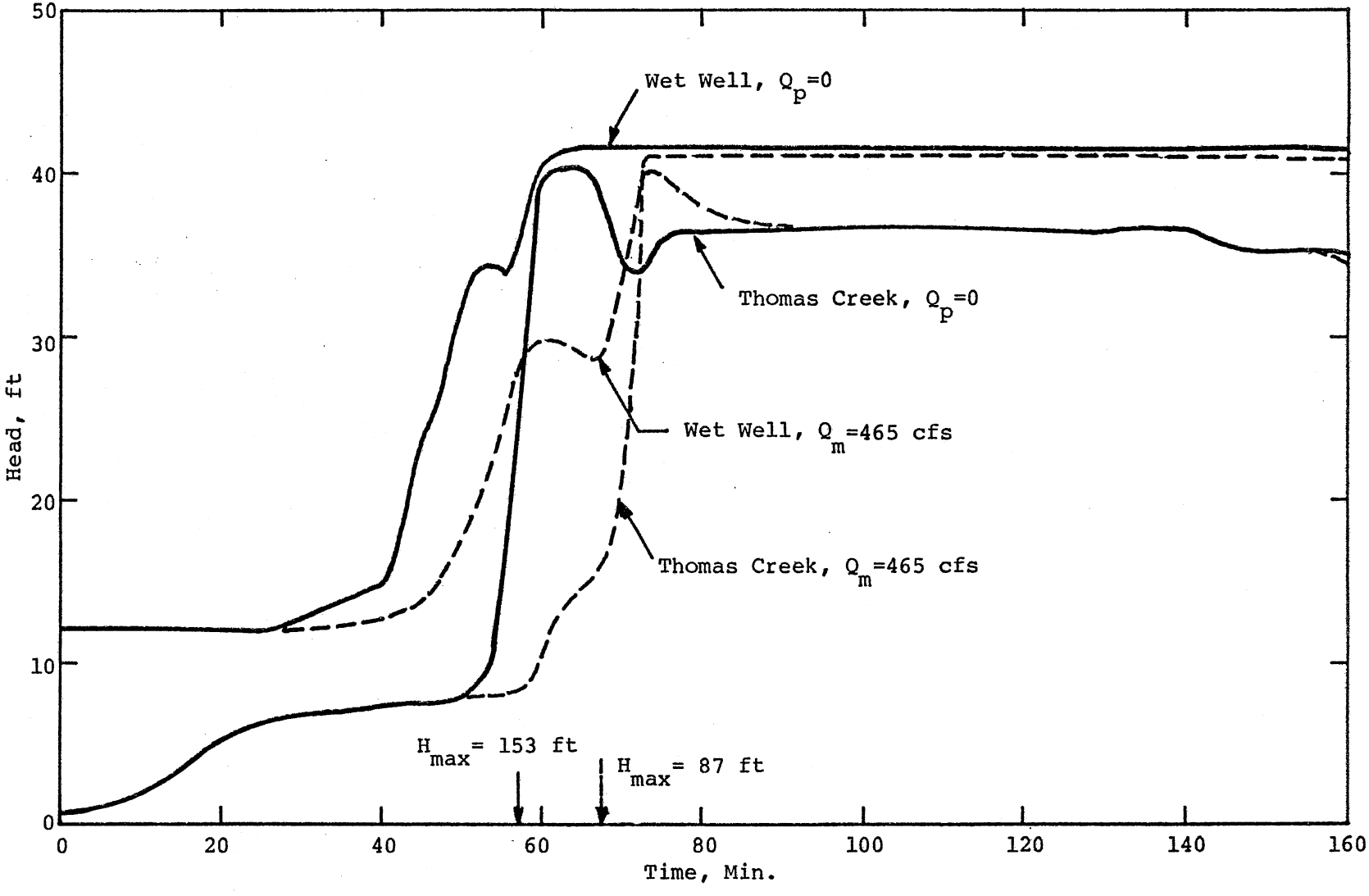

Fig. II-8. Change in Head Due to 25 Year Storm, Tunnel Initially Half Full, Runs II-8 and II-9.

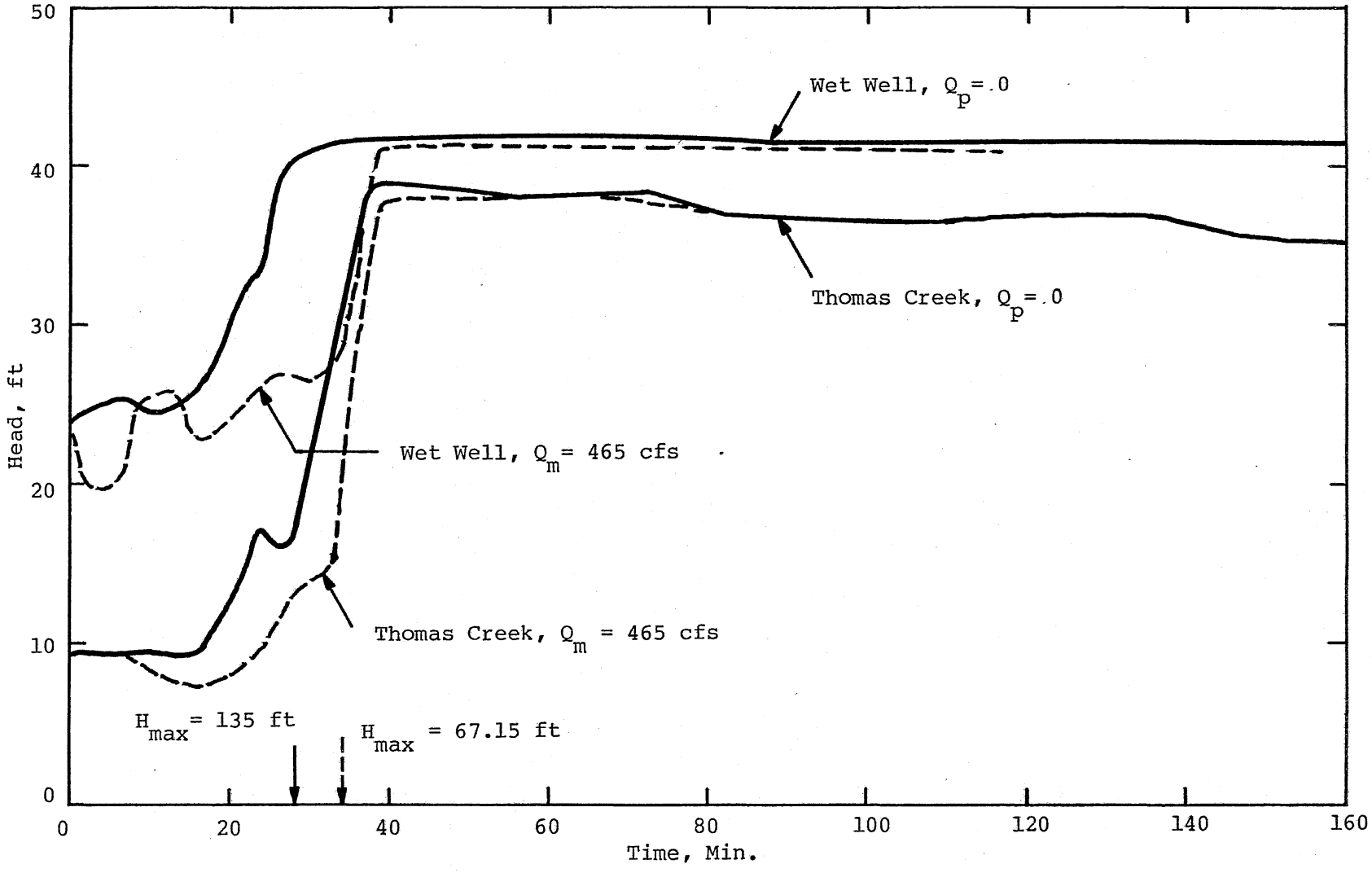

Fig. II-9. Change in Head Due to 25 Year Storm, Tunnel Initially Filled, Runs II-10 and II-11.

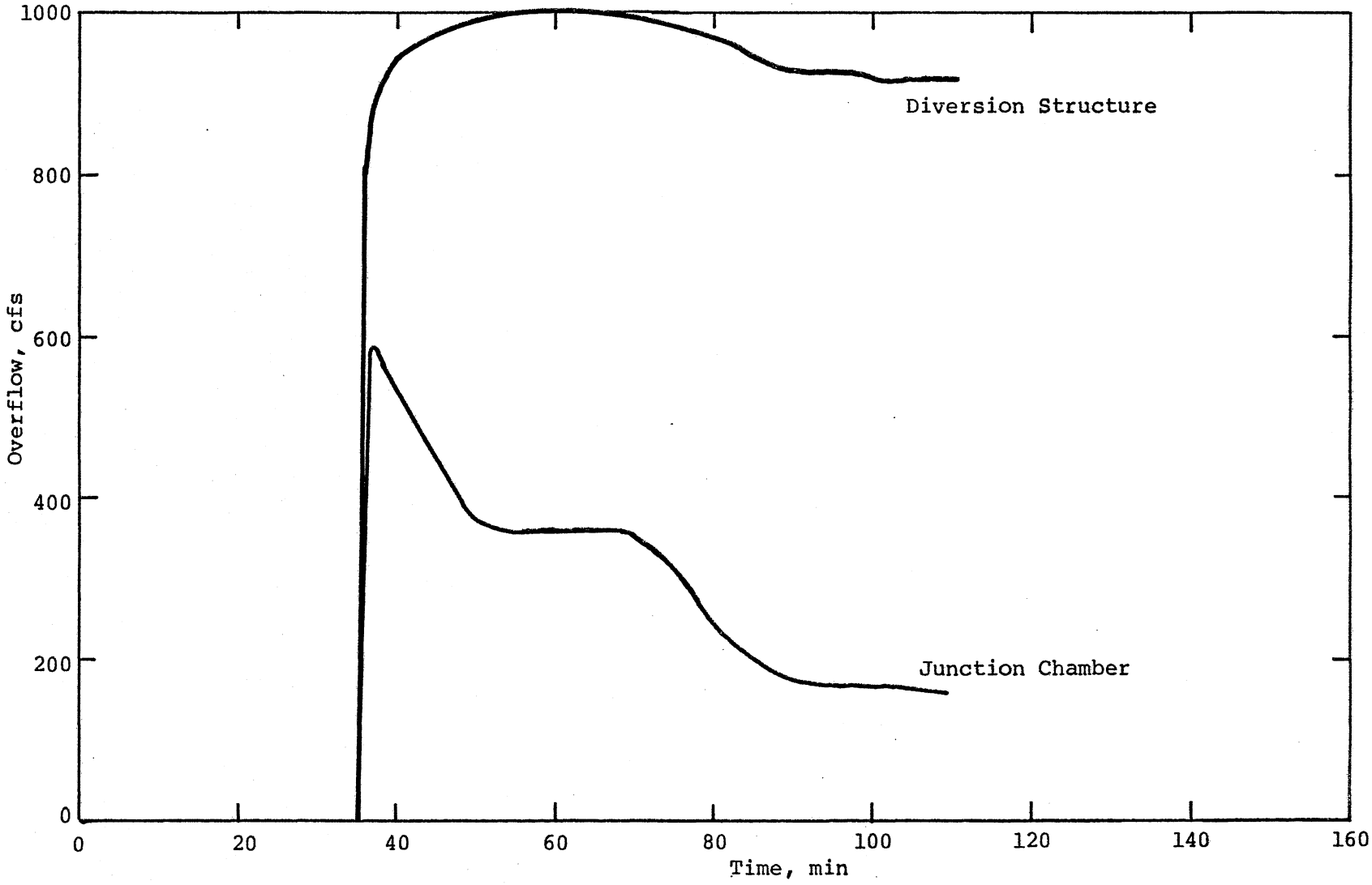

Fig. II-10. Overflow Hydrographs, 25 Year Storm, Tunnel Initially Empty, Q_m = 465 cfs, Run II-11.

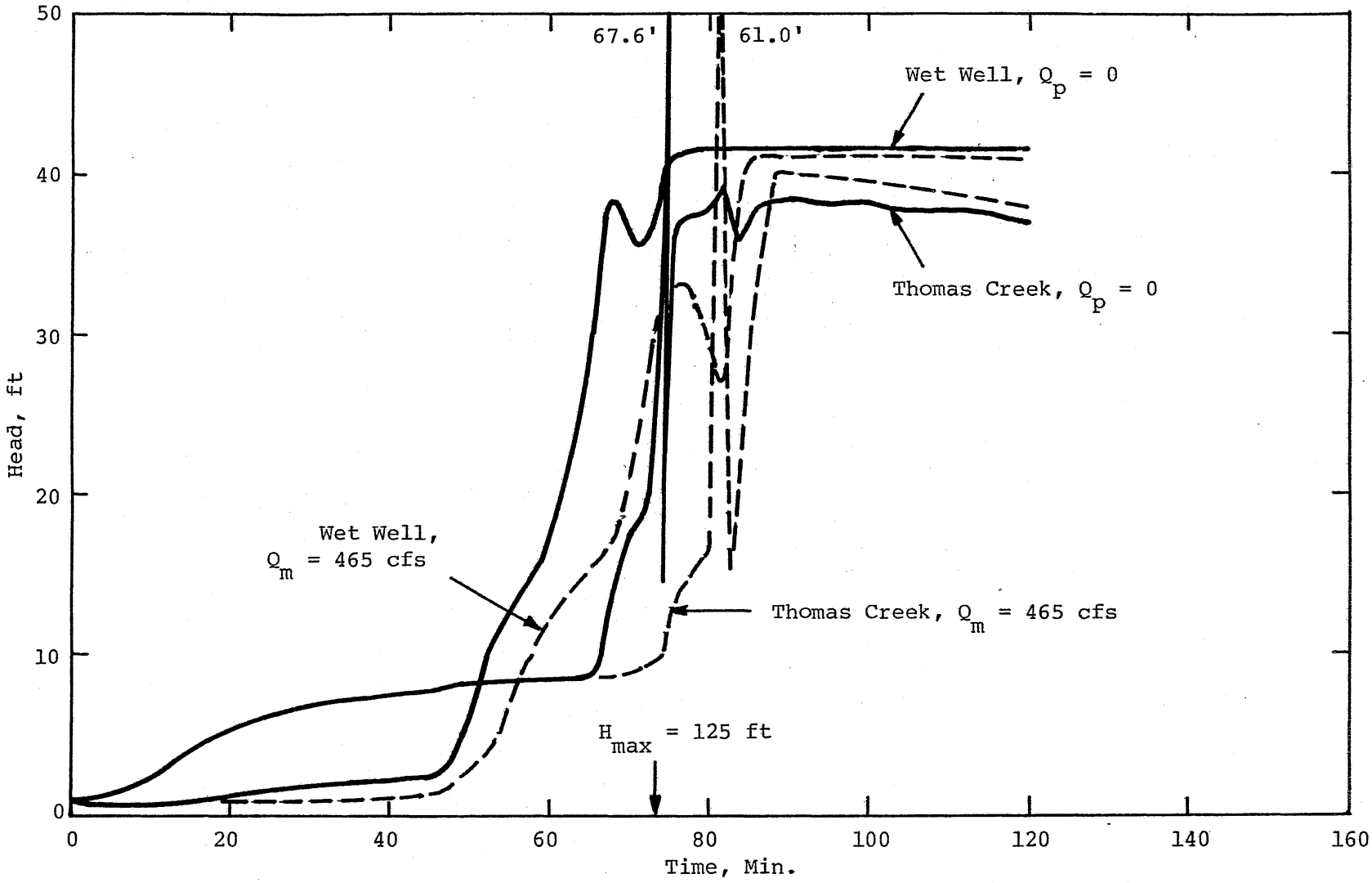

Fig. II-11. Change in Head Due to 100 Year Storm, Tunnel Initially at 1 ft, Runs II-12 and II-13.

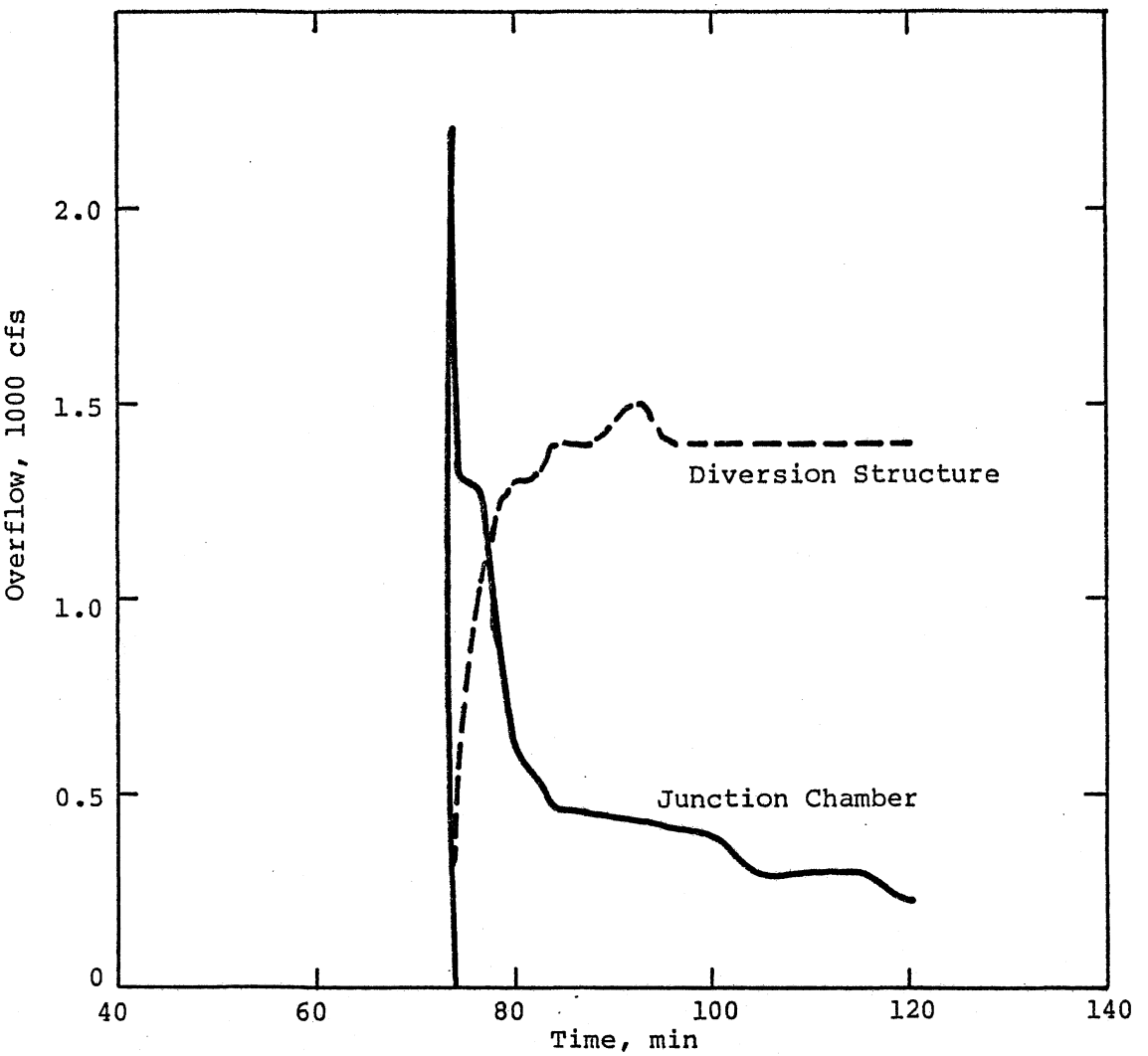

Fig. II-12. Overflow Hydrograph, 100 Year Storm, Tunnel Initially Empty, Run II-12, Q_p = 0.

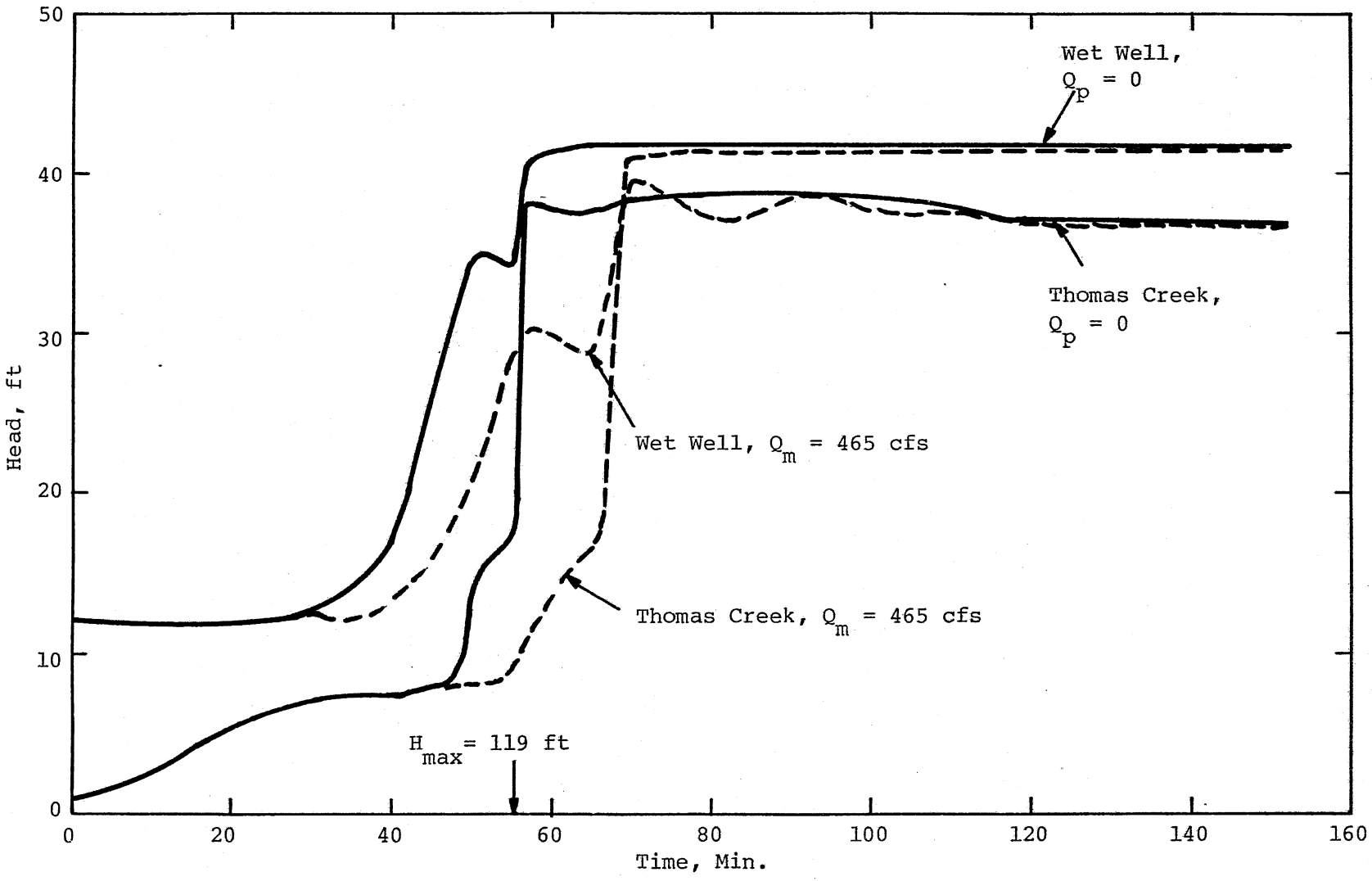

Fig. II-13. Change in Head Due to 100 Year Storm, Tunnel Initially Half Full, Runs II-14 and II-15.

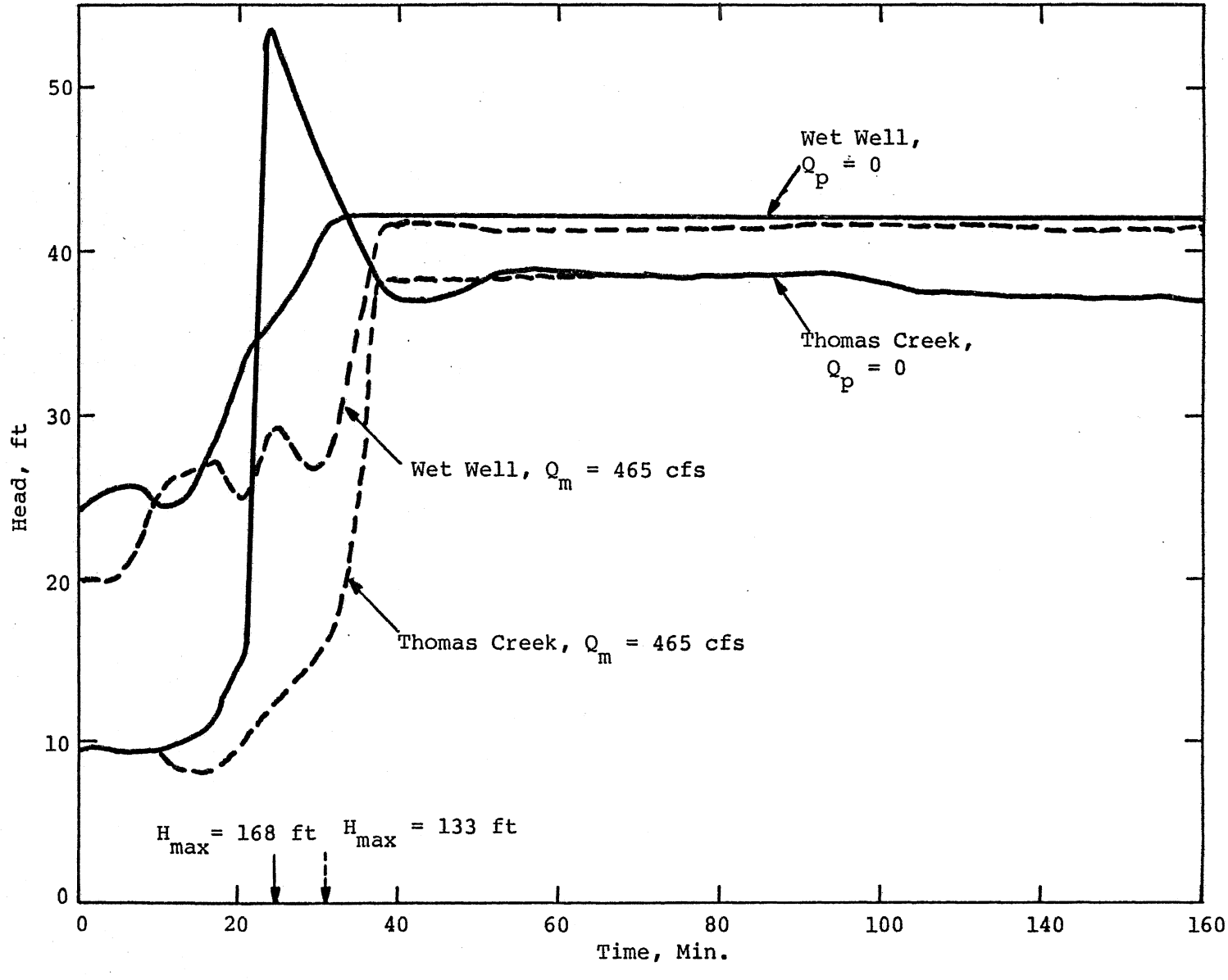

Fig. II-14. Change in Head Due to 100 Year Storm, Tunnel Initially Filled, Runs II-16 and II-17.

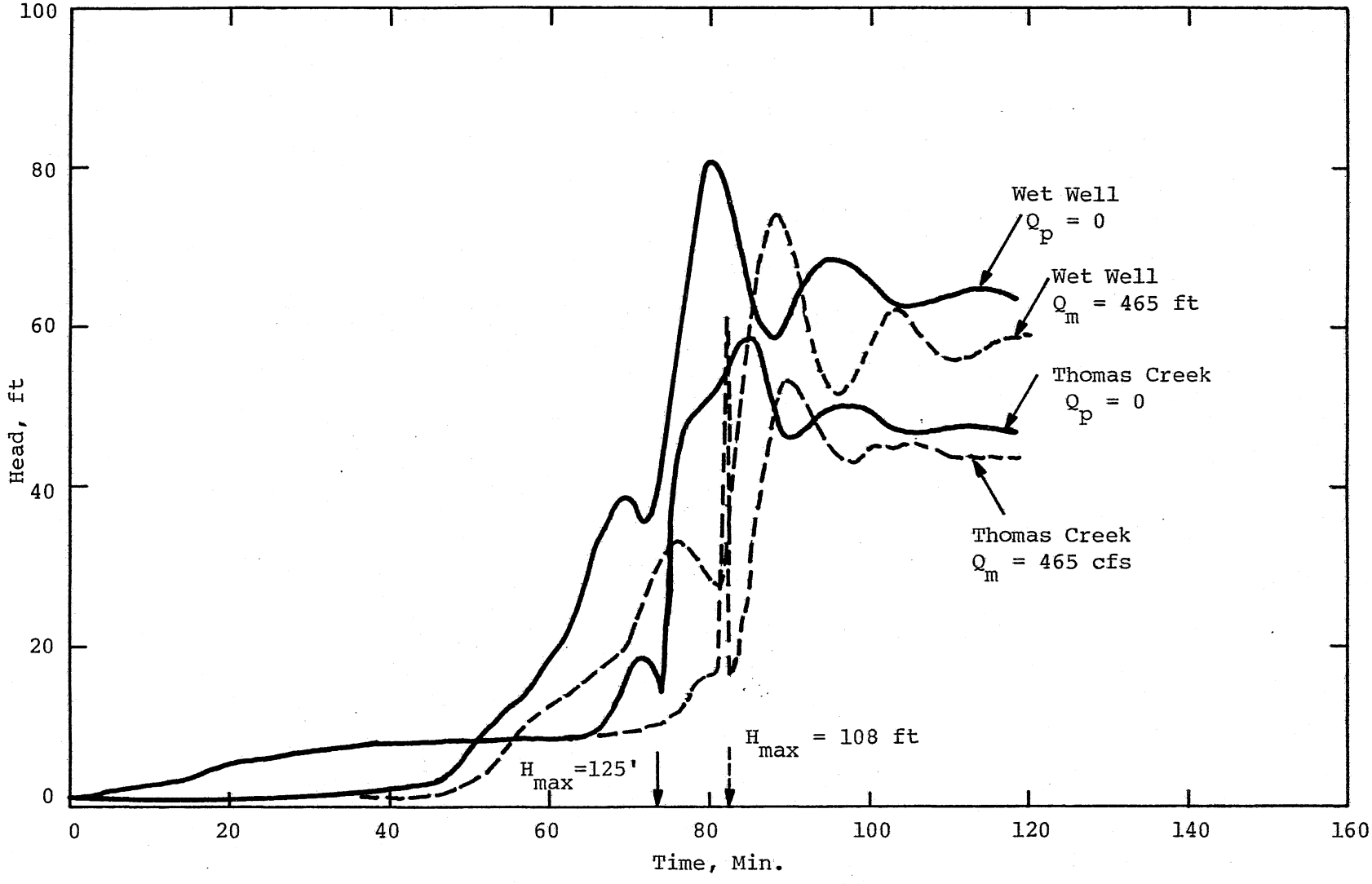

Fig. II-15. Change in Head Due to 100 Year Storm, Tunnel Initially at 1 ft, Overflow Weir at 90 ft, Runs II-18 and II-19.

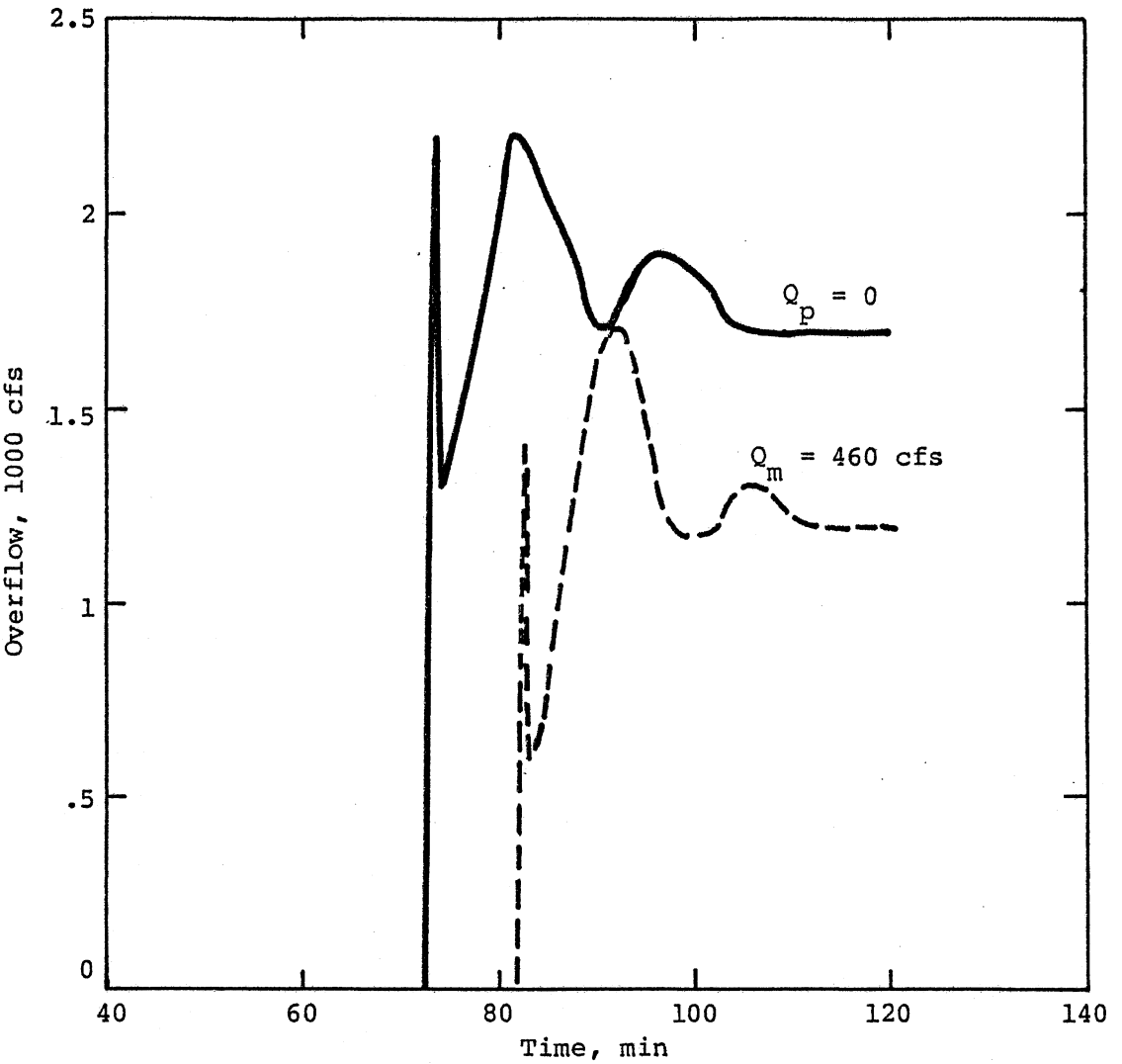

Fig. II-16. Overflow Hydrograph at Junction Chamber, 100 Year Storm, Tunnel Initially Empty, Runs II-18 and II-19.

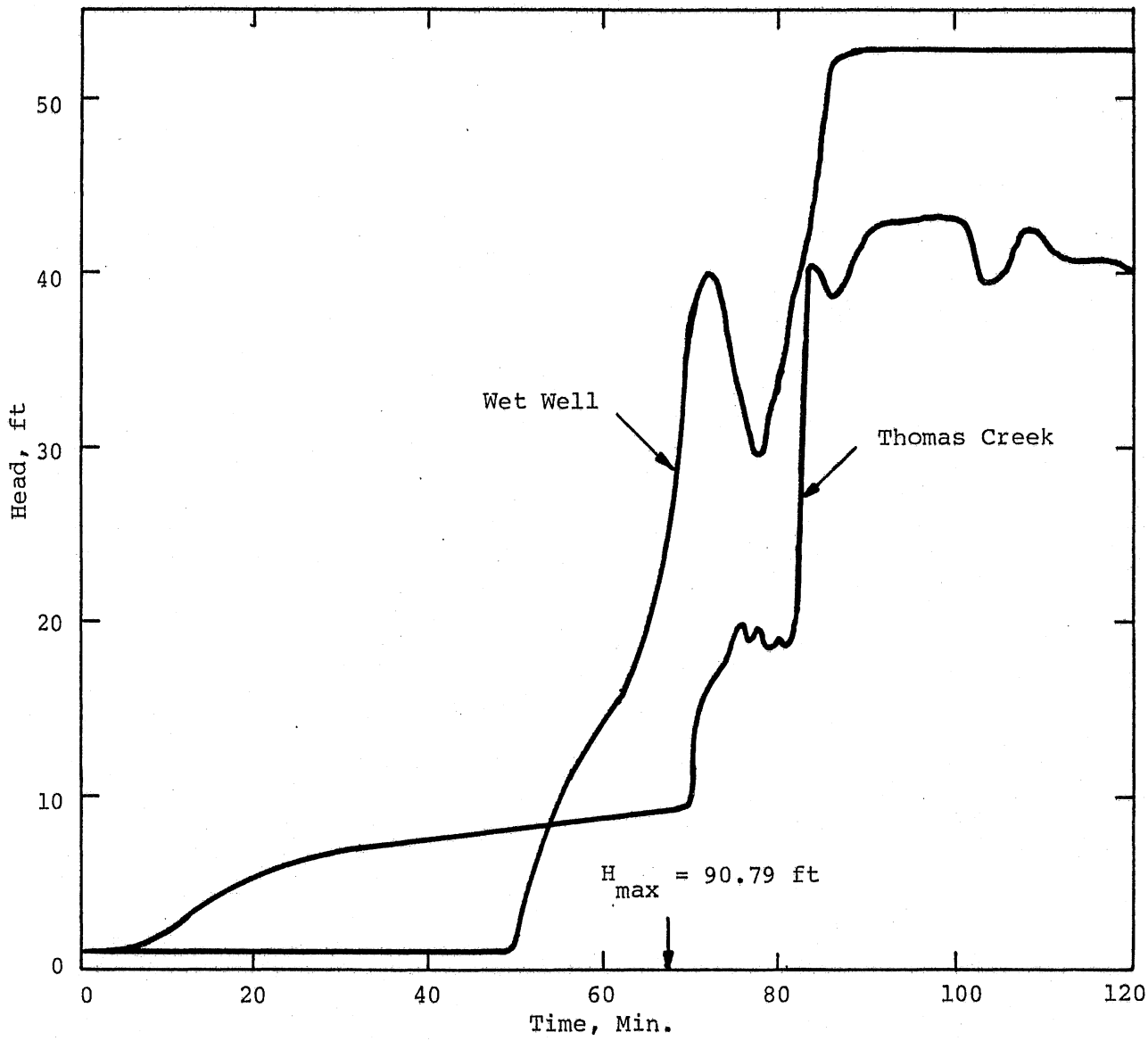

Fig. II-17. Change in Head Due to 100 Year, 1 Hour Storm, Flap Gate Removed, Overflow Weir at 51 ft, Run II-20.

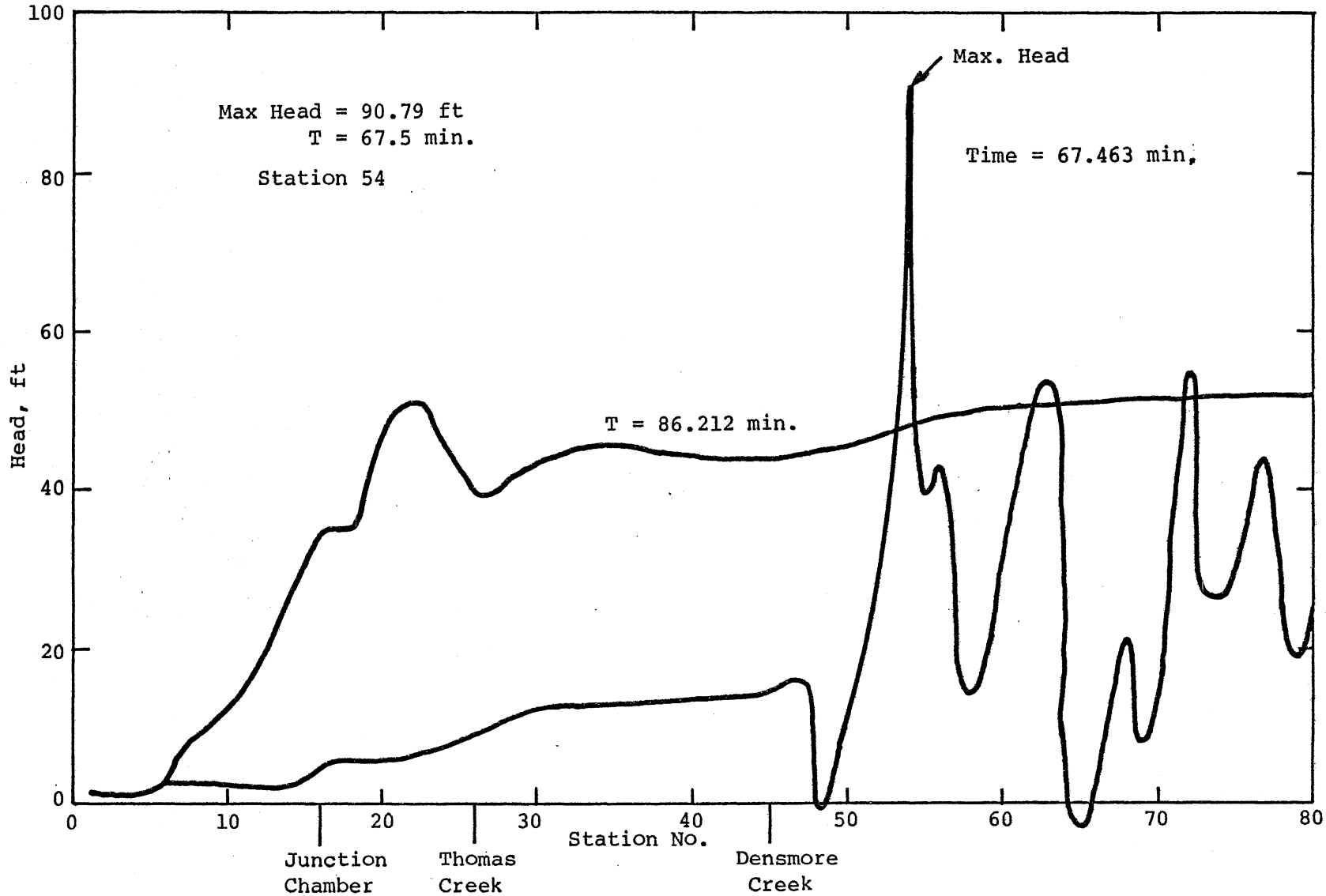

Fig. II-18. Pressure Head Distribution, 100 Year Storm, Flap Gate Removed, Overflow Weir at 51 ft, Run II-20.

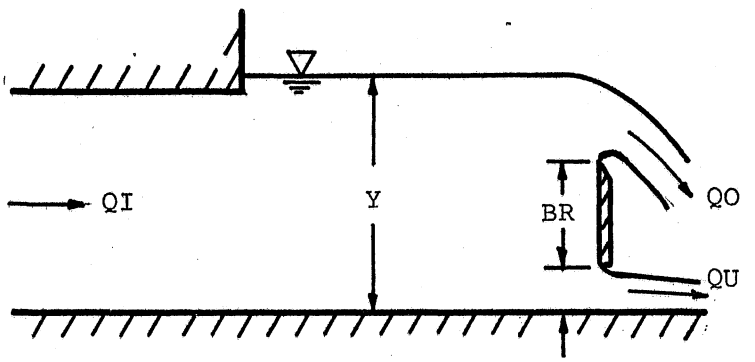

(a) Section view through roller gate

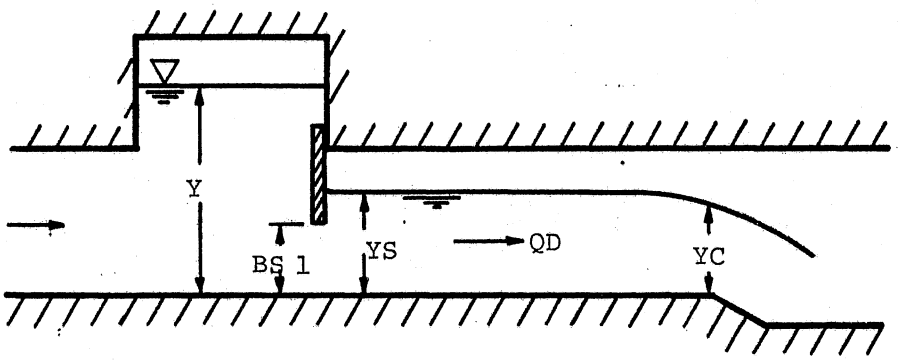

(b) Section view through sluice gates

Fig. III-1. Schematic Representation of the Control Structures.

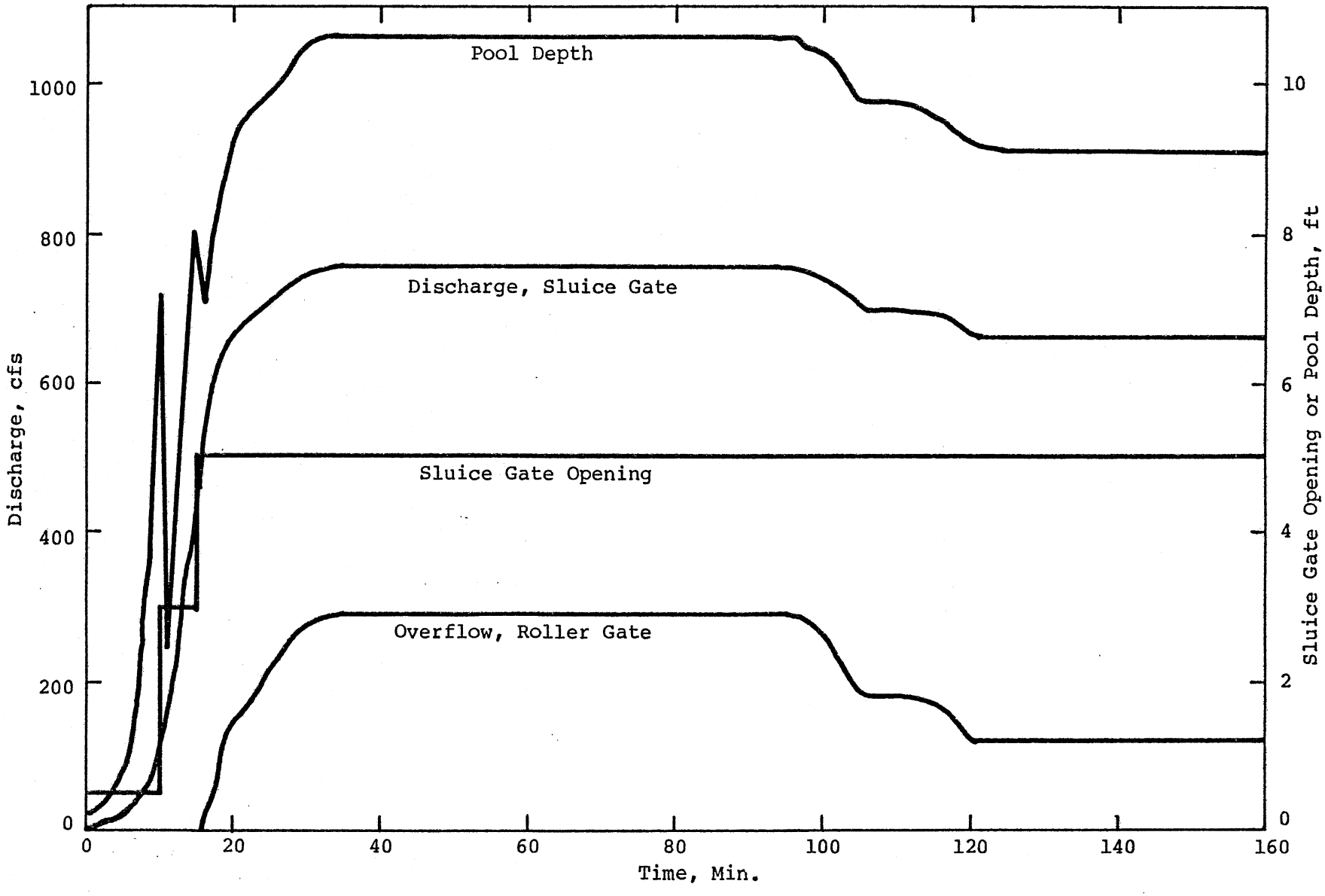

Fig. III-2. Flow at Thomas Creek, Gate Change in Steps to 2.5 ft and 5.0 ft, According to Inflow.

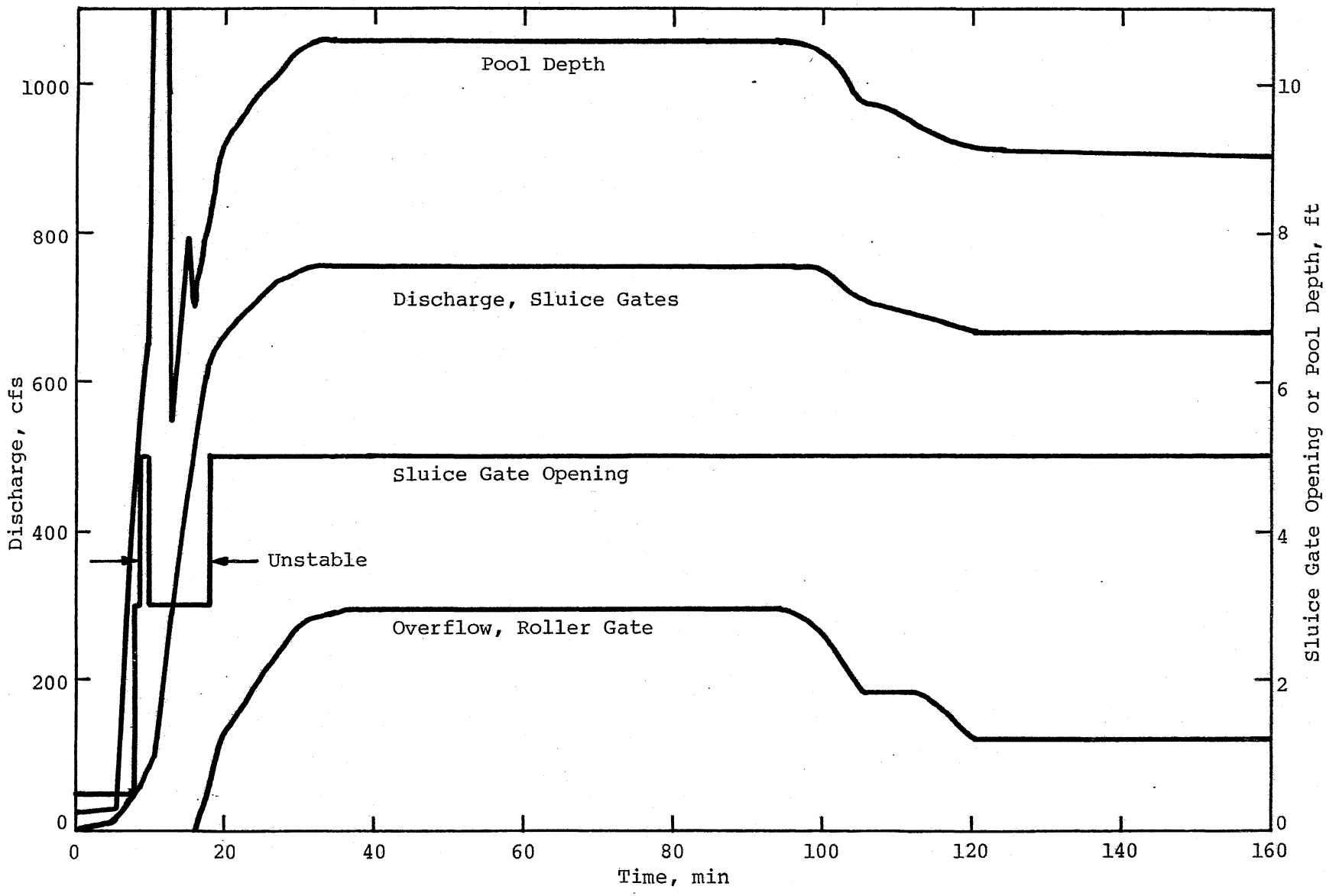

Fig. III-3. Flow at Thomas Creek, Gate Change at Steps to 2.5 ft and 5.0 ft, According to Pool Depth.

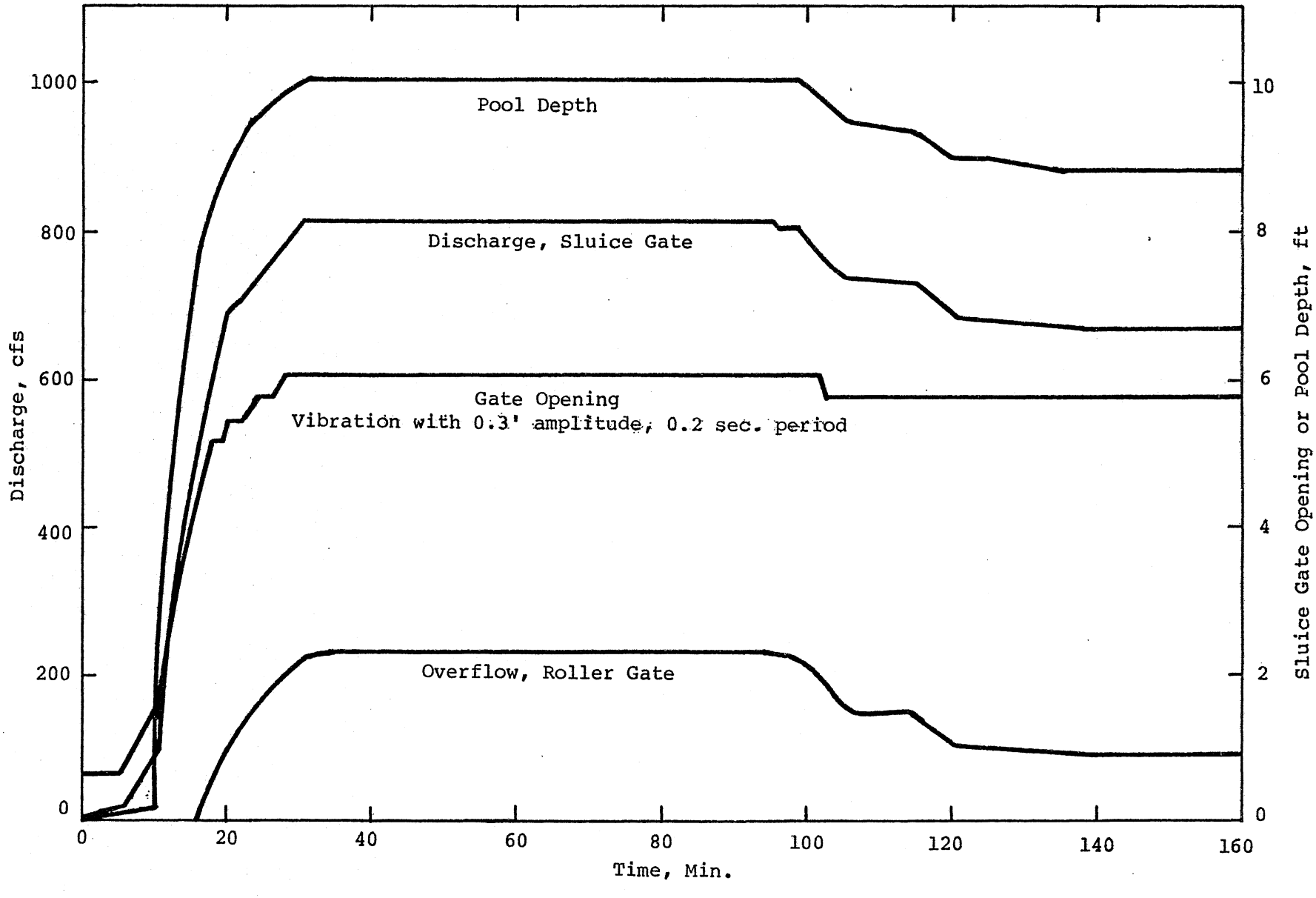

Fig.III-4. Flow at Thomas Creek, Gate Speed 3 fps, Continuously According to Pool Depth.

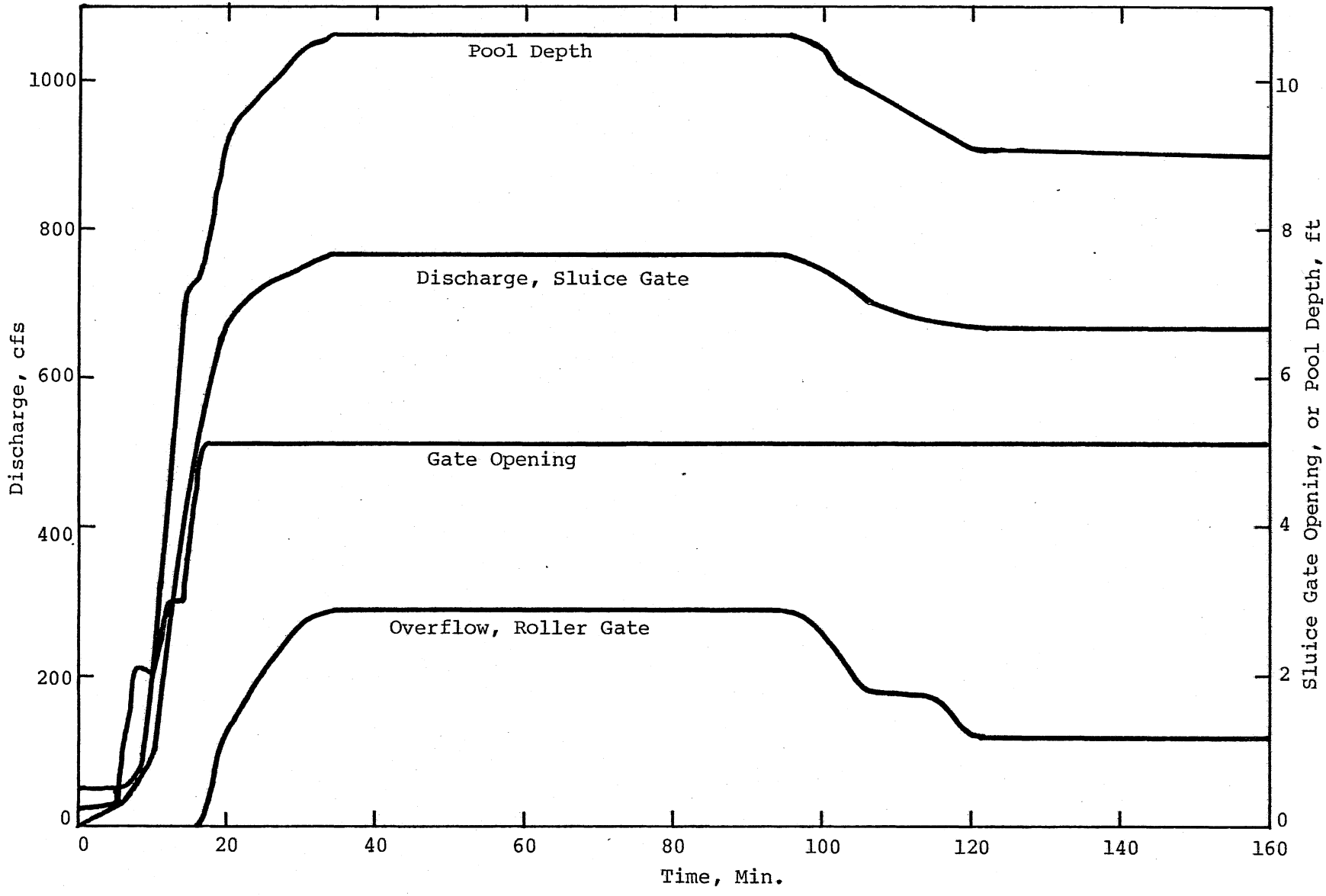

Fig. III-5. Flow at Thomas Creek, Gate Speed 0.5 ft/min, According to Pool Depth.

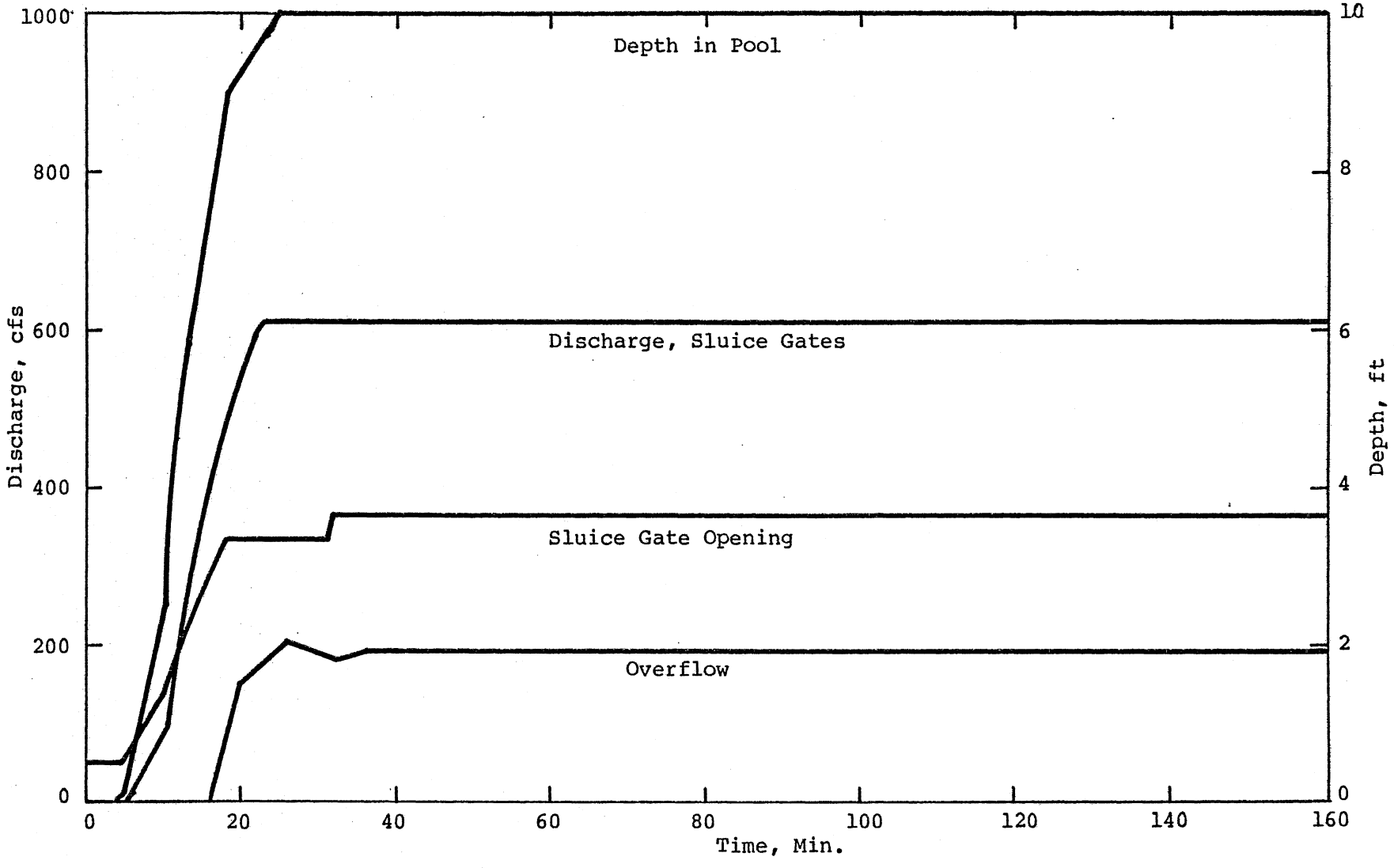

Fig. III-6. Flow at Densmore Control Structure, Outflow Limited to 600 cfs.

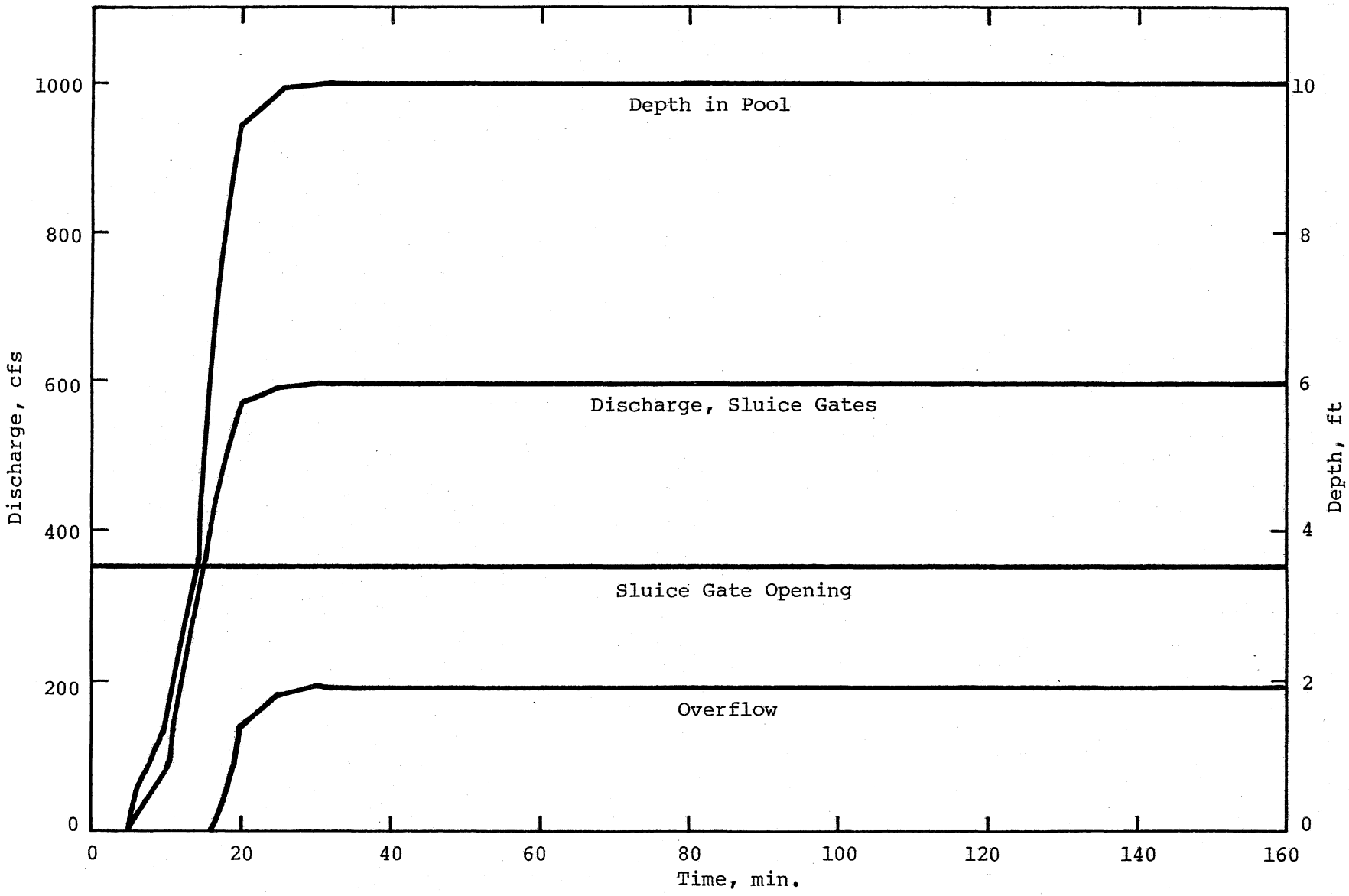

Fig. III-7. Flow at Densmore Control Structure, 100 Year Storm, Gate Opening Constant at 3½ ft.

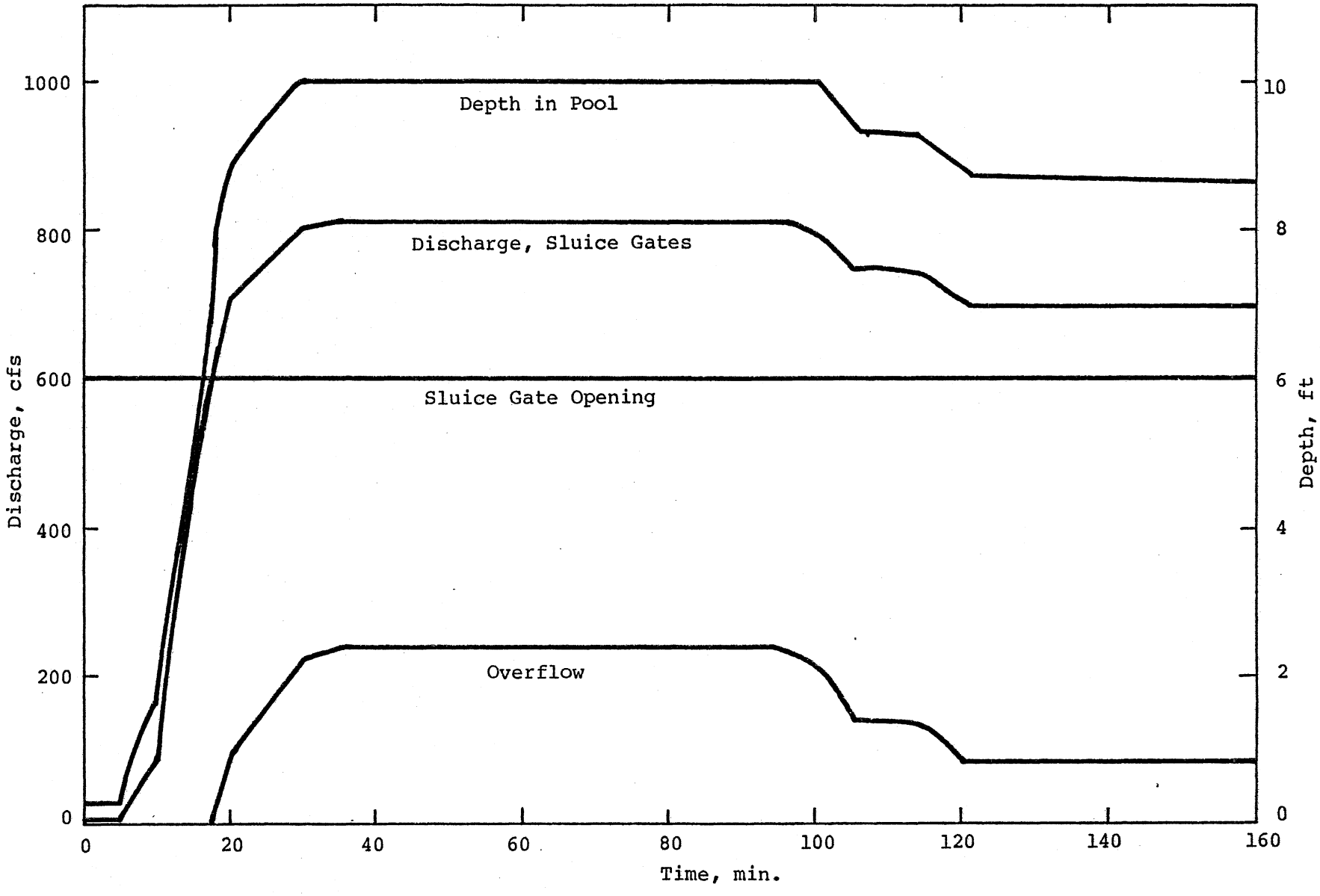

Fig. III-8. Flow at Thomas Creek, 100 Year Storm, Gate Opening Constant at 6 ft.

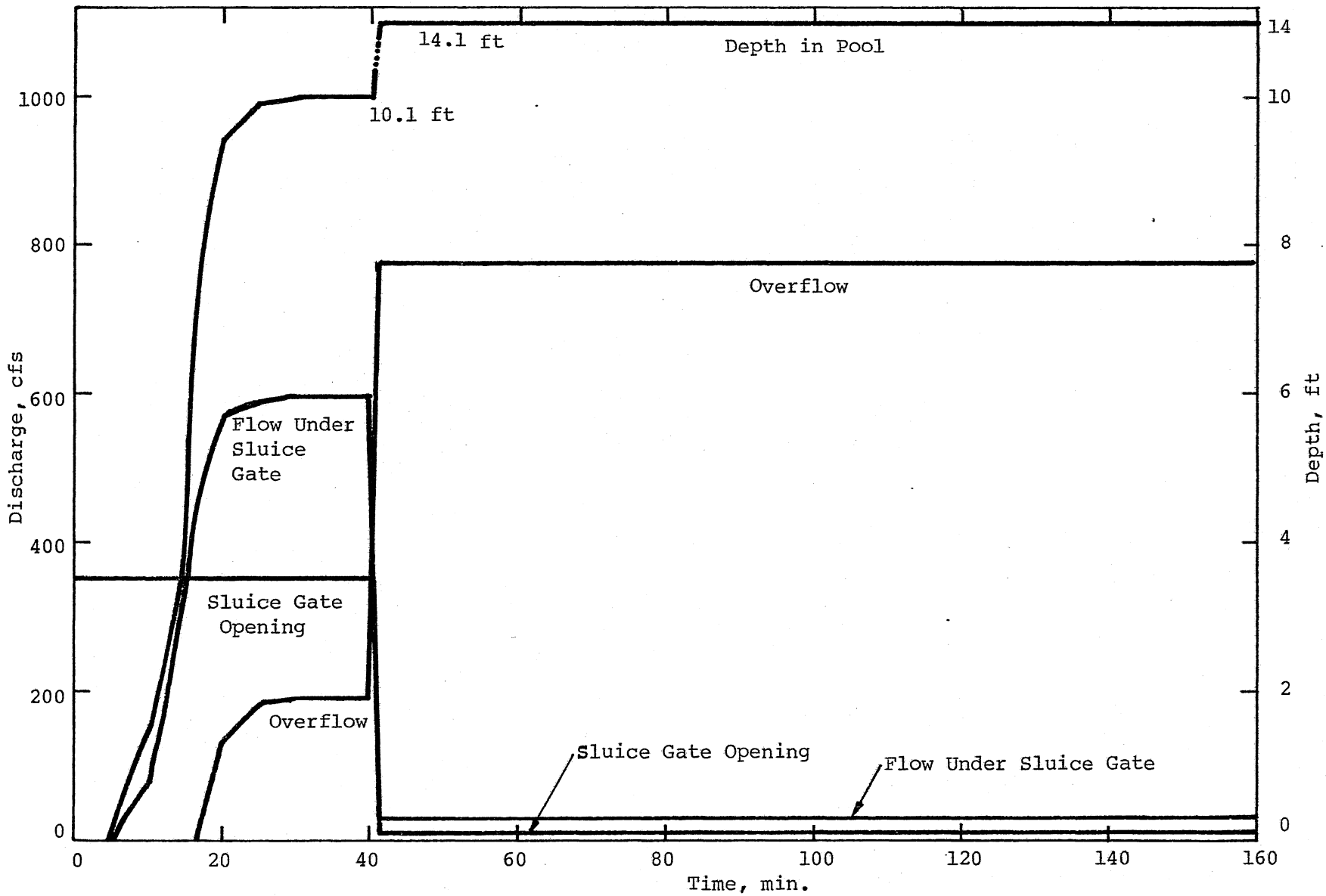

Fig. III-9. Flow at Densmore Creek, 100 Year Storm, Gate Closed at 3 fpm During Peak Inflow.

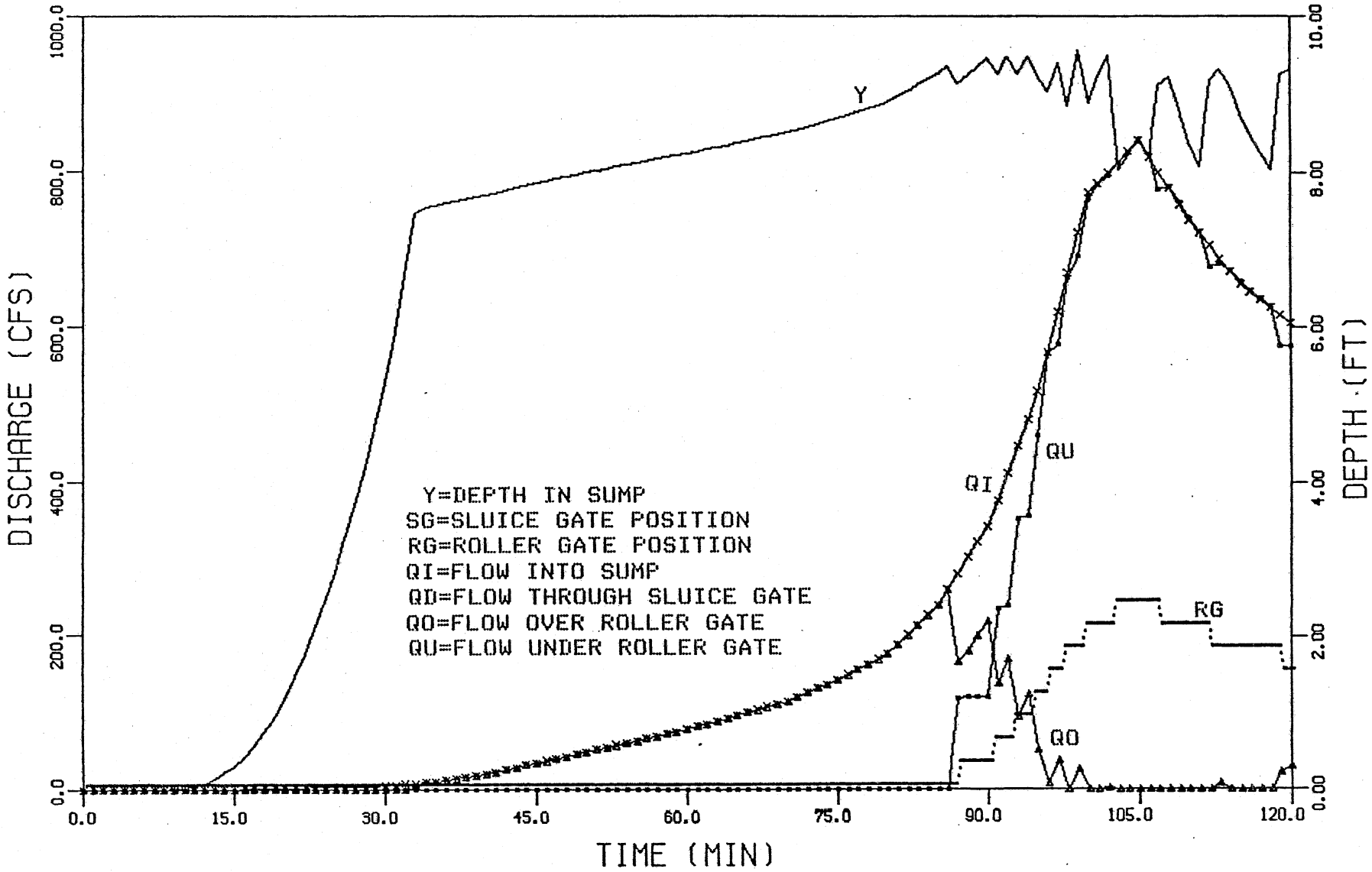

Fig. III-12. Flow at Densmore Control Structure with Roller Gate Control, Run III-11.

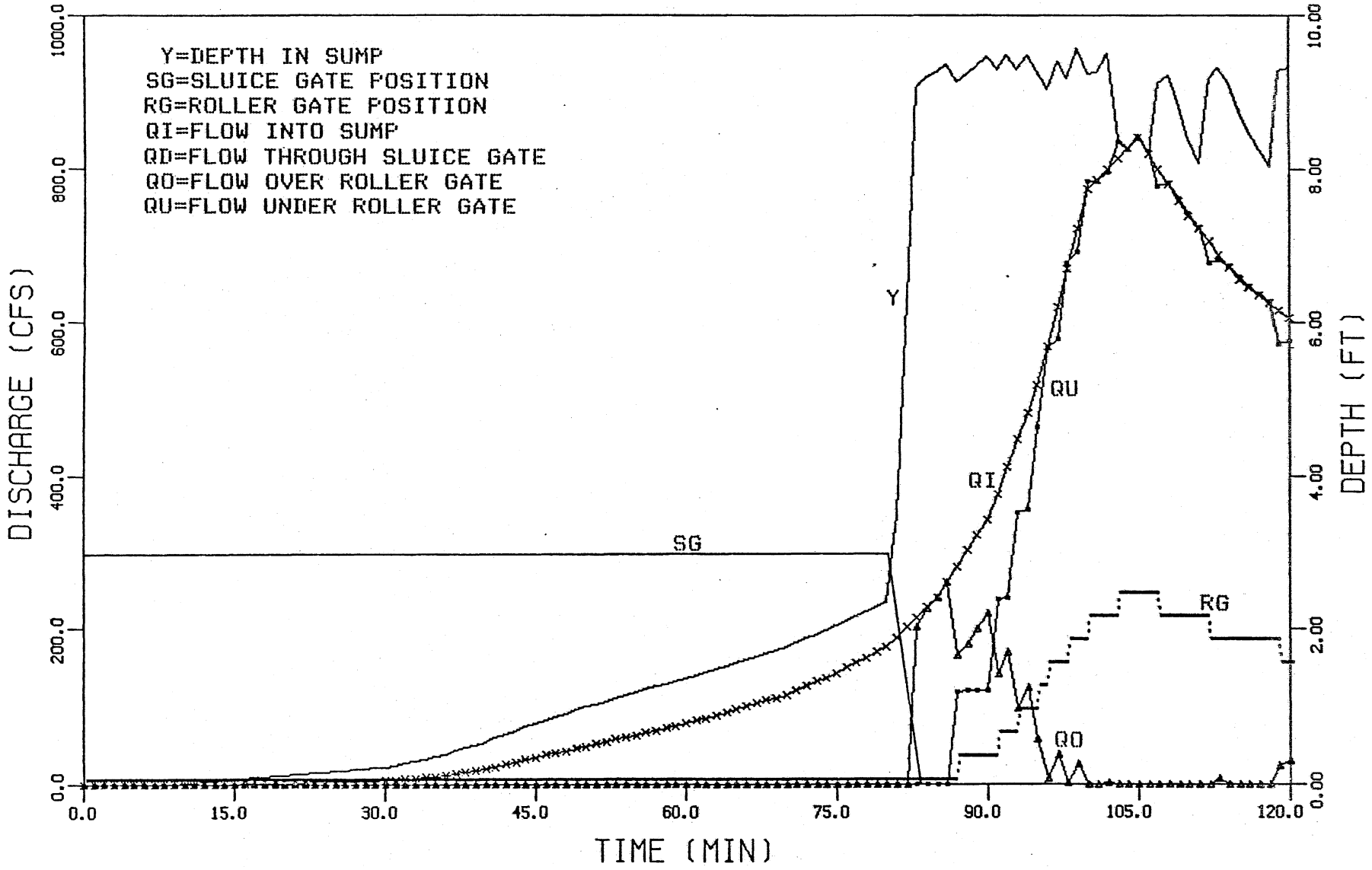

Fig. III-13. Flow at Densmore Control Structure with Roller Gate Control, Run III-12.

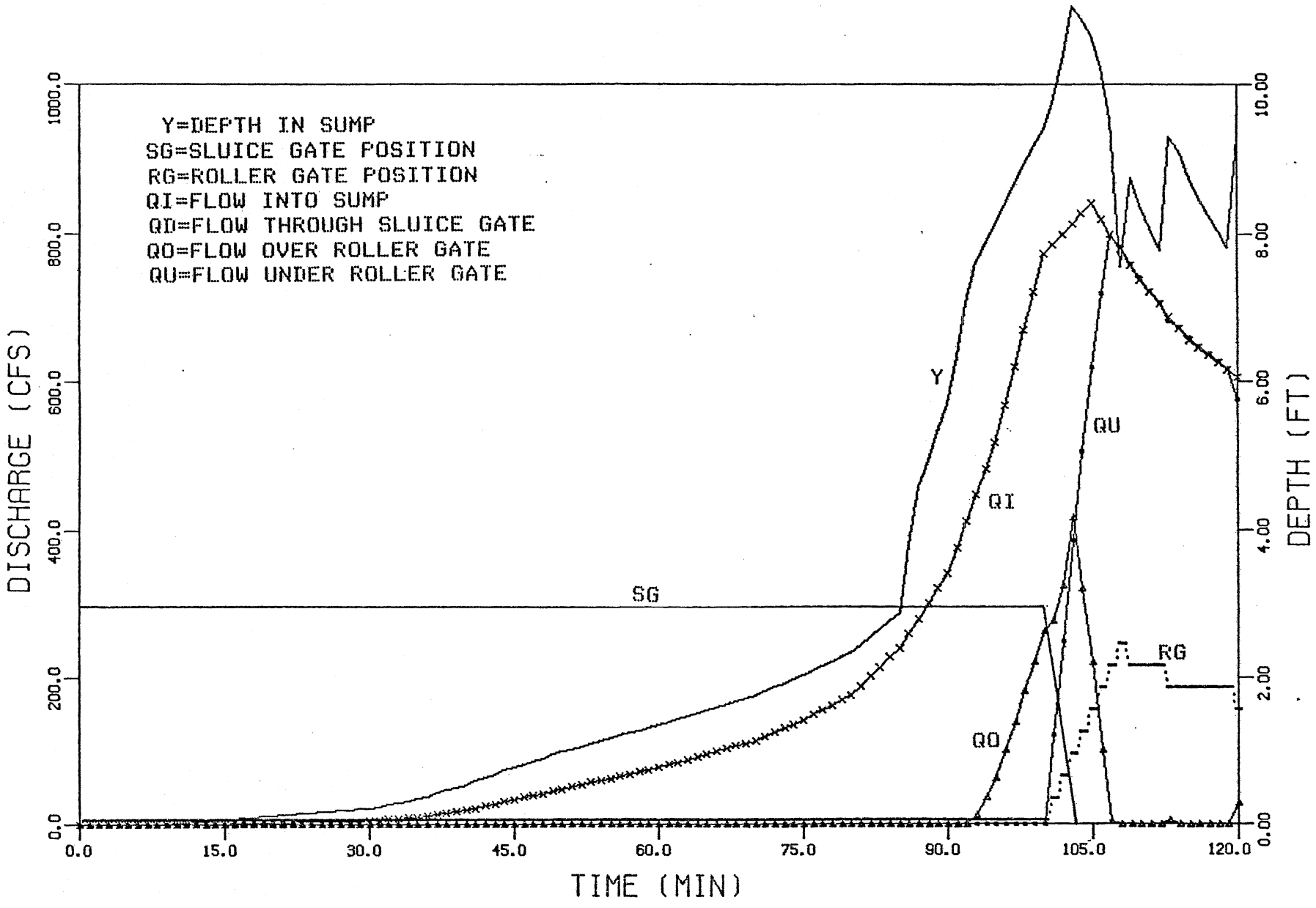

Fig. III-14. Flow at Densmore Control Structure with Roller Gate Control, Run III-13.

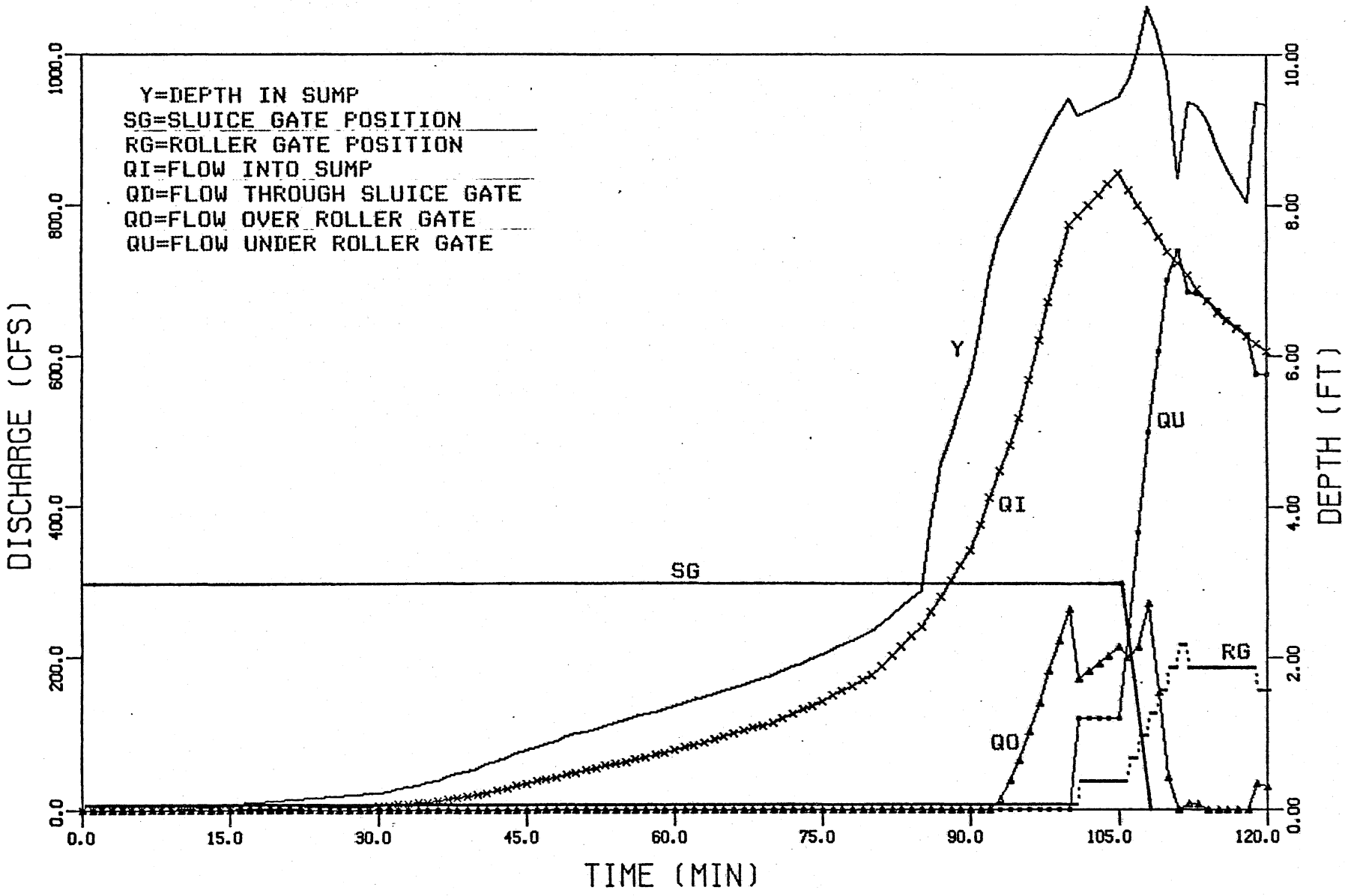

Fig. III-15. Flow at Densmore Control Structure with Roller Gate Control, Run III-14.

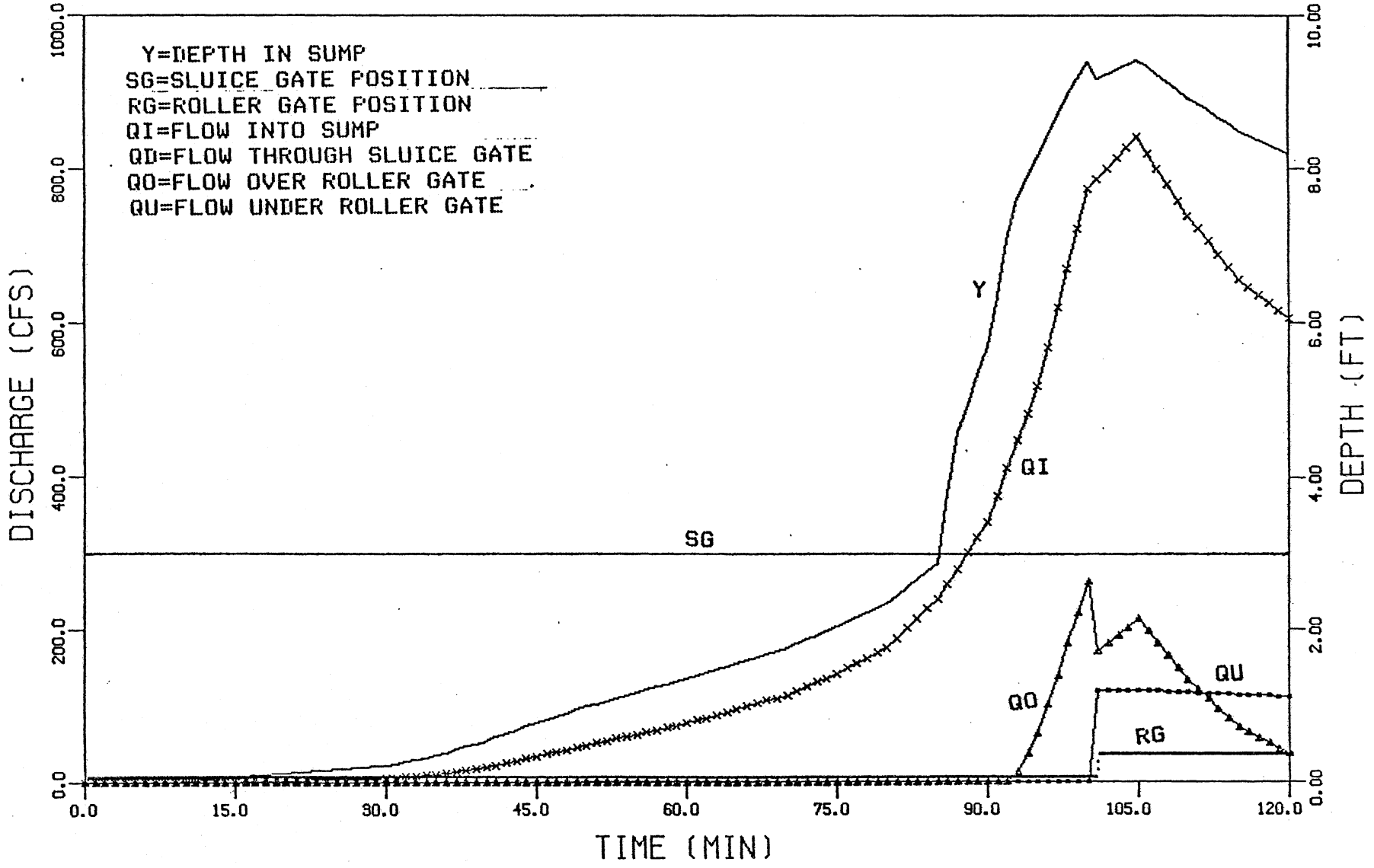

Fig. III-16. Flow at Densmore Control Structure with Roller Gate Control, Run III-15.

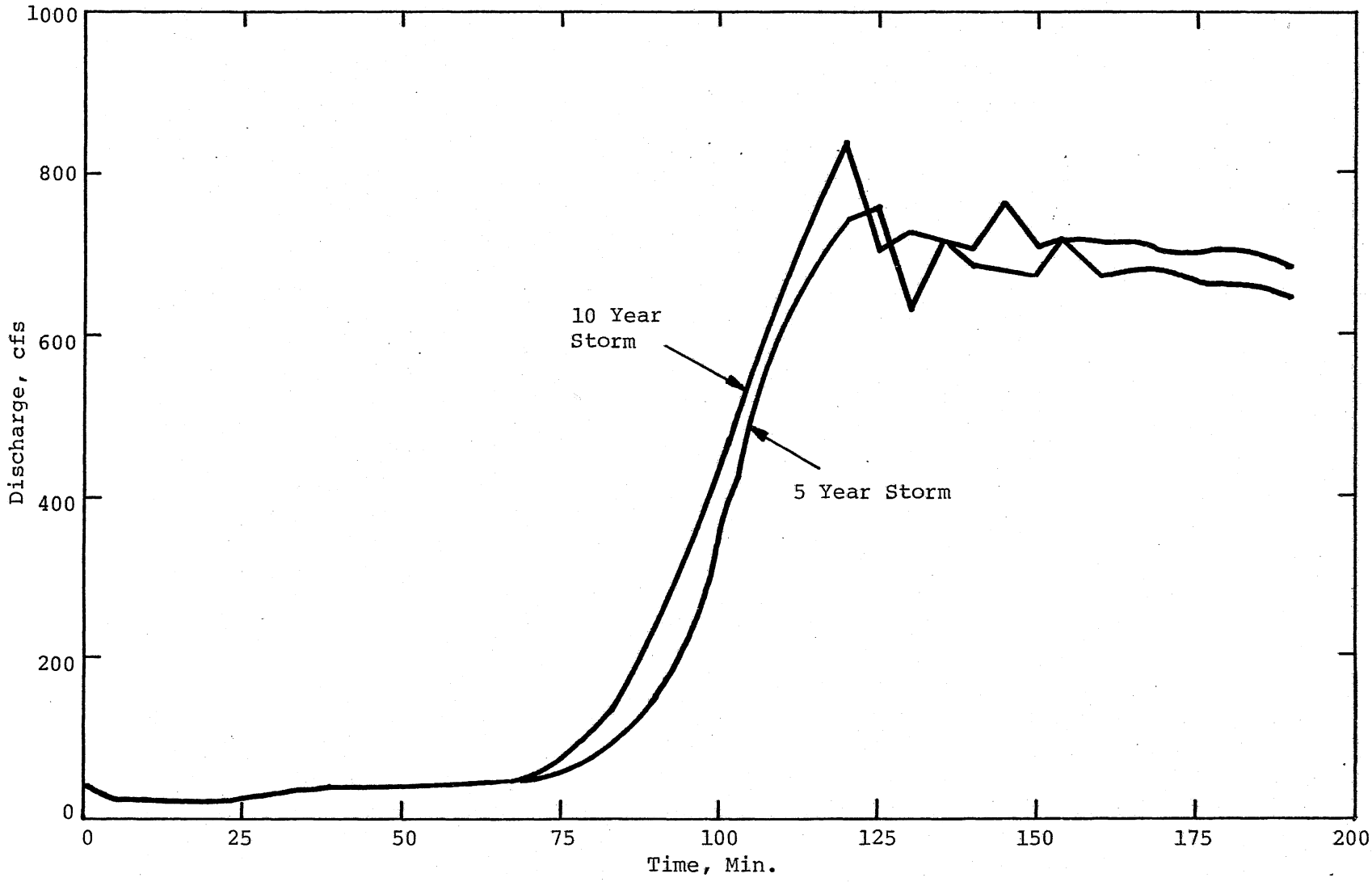

Fig. IV-1. Outflow from Culver-Goodman Tunnel.

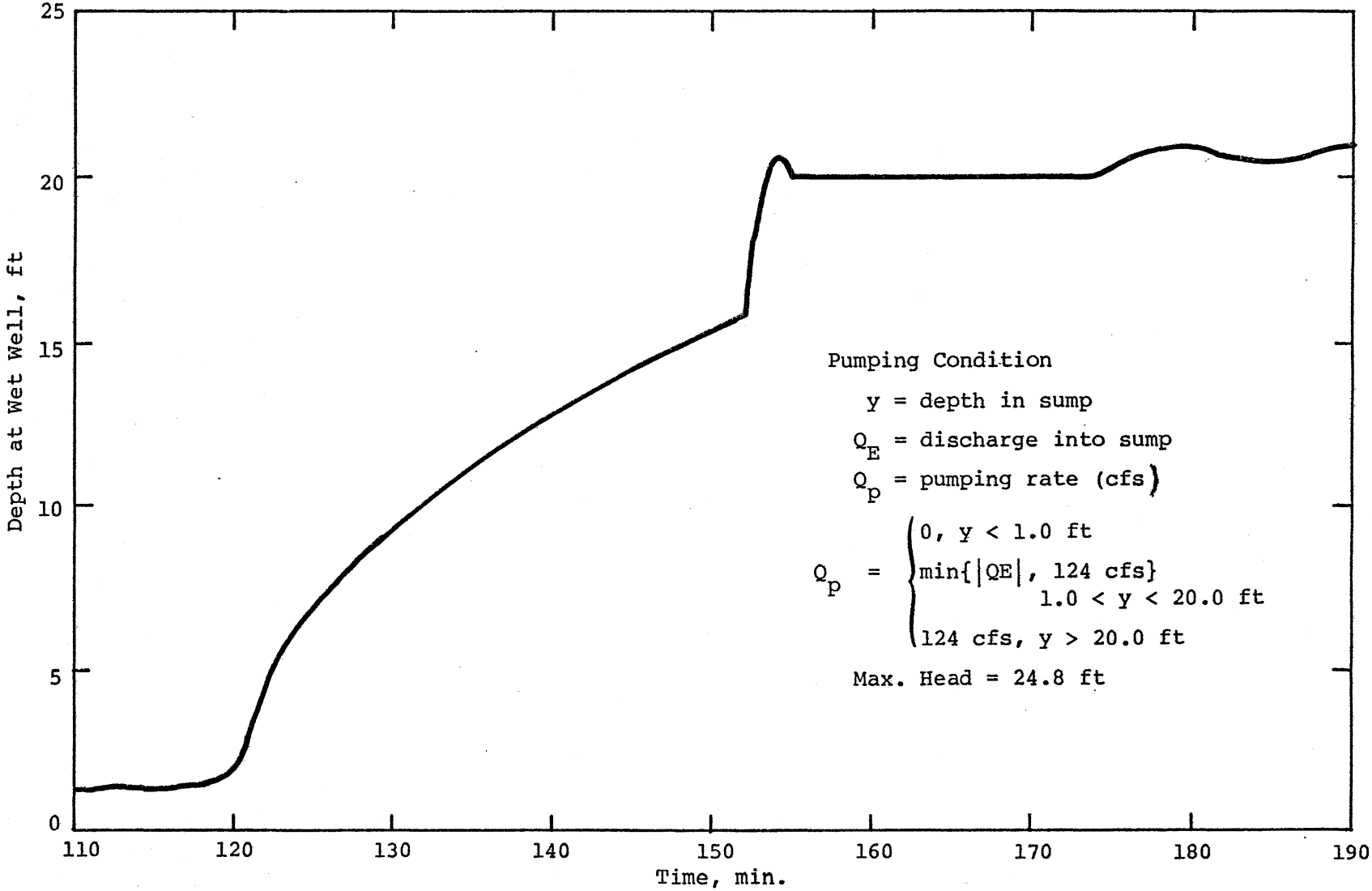

Fig. IV-2. Depth at Pump Station, 5 Year Storm, Inflow from Culver-Goodman Tunnel Unlimited, Maximum Pumping Rate 124 cfs.

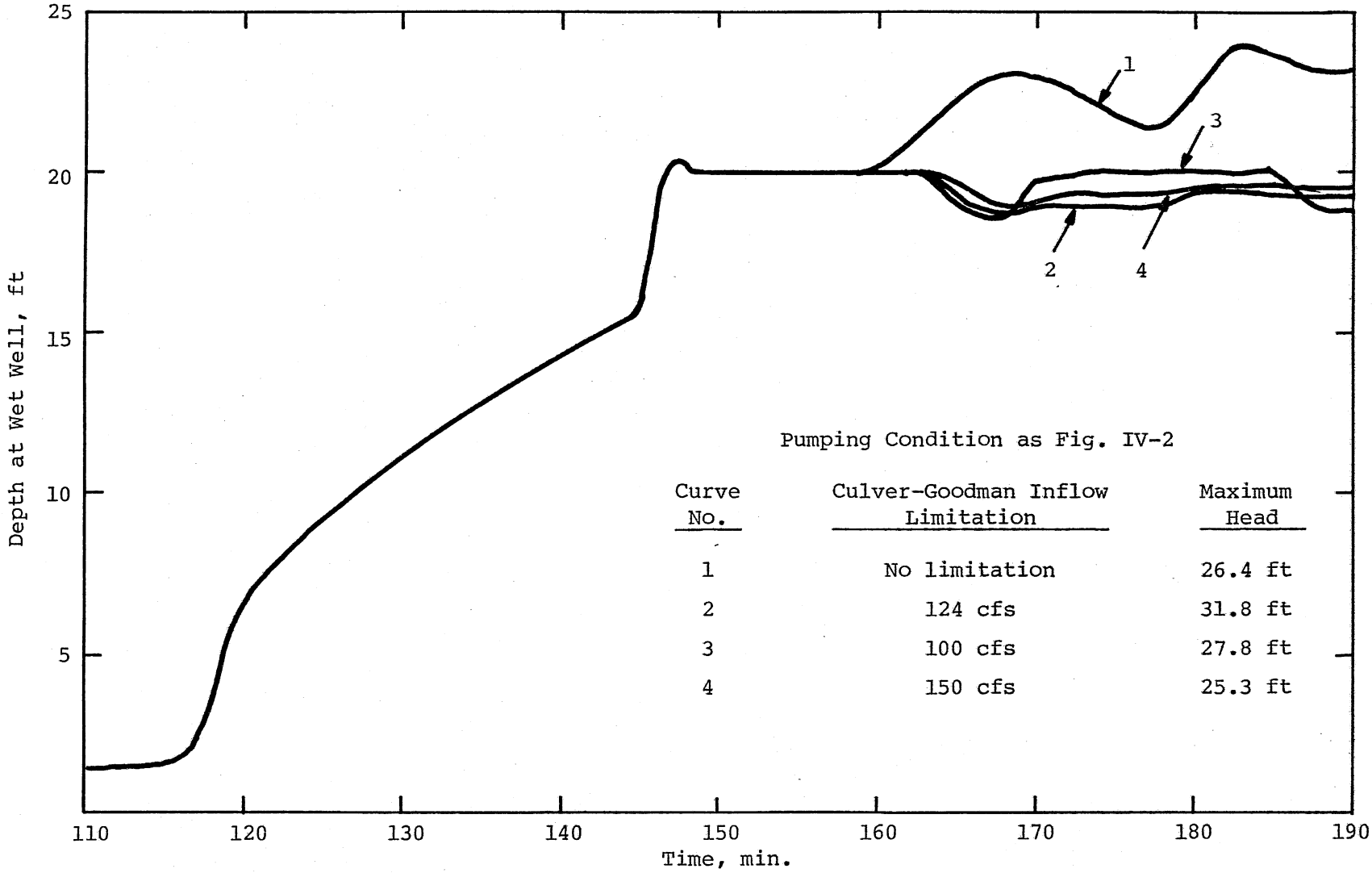

Fig. IV-3. Depth at Pump Station, 10 Year Storm, Maximum Pumping Rate 124 cfs.

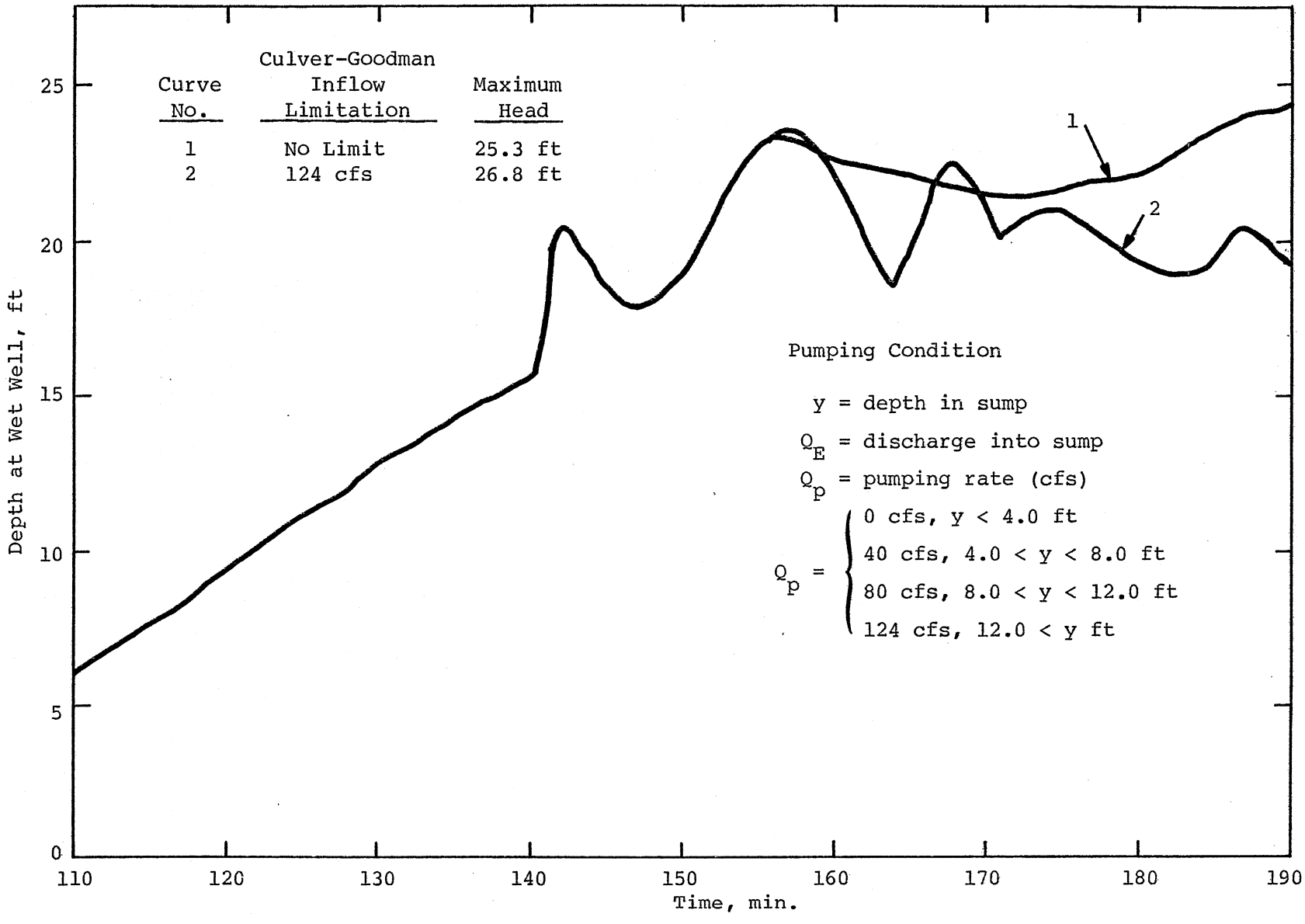

Fig. IV-4. Depth at Pump Station, 10 Year Storm, Pumping Rate Determined by Depth at Pump Station

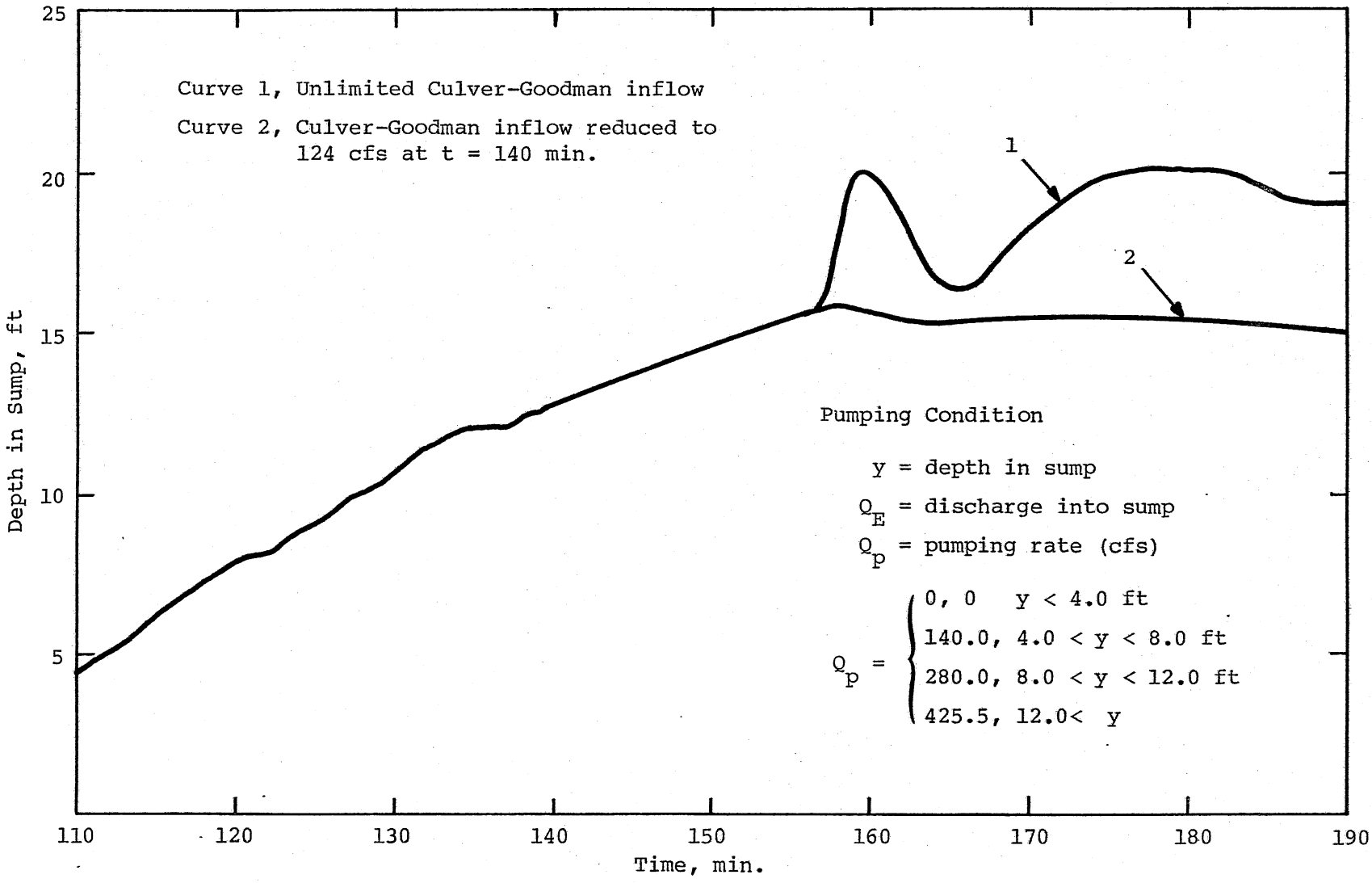

Fig. IV-5. Depth at Pump Station, 10 Year Storm, Maximum Pumping Rate 425.5 cfs.

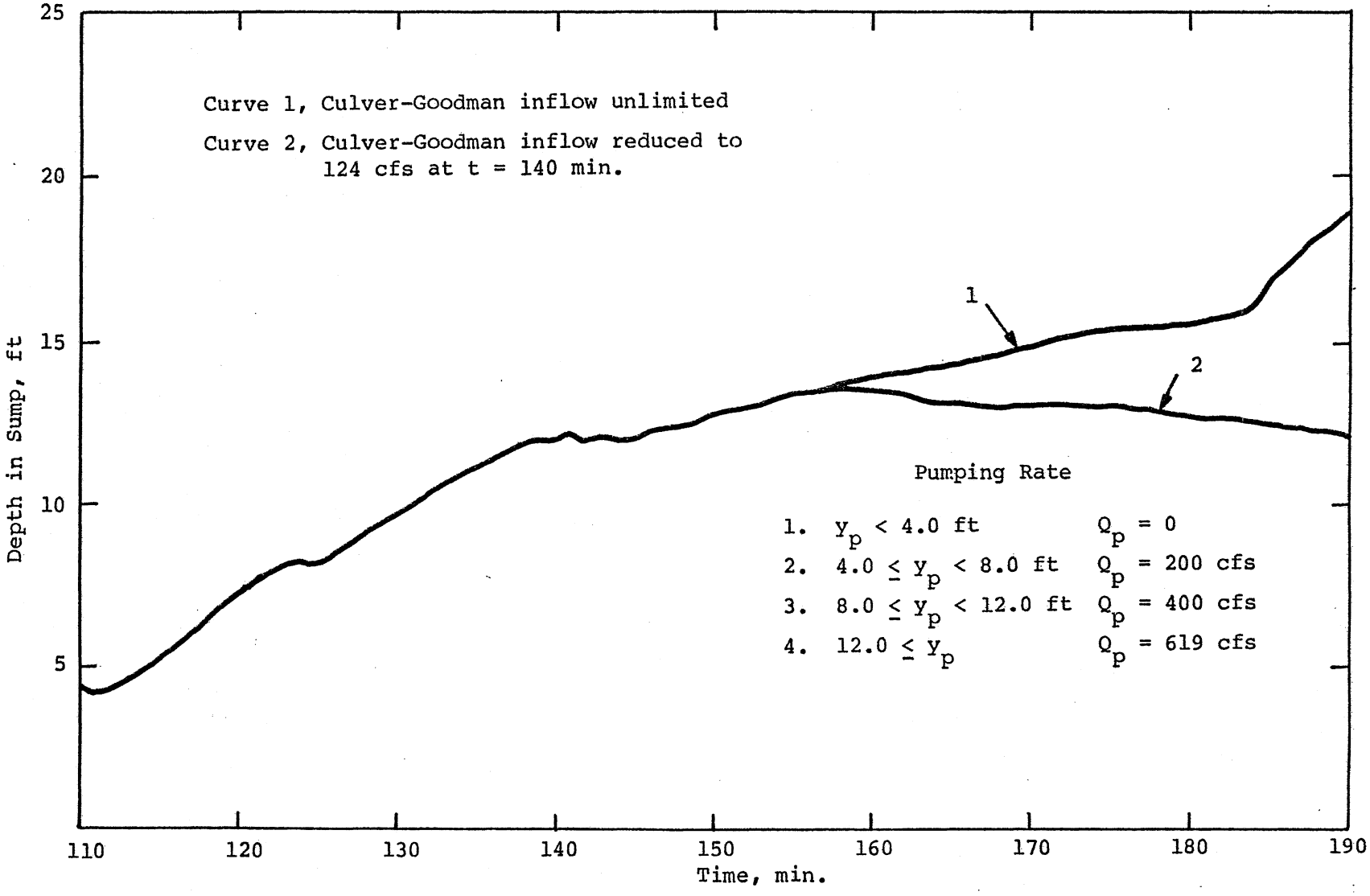

Fig. IV-6. Depth at Pump Station, 10 Year Storm, Maximum Pumping Rate 619 cfs.

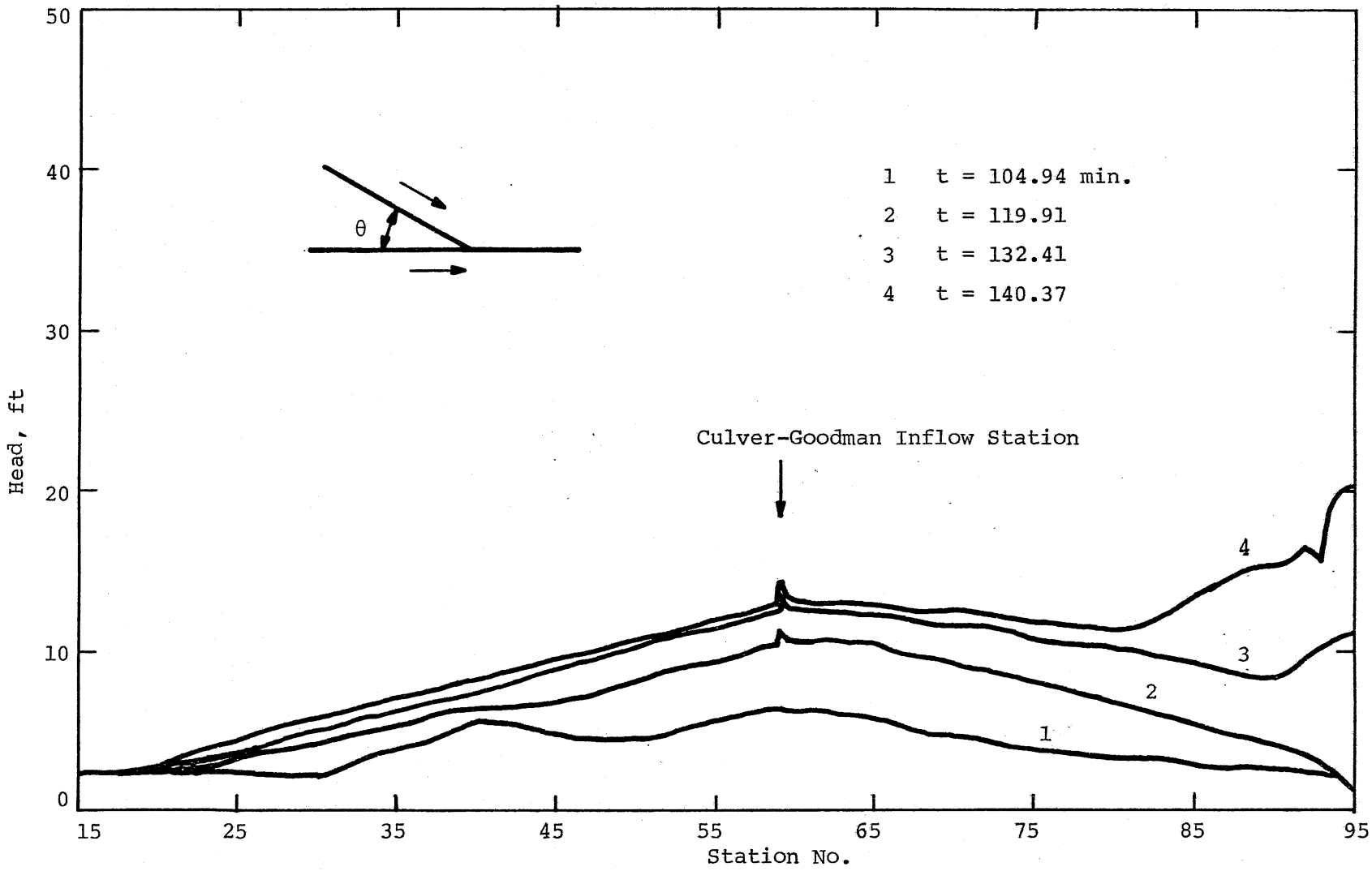

Fig. IV-7. Hydraulic Gradeline, $\theta = 30^{o}$.

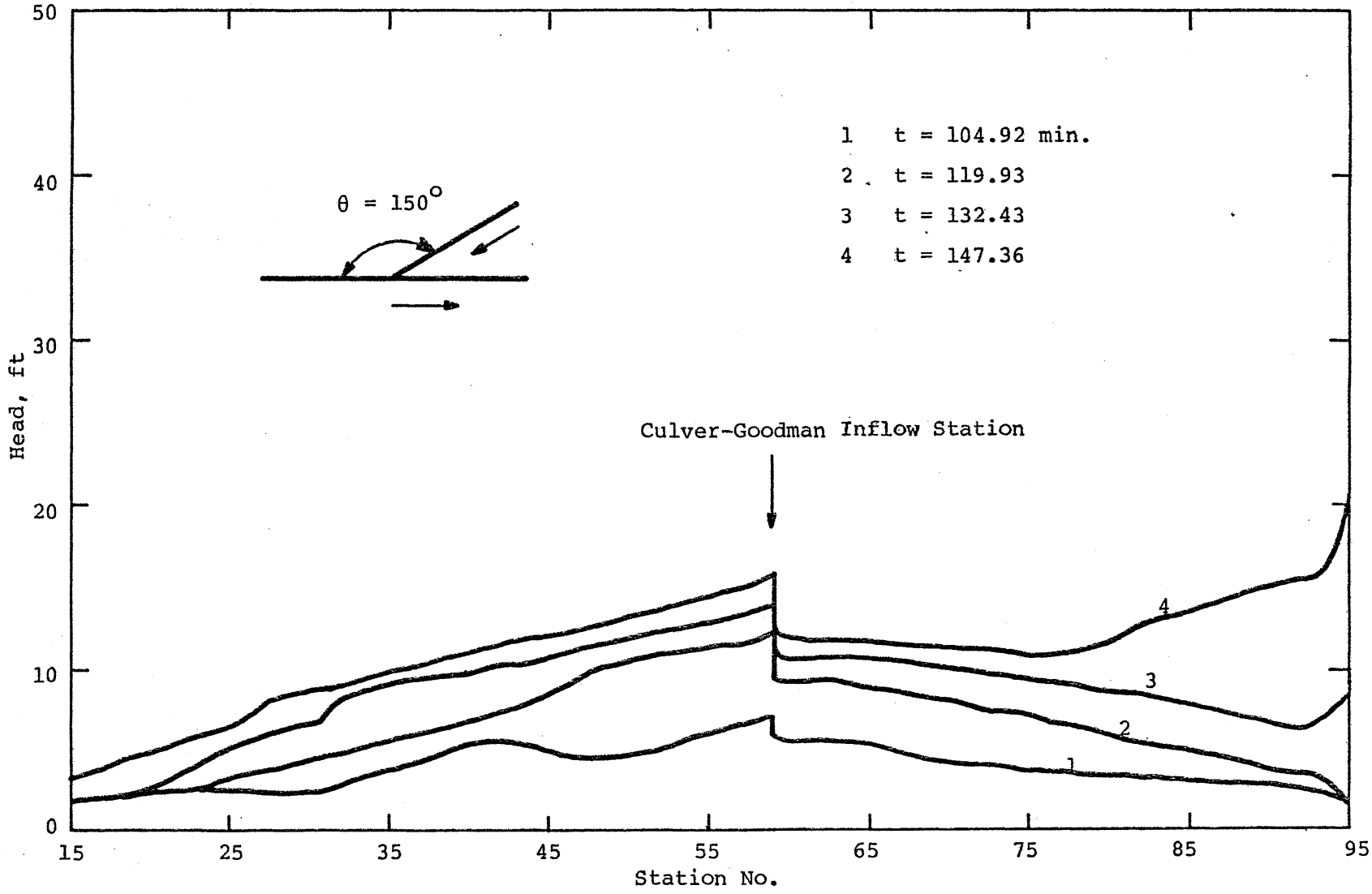

Fig. IV-8. Hydraulic Gradeline, $\theta = 150^{\circ}$.

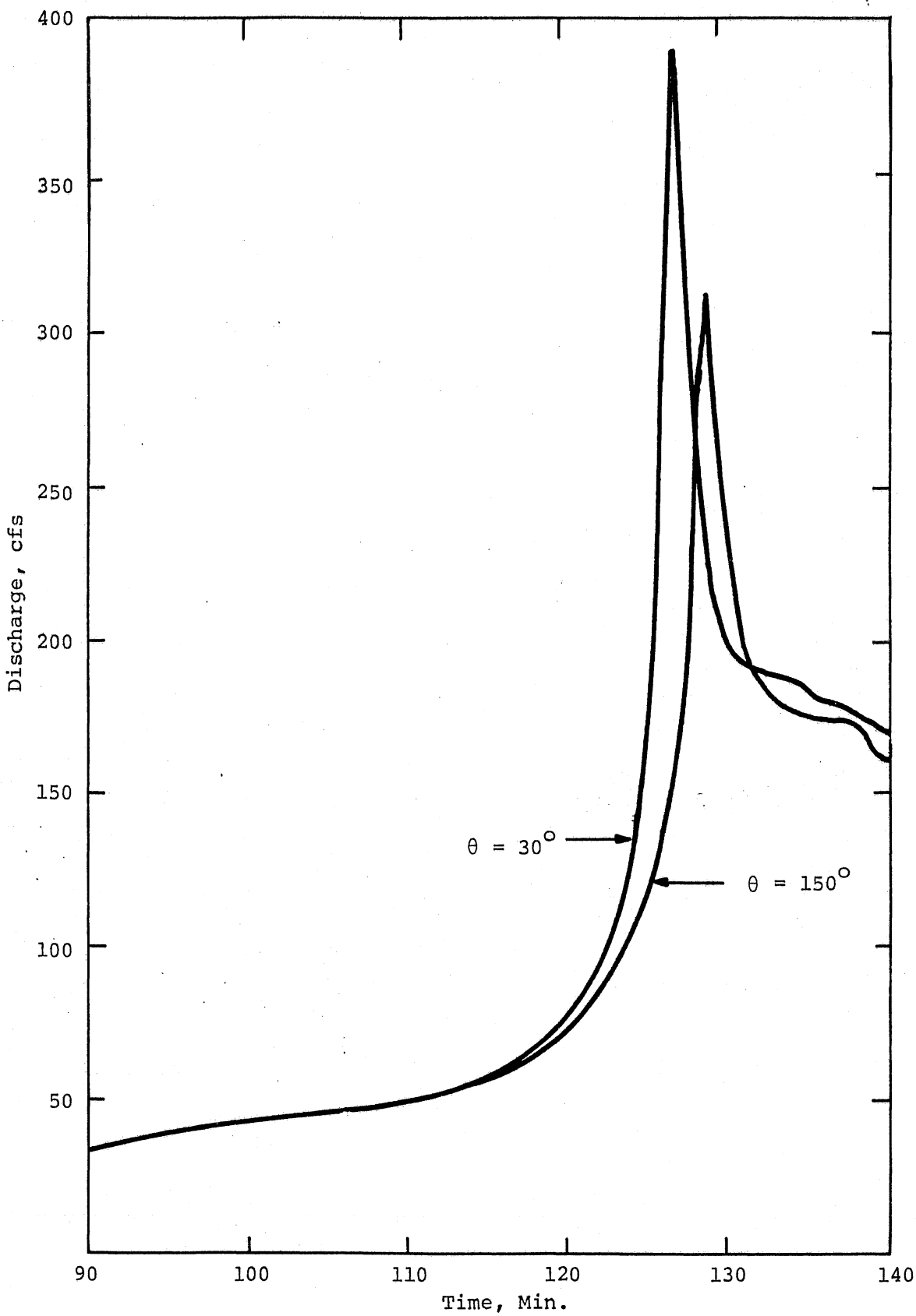

Fig. IV-9. Outflow Discharge Affected by Two Angle of Incidence.

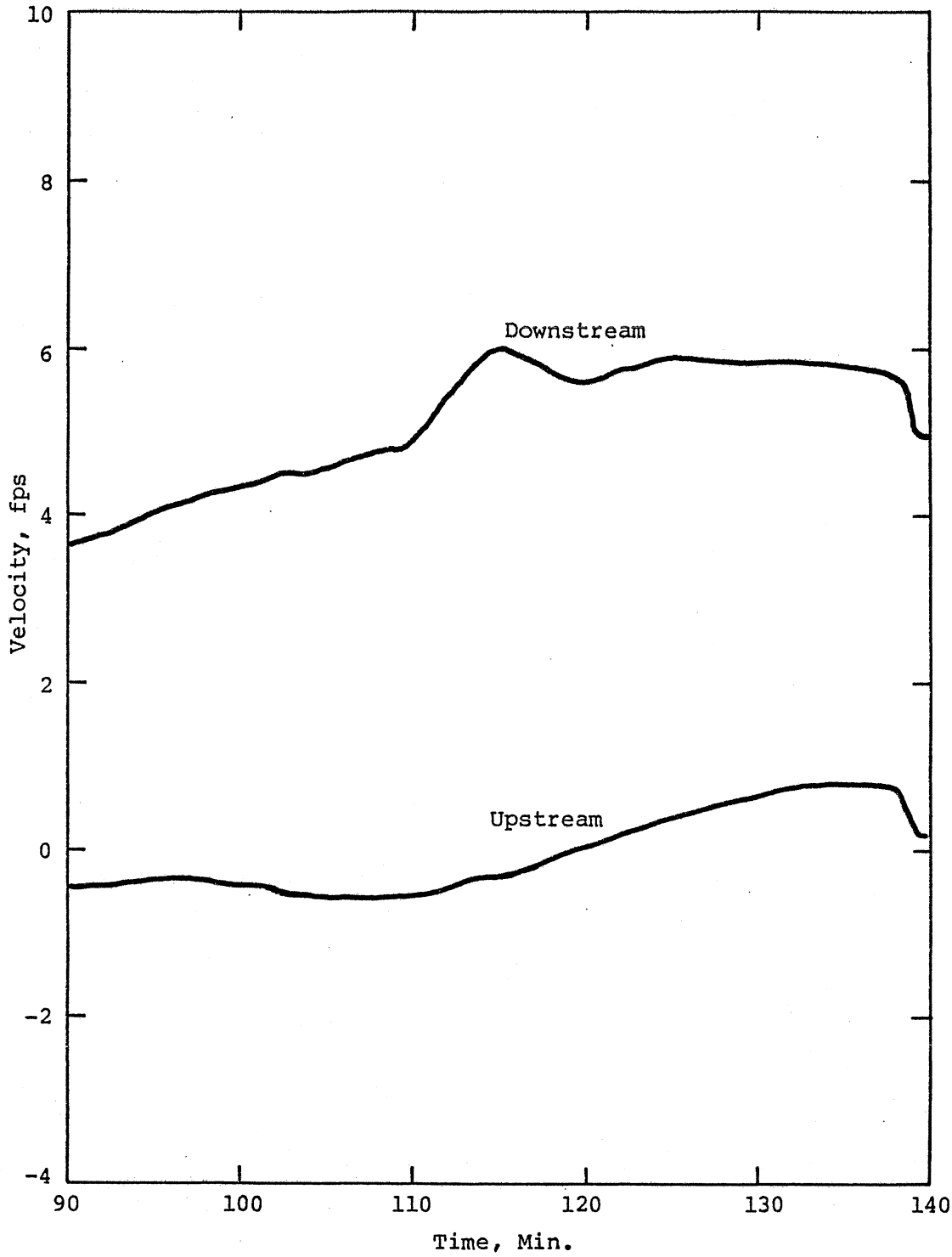

Fig. IV-10. Velocity Near the Connection, $\theta = 30^{\circ}$.

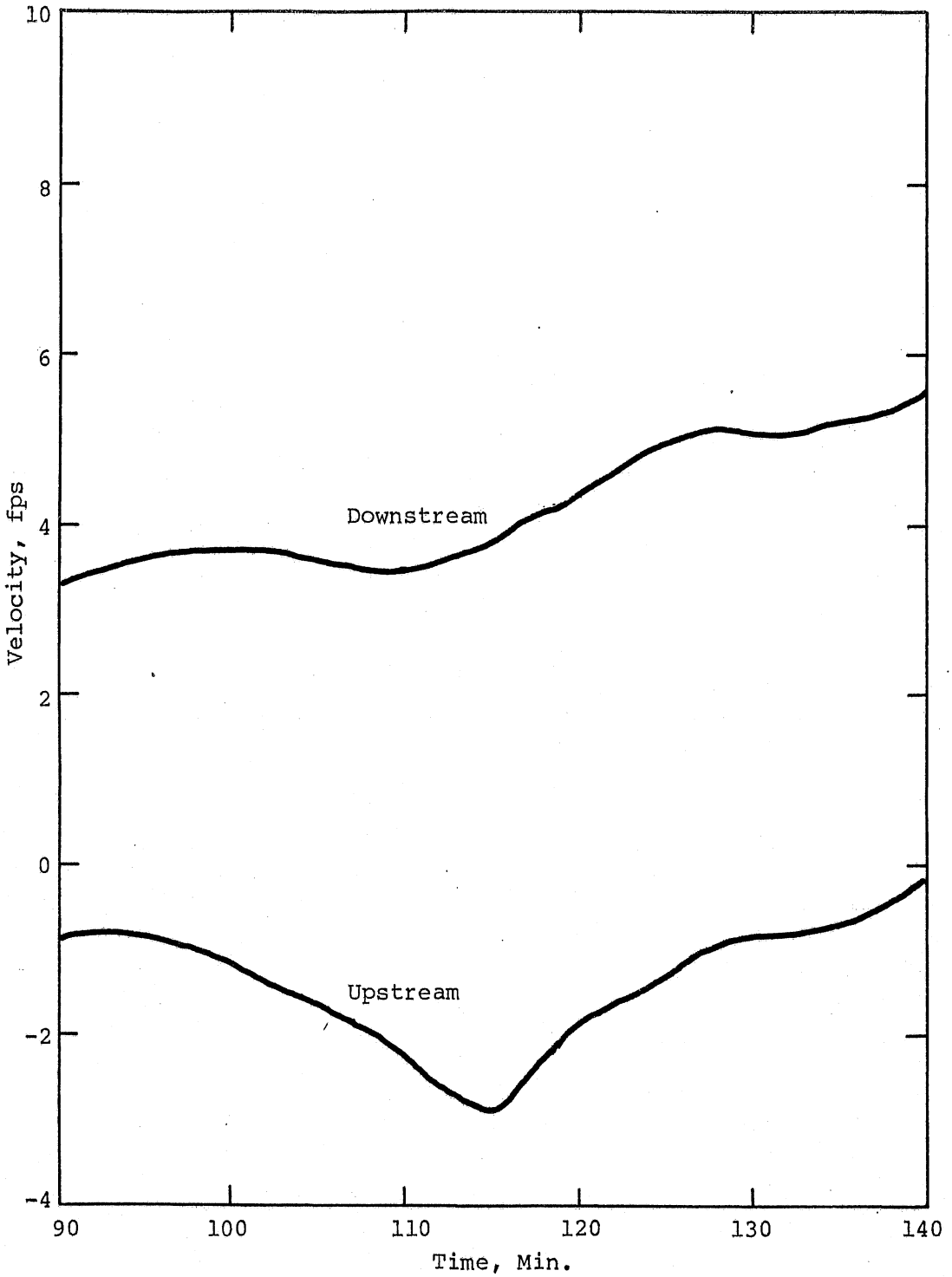

Fig. IV-11. Velocity Near the Connection, $\theta = 150^{\circ}$.

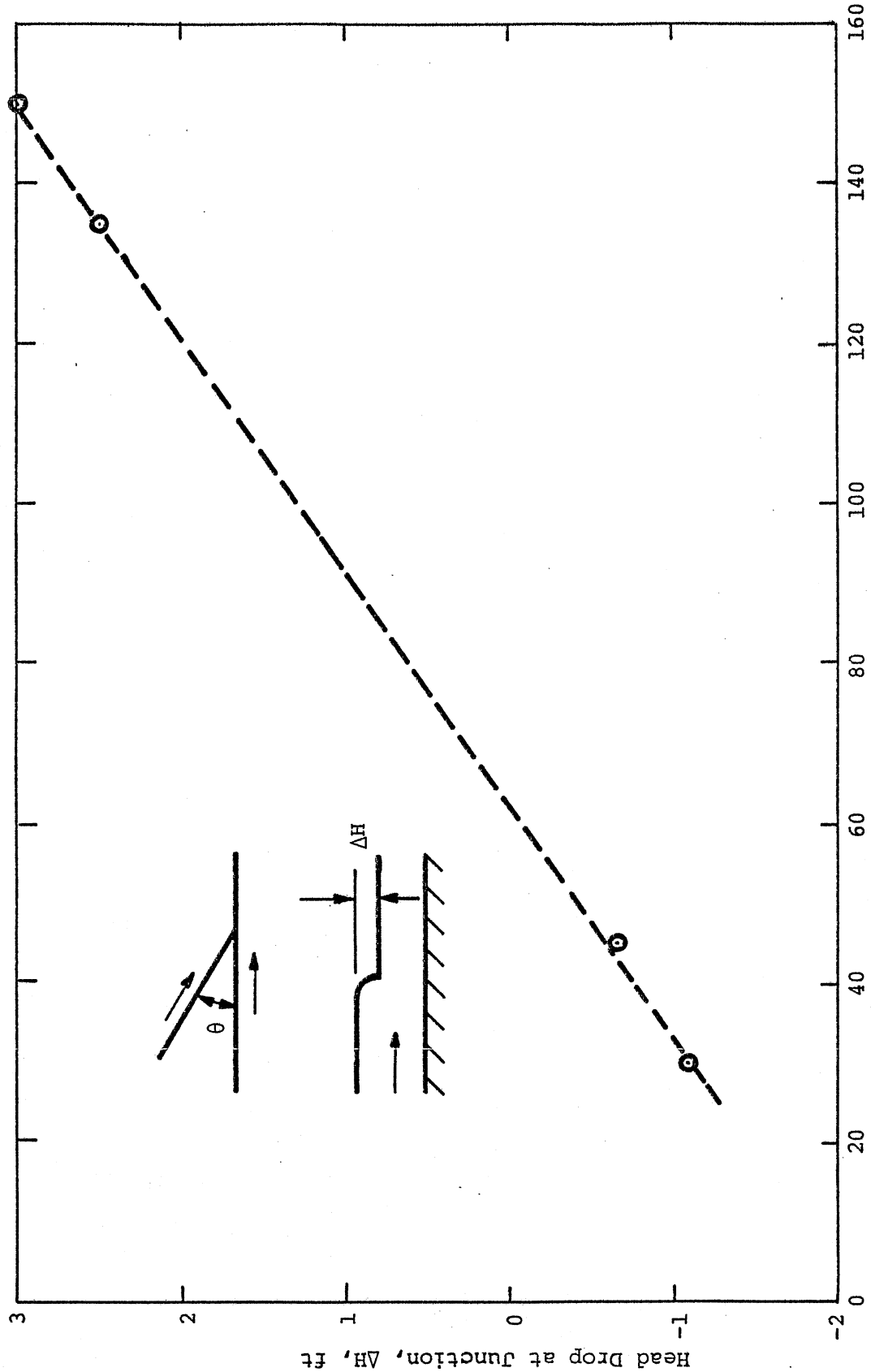

Fig. IV-12. Angle Between Inflow and Tunnel, θ degrees.

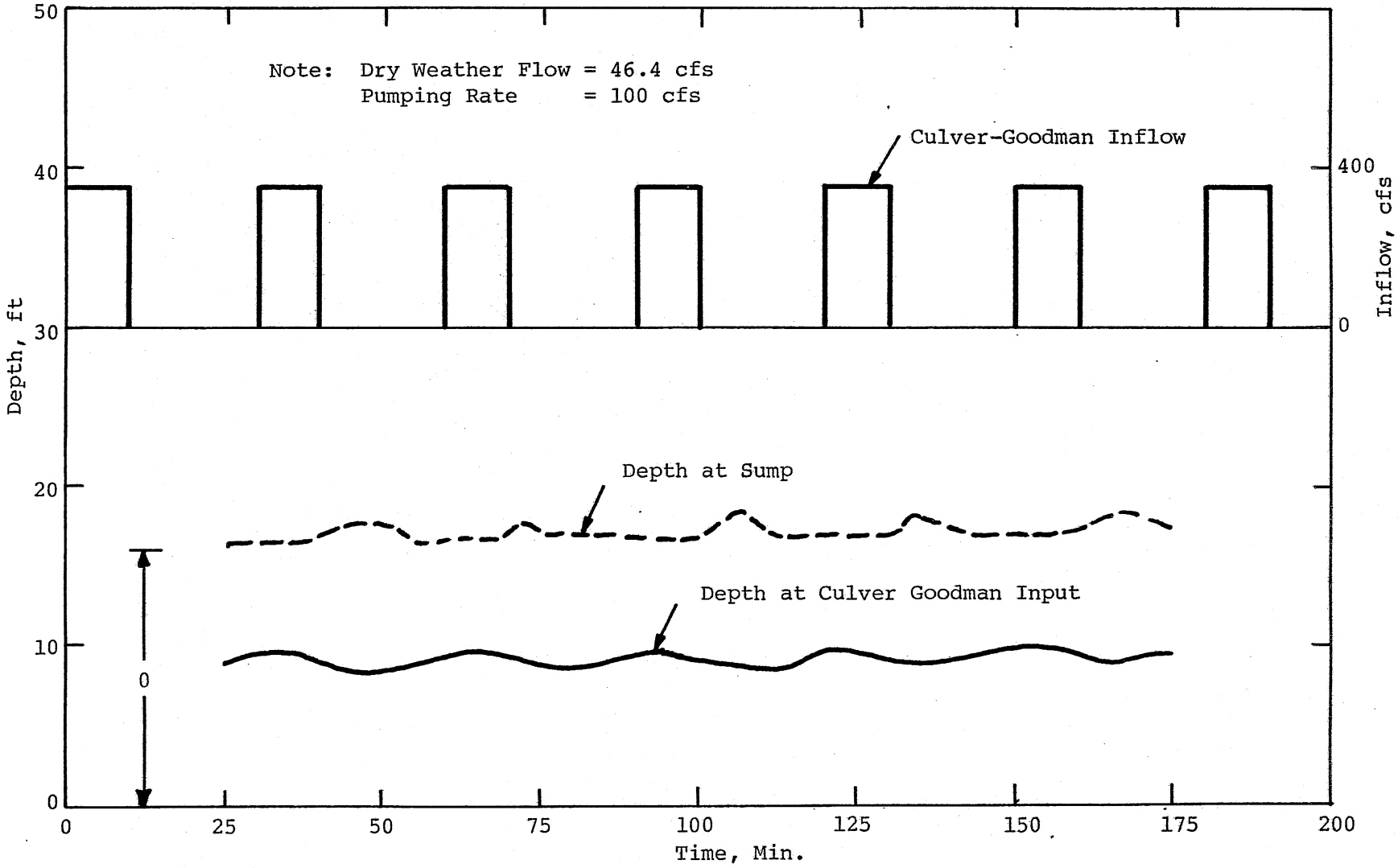

Fig. IV-13. Inflow Hydrograph and Depth, Run IV-1.

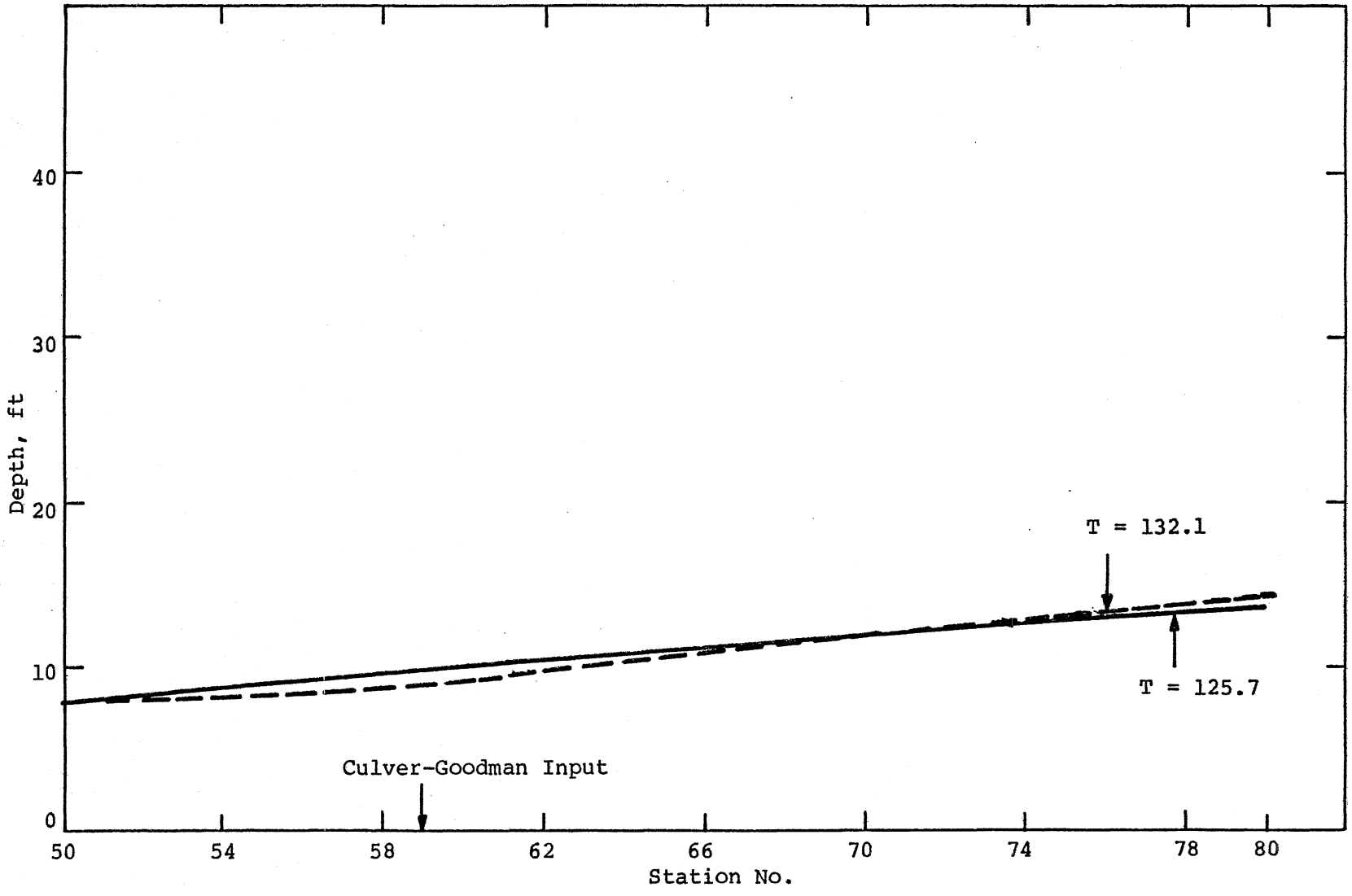

Fig. IV-14. Hydraulic Gradelines, Run IV-2.

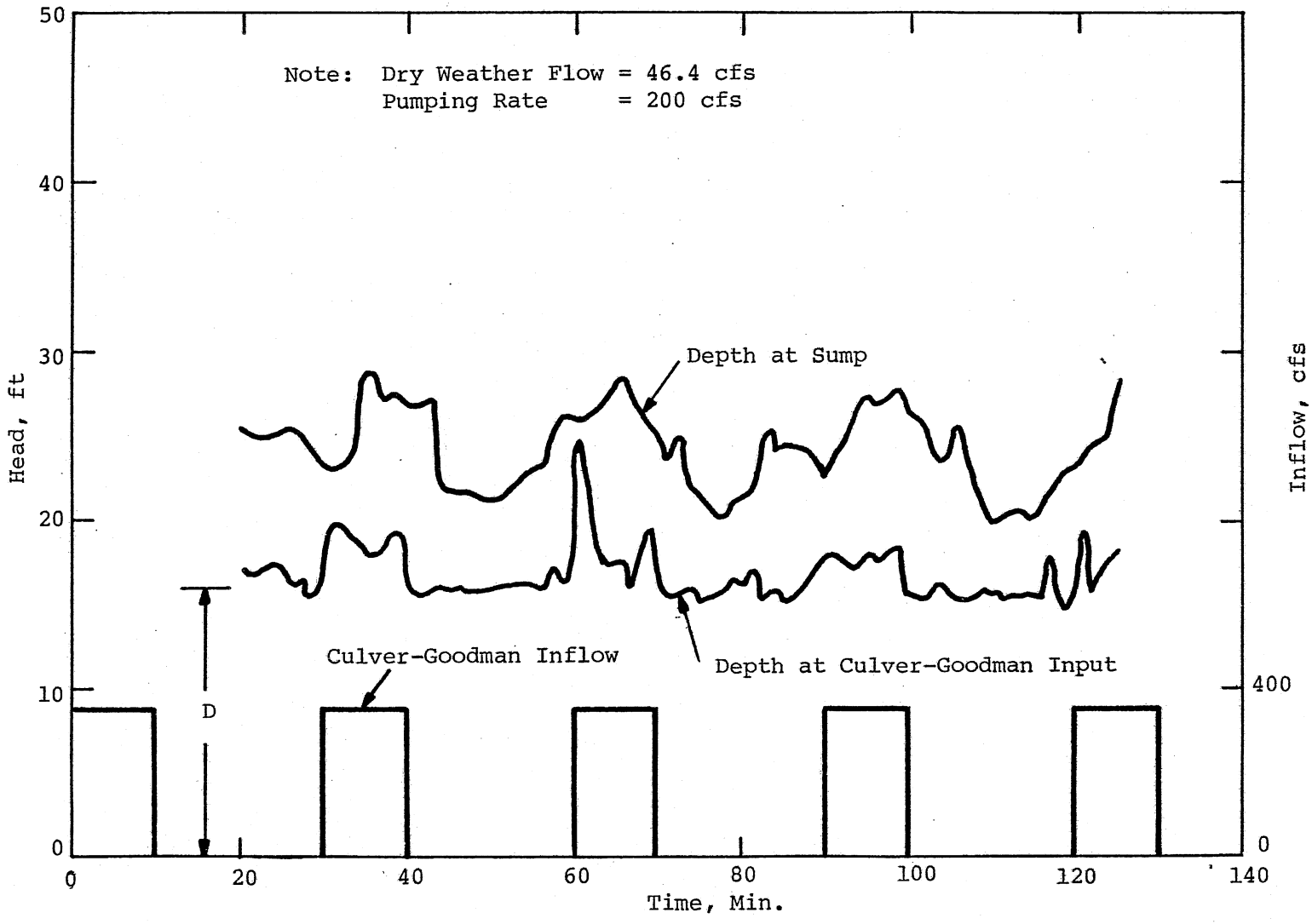

Fig. IV-15. Inflow Hydrograph and Depth, Run IV-2.

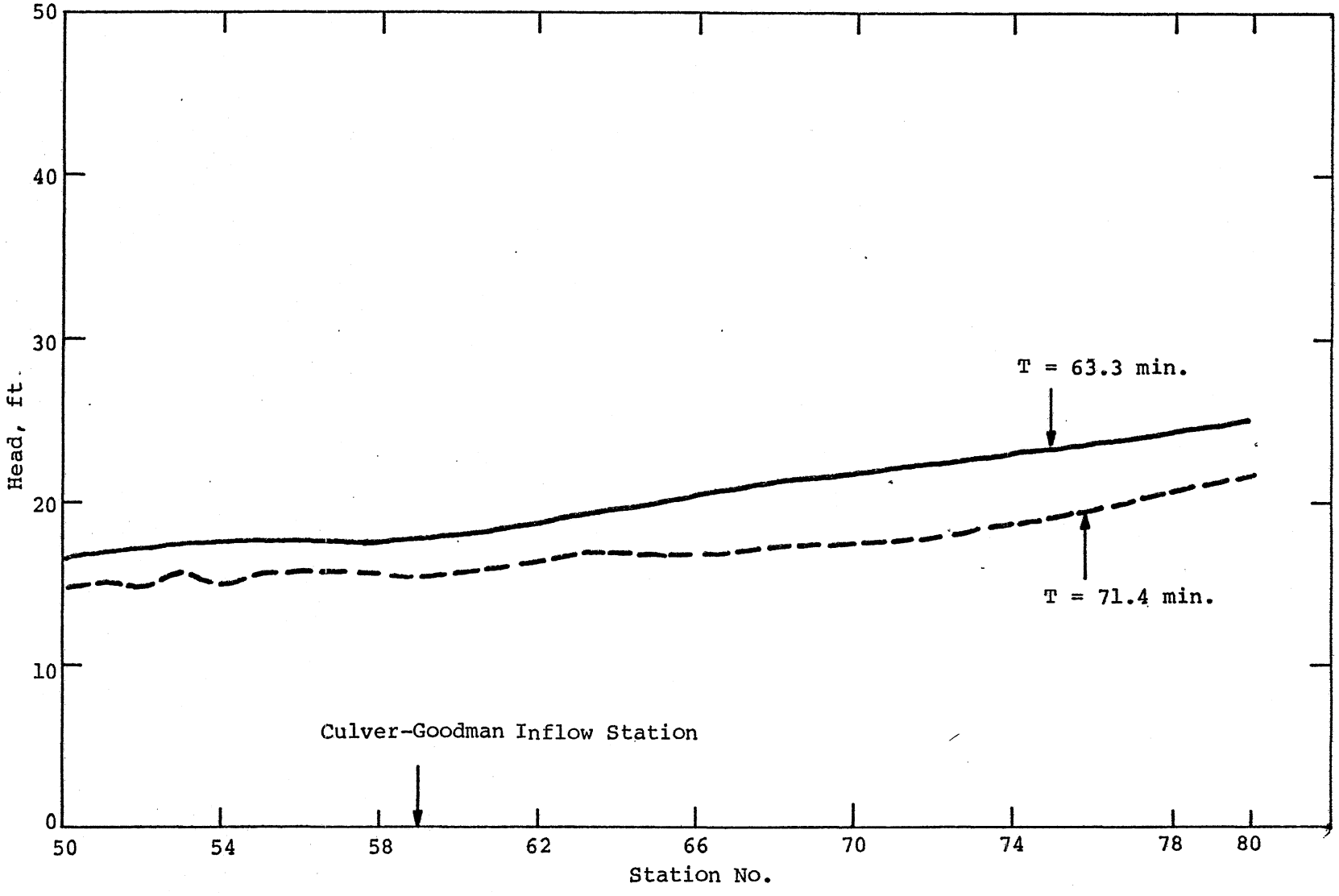

Fig. IV-16. Hydraulic Gradelines, Run IV-2.

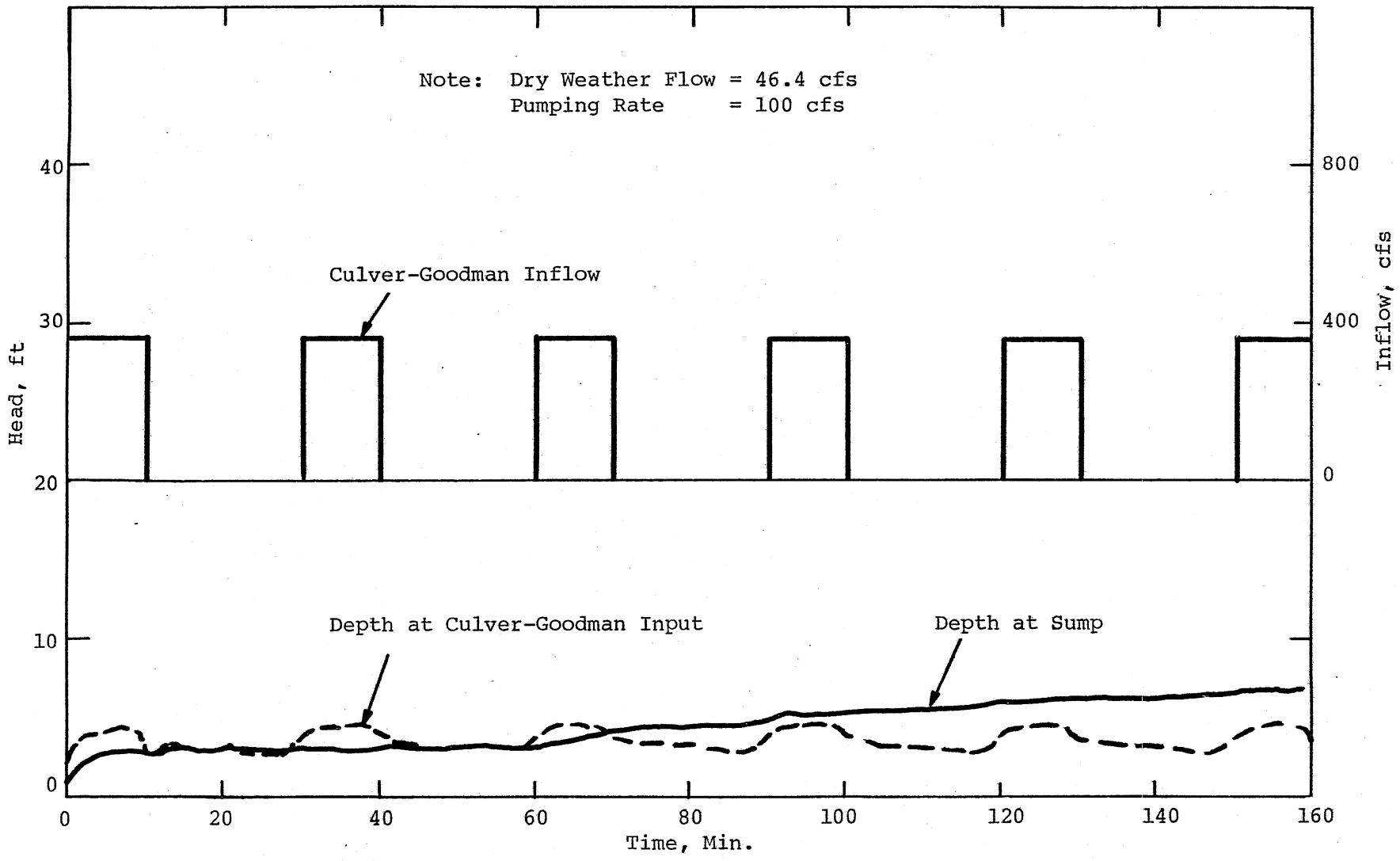

Fig. IV-17. Inflow Hydrograph and Depth, Run IV-3.

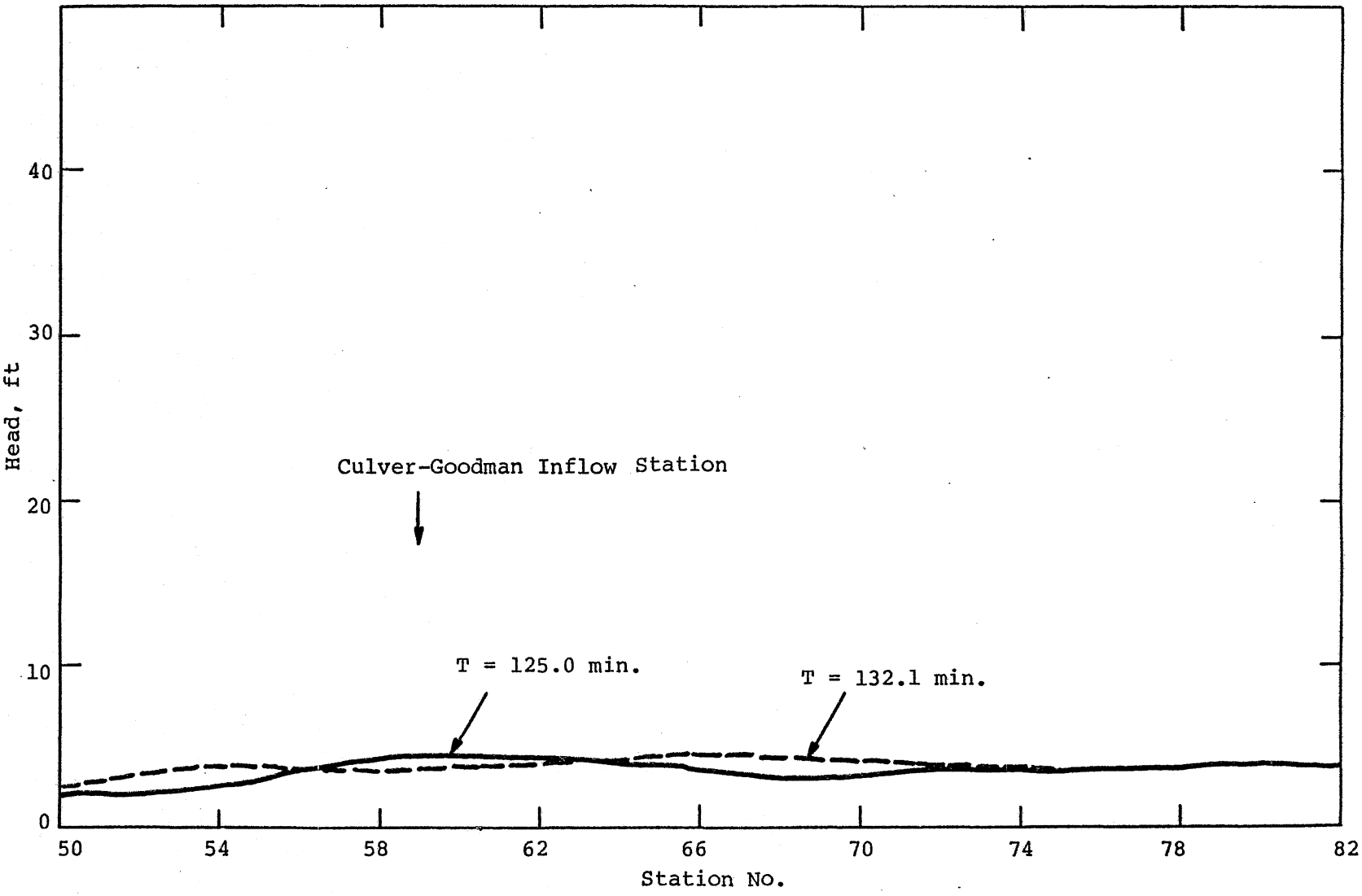

Fig. IV-18. Hydraulic Gradelines, Run IV-3.

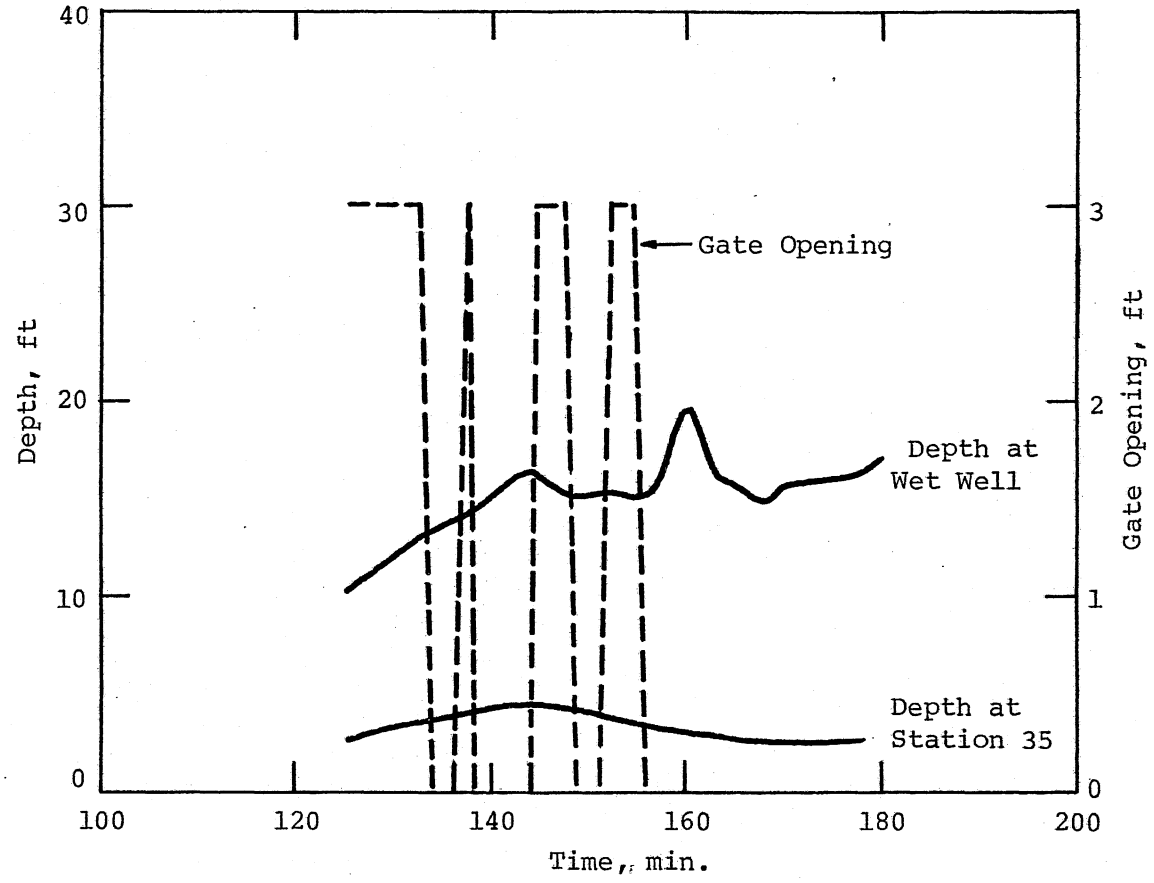

Fig. V-1. Gate Movement and Water Depth, Run V-1.

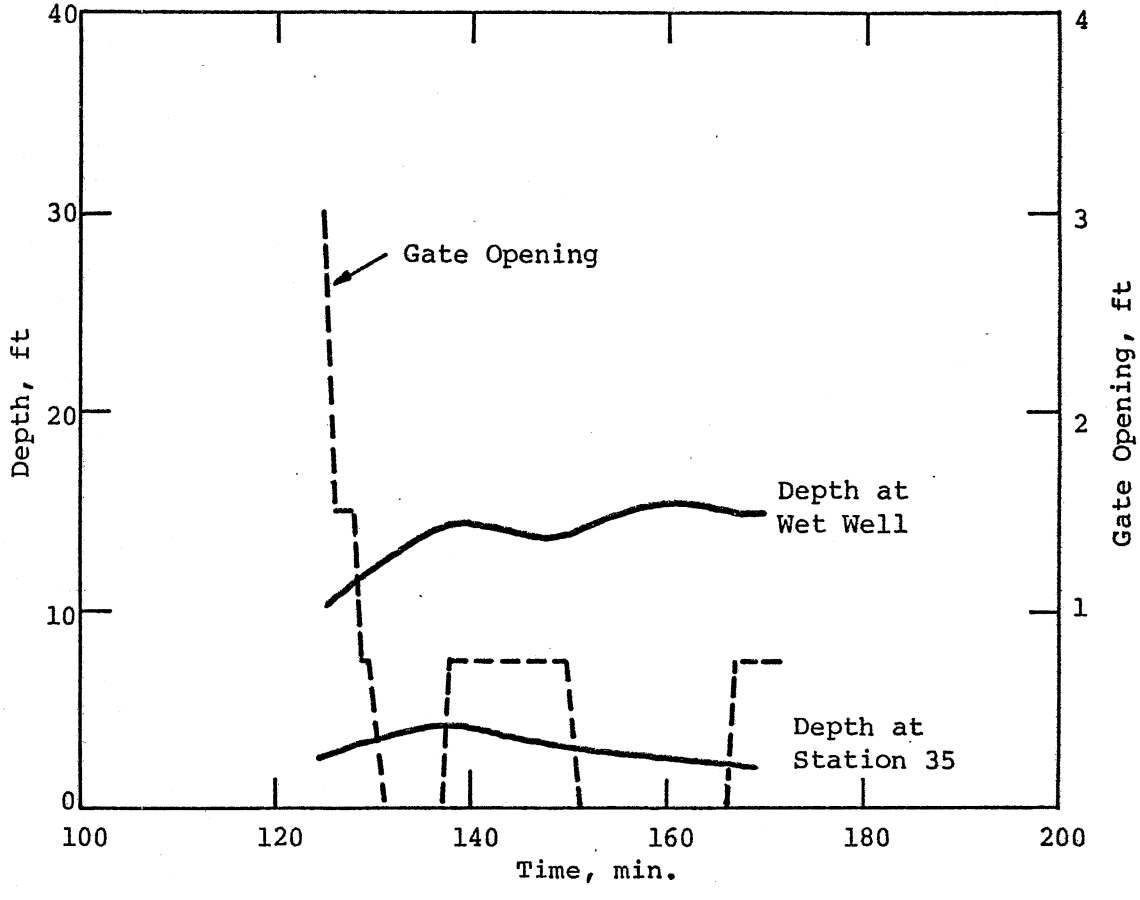

Fig. V-2. Gate Movement and Water Depth, Run V-2.

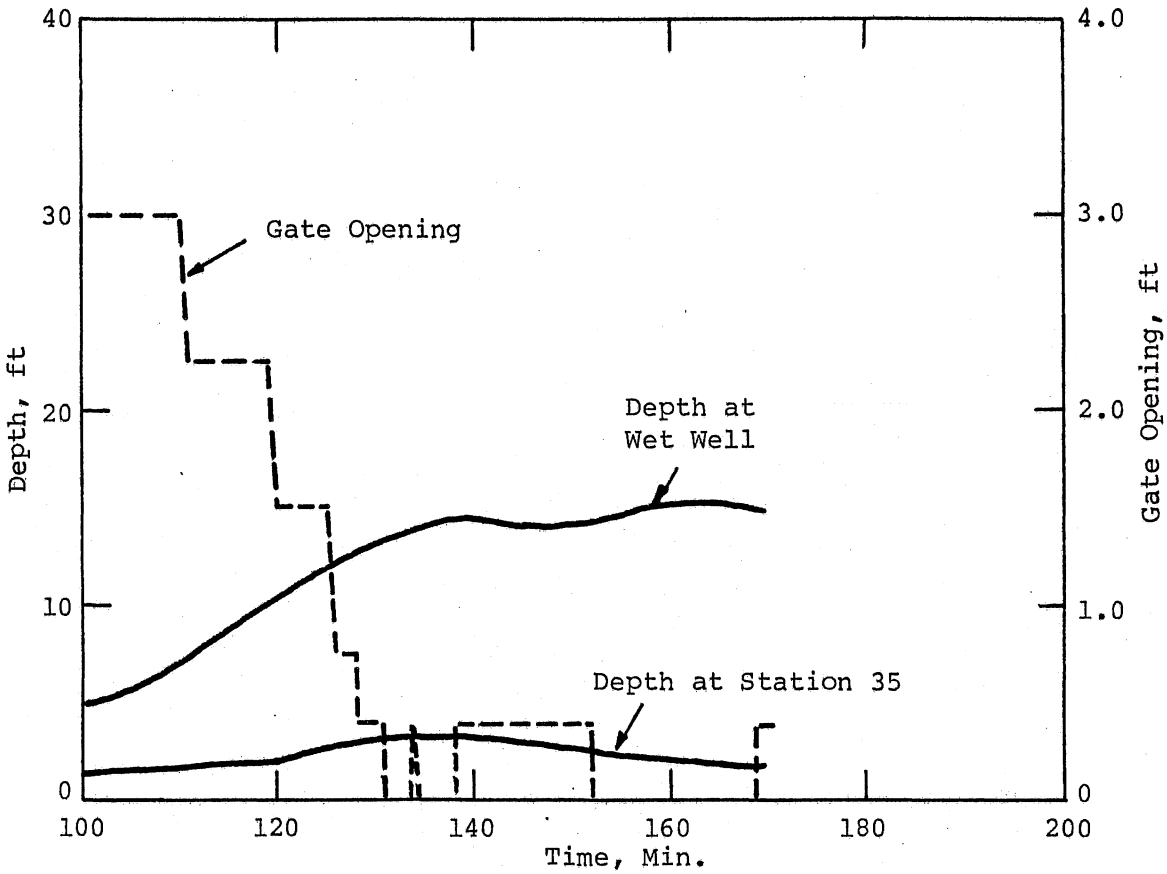

Fig. V-3. Gate Movement and Water Depth, Run V-3.

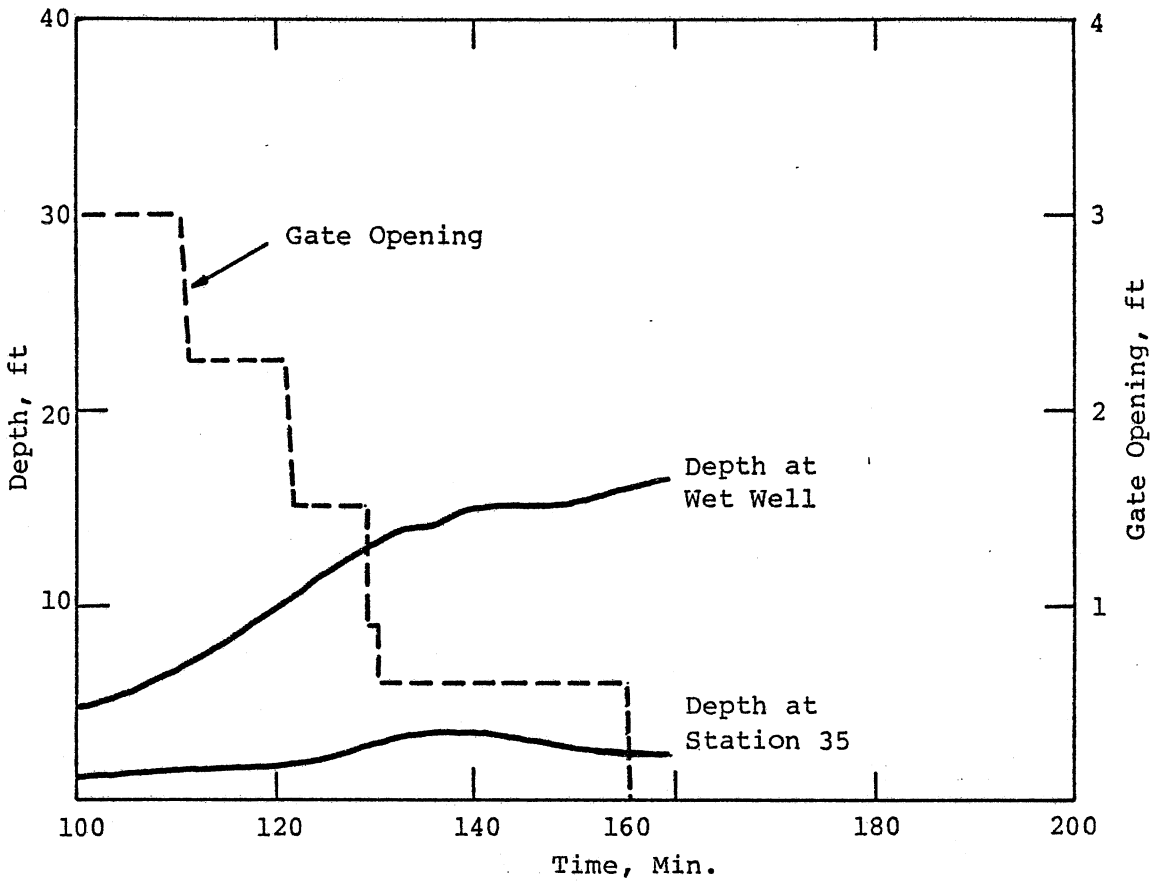

Fig. V-4. Gate Movement and Water Depth, Run V-4.

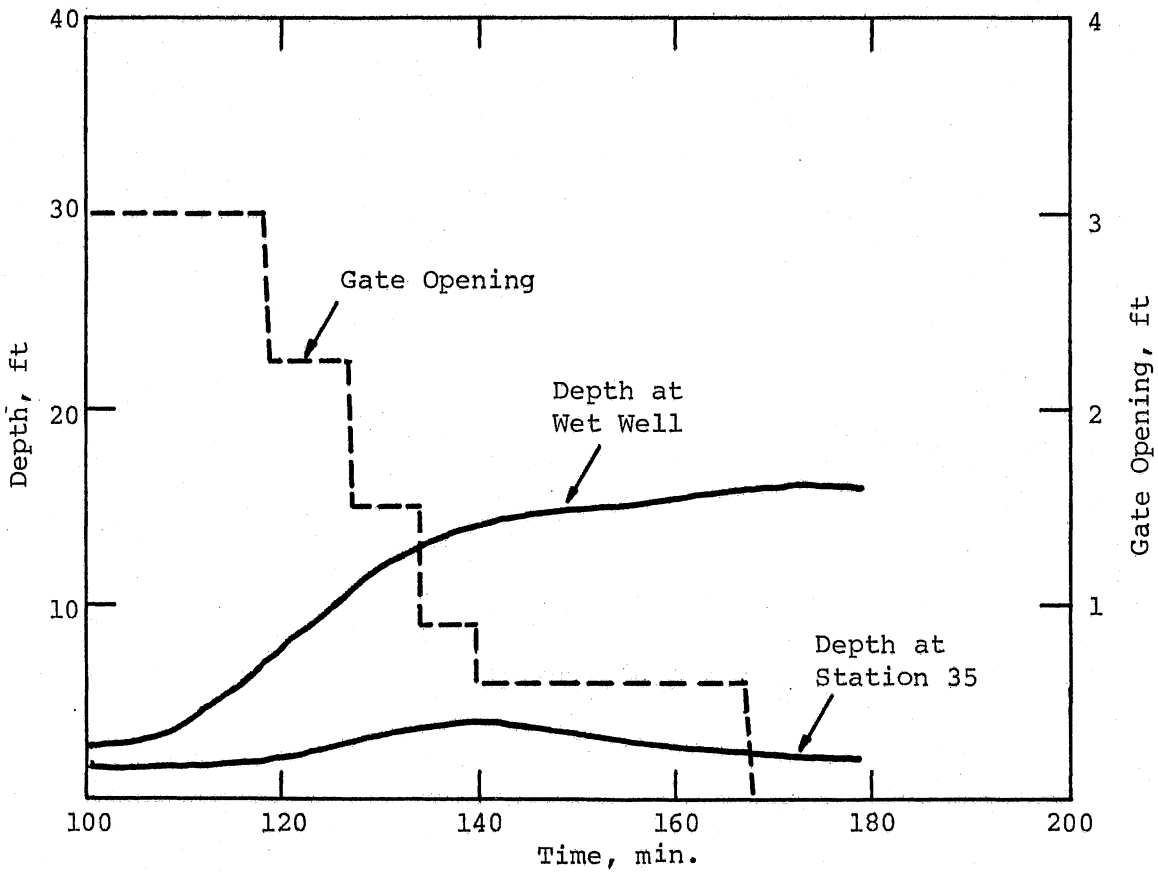

Fig. V-5. Gate Movement and Water Depth, Run V-5.

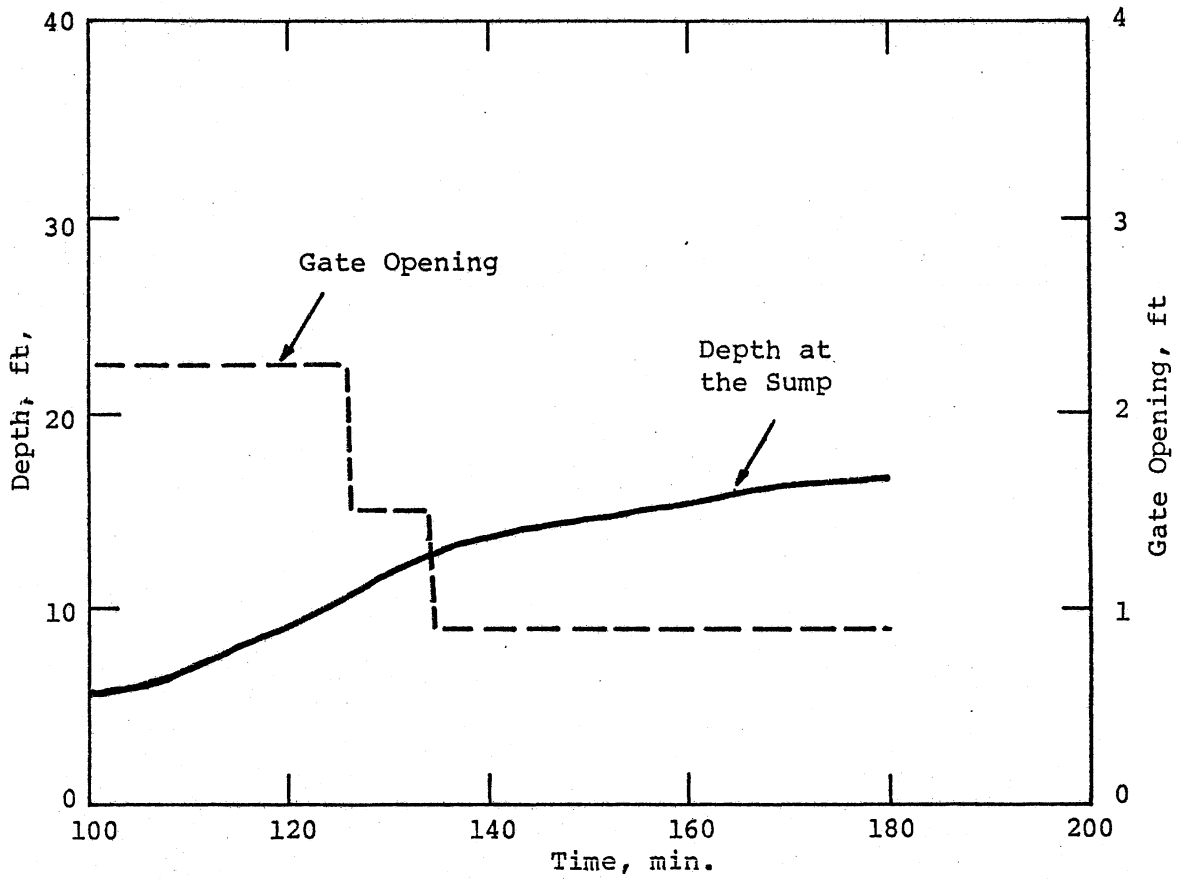

Fig. V-8. Gate Movement and Water Depth, Run V-8.

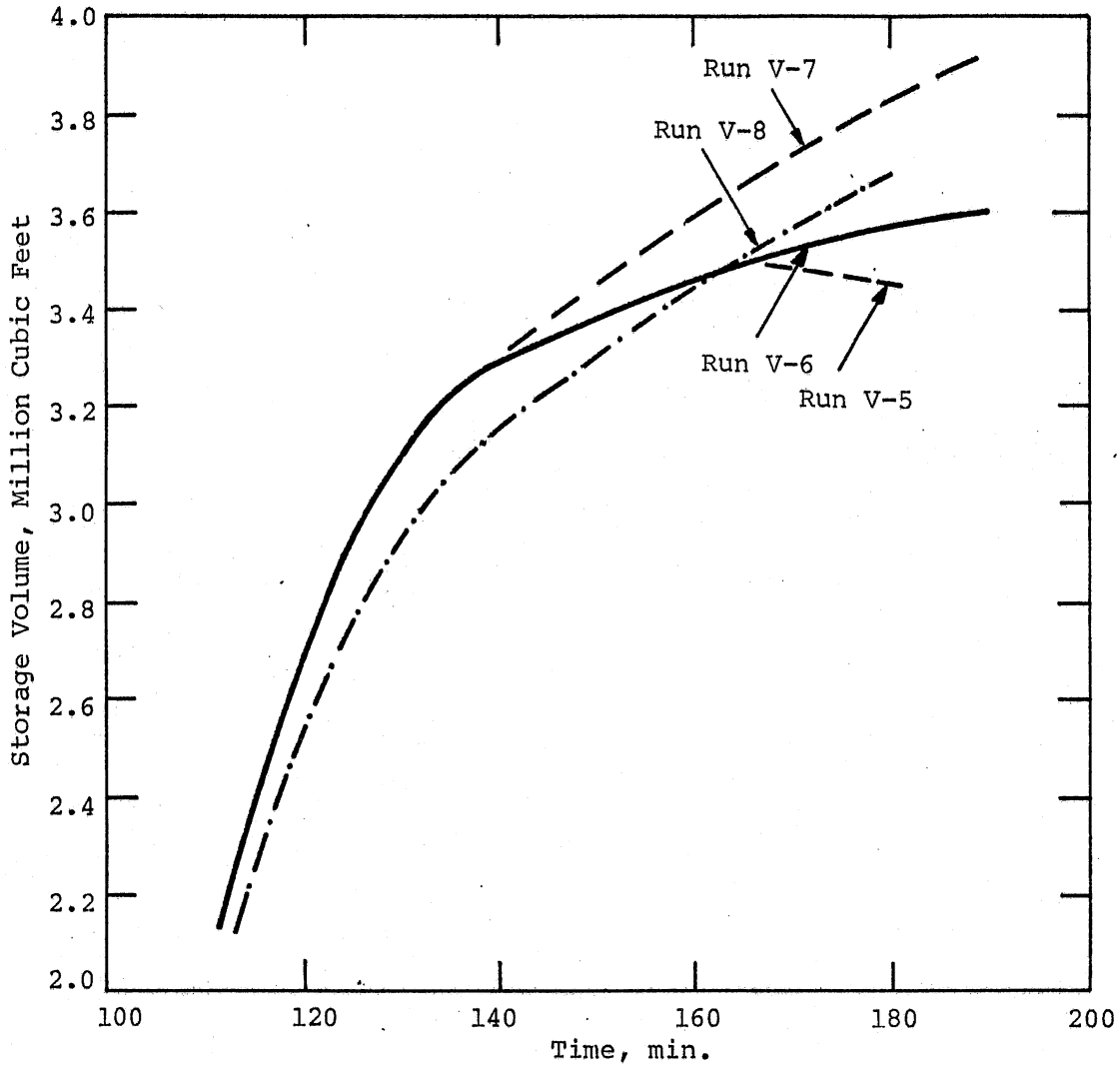

Fig. V-9. Water Stored in Cross-Irondequoit Tunnel.

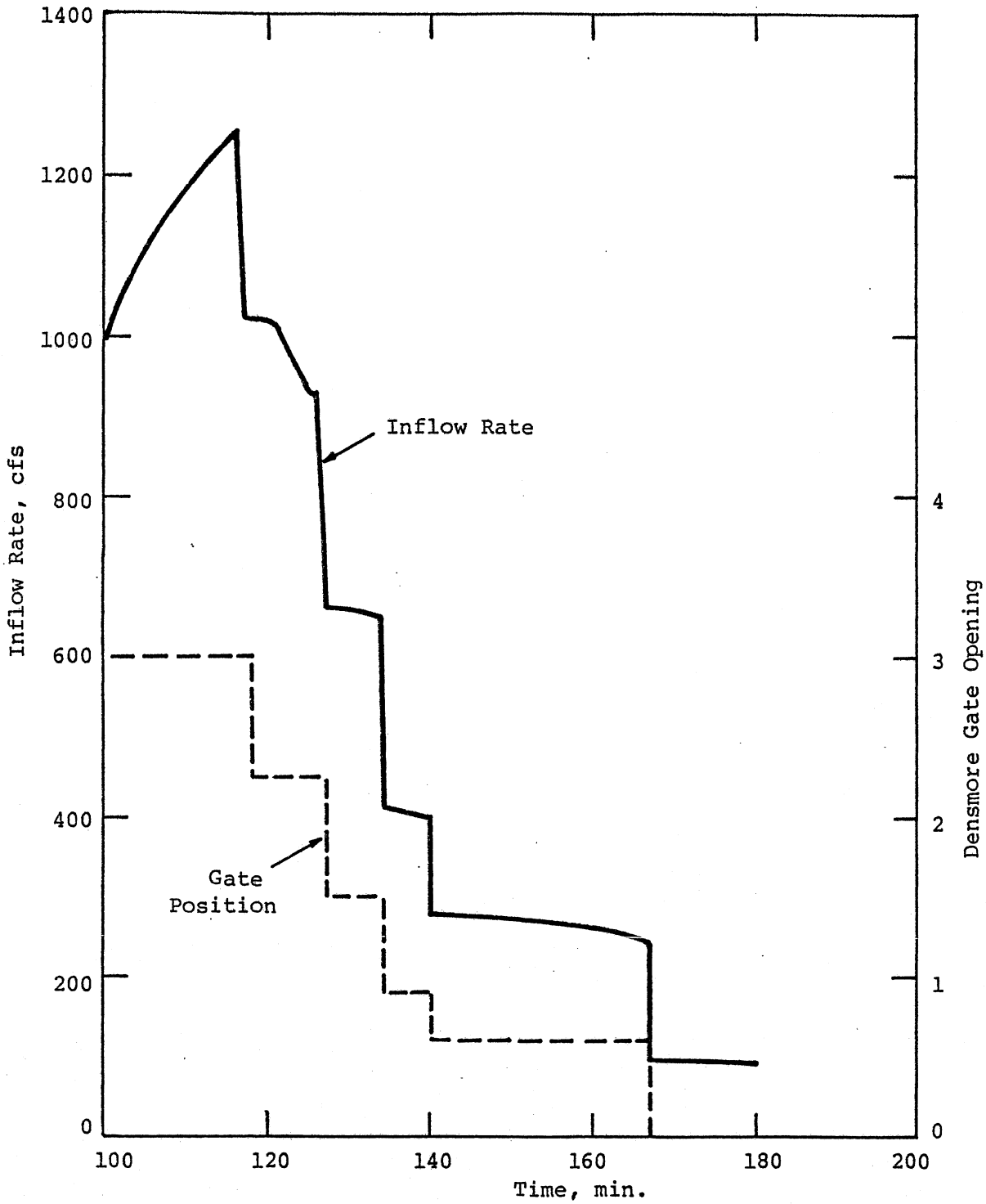

Fig. V-10. Total Inflow into the Tunnel and Gate Position at Densmore Creek, Run V-5.

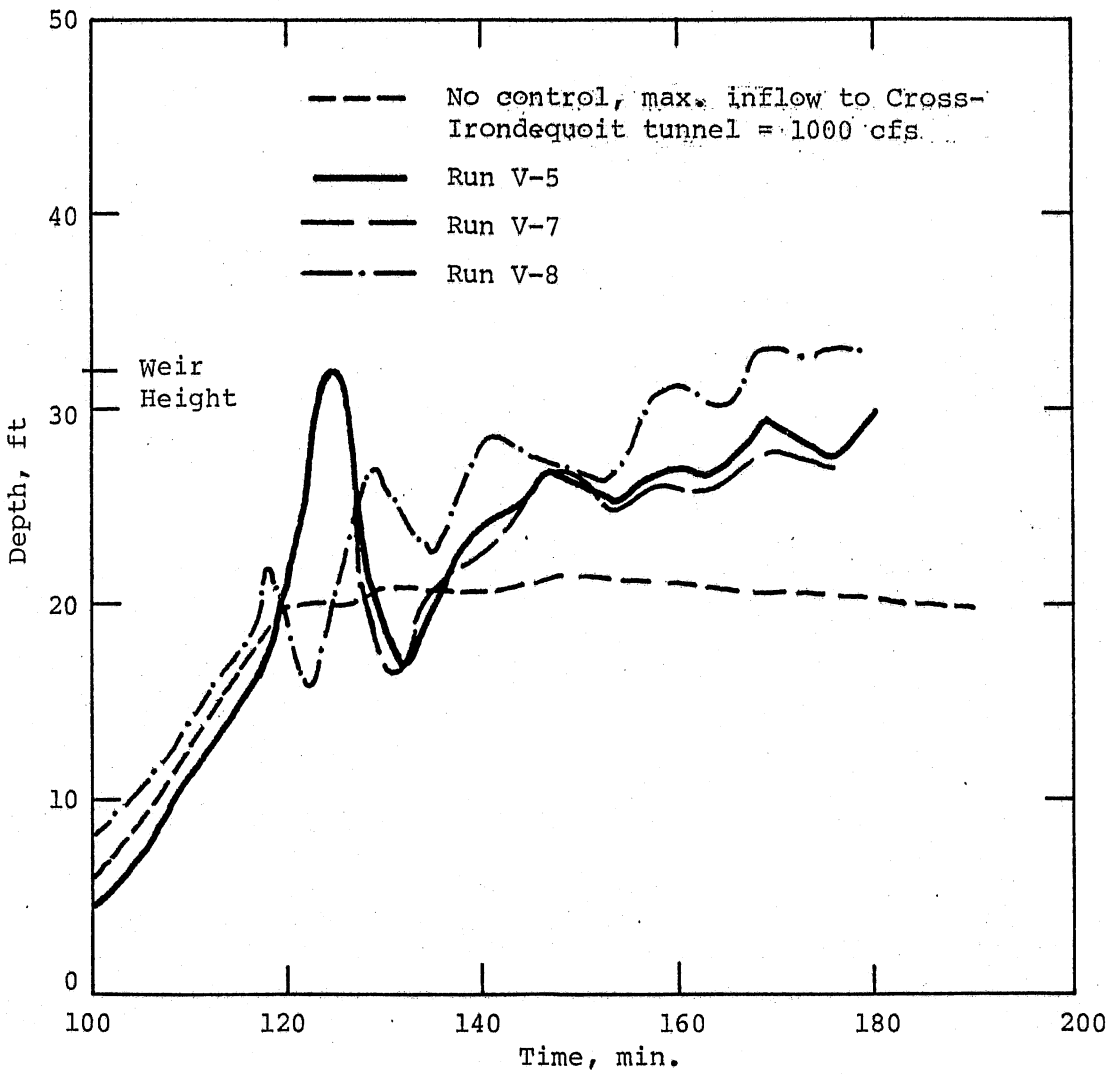

Fig. V-11. Depth Fluctuations at Culver-Goodman Tunnel Control Structure for Different Control Algorithms.

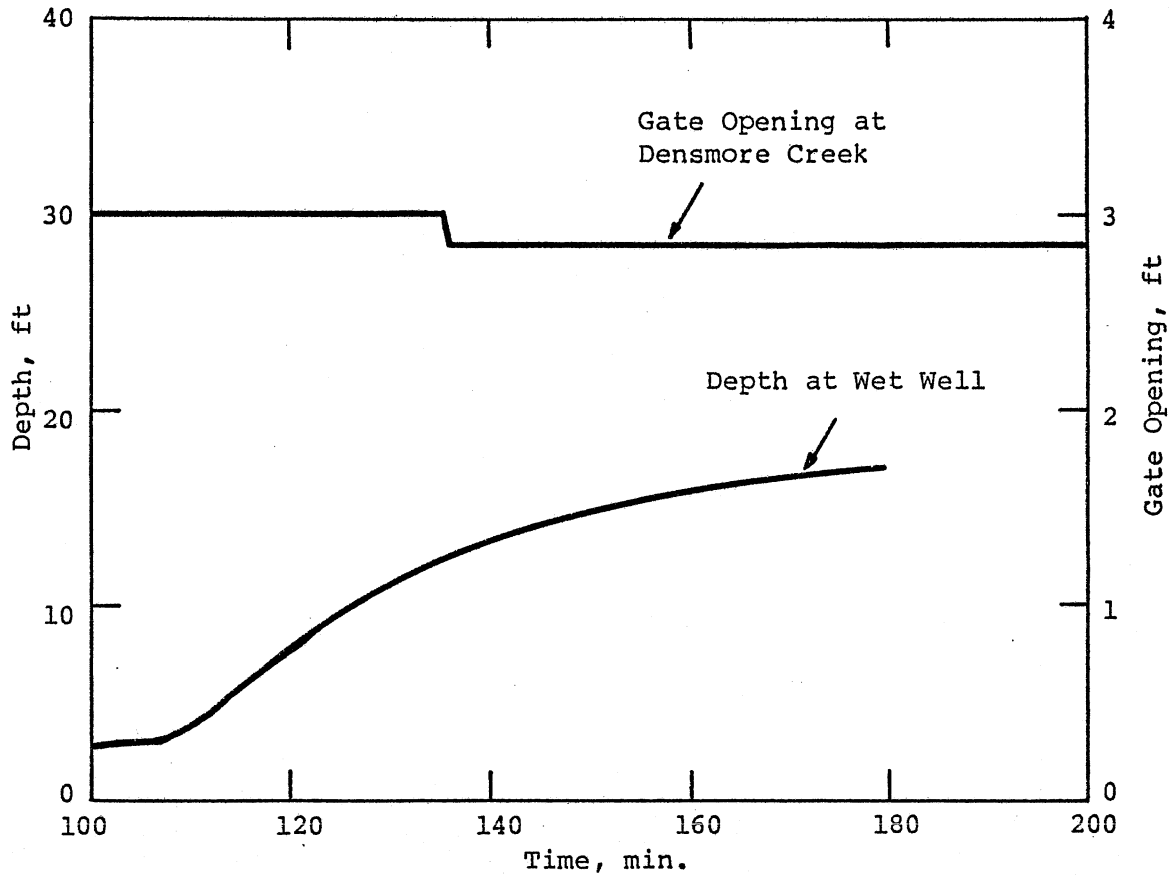

Fig. V-12. Depth in Wet Well and Gate Opening at Densmore Creek, Run V-9.

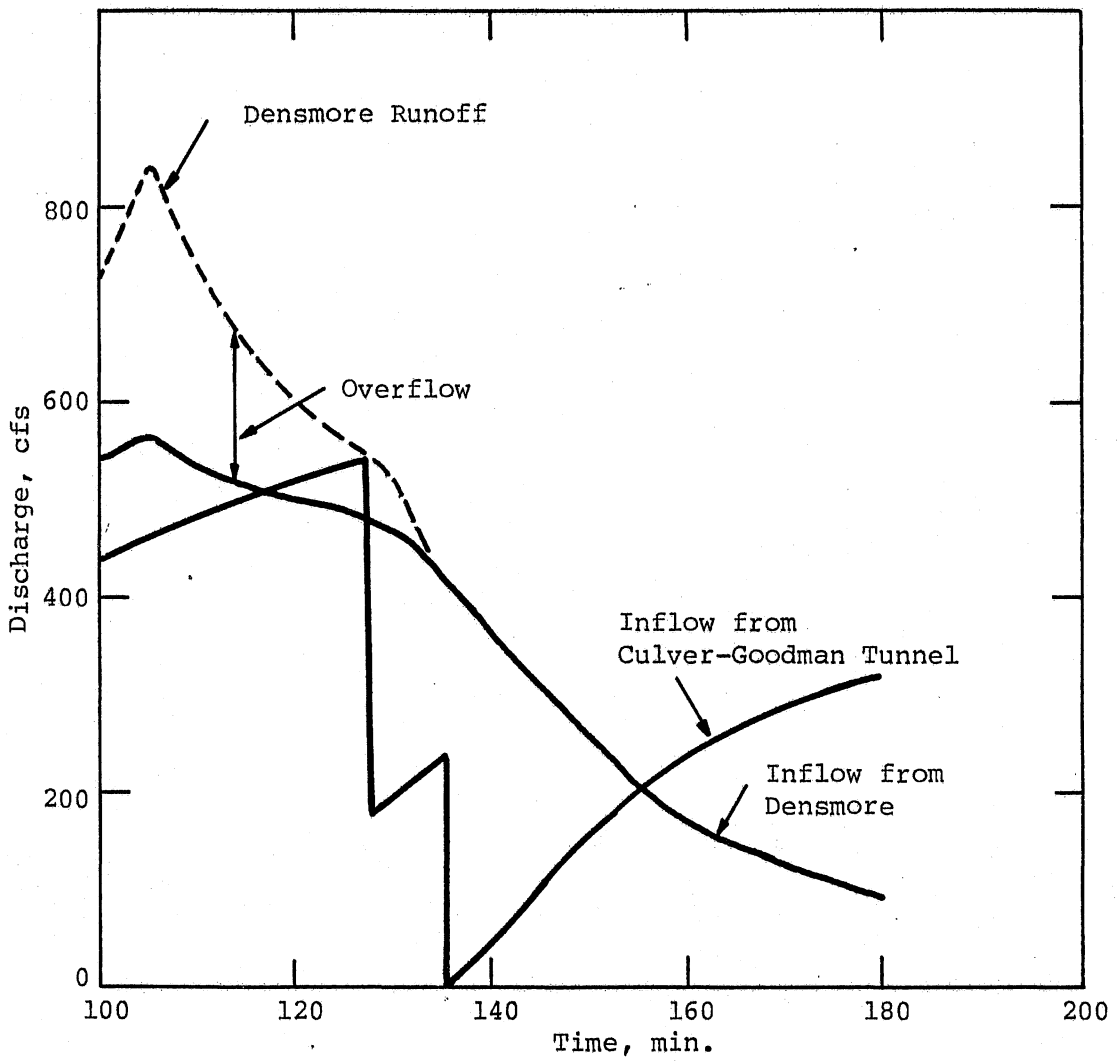

Fig. V-13. Comparison of Hydrograph, at Densmore Creek and the Culver-Goodman Control Structure, Run V-9.

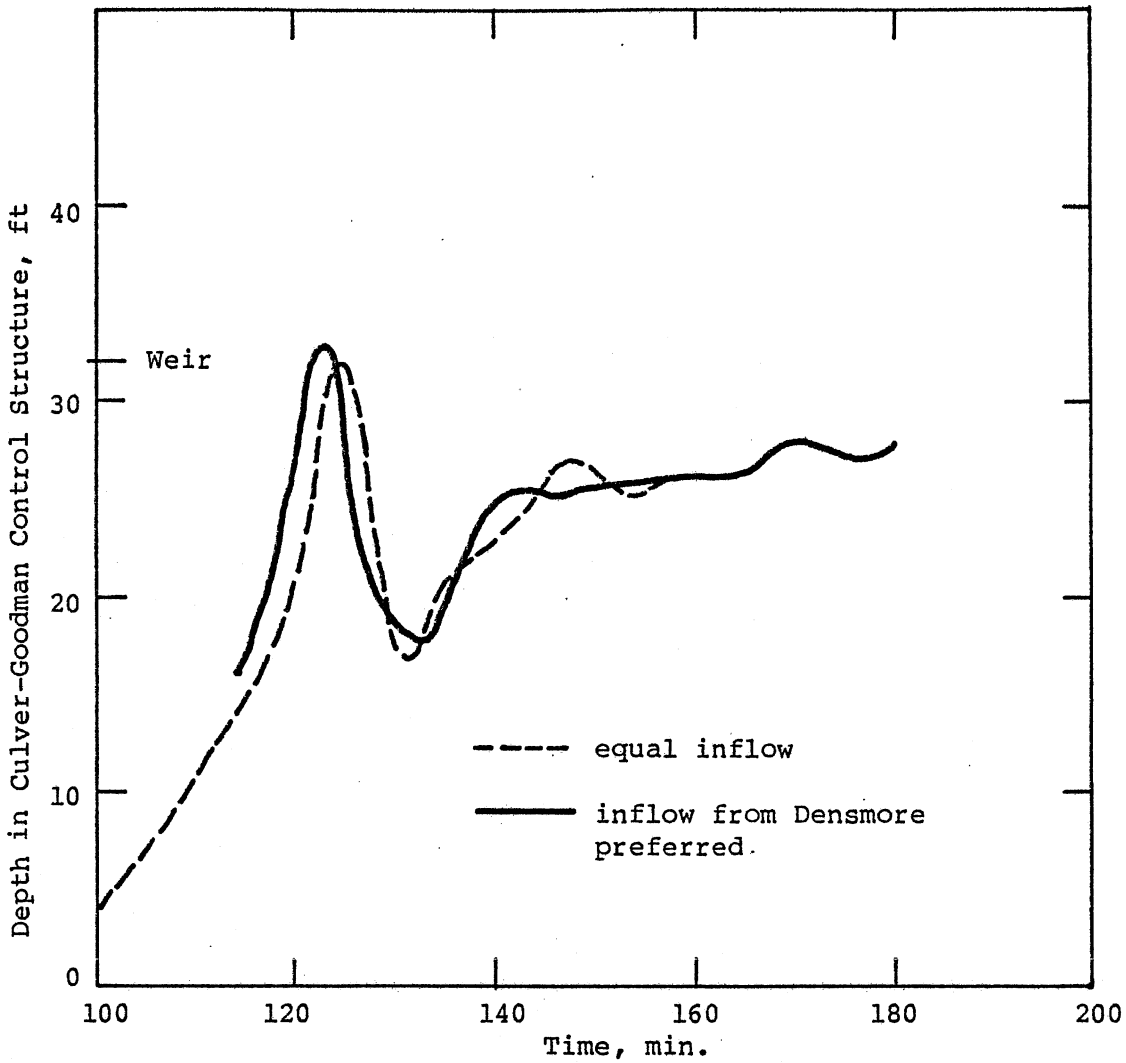

Fig. V-14. A Comparison of the Effect of Operating the Controls at Culver-Goodman and Densmore in Tandem versus Giving Priority to Densmore over the Culver-Goodman Tunnel.

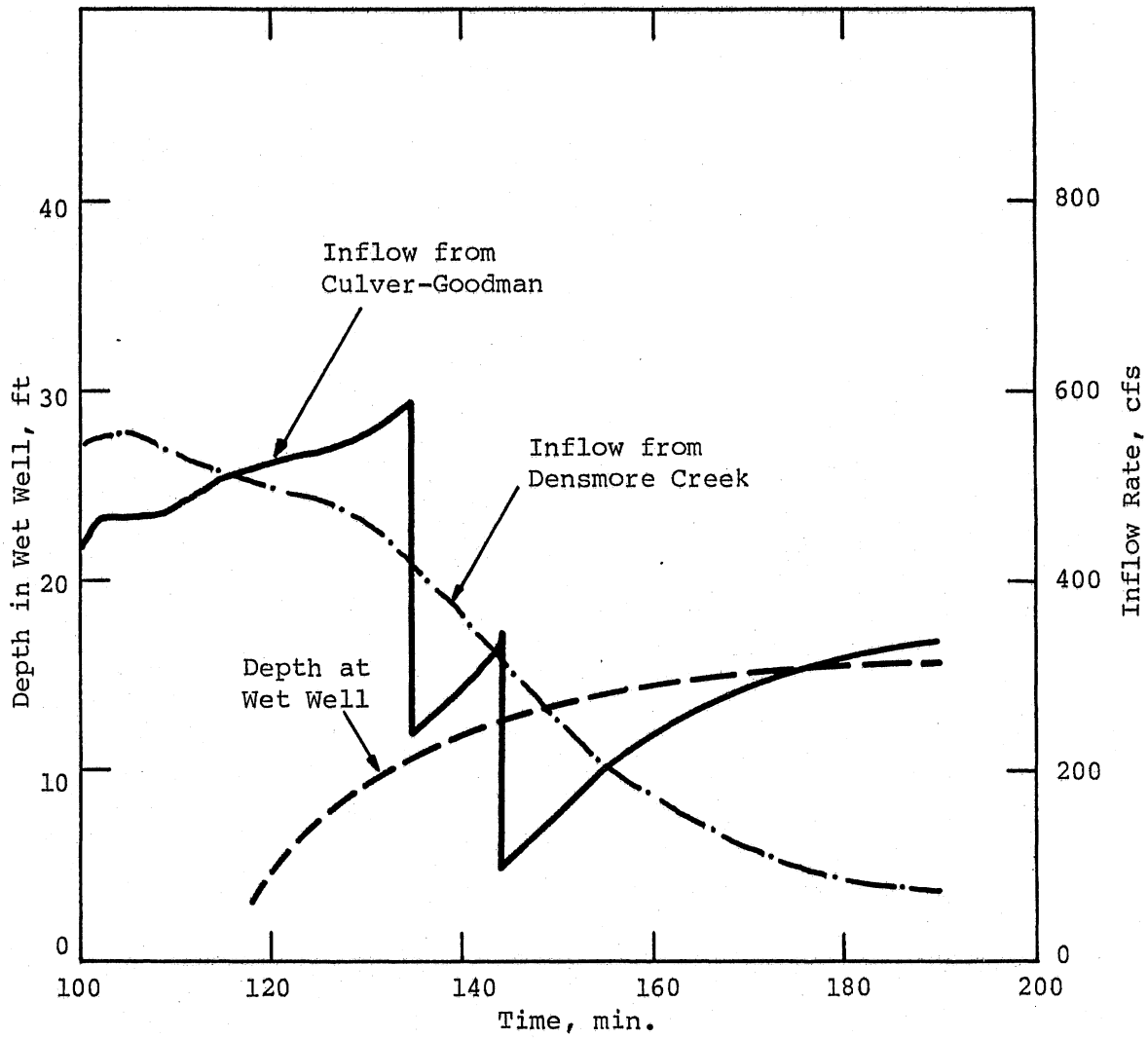

Fig. V-15. Inflow Hydrographs and the Depth at Wet Well with Increased Pumping Rate, Run V-10

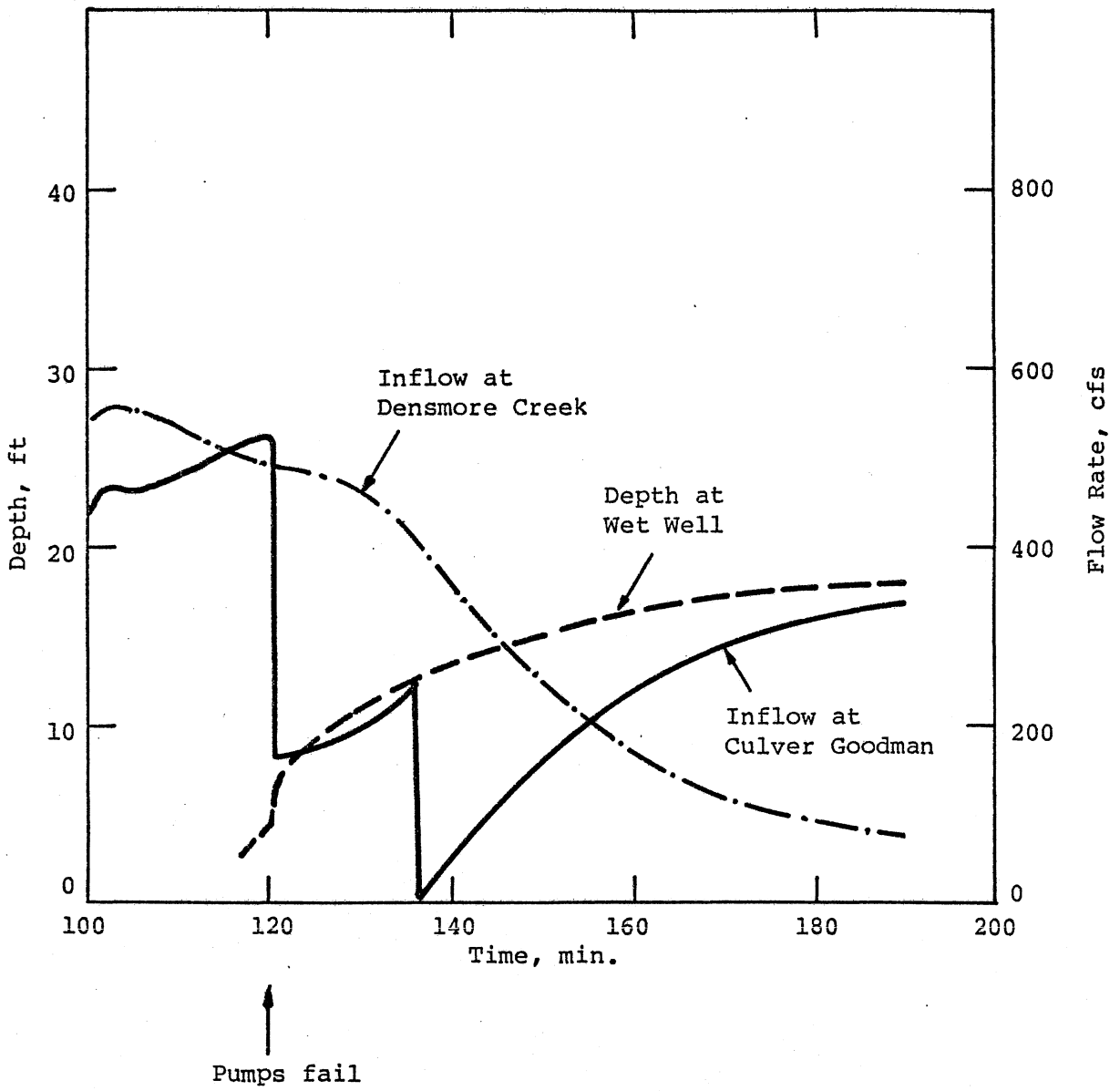

Fig. V-16. Effect of Pump Failure on the Flow Control, Run V-15

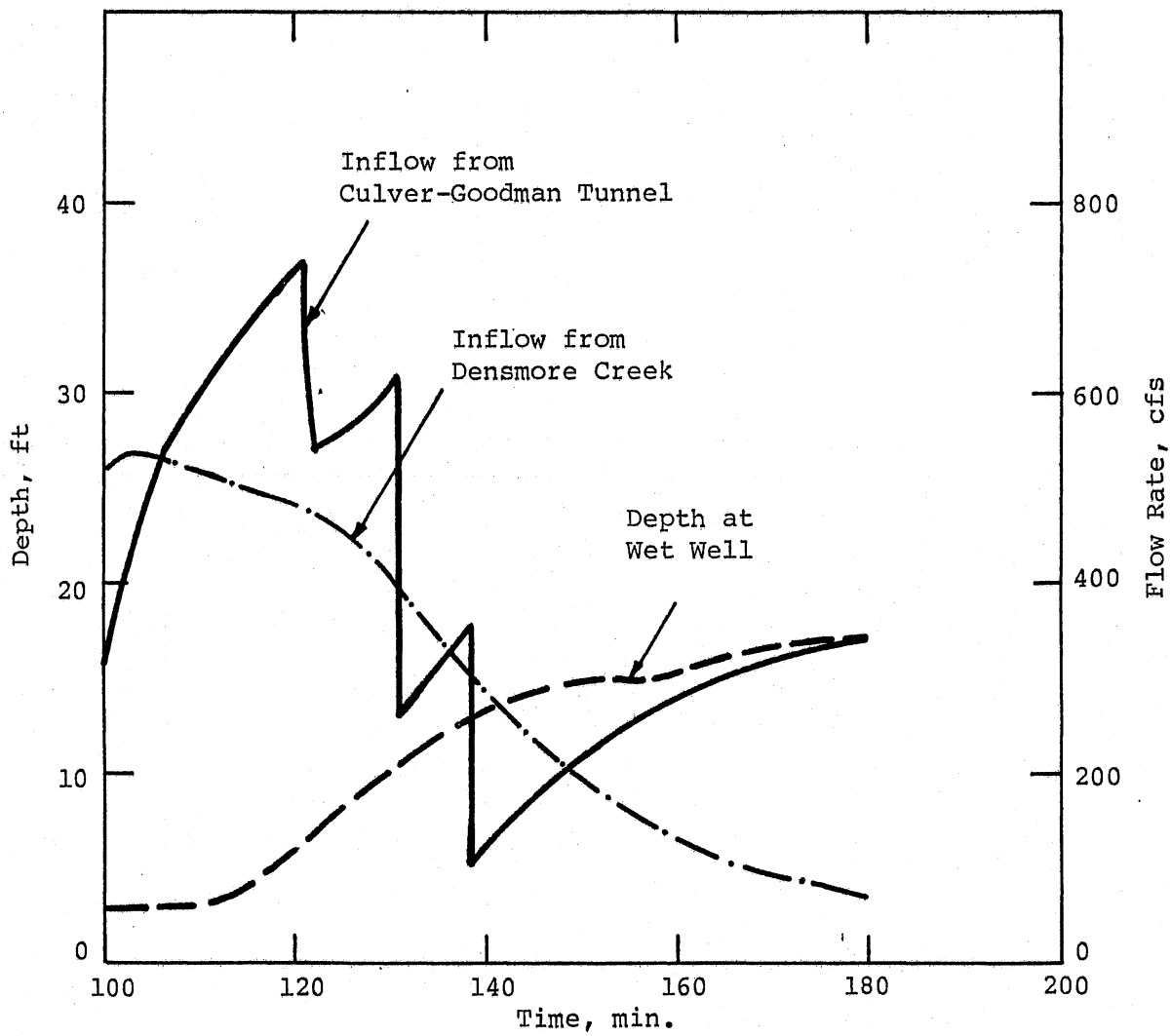

Fig. V-17. Effectiveness of Control Algorithm on 5-Year Storm, Run V-11.

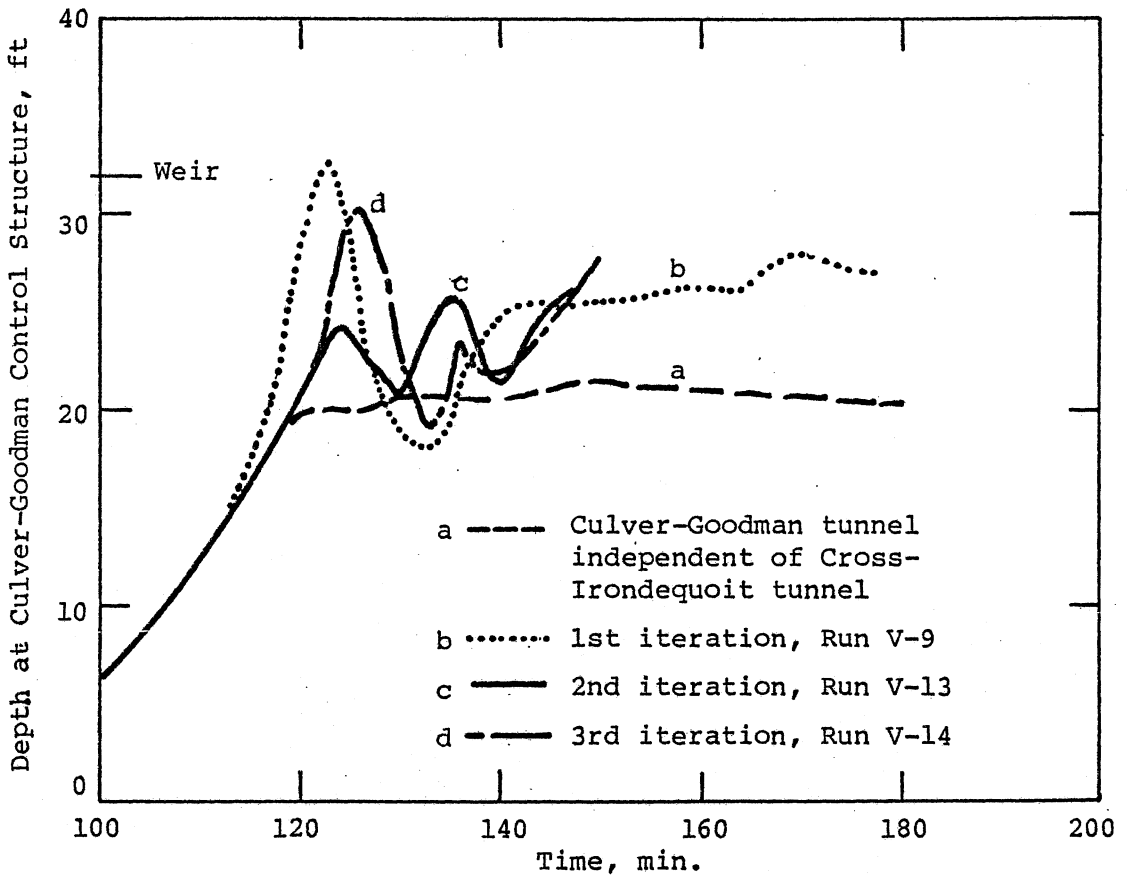

Fig. V-18. Water Depths in Culver-Goodman Tunnel Control Structure when Coupled with Cross-Irondequoit Tunnel Operation.

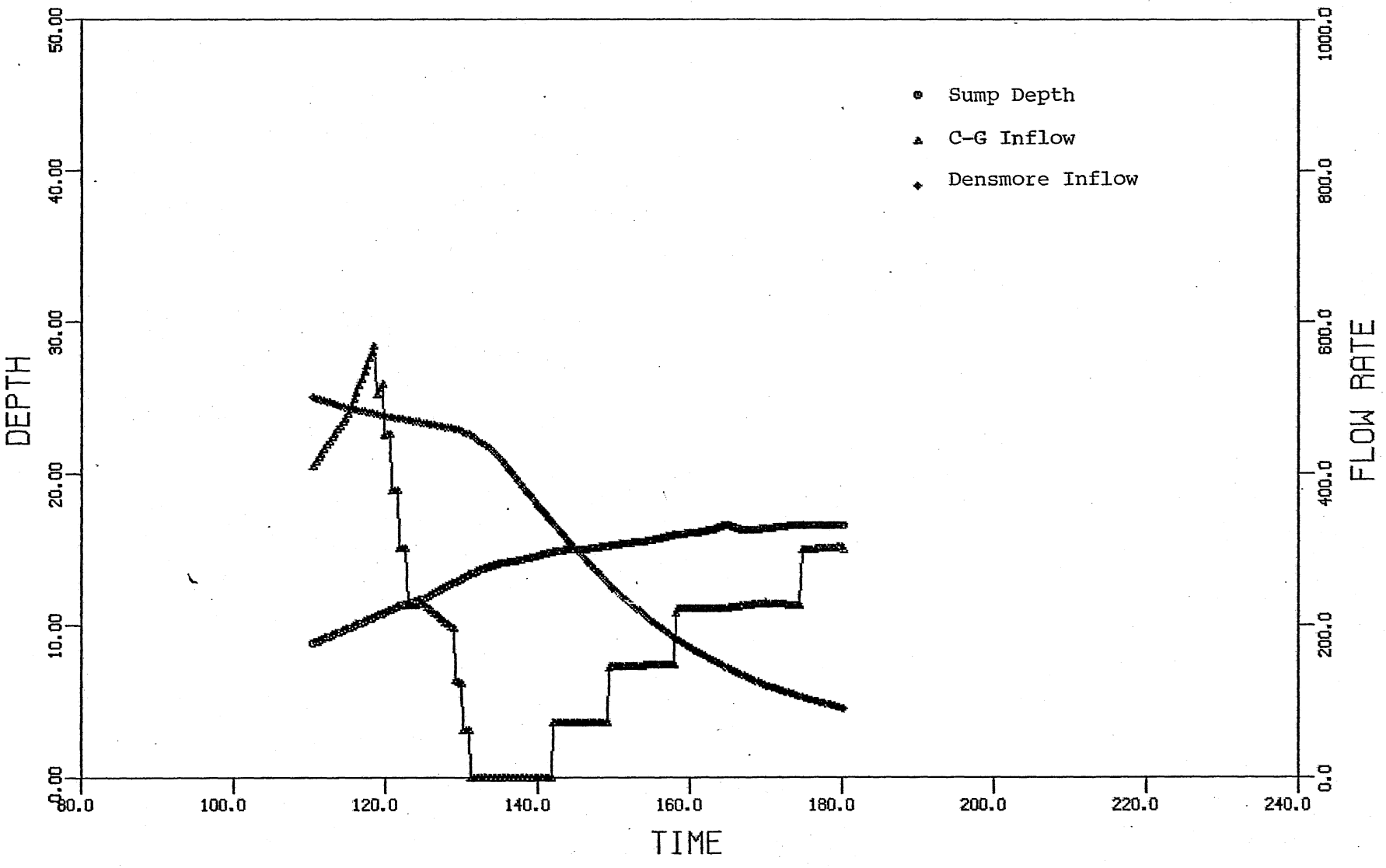

Fig. V-19. Depth at Wet Well and the Controlled Inflow Hydrograph, Run V-13, First Iteration.

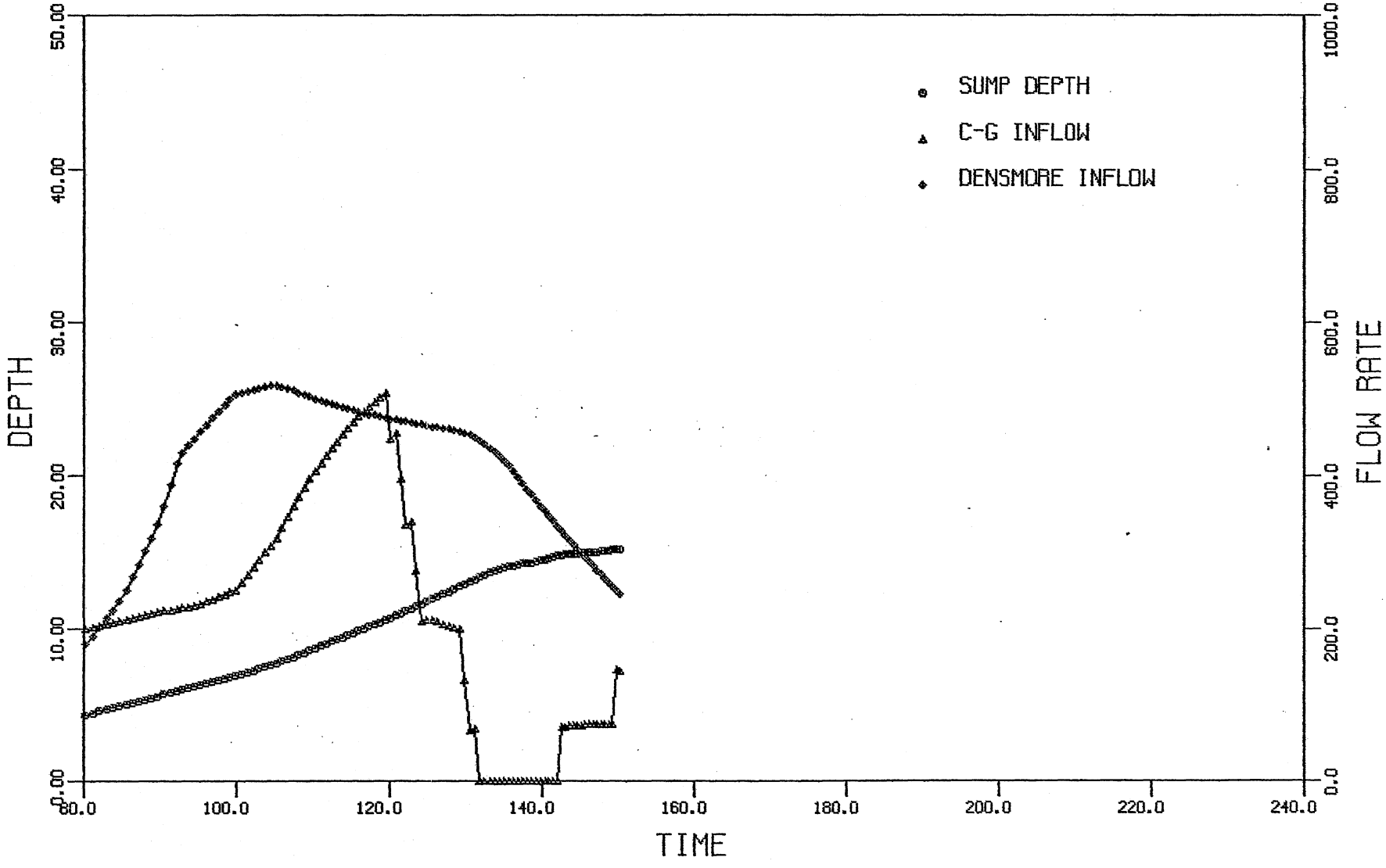

Fig. V-20. Depth at Wet Well and the Controlled Inflow Hydrograph, Run V-14, Second Iteration.

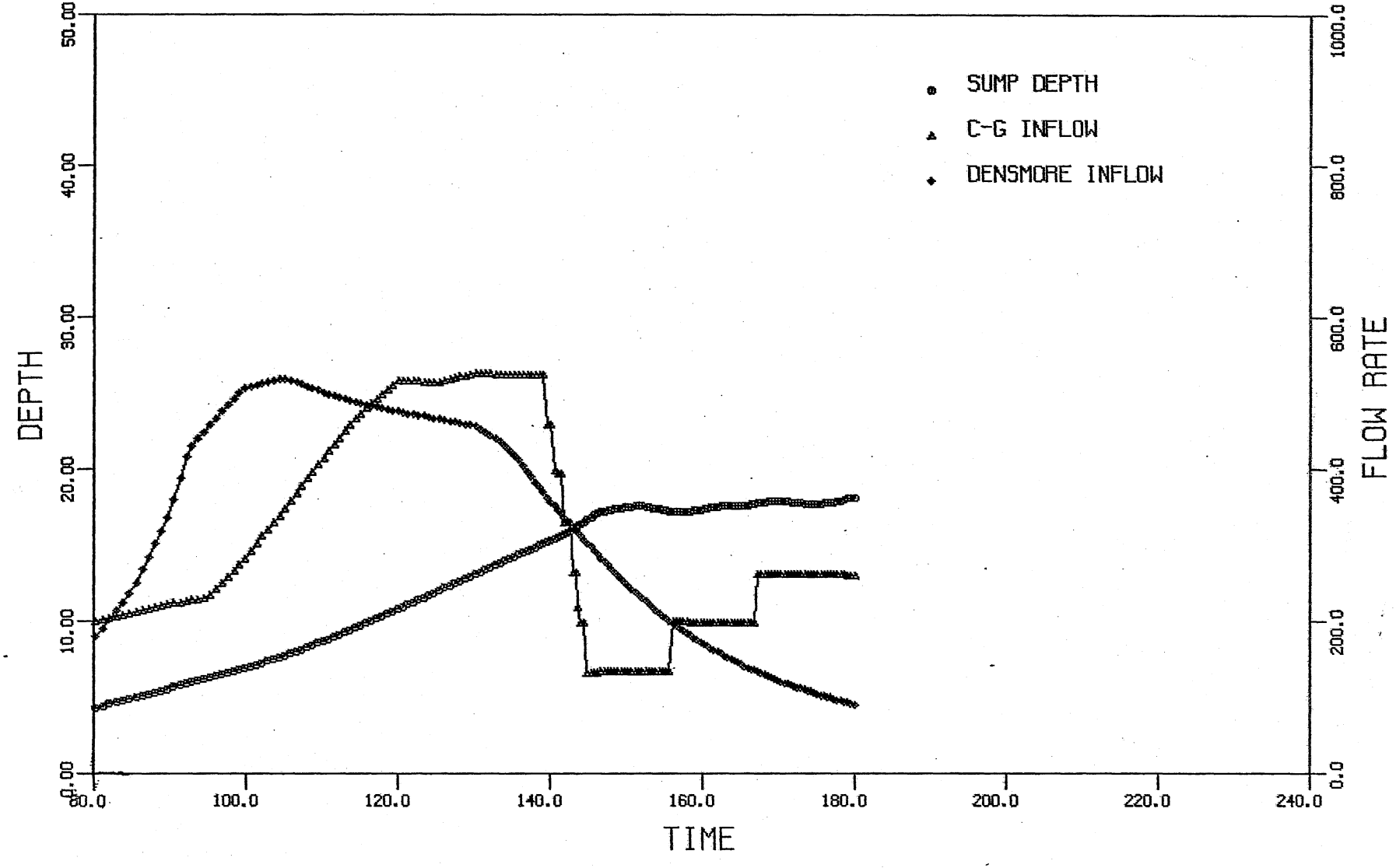

Fig. V-21. Depth at Wet Well and the Controlled Inflow Hydrograph, Run V-15.

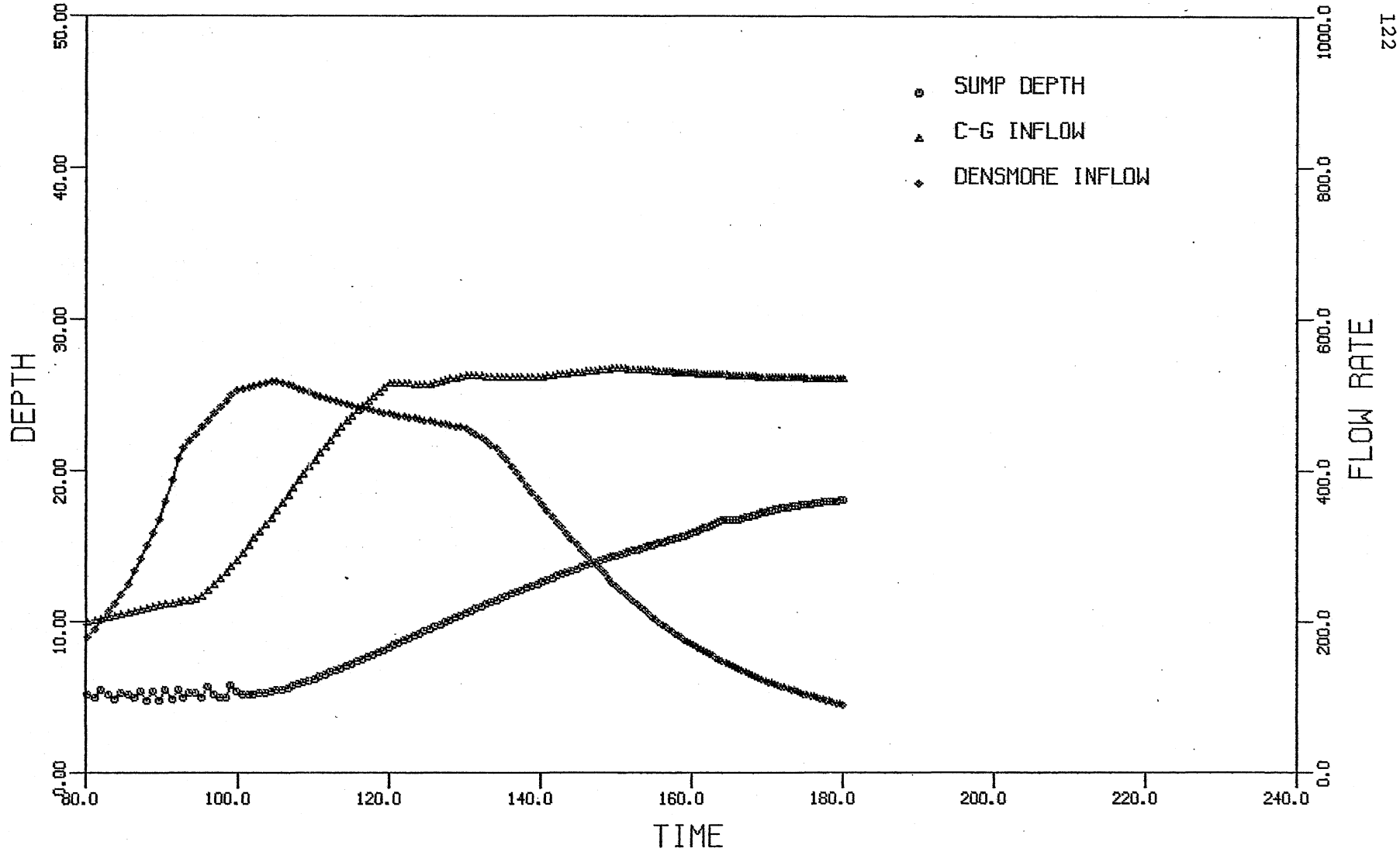

Fig. V-22. Depth at Wet Well and the Controlled Inflow Hydrograph, Run V-16.

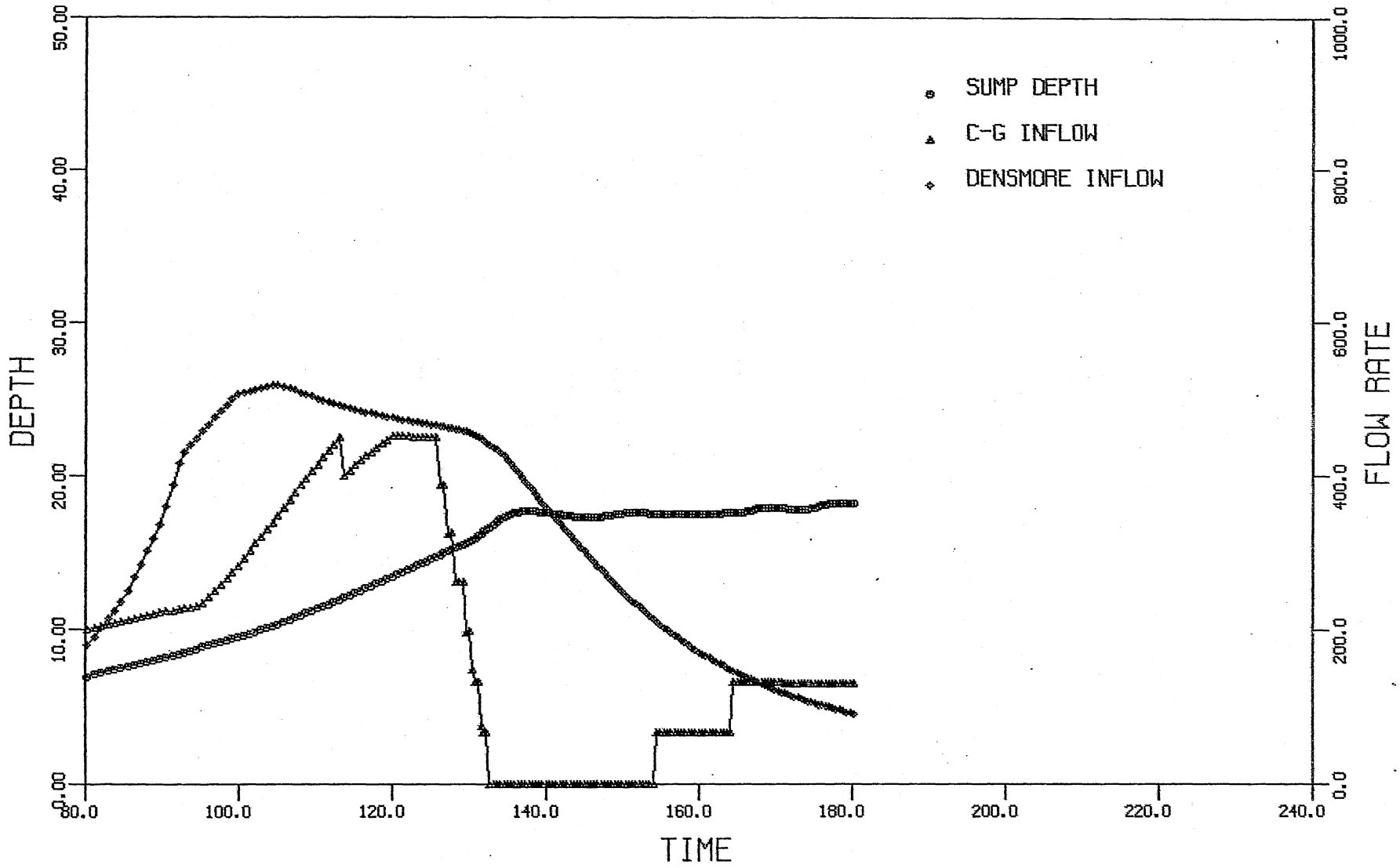

Fig. V-23. Depth at Wet Well and the Controlled Inflow Hydrograph, Run V-17.

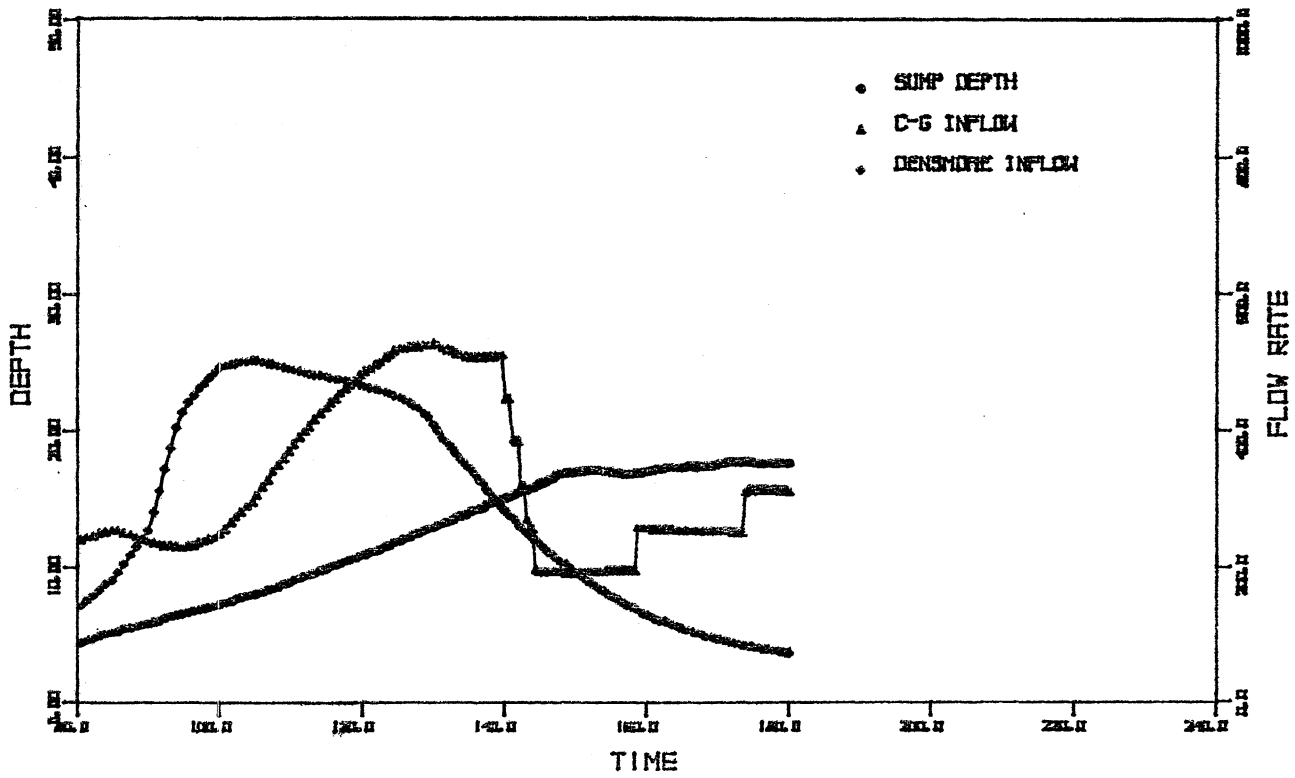

Fig. V-24. Depth at Wet Well and the Controlled Inflow Hydrograph, Run V-18, 5 Year Storm.

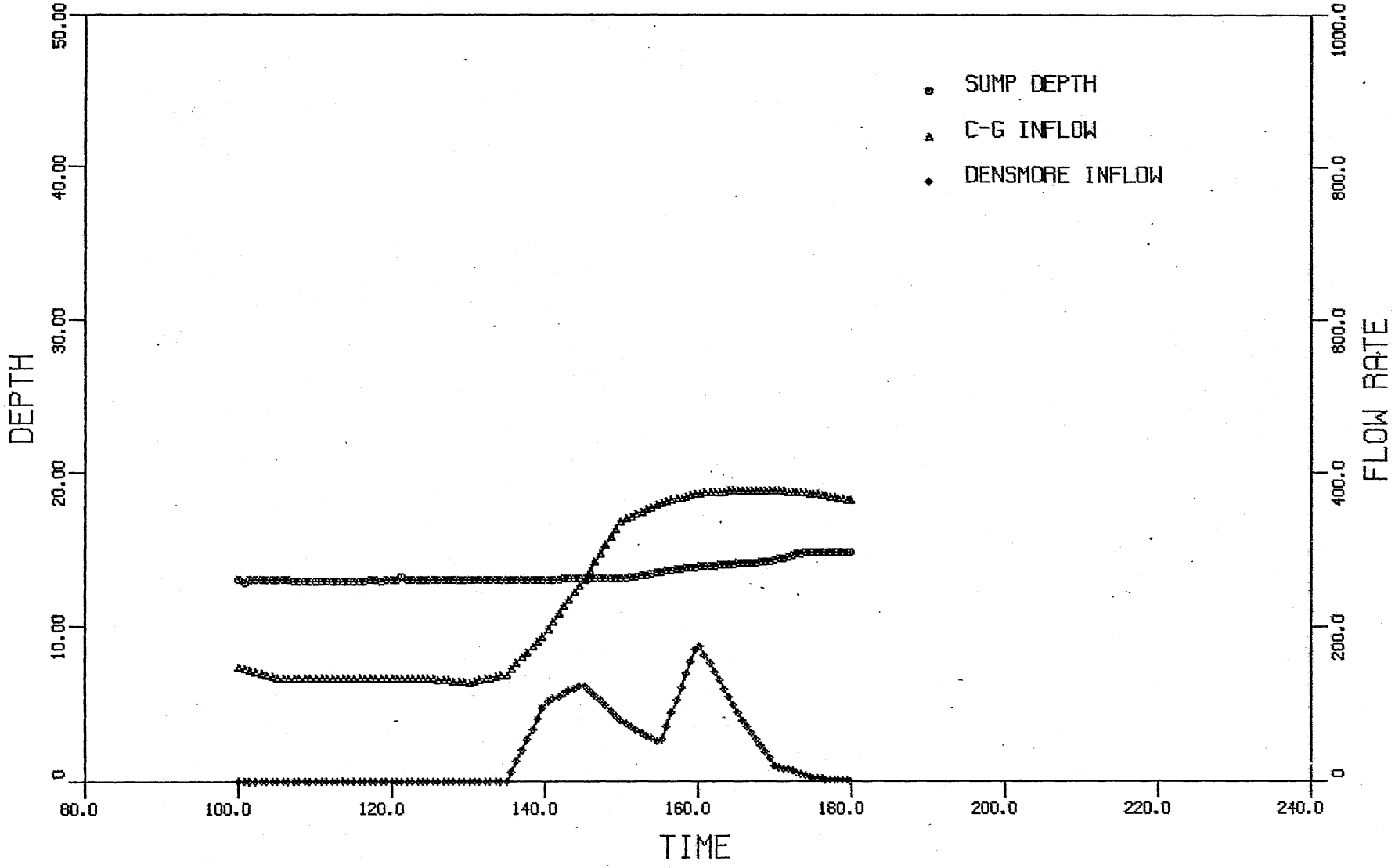

Fig. V-25. Depth at Wet Well and Controlled Inflows Due to 1 Year Storm, Run V-19.

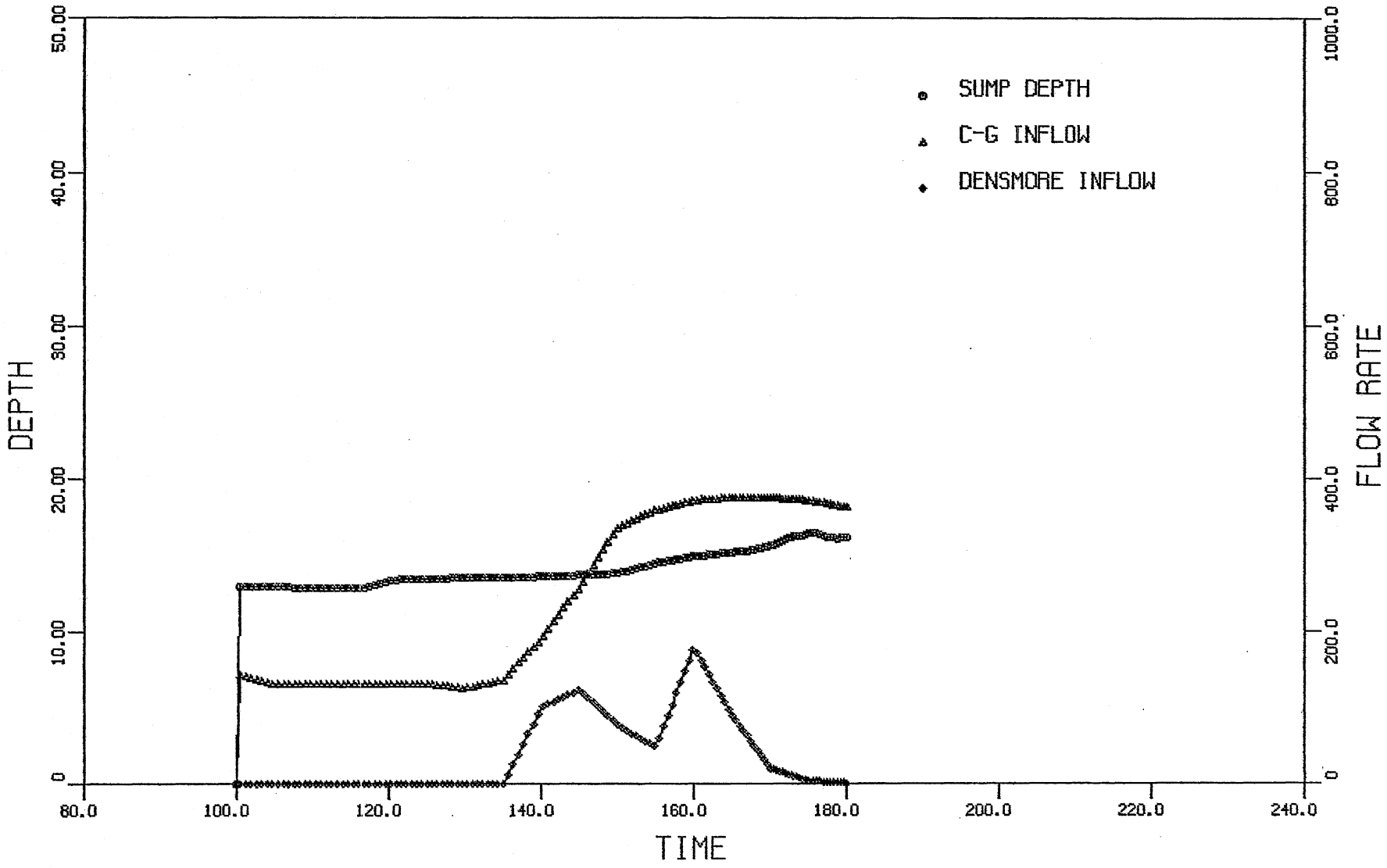

Fig. V-26. Depth at Wet Well and Controlled Inflows Due to 1 Year Storm, Run V-20.

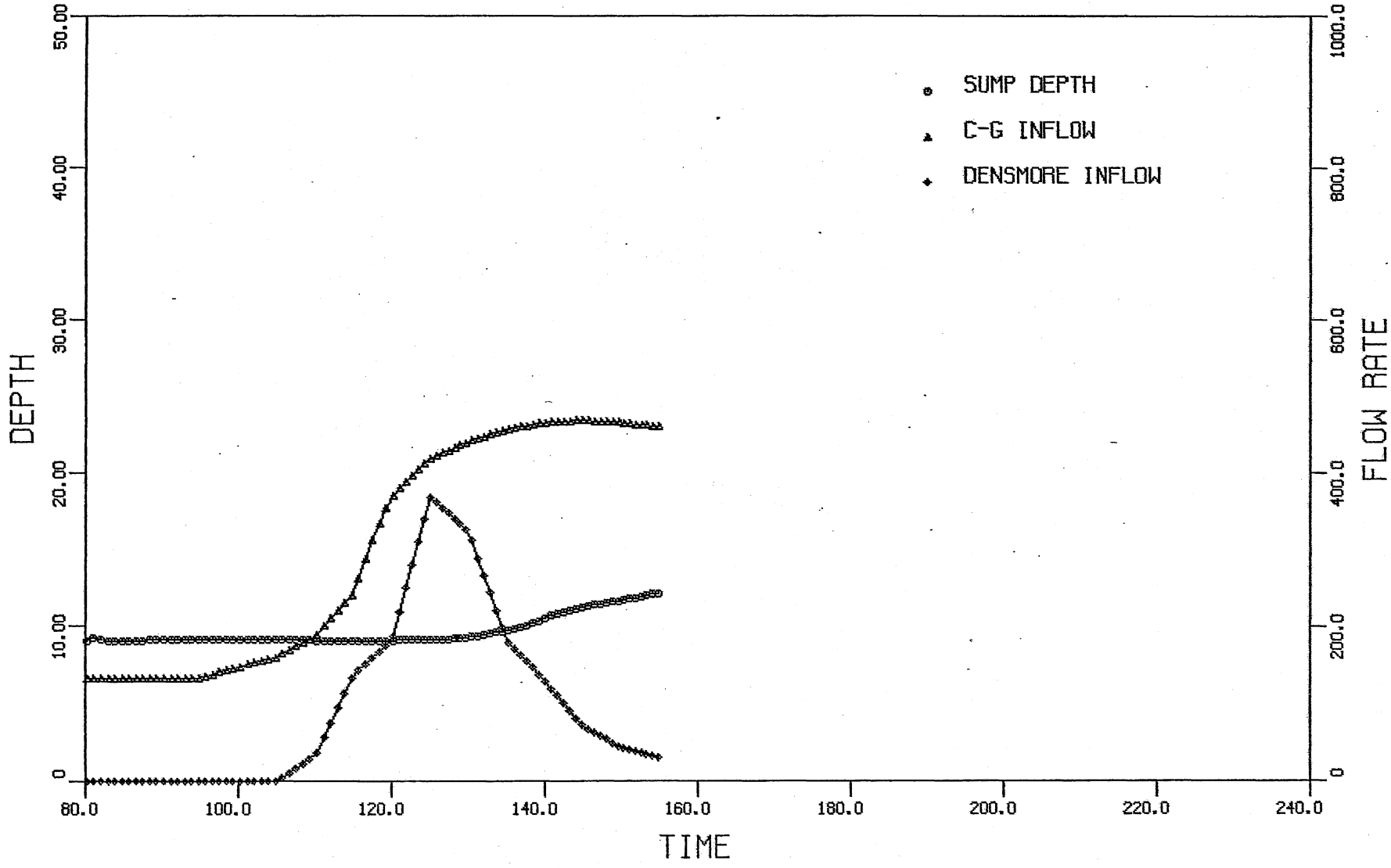

Fig. V-27. Depth at Wet Well and Controlled Inflows Due to 2 Year Storm, Run V-21.

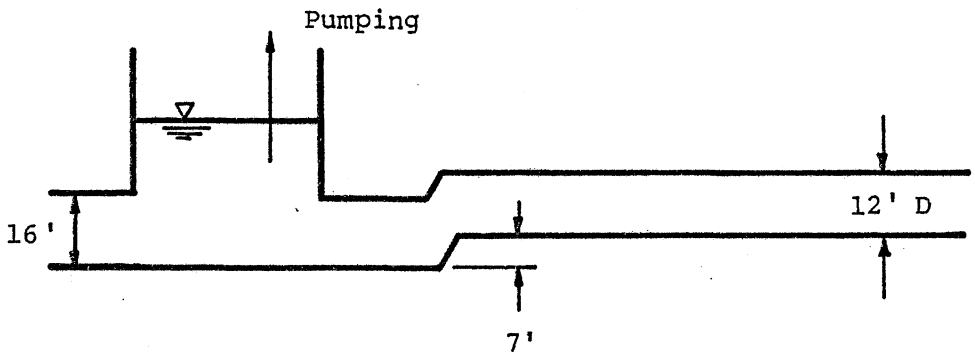

Fig. V-28. Sketch of West Side Interceptor Connection.

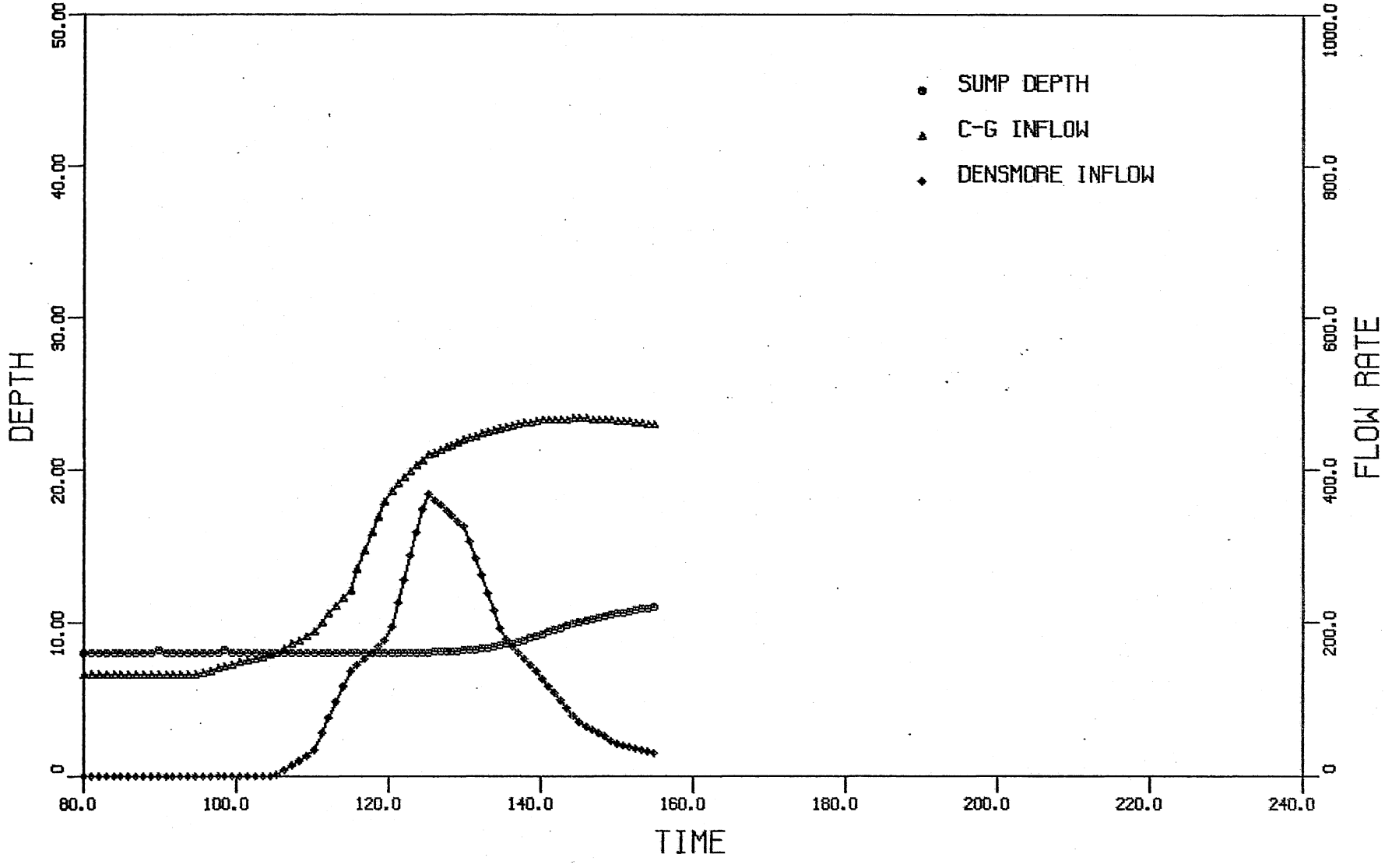

Fig. V-29. 2 Year Storm with West Side Interceptor,Initial Condition 8 ft at Downstream End and Pumping Rate 124 cfs, Run V-22.

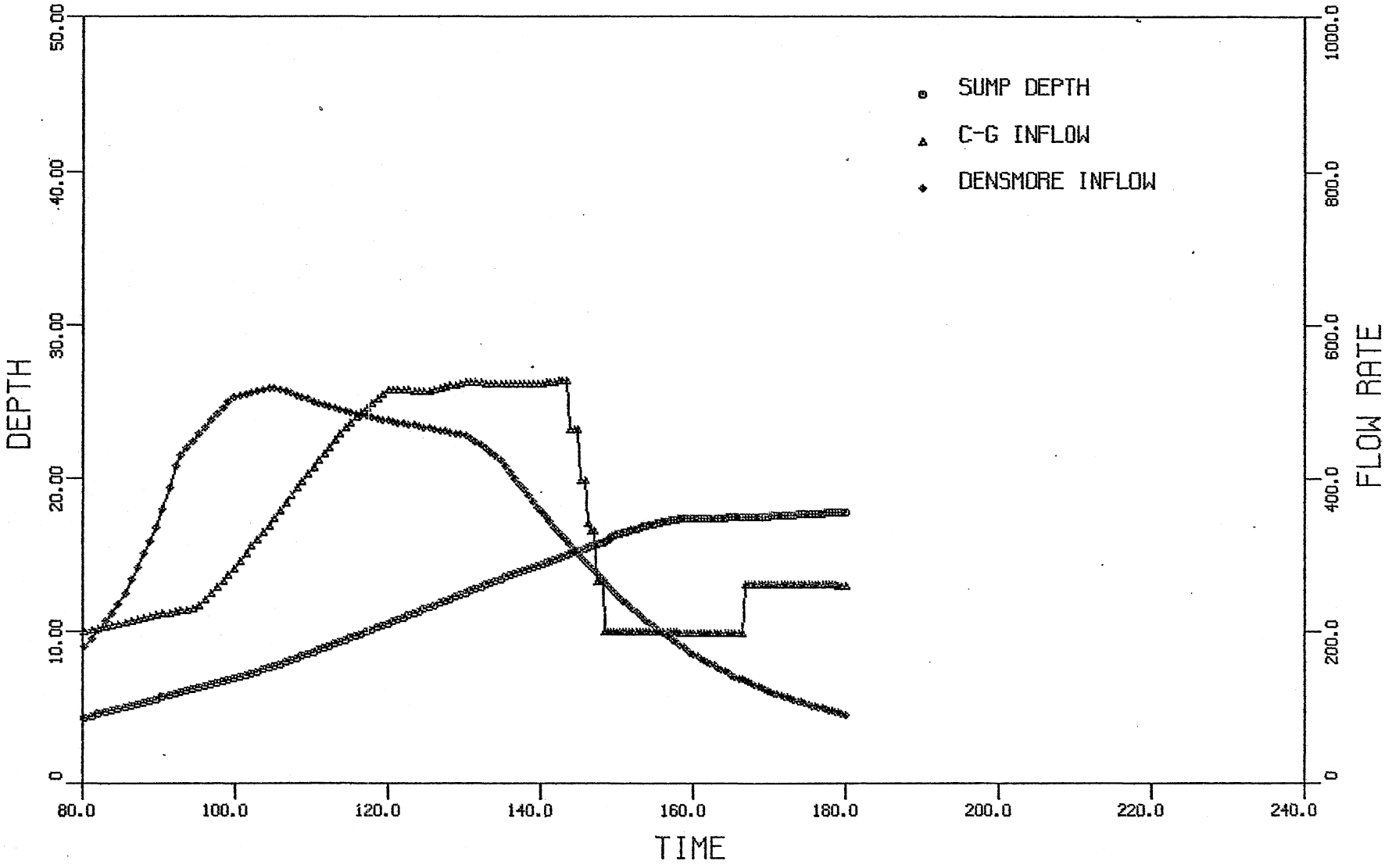

Fig. V-30. 10 Year Storm with West Side Interceptor. Tunnel Initially Empty and a Pumping Rate of 124 cfs, Run V-23.

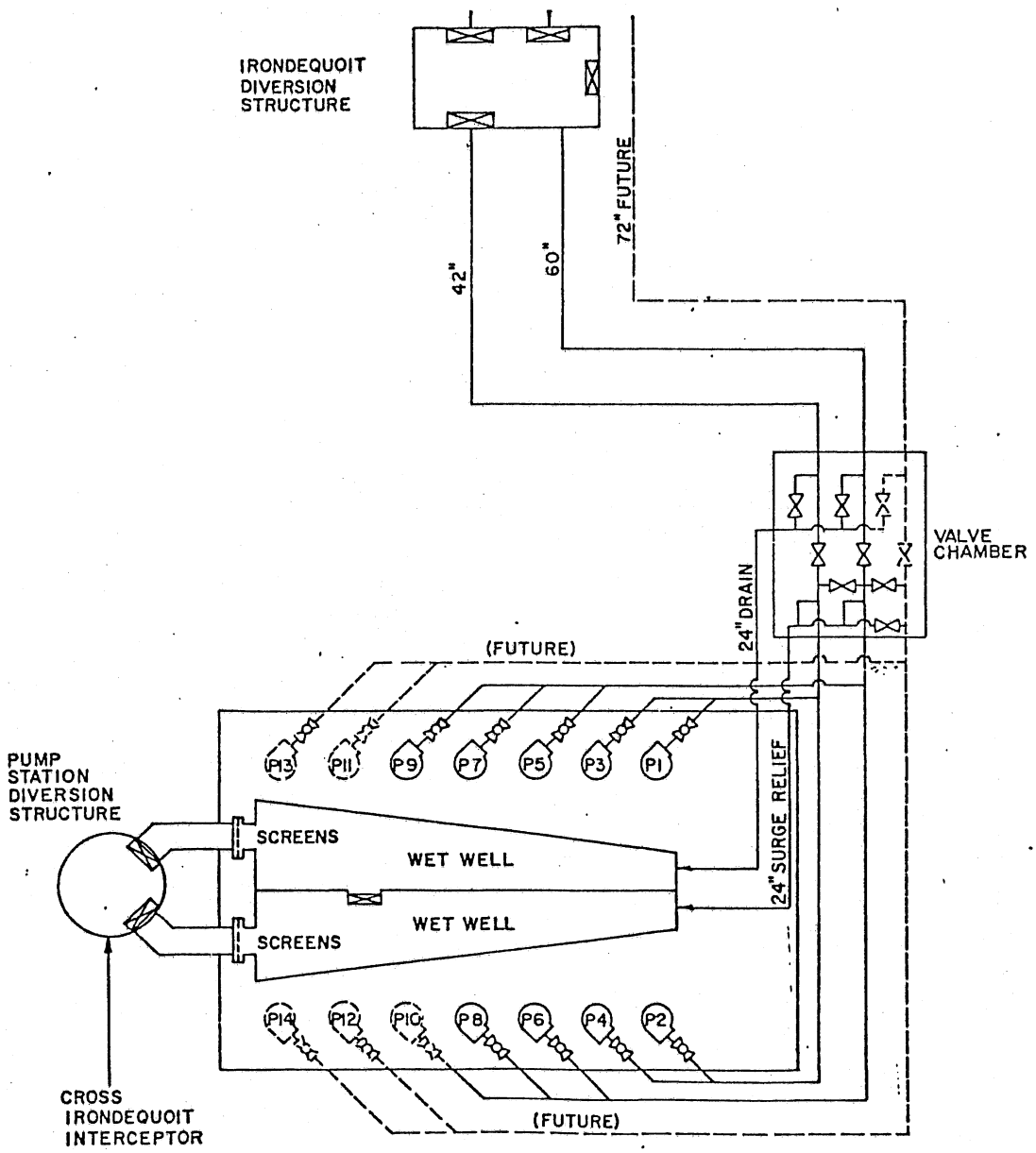

Fig. VI-1. Cross Irondequoit Pump Station.

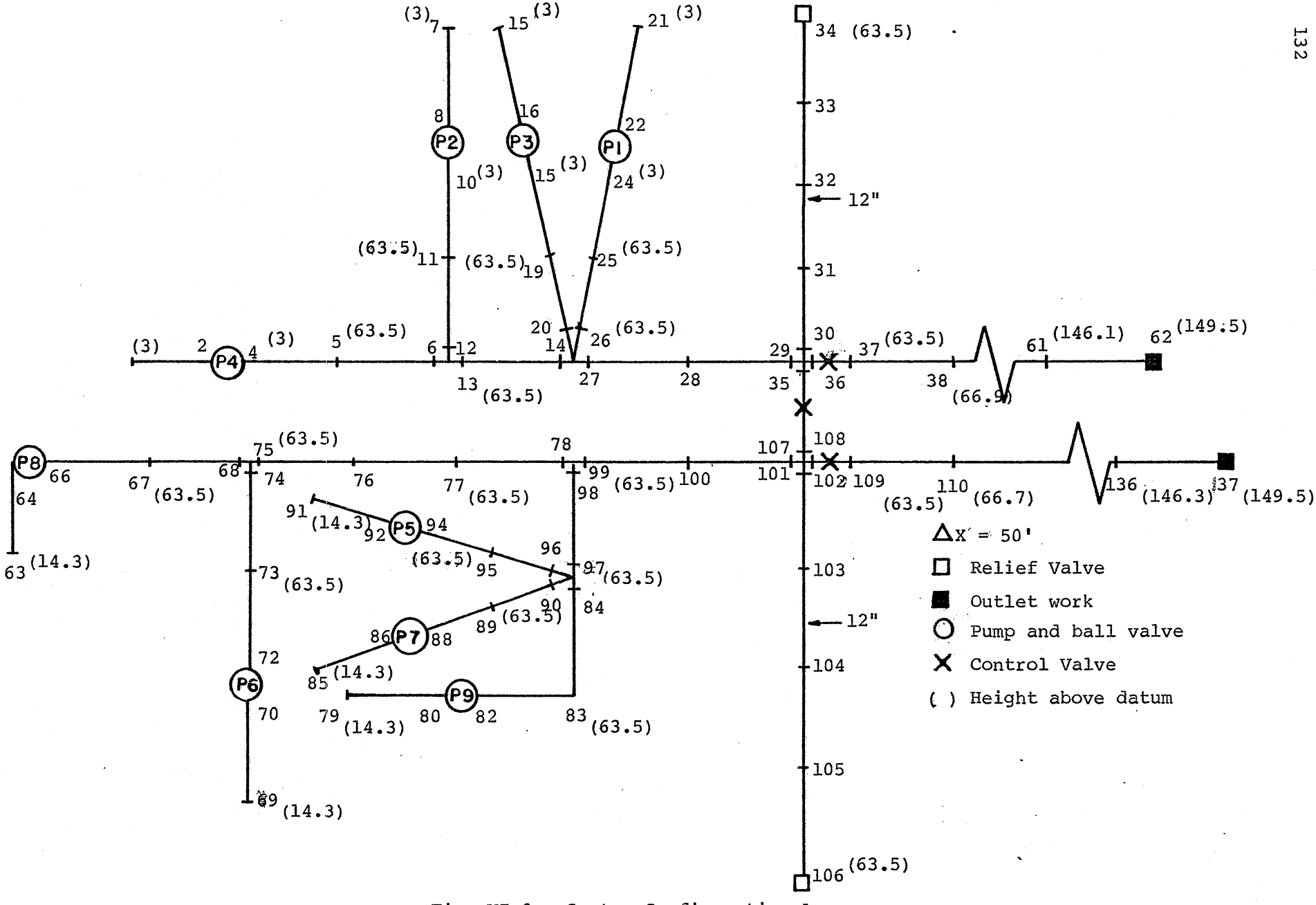

Fig. VI-2. System Configuration A.

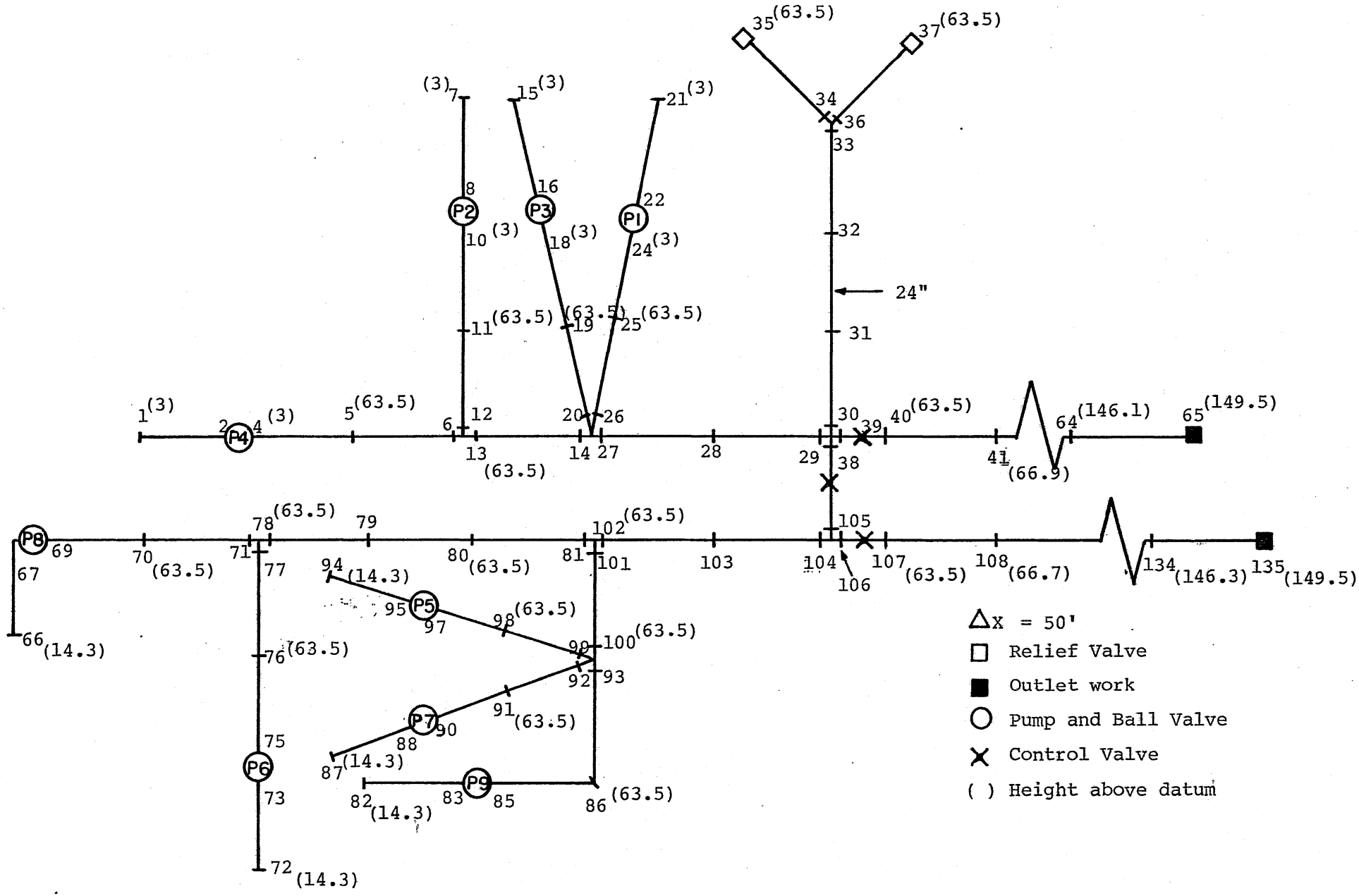

Fig. VI-3. System Configuration B.

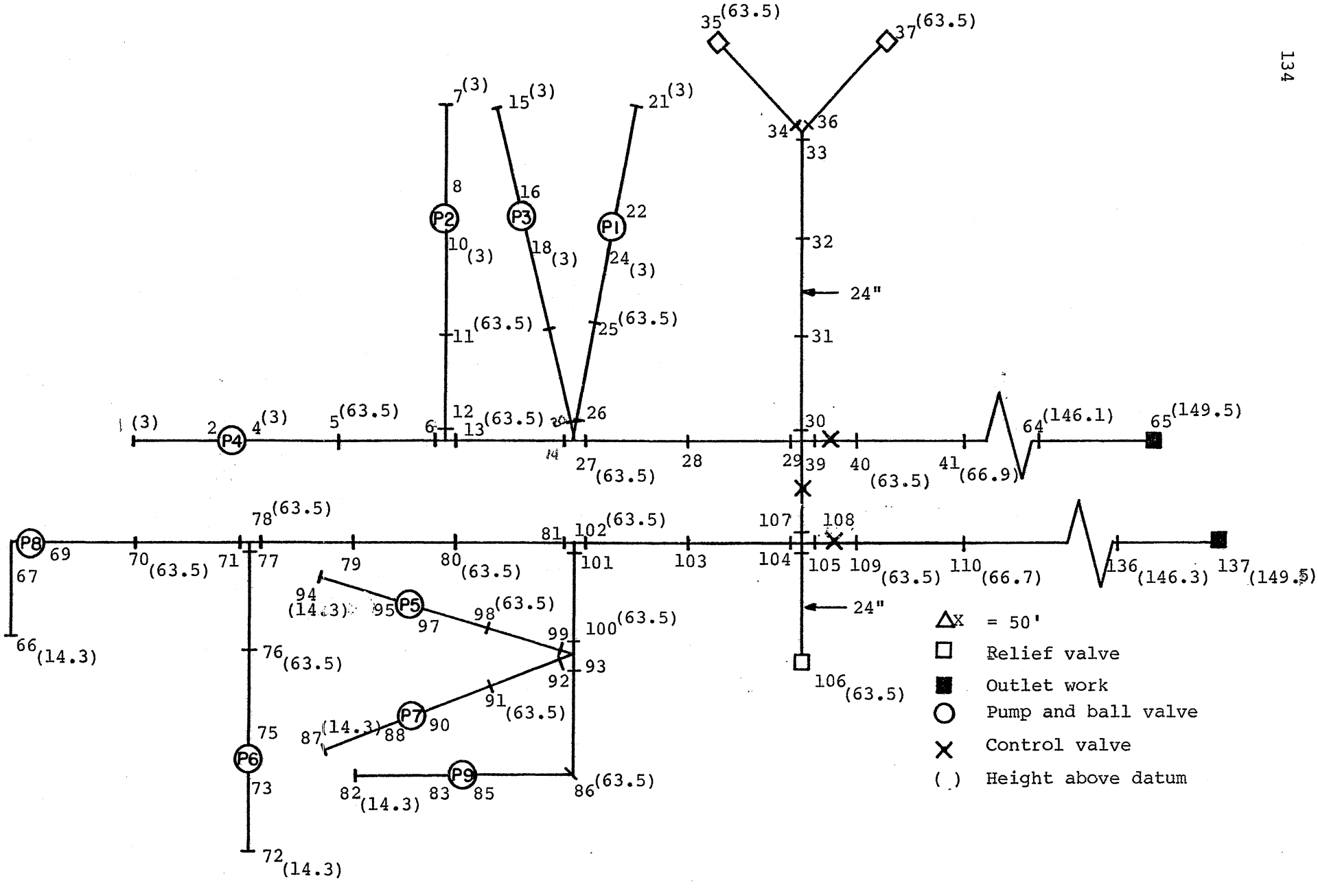

Fig. VI-4. System Configuration C.

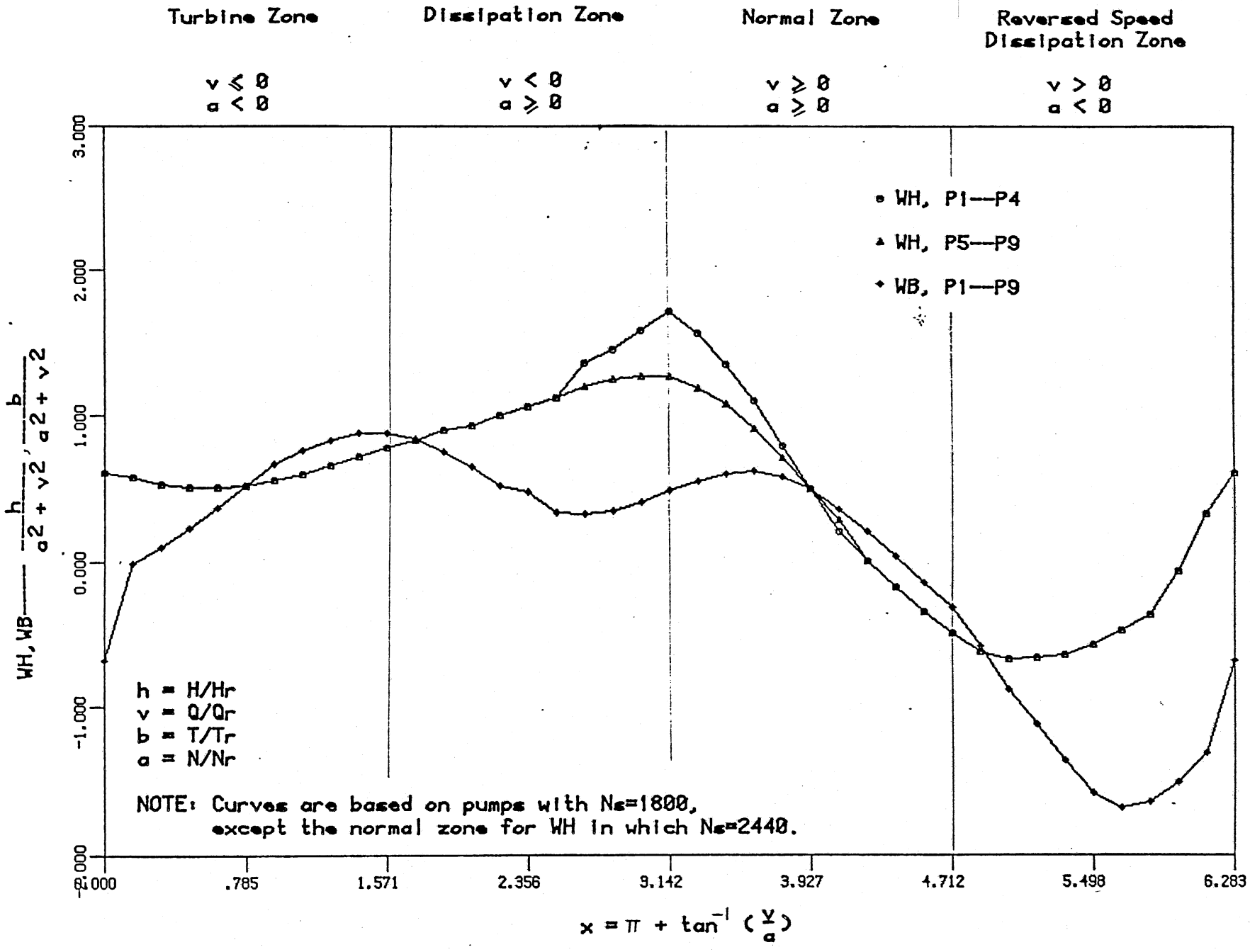

Fig. VI-5. Complete Pump Characteristics.

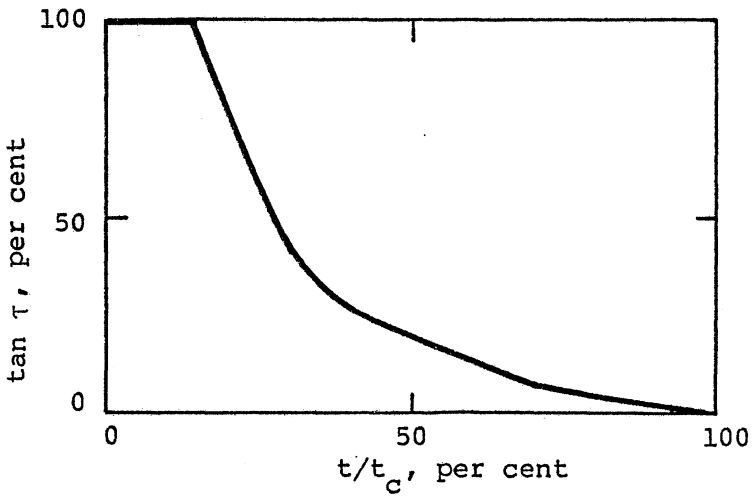

Fig. VI-6. Ball Valve Operating Characteristic.

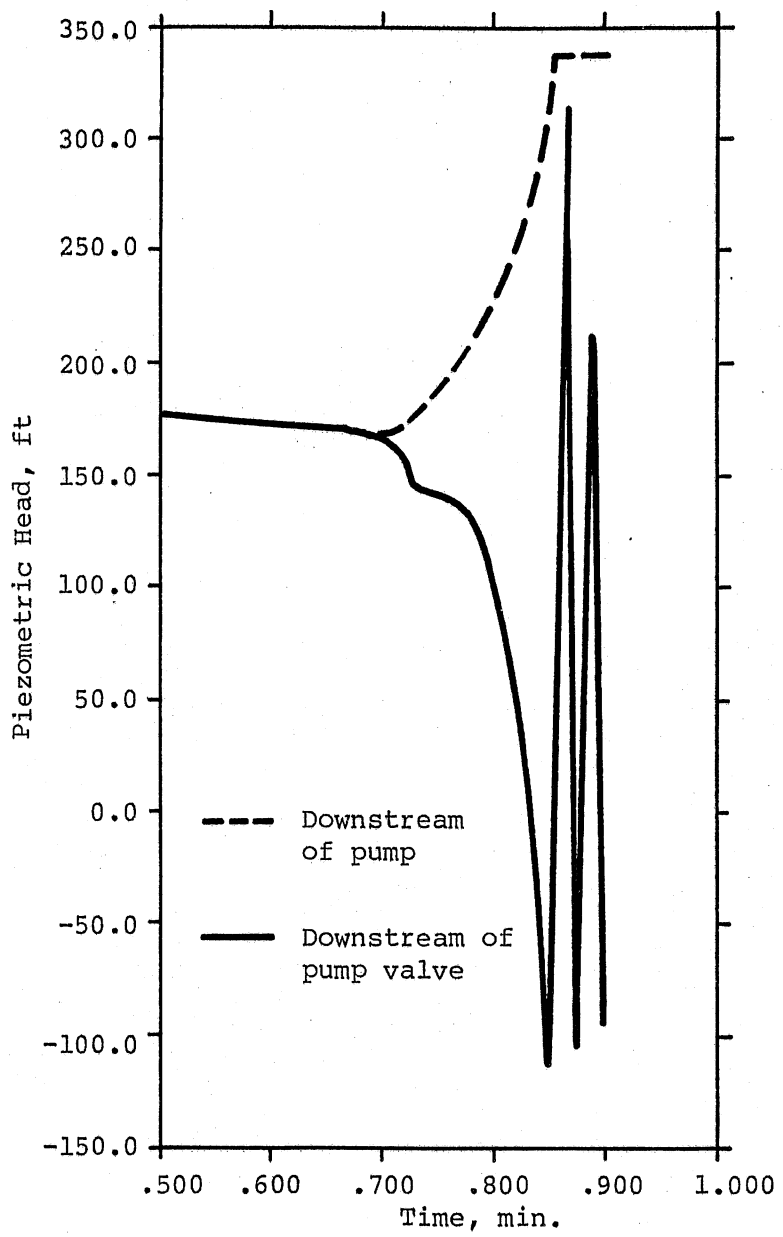

Fig. VI-7. Piezometric Heads at Pump 4, Pump Shutdown, Run VI-1.

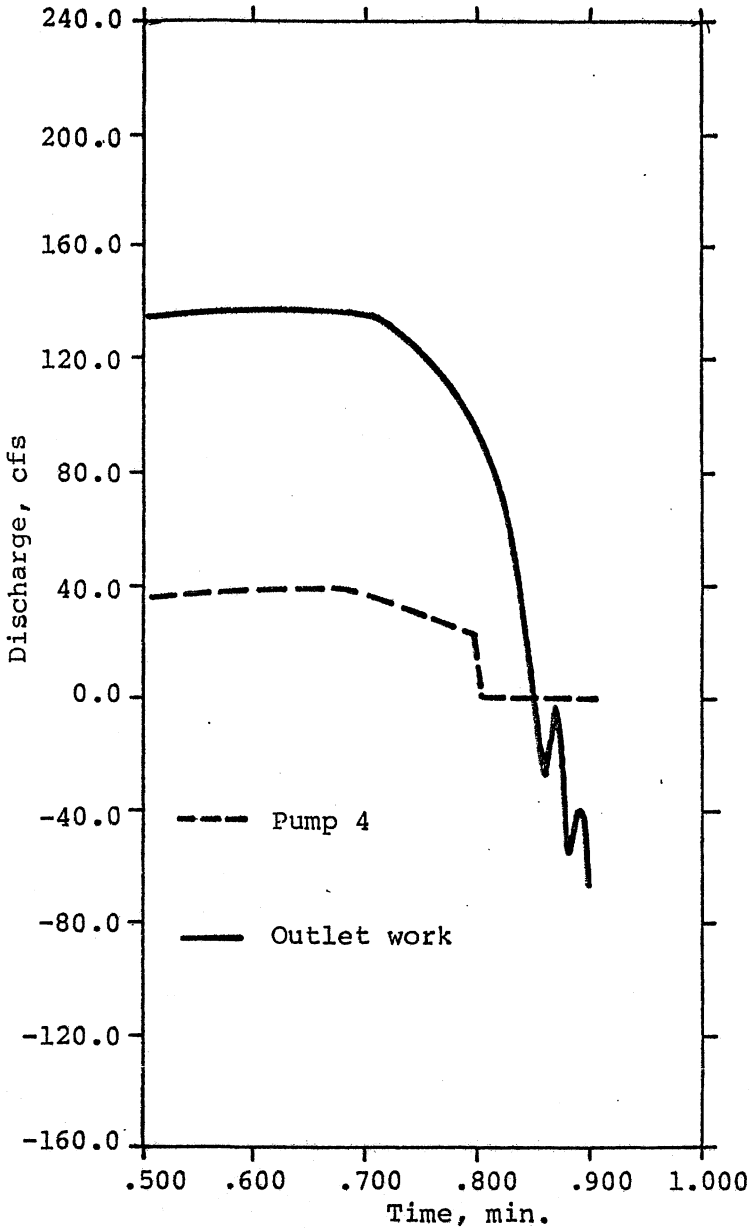

Fig. VI-8. Pumping Rate and Discharge on the 42" Pipe, Pump Shutdown, Run VI-1.

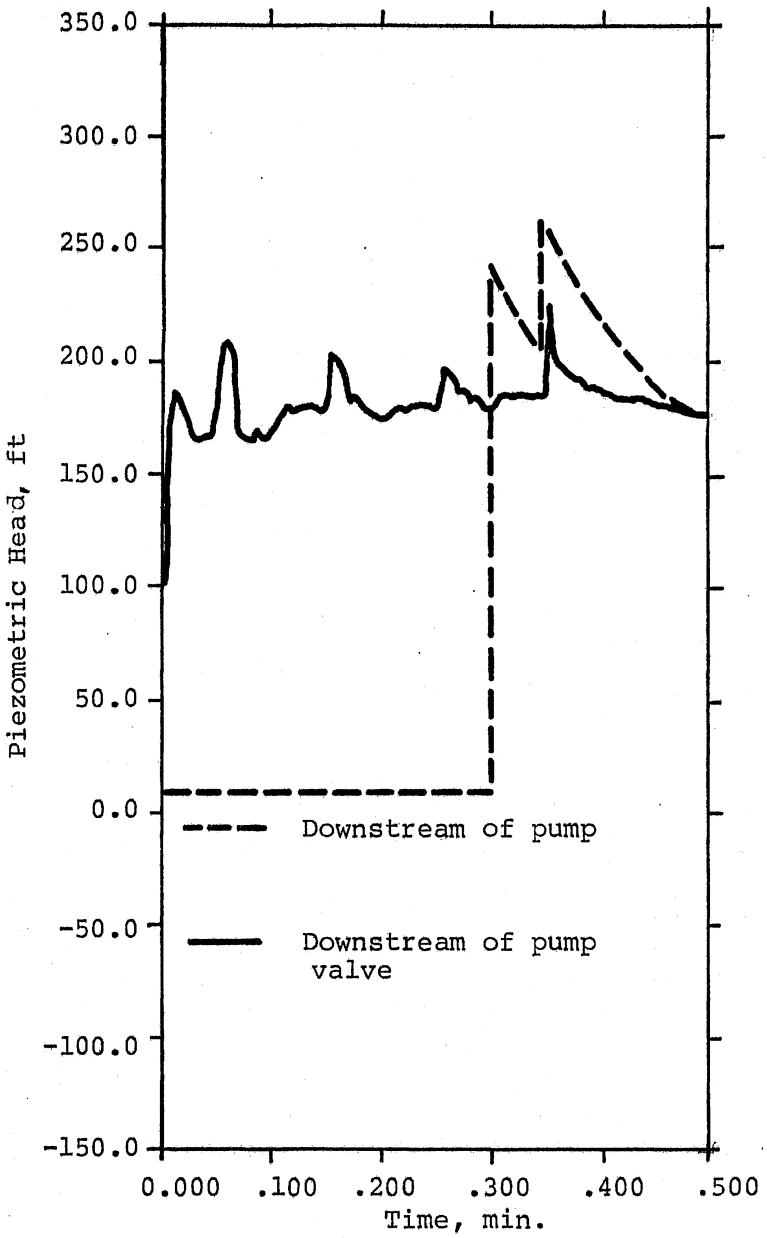

Fig. VI-9. Piezometric Heads at Pump 4, Pump Start-up, Run VI-2.

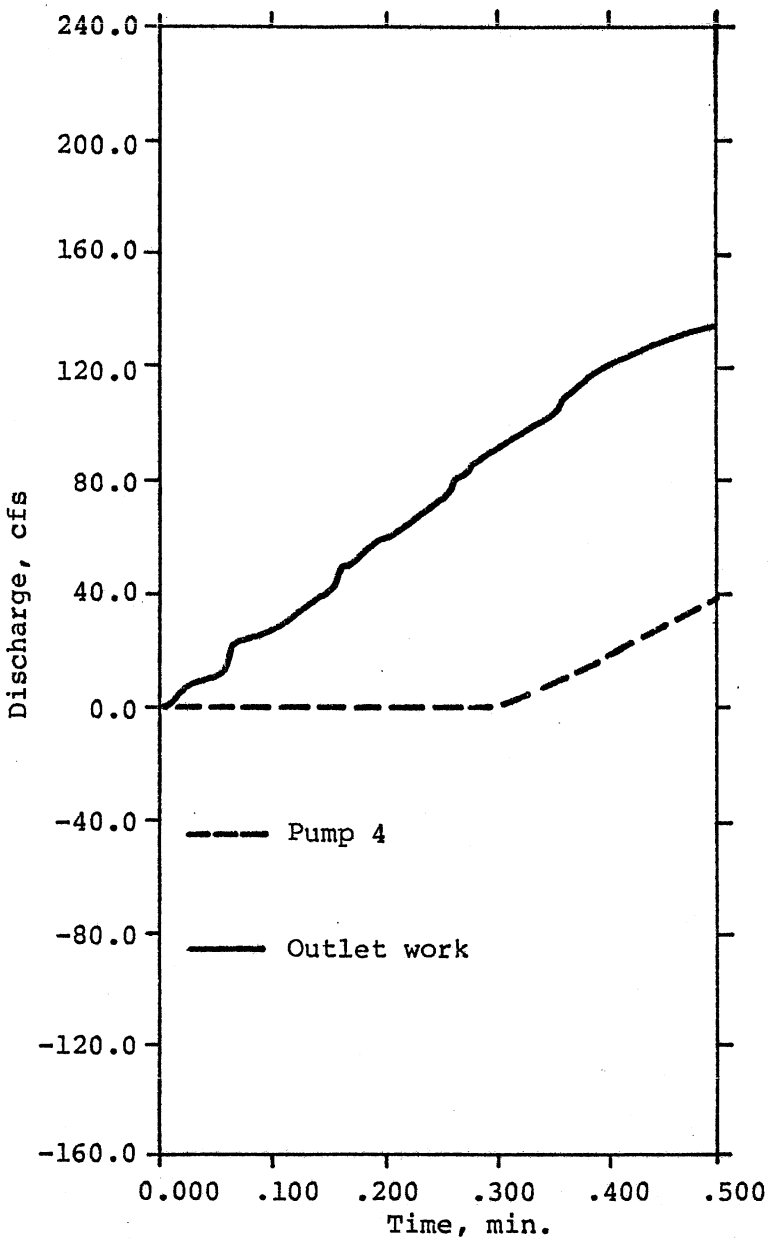

Fig. VI-10. Pumping Rate and Discharge on the 42" Pipe, Pump Start-up, Run VI-2.

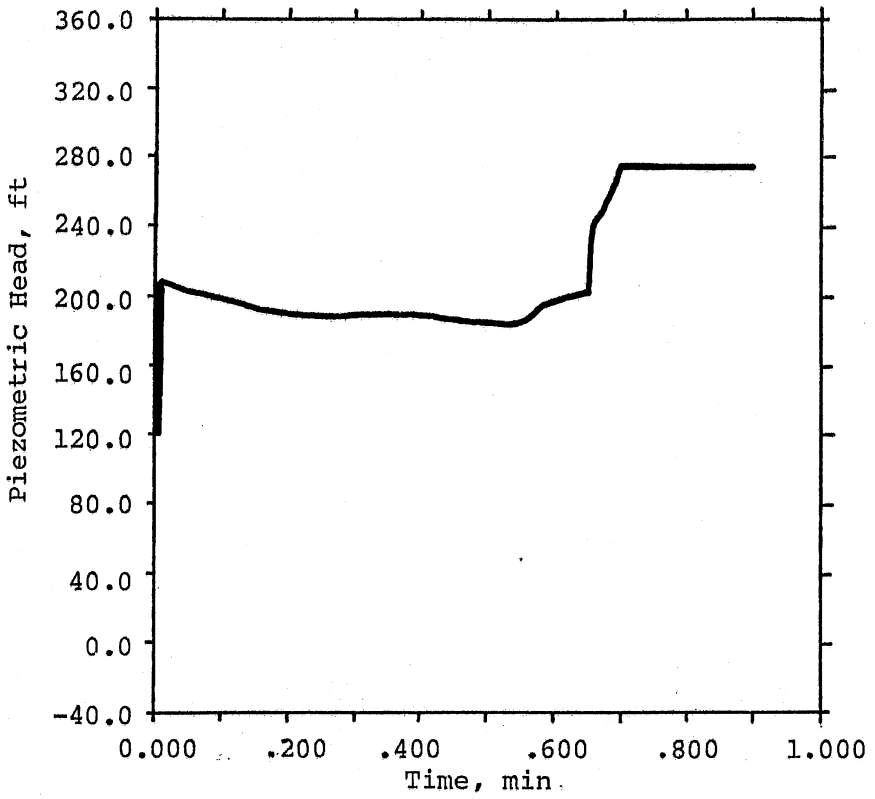

(a) Downstream of Pump.

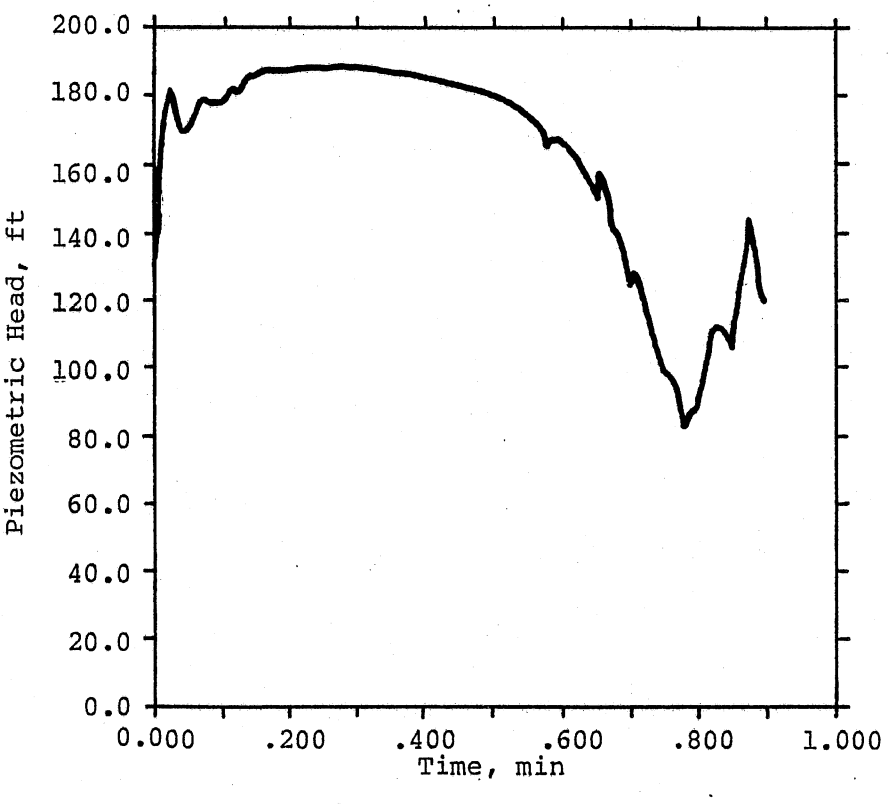

(b) Downstream of Pump Valve.

Fig. VI-11. Piezometric Heads at Pump 5, Pump Start-up and Shutdown, Run VI-3.

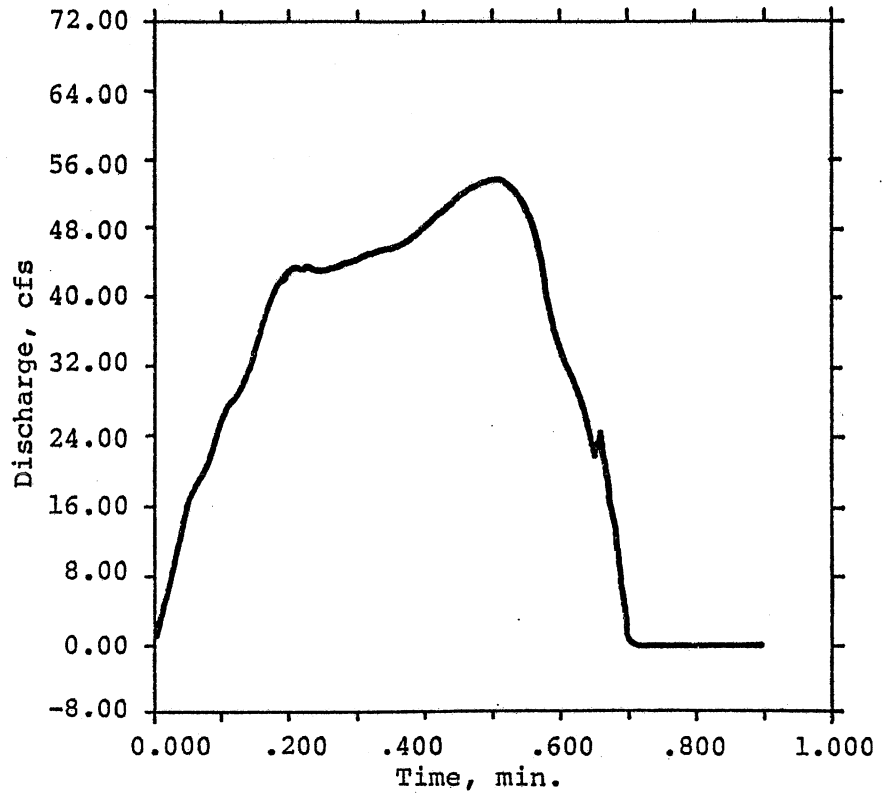

(a) Pump No. 5.

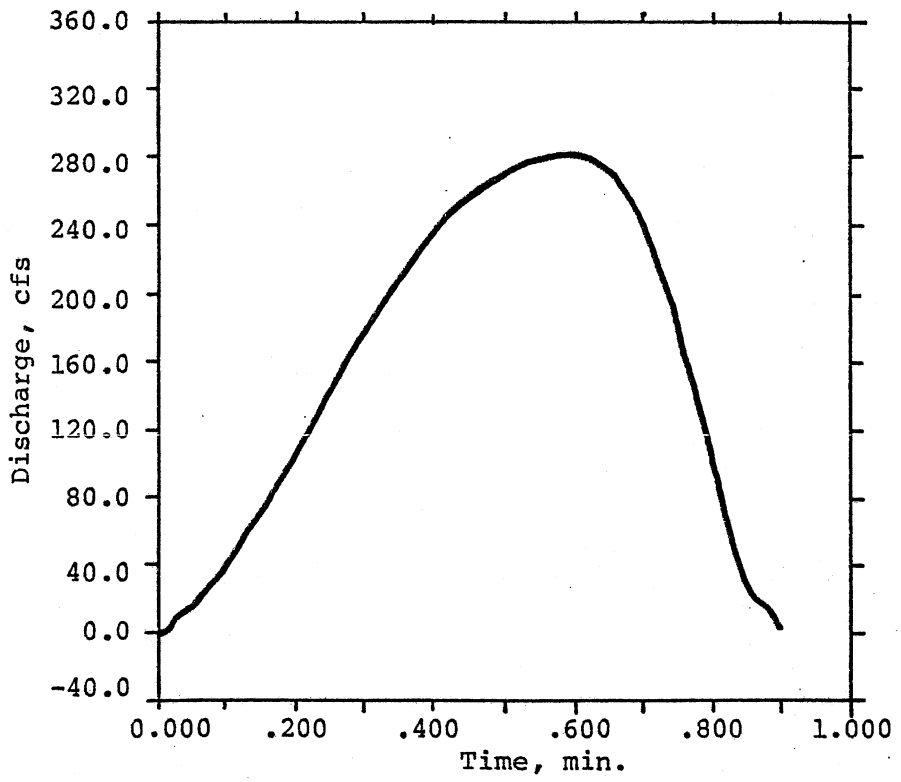

(b) Total Discharge.

Fig. VI-12. Pumping Rate and Discharge on the 60" Pipe, Run VI-3.

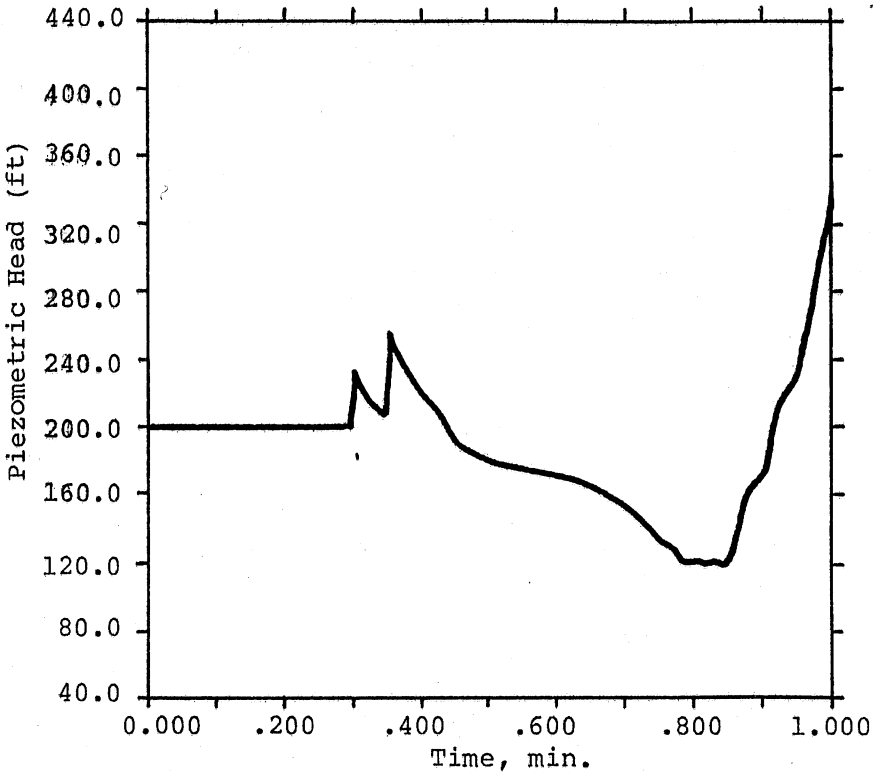

(a) downstream of pump.

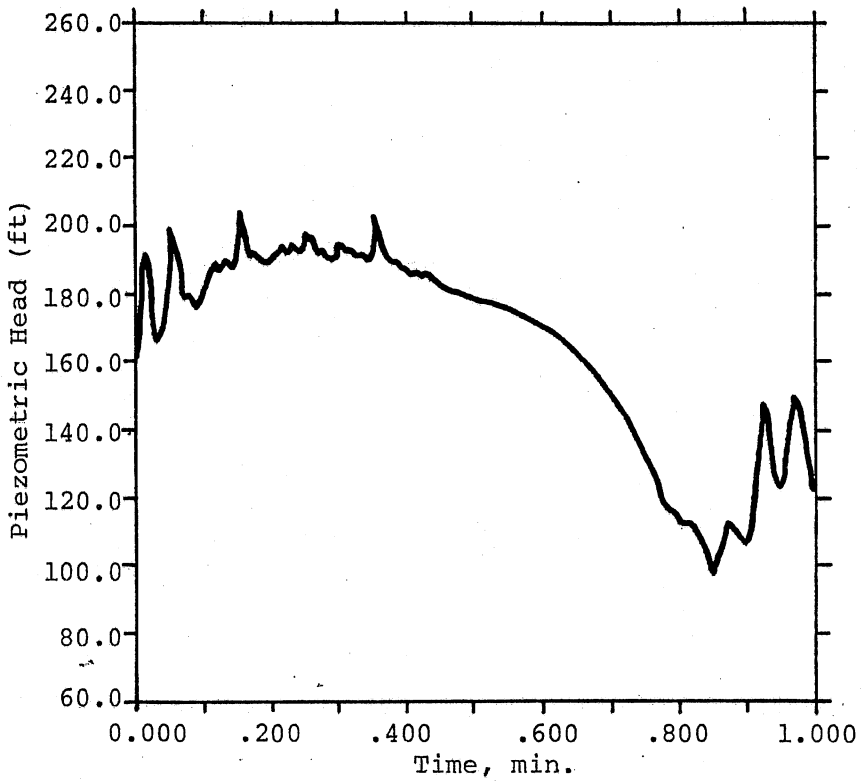

(b) downstream of pump valve.

Fig. VI-13. Piezometric Heads of Pump 4, Run VI-4.

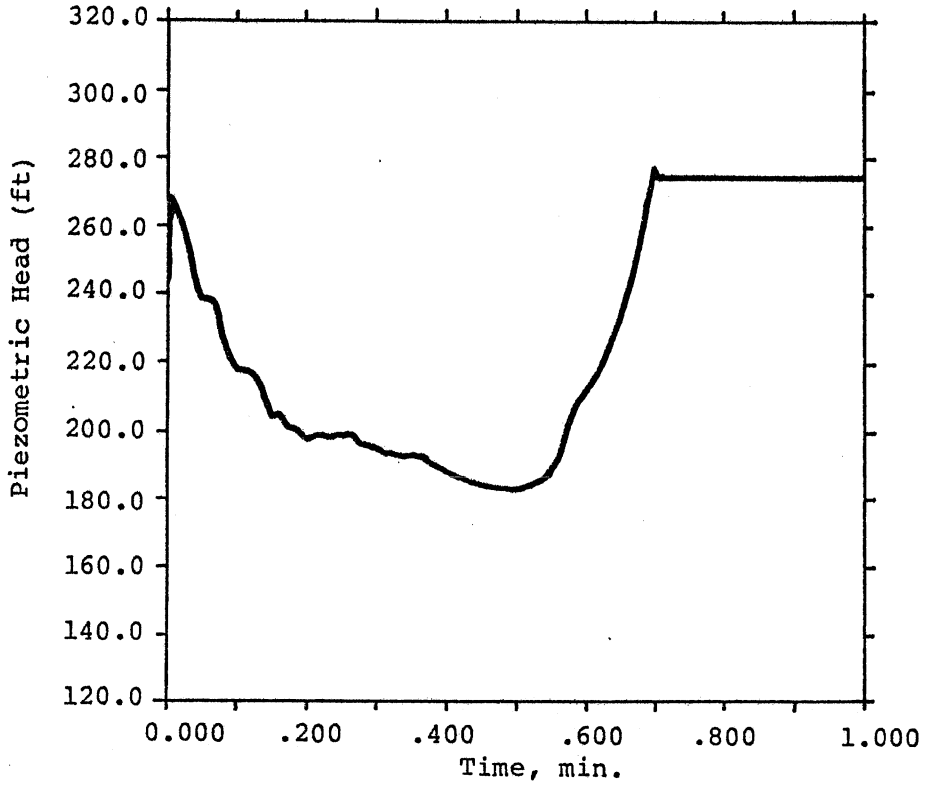

(a) downstream of pump.

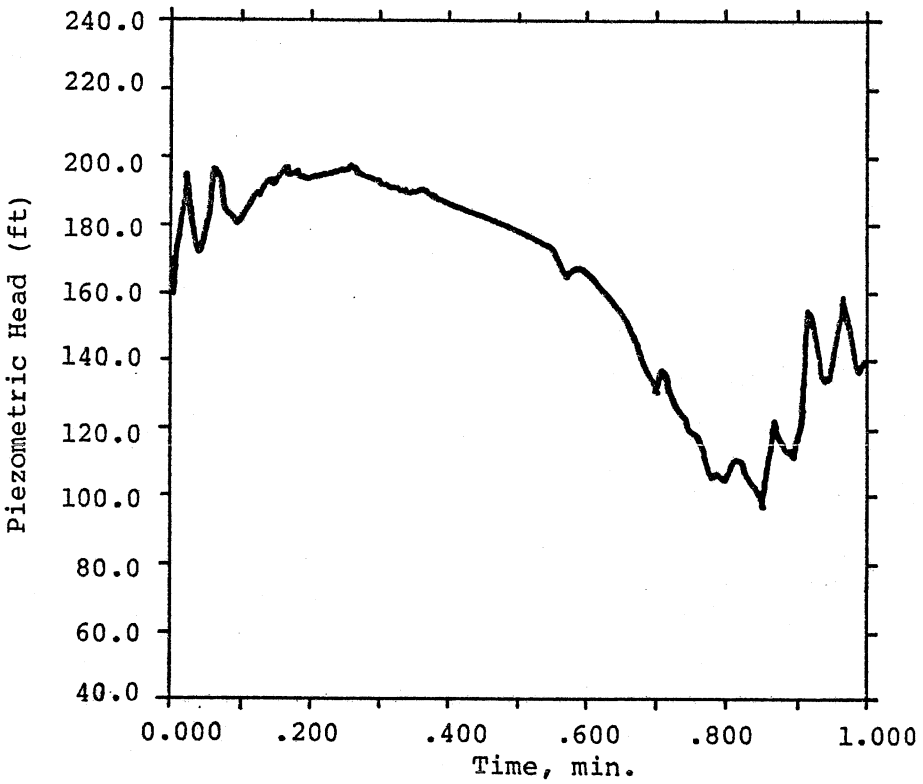

(b) downstream of pump valve.

Fig. VI-14. Piezometric Heads at Pump 5, Run VI-4.

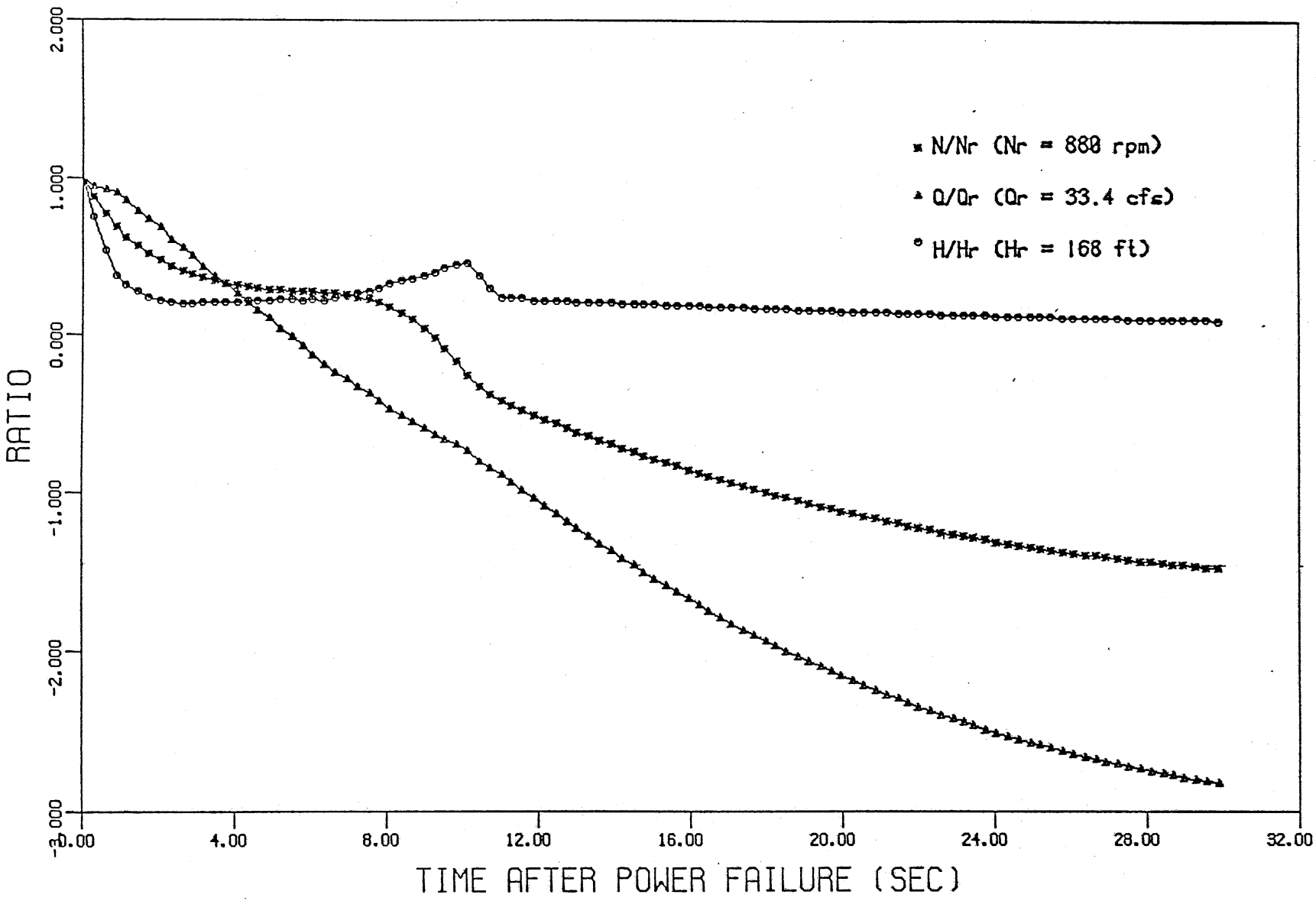

Fig. VI-15. N, Q, H Curves for Pump No. 1 with Valve Opened, Run VI-5.

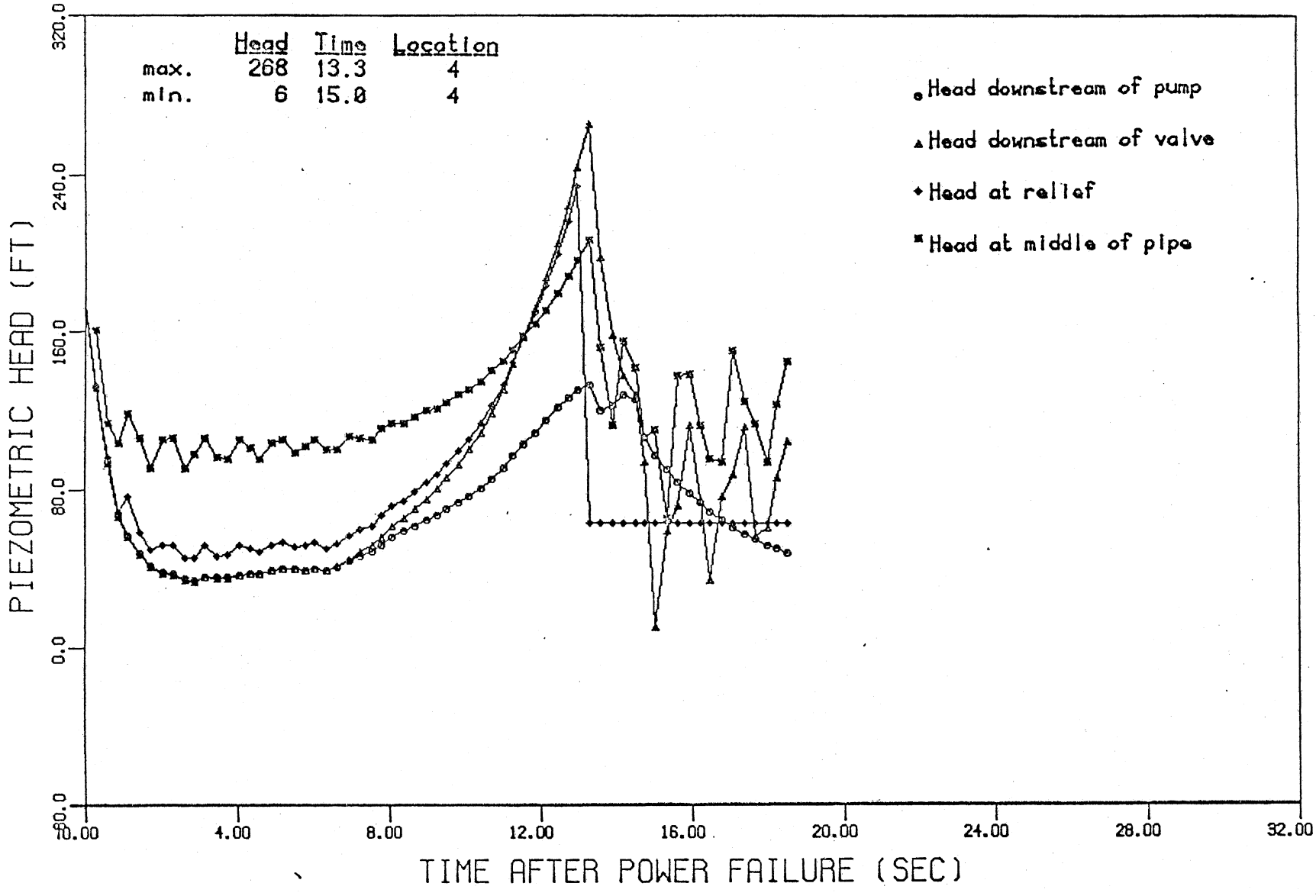

Fig. VI-22. Piezometric Heads in 42" Pipe, Closure 15 sec., Run VI-9.

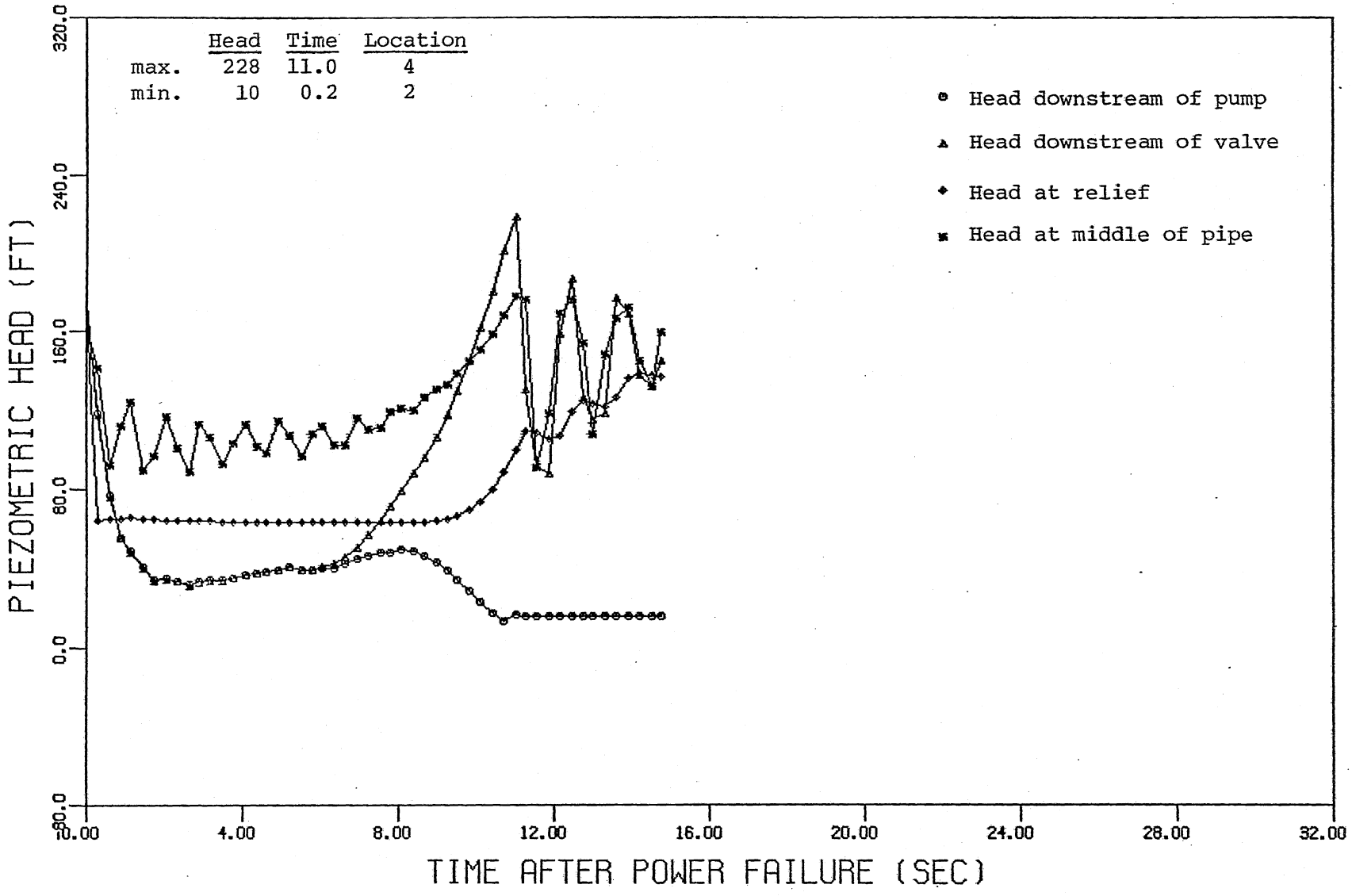

Fig. VI-23. 42" Pipe with Closure in 11 sec., 2 Anticipation Valves, Run VI-11.

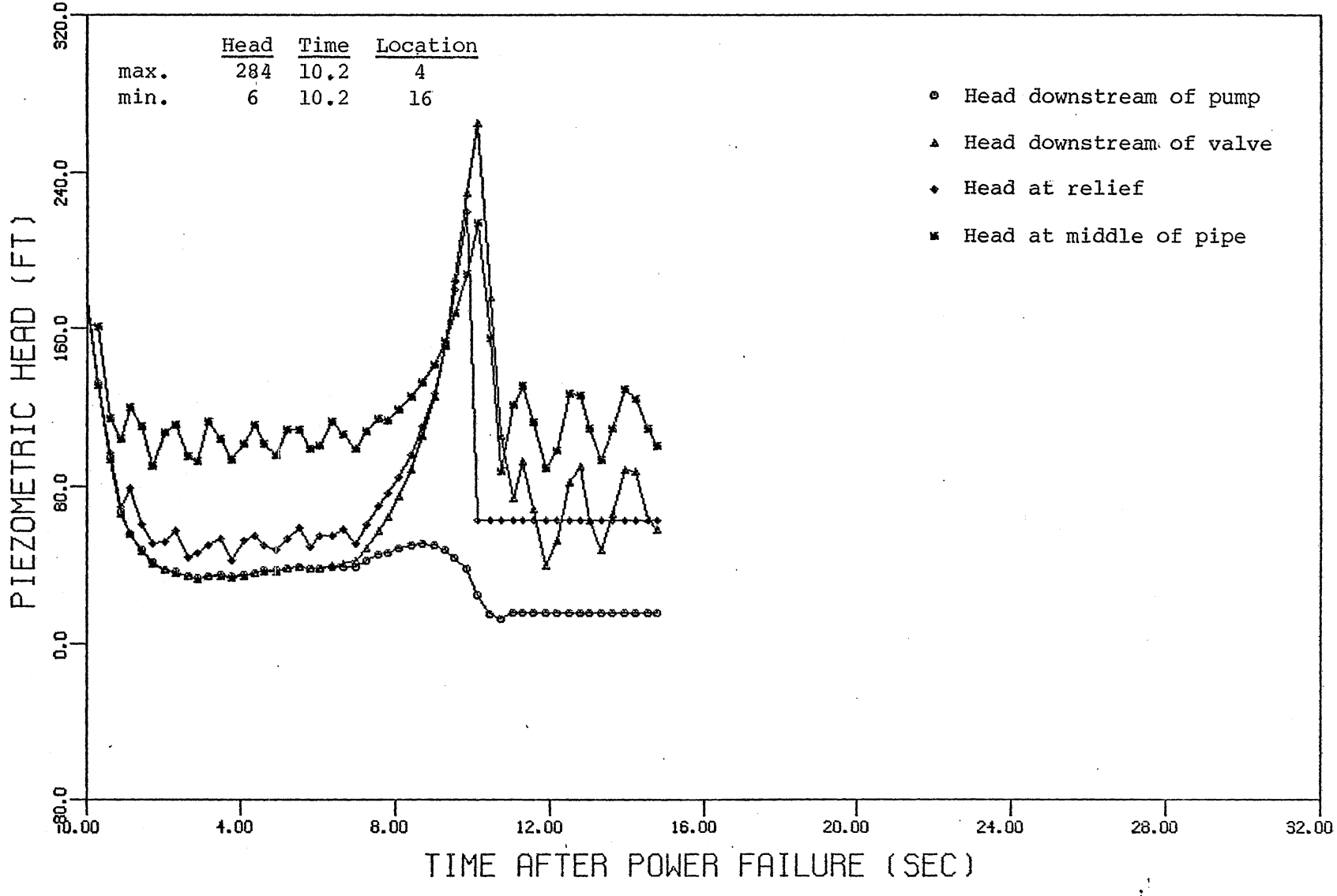

Fig. VI-24. 42" Pipe with Closure in 11 sec., 8 Surge Relief Valves, Run VI-13.

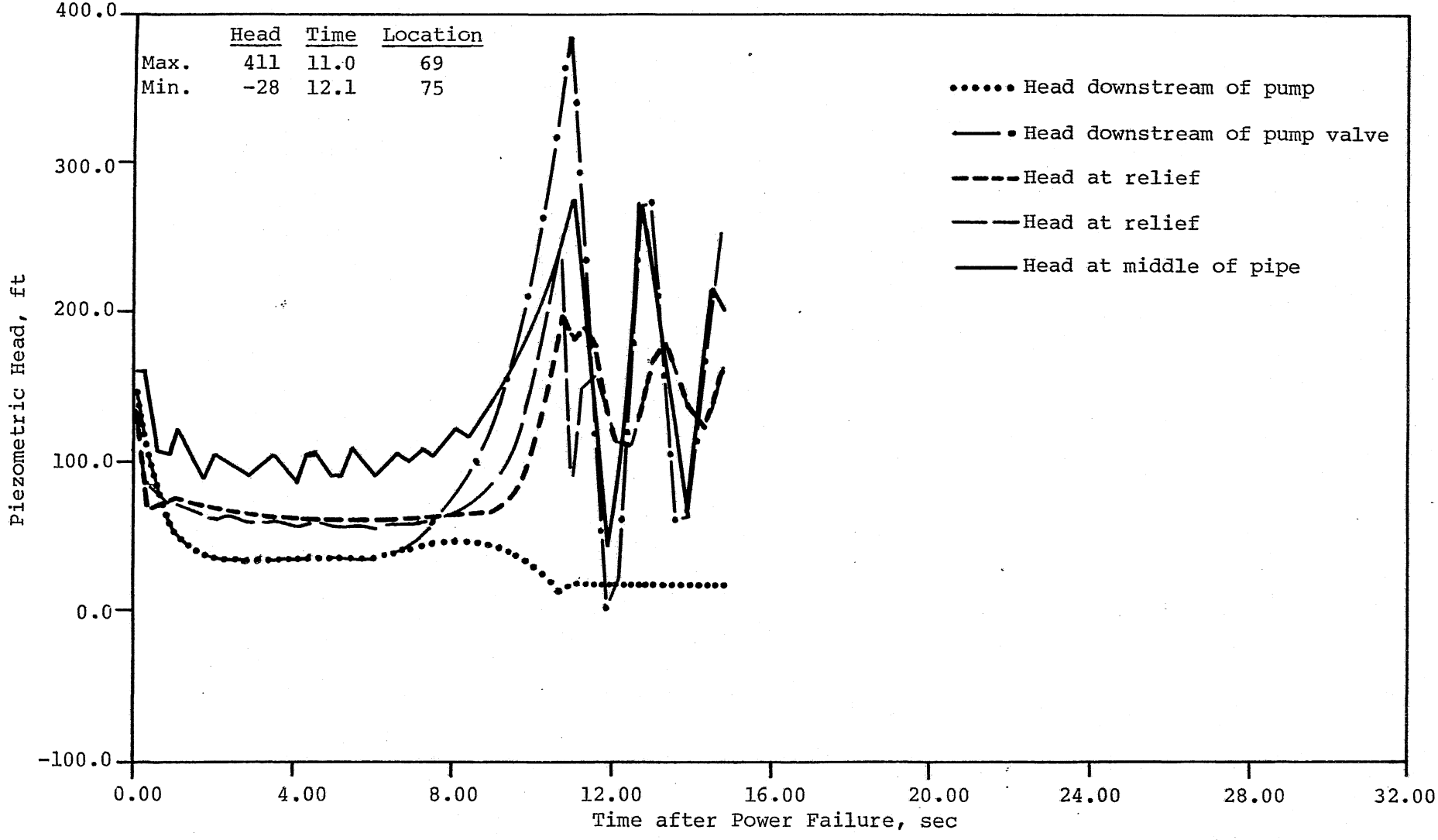

Fig. VI-25. Both Force Mains in Operation, Configuration B, 2 Anticipation Valves, 2 Surge Relief Valves, Heads in 42 Inch Main, Run VI-14.

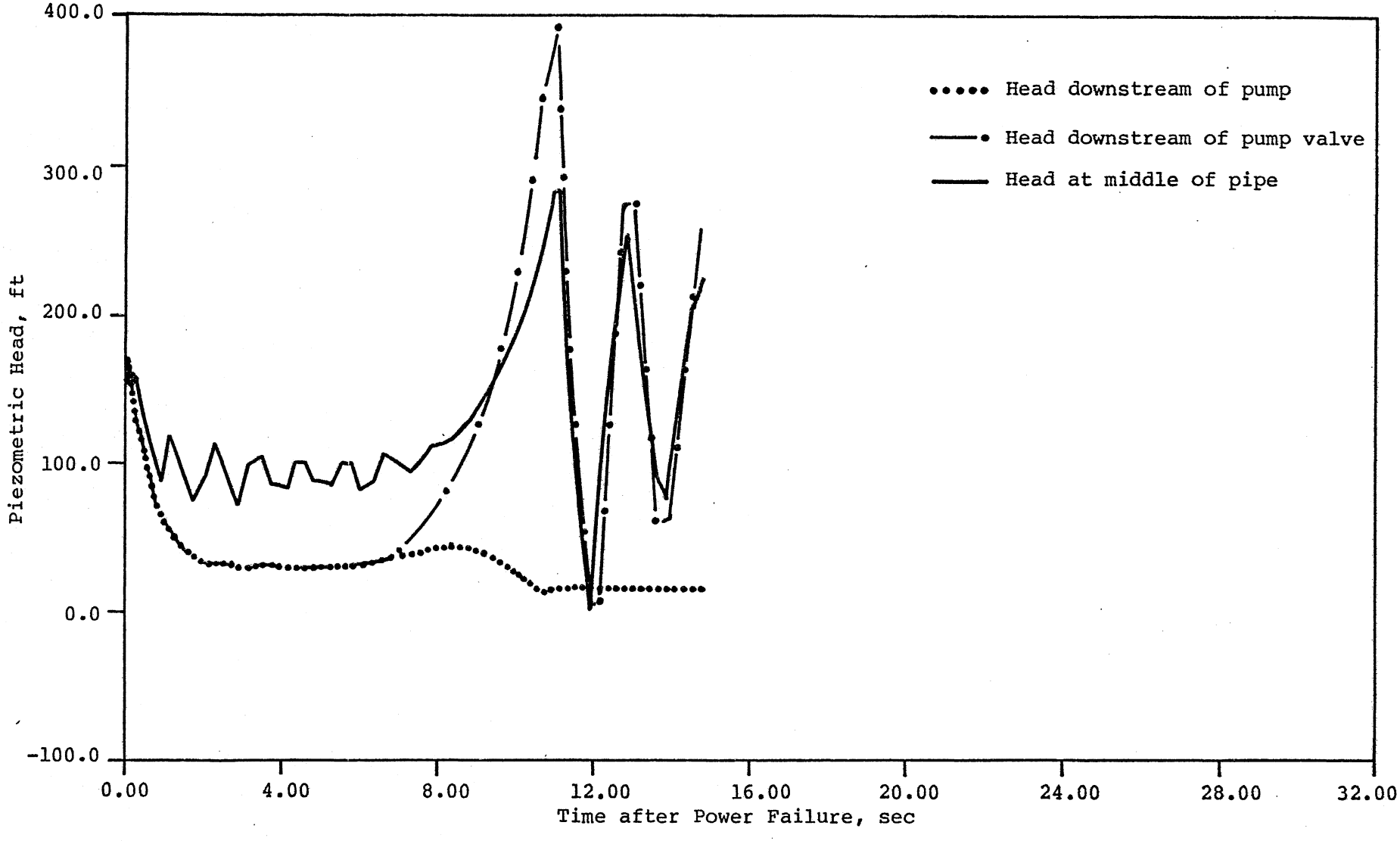

Fig. VI-26. Heads in 60 Inch Main, Run VI-14.

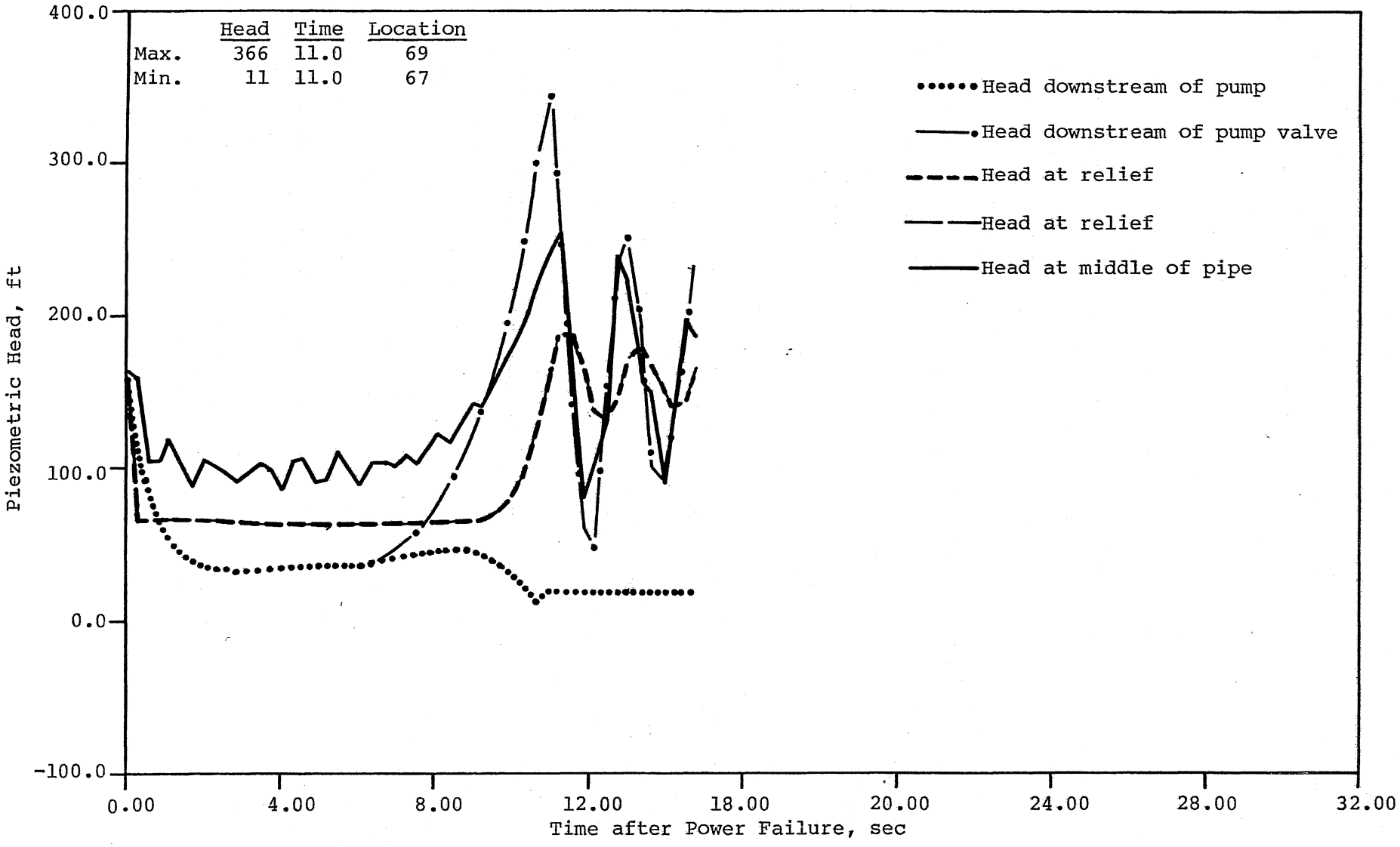

Fig. VI-27. Both Force Mains in Operation, Configuration B, 4 Anticipation Valves, Head Predicted for 42 Inch Main, Run VI-15.

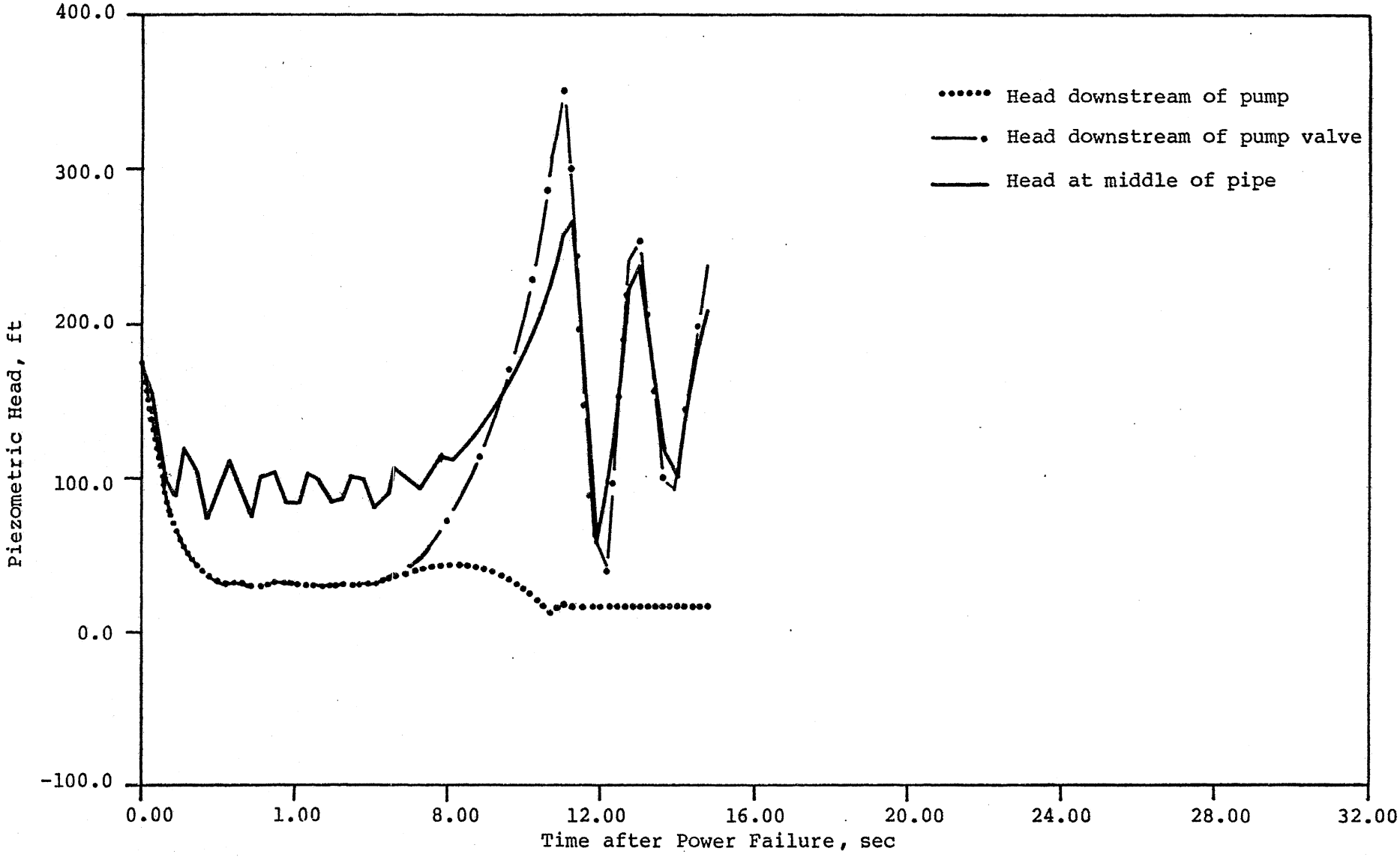

Fig. VI-28. Head Predicted for 60 Inch Main, Run VI-15.

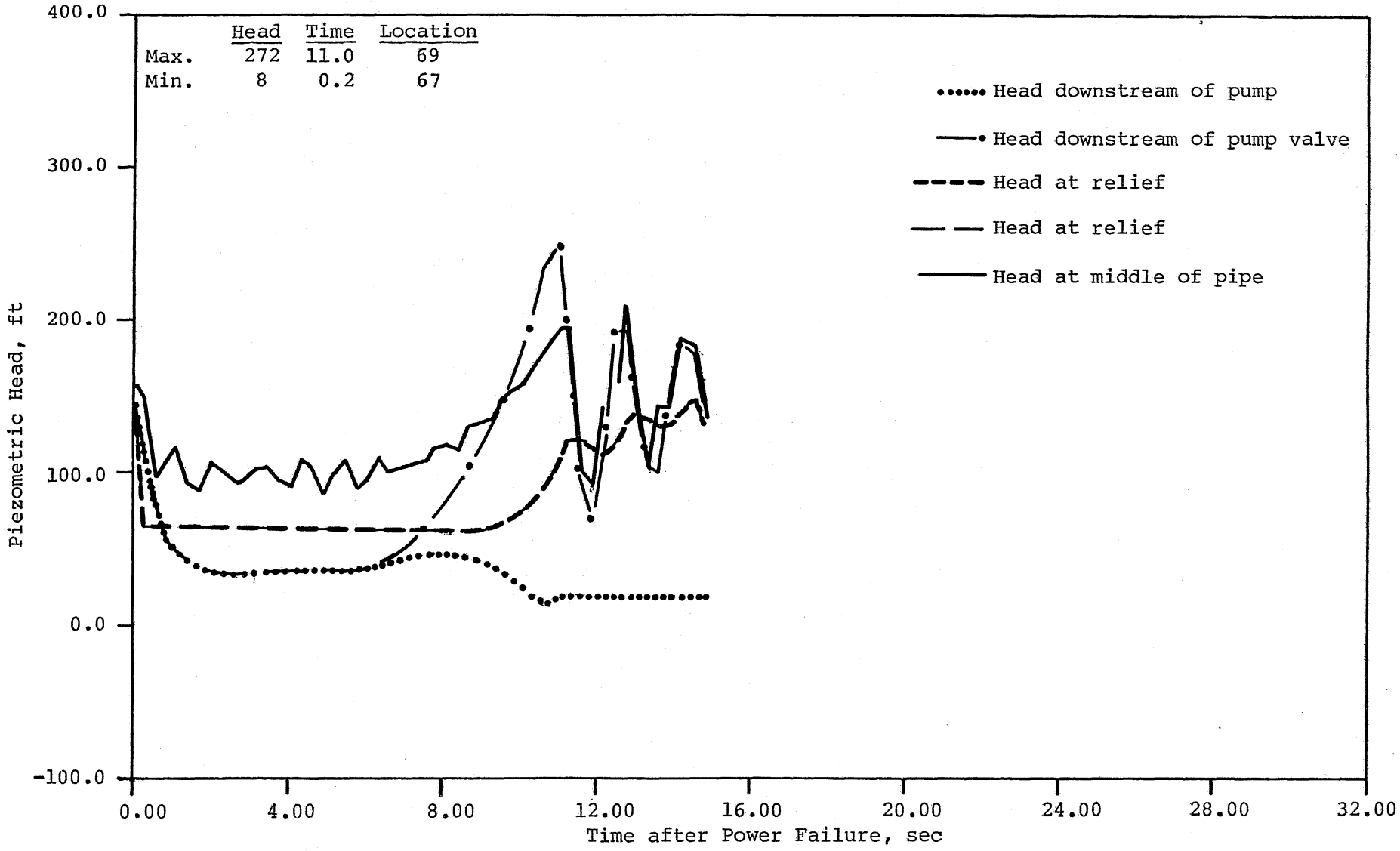

Fig. VI-29. Both Force Mains in Operation, Configuration B, 10 Anticipation Valves, Head Predicted for 42 Inch Main, Run VI-16.

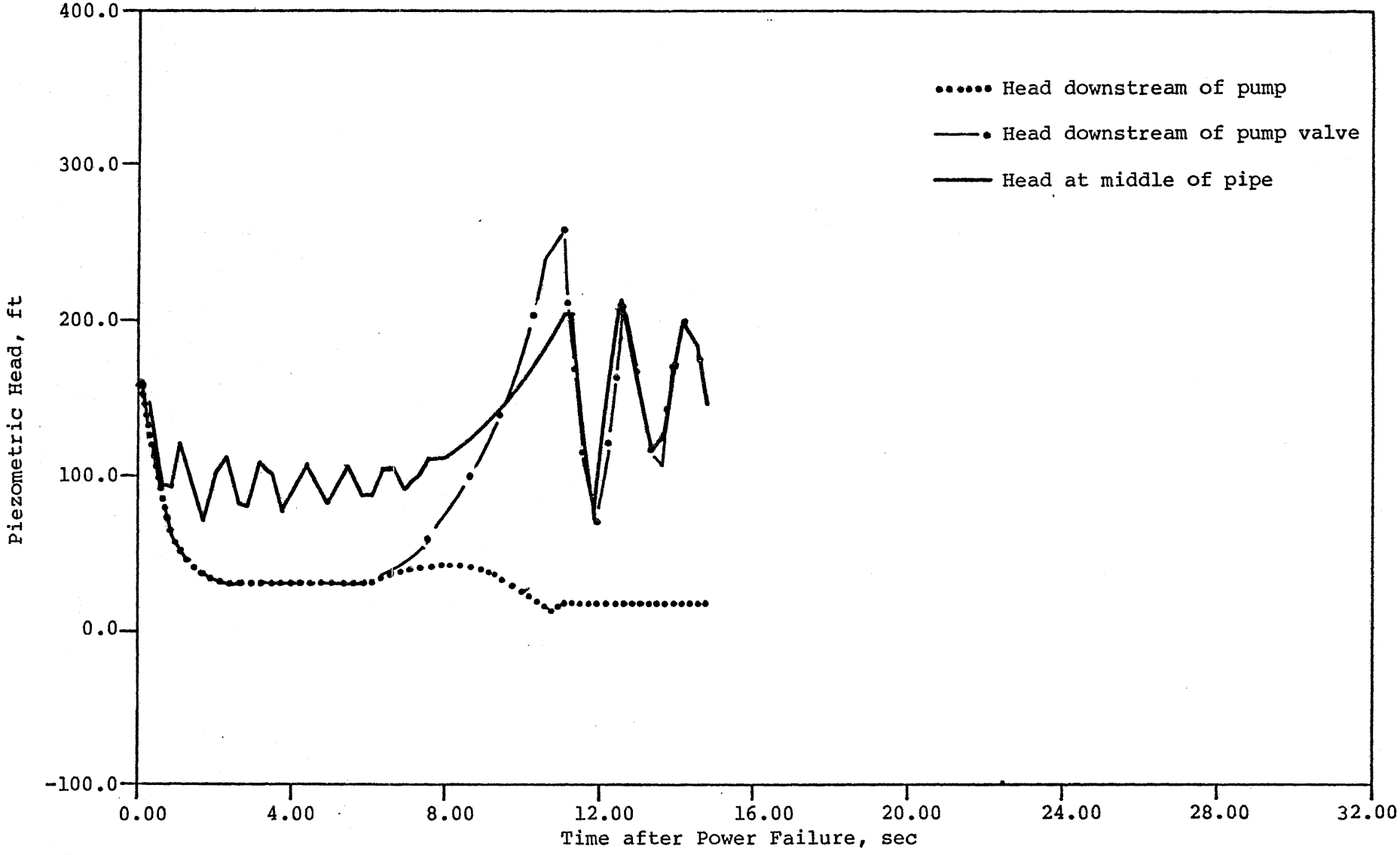

Fig. VI-30. Heads in 60 Inch Main, Run VI-16.

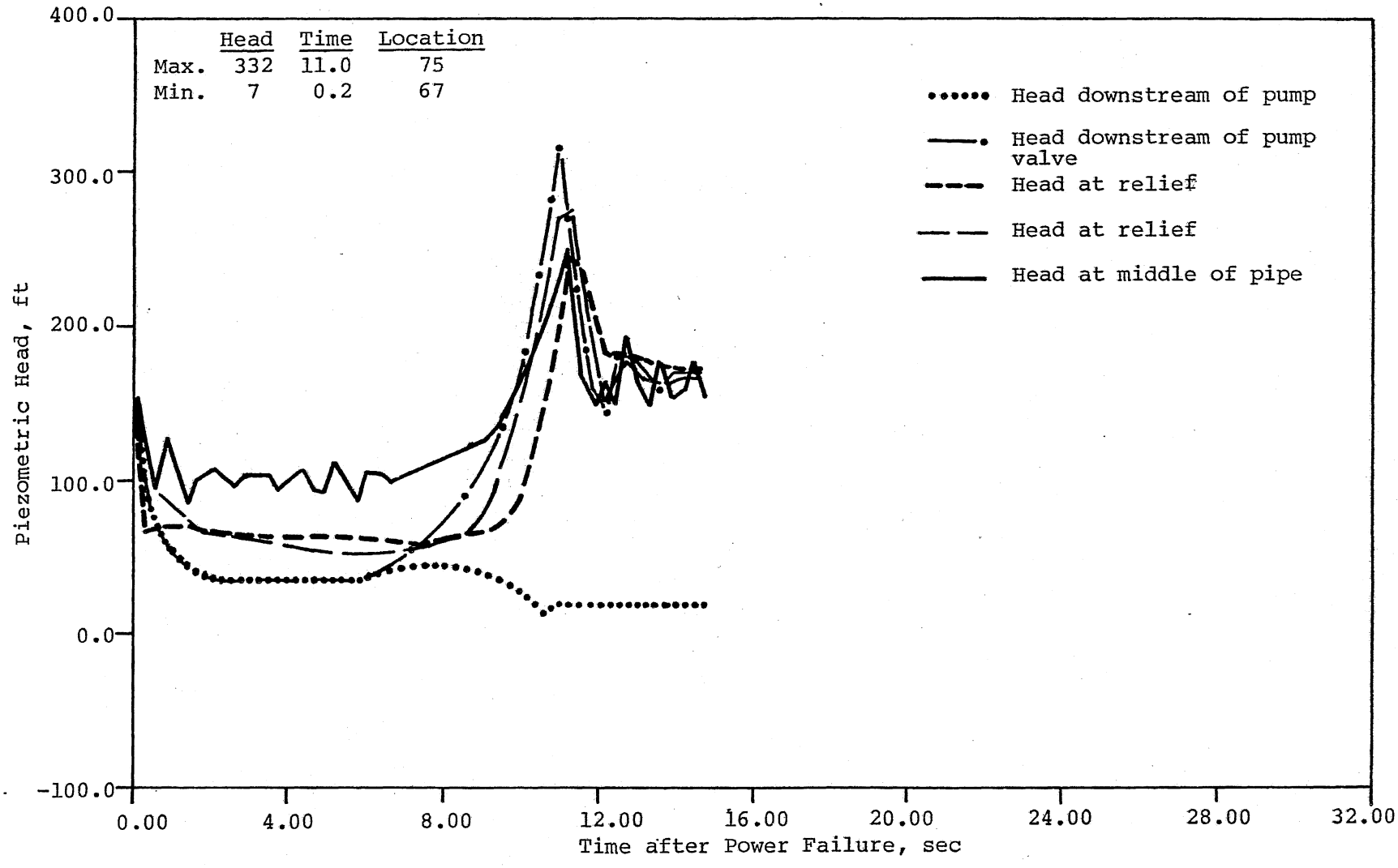

Fig. VI-31. Configuration C, 4 Anticipation Valves, 2 Surge Relief Valves, Head in 42 Inch Main, Run VI-17.

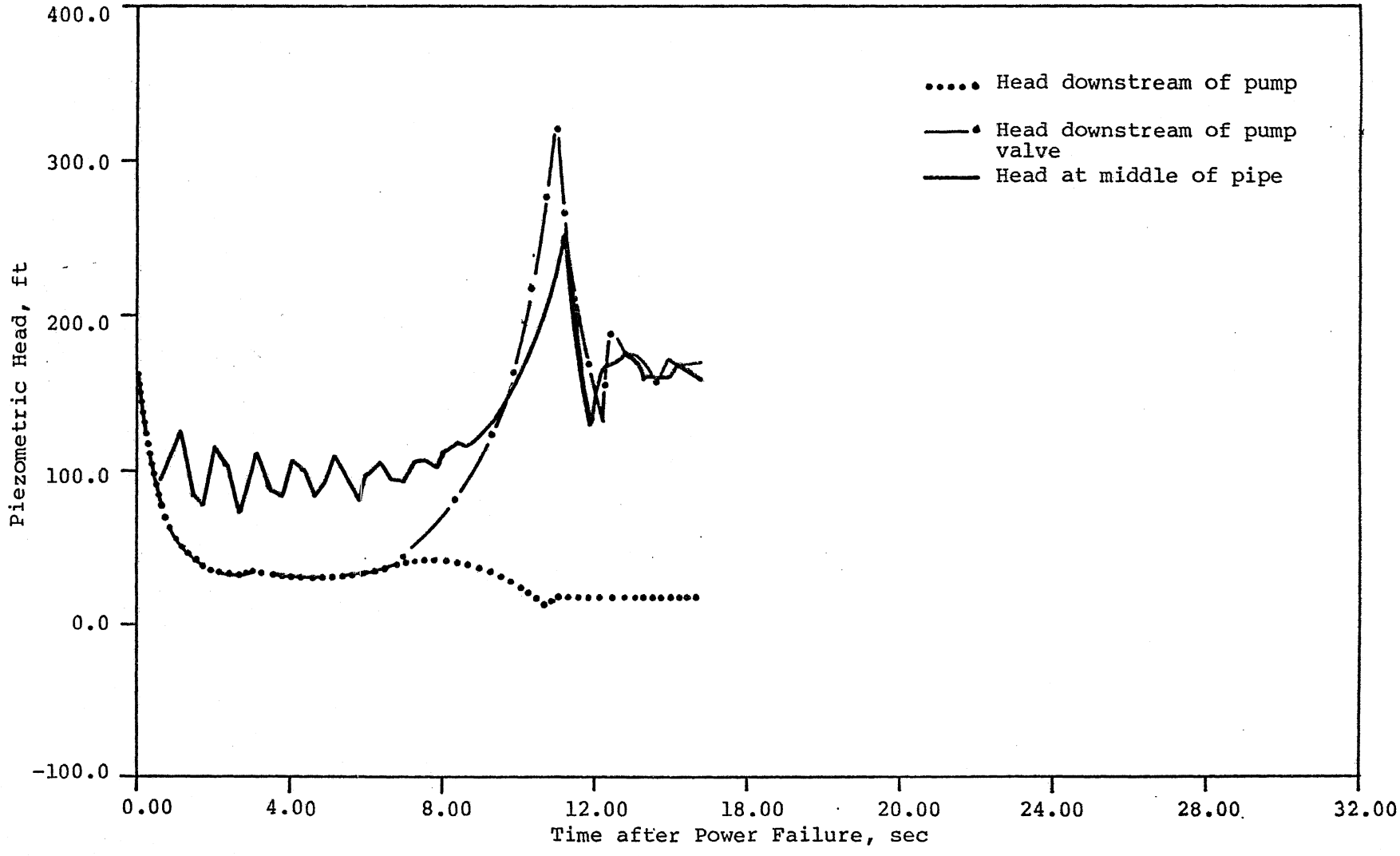

Fig. VI-32. Head in 60 Inch Main, Run VI-17.

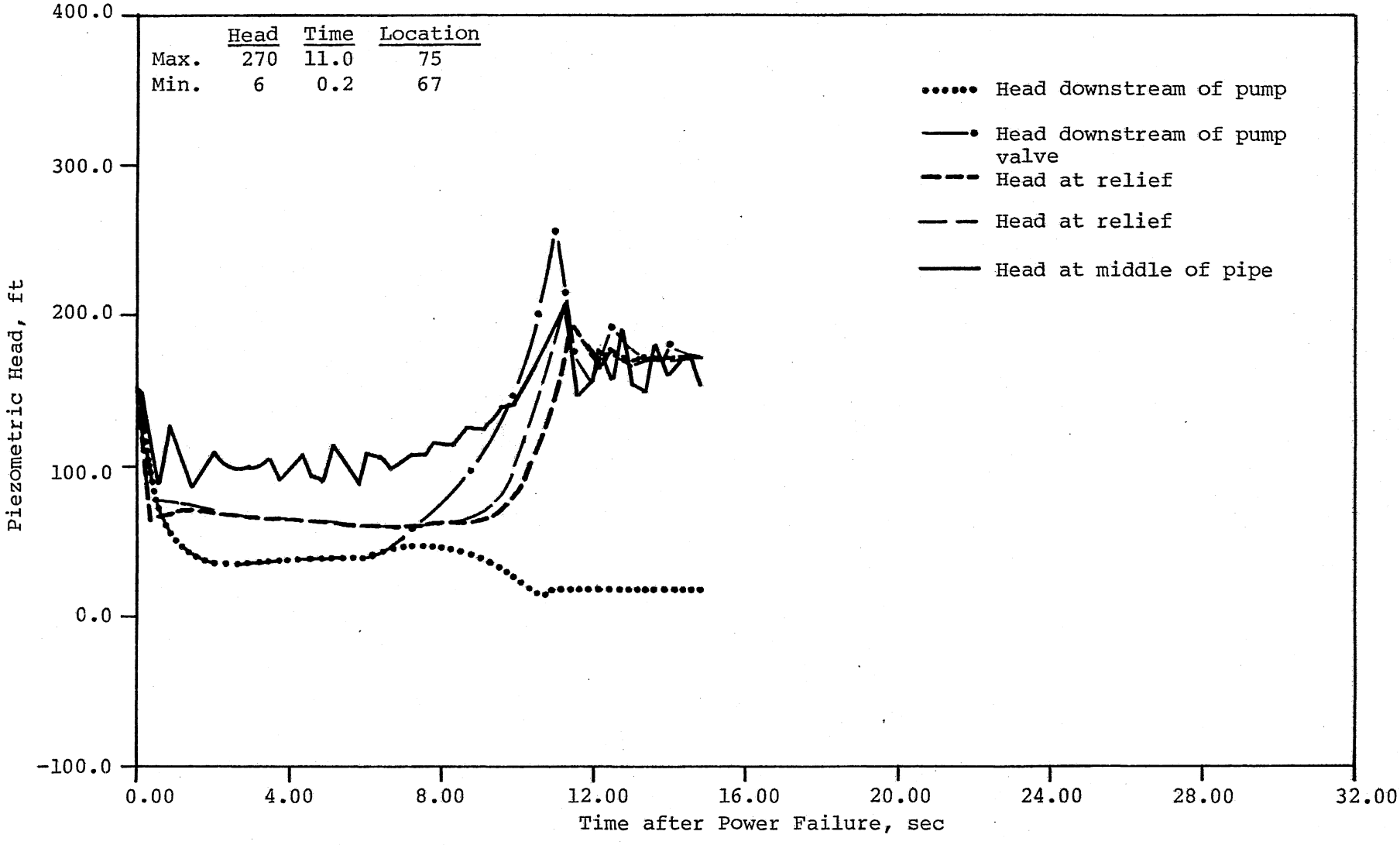

Fig. VI-33. Configuration C, 6 Anticipation Valves, 2 Surge Relief Valves, Head in 42 Inch Main, Run VI-18.

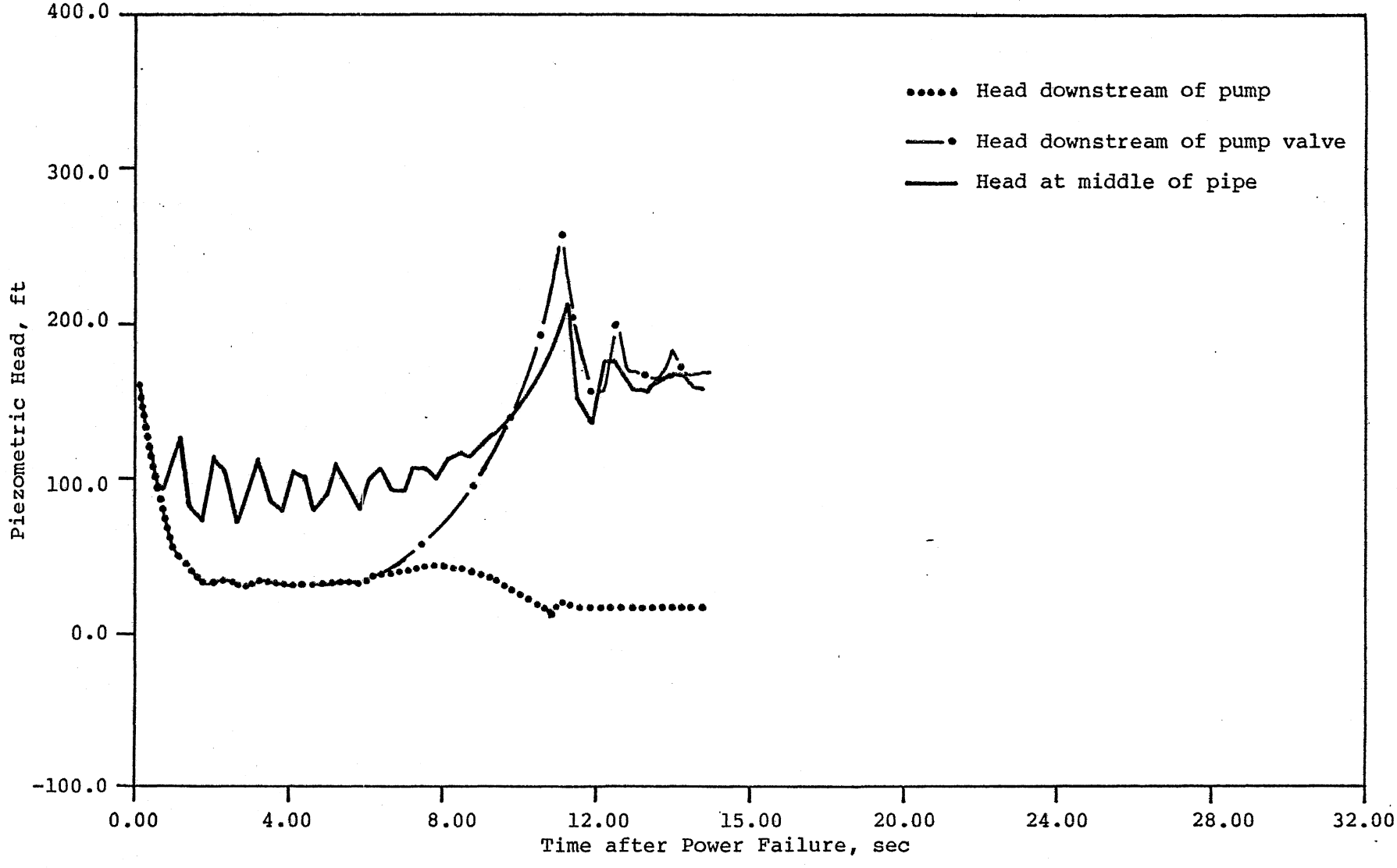

Fig. VI-34. Head in 60 Inch Main, Run VI-18.

REFERENCES

1. Song, C. S., Ring, T. M., Young, A.C. H., Leung, K. S. G., "Hydraulic Transient Analysis for the Culver-Goodman Tunnel, Rochester, N. Y.," St. Anthony Falls Hydraulic Laboratory, Project Report No. 157, Dec. 1975.
2. Donsky, Benjamin, "Complete Pump Characteristics and the Effects of Specific Speeds on Hydraulic Transients," Jour. of Basic Engineering, ASME, pp. 685-699, Dec., 1961.
3. Cardle, J. A., "Hydraulic Transients in Storm Sewer Systems," M. S. thesis (unpublished), University of Minnesota, 1978.
4. ASCE Task Committee, "Aerated Flow in Open Channels," Proceedings, ASCE, Vol. 87, No. HY3, May, 1961, p. 73.
5. Straub, L. G. and Anderson, A. G., "Experiment on Self-Aerated Flow in Open Channels," Trans. ASCE, Vol. 125, 1960, p. 456.
6. Song, C. S., "Two-Phase Flow Hydraulic Transient Model for Storm Sewer Systems," Second International Conference on Pressure Surges, The City University, London, 1976.
7. Streeter, Victor, L. and Wylie, E. Benmamin, *Fluid Transients*, McGraw-Hill Book Company, New York, 1978.
8. Chandhry, M. H., *Applied Hydraulic Transients*, Van Nortrand Reinhold Co., New York, 1979.

APPENDIX A

DESCRIPTION OF THE MIXED FLOW HYDRAULIC TRANSIENT MATHEMATICAL MODEL

General

This mathematical model is based on the full equations of continuity and motion (St. Venant equations) applicable to one dimensional unsteady flow in open channel and closed conduits. The governing equations for open channel flow are

$$\frac{\partial y}{\partial t} + V\frac{\partial y}{\partial x} + \frac{c^2}{g}\frac{\partial V}{\partial x} = 0 \qquad \text{(A-1)}$$

and

$$g\frac{\partial y}{\partial x} + \frac{\partial V}{\partial t} + V\frac{\partial V}{\partial x} + g(s_f - s_o) = 0 \qquad \text{(A-2)}$$

in which c is the gravity wave speed given by

$$c = \sqrt{\frac{gA}{T}} \qquad \text{(A-3)}$$

The corresponding equations for closed conduit flow are

$$\frac{\partial H}{\partial t} + V\frac{\partial H}{\partial x} + \frac{a^2}{g}\frac{\partial V}{\partial x} = 0 \qquad \text{(A-4)}$$

and

$$g\frac{\partial H}{\partial x} + \frac{\partial v}{\partial t} + V\frac{\partial v}{\partial x} + g(s_f - s_o) = 0 \qquad \text{(A-5)}$$

in which a is the speed of the pressure wave.

The following is a list of the symbols used in the above equations:

y = depth of flow

H = piezometric head

A = area of flow

s_f = friction slope

s_o = slope of channel or pipe

V = velocity of flow,

g = acceleration due to gravity,

T = top width of flow

t = time

x = distance measured along channel or pipe

There are a number of different approaches available for solving the above differential equations, but in view of the complex geometrical configuration to be dealt with, the method of characteristic appears to be the most suitable. The characteristic equations are, for open channel flow,

$$\frac{dx}{dt} = V \pm C \tag{A-6}$$

$$\frac{dy}{dt} \pm \frac{C}{g}\frac{dV}{dt} \pm C(s_f - s_o) = 0 \tag{A-7}$$

and for closed conduit flow

$$\frac{dx}{dt} = V \pm a \tag{A-8}$$

$$\frac{dH}{dt} \pm \frac{a}{g}\frac{dV}{dt} \pm a(s_f - s_o) = 0 \tag{A-9}$$

Note that the two sets of characteristic equations have identical forms. For the characteristic method to converge, the following stability criteria must be enforced.

Open Channel Flow $\quad \Delta t \leq \Delta x/|V \pm C|$ (A-10)

Closed Conduit Flow $\quad \Delta t' \leq \Delta x/|V \pm a|$ (A-11)

When mesh sizes are chosen according to the above stability criteria, the characteristic lines issuing from a nodal point P will intersect the line representing the previous time, as shown in Fig. A-1, provided that the flow is subcritical. These intersects are denoted R and S in Fig. A-1. Accordingly, the characteristic differential equations, Eqs. A-7 and A-9, can be written as:

for open channel flows,

$$C^+ : y_P - y_R + \frac{C_R}{g}(V_P - V_R) + C_R(S_f - S_o)_R \ \Delta t = 0 \qquad \text{(A-12)}$$

$$C^- : y_P - y_S - \frac{C_S}{g}(V_P - V_S) - C_S(S_f - S_o)_S \ \Delta t = 0 \qquad \text{(A-13)}$$

and for closed conduit flows,

$$C^+ : H_P - H_R + \frac{a}{g}(V_P - V_R) + a(S_f - S_o)_R \ \Delta t' = 0 \qquad \text{(A-14)}$$

$$C^- : H_P - H_S - \frac{a}{g}(V_P - V_S) - a(S_f - S_o)_S \ \Delta t' = 0 \qquad \text{(A-15)}$$

When the flow at the nodal points, A, B, and C is known, then the corresponding values at the intersects R and S can be obtained by linear interpolations. In principle, a set of unknowns (Y_P, V_P) or (H_P, V_P) can be readily obtained by solving Eqs. (A-12) and (A-13) or Eqs. (A-14) and (A-15), respectively.

The computation at the interface requires a special treatment. According to Eq. A-3, $c \to \infty$ as $T \to o$. To overcome this physically unrealistic situation, Song [6] assumed that the phase change will occur at a depth slightly less than the diameter D so that the flow is regarded as open channel when

$$y \leq D - \varepsilon \qquad \text{(A-16)}$$

but closed conduit when

$$y > D - \varepsilon \qquad \text{(A-17)}$$

In Model II the motion of the interface shown in Fig. A-2 is determined by the volumetric increase or decrease in storage in the segment containing the interface. The rate of change of the storage is given by

$$\Delta Q = V_{i-1} A_{i-1} - V_i A_i \qquad \text{(A-18)}$$

For a small time interval Δt, ΔQ is assumed to be constant, so that the change in storage is

$$\Delta S = \Delta Q \ \Delta t' \qquad \text{(A-19)}$$

Using this change in storage, the new interface position, x_2, can be calculated and the interface velocity found. The head at the interface is considered to be $D - \varepsilon$, where ε is considered to be known, and the head is assumed to vary linearly between the interface and station i-1, so that the head at station i can be found by linear interpolation. These conditions, plus an open channel characteristic equation and a closed conduit characteristic equation, determine the flow condition at the stations adjacent to the interface.

In Model III, a more exact formulation of the conditions at the interface is made. Assuming that the interface is originally located at point C in Fig. A-3 and moving to the left at speed W, the new location of the interface after $\Delta t'$ is indicated by point p'. The distance moved is

$$\Delta x' = W\Delta t' \tag{A-20}$$

Since there is a jump in the depth of ε across the interface, there is also a jump in V across the interface. The depth just upstream of the interface is assumed to be $D - \varepsilon$. The head just downstream of the interface, Hp2, the velocity just upstream of the interface, Vp1, and the velocity just downstream of the interface, Vp2, are unknowns. There are a total of four unknowns at the interface, including W. There are available two characteristic equations corresponding to $\overline{p'R}$ and $\overline{p'S}$ characteristic lines. In addition, it is possible to write a continuity equation across the jump as

$$(VP1 + W)A_1 = (VP2 + W)A_2$$

where A_1 and A_2 are the known cross-sectional areas. The momentum equation across the interface is

$$F_1 - F_2 = \rho(VP1 + W)A_1\ (VP2 - VP1) \tag{A-22}$$

where F_1 is the force due to hydrostatic pressure in the flow depth $D - \varepsilon$ and F_2 is the force due to the head of Hp2 in closed conduit. There are four equations and four unknowns at the interface, assuming ε is given.

Boundary Conditions

There are many abrupt changes in sizes and shapes, junctions, and flow control structures, etc. where special boundary conditions are required. A few typical boundary conditions for this system are described below.

1. Upstream End

At an upstream end it is generally assumed that the inflow is given by a known runoff hydrograph previously computed. That is

$$Q = Q(t) \tag{A-23}$$

This equation plus a negative characteristic equation, either Eq. A-13 or Eq. A-15, provides the necessary equations for the determination of the two unknowns.

2. Expansion or Contraction

A typical expansion joint is sketched in Fig. A-4. Since there is an abrupt change in the flow across the joint, the joint is represented by two stations, C1 and C2. There are four unknowns, Y_{p1} (H_{p1}), V_{p1}, y_{p2} (H_{p2}), and V_{p2}. Two characteristic equations are available - the C+ equation for station 1 and C- equation for station 2. The two additional equations required are the continuity equation

$$V_{p1} A_{p1} = V_{p2} A_{p2} \tag{A-24}$$

and a fairly common assumption that the piezometric head is unchanged between station 1 and station 2. That is

$$H_{p1} = H_{p2},\ y_{p1} = y_{p2},\ \text{or}\ H_{p1} = Y_{p2} \tag{A-25}$$

whichever may be appropriate. Although it is possible to specify the expansion loss in lieu of Eq. A-25, this equation is simpler and produces satisfactory results.

3. Dropshaft Inlet

There are a number of different flow conditions possible at a dropshaft, but only two simple cases are shown in Fig. A-5. Sketch (a) indicates the open channel condition at the dropshaft with known point input Q(t). There are three unknowns, V_{p1}, V_{p2}, and y_p. Two characteristic

equations are available. The third equation is furnished by the continuity relation,

$$V_{p1} A_{p1} + Q = V_{p2} A_{p2} \qquad \text{(A-26)}$$

Sketch (b) shows the flow condition when both sides of the dropshaft act as closed conduits. The inflow Q is again given, and therefore four unknowns, V_{p1}, V_{p2}, V_{p3}, and H_p, must be determined. Two characteristic equations plus two boundary conditions are needed. The continuity relation at the junction gives:

$$V_{p1} A_1 + V_{p3} A_3 = V_{p2} A_2 \qquad \text{(A-27)}$$

In this case the dropshaft acts as a surge tank described by a storage equation:

$$Q(t) - V_3 A_3 = \frac{dH}{dt} \qquad \text{(A-28)}$$

4. Downstream End

There is both the possibility of pumping and of overflow at the downstream boundary. The configuration is shown schematically in Fig. A-6. The unknowns V and y are computed by combining the appropriate c^+ characteristic equation with the storage equation, which is

$$VA - Q_p - Q_w = A_s \frac{dy}{dx} \qquad \text{(A-29)}$$

where A is the flow area in the pipe and A_s is the surface area of the sump. The pumping rate Q_p is specified and Q_w can be readily calculated by using the weir equation.

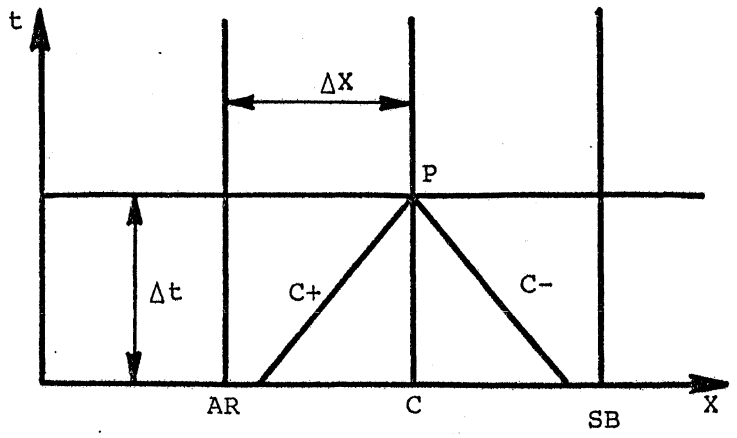

Fig. A-1. Fixed Grid System for Single Phase Flow.

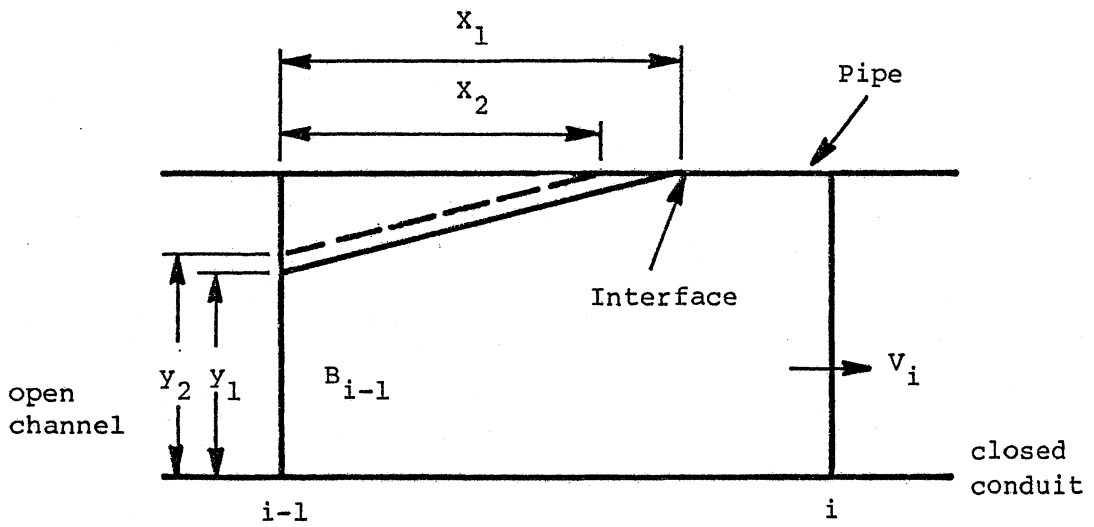

Fig. A-2. Definition Sketch for a Mixed-Flow Segment in Model II.

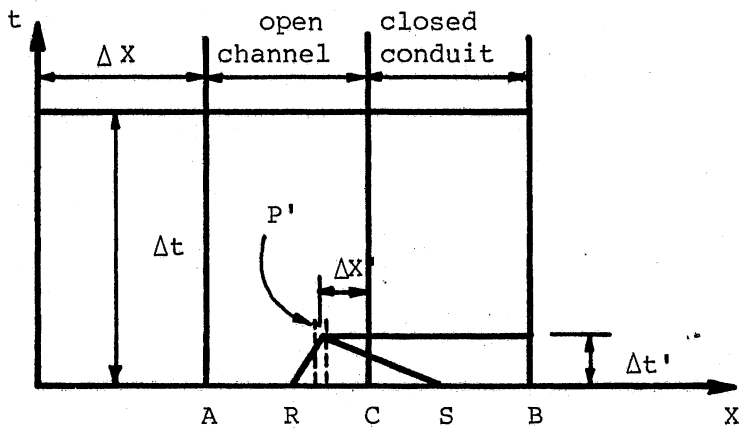

Fig. A-3. Fixed Grid System for Mixed Flow, Moving Interface.

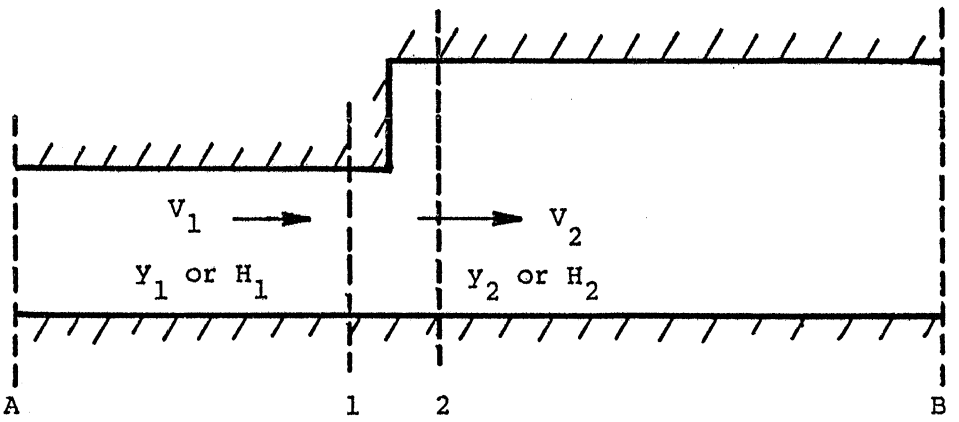

Fig. A-4. Expansion Joint.

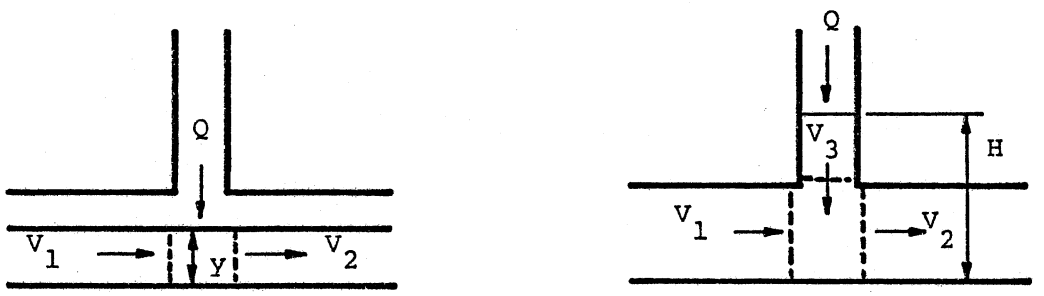

Fig. A-5. Flow Conditions at Dropshaft.

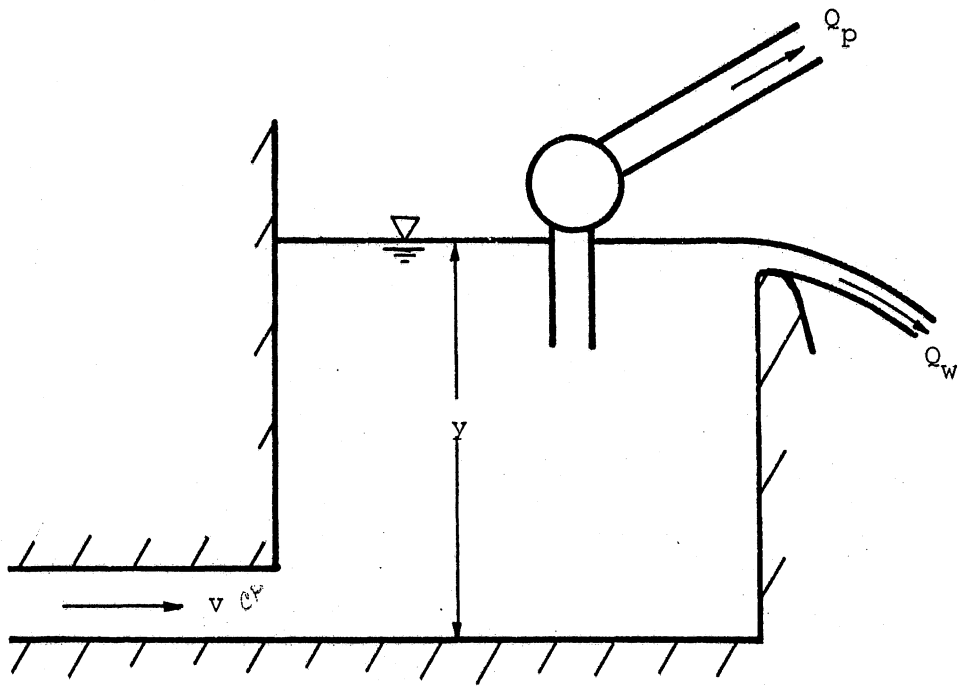

Fig. A-6. Downstream Boundary Condition.

APPENDIX B

DIVERSION STRUCTURE MODEL

The model is essentially a flow balance model in which inflow is equal to storage plus outflow. Figure III-1 describes the structure and parameters used in the model.

1. Inflow

   Inflow is taken from a 10 year storm hydrograph.

2. Channel

   A control point is located downstream of the sluice gate where the slope of the channel changes. Due to the existence of critical flow at the control point, the equation

$$QD = W\sqrt{g}\,(YC)^{3/2} \tag{B-1}$$

   where W = width of channel at control point can be written.

3. Sluice Gates

   An orifice equation is used when $Y > BS1$,

$$QD = Cd\ Ws\ BS1\sqrt{2g(Y-YS)} \tag{B-2}$$

   or else the equation of equal depths

$$Y = YS \tag{B-3}$$

   is employed.

4. Roller Gate

   Overflow from the roller gate is given by weir equation

$$QD = Cd\ \frac{2}{3}\ WR\ \sqrt{2g}\ [Y-(BR+BR1)]^{3/2} \tag{B-4}$$

   whereas flow under it is given by the orifice equation

$$QU = Cd\ BR1\ WR\ \sqrt{2g(Y-\ Cd\ BR1)} \tag{B-5}$$

5. Continuity

The rate of change of storage in the structure is given by the relationship,

$$QI = QD + QD + A \frac{dy}{dt} \qquad (B-6)$$

APPENDIX C

DESCRIPTION OF THE FORCE MAIN MODEL

The force main mathematical model is based on the equations of motion and continuity applicable to one dimensional unsteady flows in closed conduits. These equations are Eqs. A-4 and A-5 in Appendix A. The method of characteristics, as described in Appendix A, is also used in this model. Many of the boundary conditions such as the junction condition are also applicable here and will not be repeated.

Some boundary conditions special to this model are listed below.

1. Intake

The orifice equation

$$Q = \pm C_d A\sqrt{2g\,|H_o - H_p|} \qquad \text{(C-1)}$$

is used to represent the valve located in each suction line. A positive sign is chosen when $H_o > H_p$ in Eq. C-1. This equation and a characteristic equation are used, simultaneously, to determine the head and the discharge.

2. Relief and Anticipation Values

Surge relief valves and surge anticipation valves are all treated as orifices and Eq. C-1 is used. In the case of the surge relief valve, the orifice equation is activated when Hp exceeds a predetermined value. For the surge anticipated valve, the equation is activated when power failure occurs. The station is regarded as a dead end when the orifice equation is not in force.

3. Valve Chamber

The two force mains are interconnected with a 30 inch pipe at the valve chamber. There are three valves in the chamber, one each on the 42 in. main, 60 in. main, and the 30 in. connection. There is also a 12 in. relief line attached to each force main. Because they are located very close to each other, they must be treated as a group, and all variables solved simultaneously. An idealized configuration of the valve chamber is sketched in Fig. C-1. The system is defined by 10 stations and 20 unknowns. Six characteristic equations, one each for

Stations 1, 2, 5, 6, 7, and 10, can be written. Two continuity equations at the junctions,

$$V_{p1} A_1 = V_{p2} A_2 + V_{p3} A_3 + V_{p4} A_4 \qquad (C-2)$$

$$V_{p6} A_6 + V_{p8} A_8 = V_{p7} A_7 + V_{p9} A_9 \qquad (C-3)$$

and three continuity equations across the valves,

$$V_{p4} = V_{p5} \qquad (C-4)$$

$$V_{p3} = V_{p8} \qquad (C-5)$$

$$V_{p9} = V_{p10} \qquad (C-6)$$

can be written. Three orifice equations similar to Eq. C-1 are written for the three valves. In addition, it is also reasonable to assume constant head at each of the two junctions. Thus,

$$H_{p1} = H_{p2} = H_{p3} = H_{p4} \qquad (C-7)$$

$$H_{p6} = H_{p7} = H_{p8} = H_{p9} \qquad (C-8)$$

All together there are 20 independent equations which are solved for the 20 unknowns by the Newton-Raphson method.

4. Pump

A typical pump ball valve unit is sketched in Fig. C-2. This system is represented by three stations and the associated six unknowns. During the transient condition after power failure, the rotational speed and the torque of the pump will also vary, making a total of eight variables to be found.

There are two characteristic equations, one each at stations 1 and 3, two continuity equations and an orifice equation for the valve. Three additional equations are needed to solve the problem. Pump manufacturers may furnish two pump characteristic curves relating head discharge, speed, and torque. These characteristic curves are usually plotted, as shown in Fig. VI-5, in dimensionless form

$$WH = f_1(x) \tag{C-9}$$

and

$$WB = f_2(x) \tag{C-10}$$

in which WH, WB, and x are defined as

$$WH = \frac{h}{a^2 + v^2} \tag{C-11}$$

$$WB = \frac{b}{a^2 + v^2} \tag{C-12}$$

$$x = \pi + \tan^{-1} \frac{v}{a} \tag{C-13}$$

Finally, the equation of motion of the rotating system without power written as follows completes the required set of equations.

$$b = - WR^2 \frac{2\pi N_R}{60 T_R} \frac{da}{dt} \tag{C-14}$$

In the above equation, WR^2 = combined polar moment of inertia of the pump, motor, shaft, and liquid entrained in the pump impeller. For a more detailed description of pump transient analysis see Streeter and Wylie [7] and Chandhry [8].

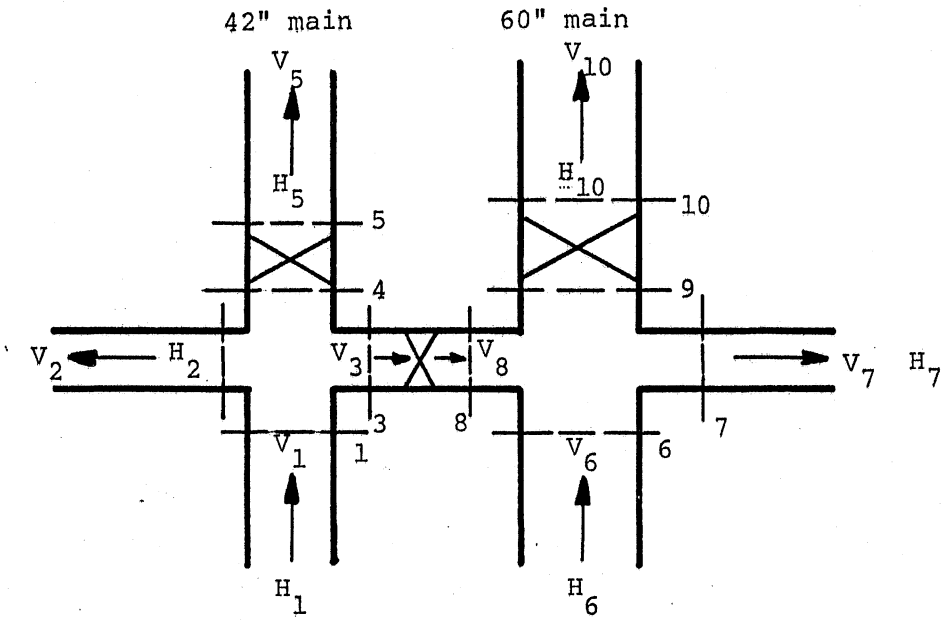

Fig. C-1. Valve Chamber.

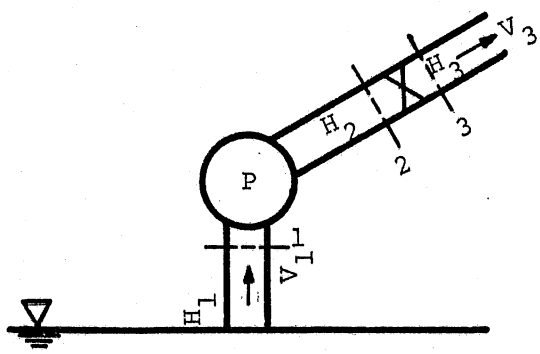

Fig. C-2. Pump and Control Valve.

APPENDIX D

INPUT HYDROGRAPHS

Two sets of inflow hydrographs plus the base flows into the Cross-Irondequoit tunnel system were developed by O'Brien and Gere Engineers, Inc. using the Environmental Protection Agency's SWMM model. These hydrographs and base flows were then used by the St. Anthony Falls Hydraulic Laboratory on the input into the mixed flow model of this tunnel system.

The first set of hydrographs included the 100 year, 1 hour storm; the 25 year, 1 hour storm; and 1 year, 1 hour storm; and a typical storm having a recurrence interval of less than 1 year. These hydrographs were developed without considering the effect of the Culver Goodman tunnel. The major inflow points were at Thomas Creek and at Densmore Creek. The total inflow into the Cross Irondequoit tunnel for these storms is plotted in Fig. D-1.

The other set of hydrographs included the Culver-Goodman tunnel. This set consisted of the 10 year, 1 hour storm; the 5 year, 1 hour storm; the 2 year, 1 hour storm; and the 1 year, 1 hour storm. In this case, the major inflow points into the Cross-Irondequoit tunnel were found to be at Densmore Creek and at the Culver-Goodman inflow near Densmore Creek, while the inflow at Thomas Creek was virtually eliminated. The total inflow into the combined Culver Goodman Cross Irondequoit system is plotted in Fig. D-2.

It should be noted that the inclusion of the proposed west side interceptor did not affect the inflow hydrograph.

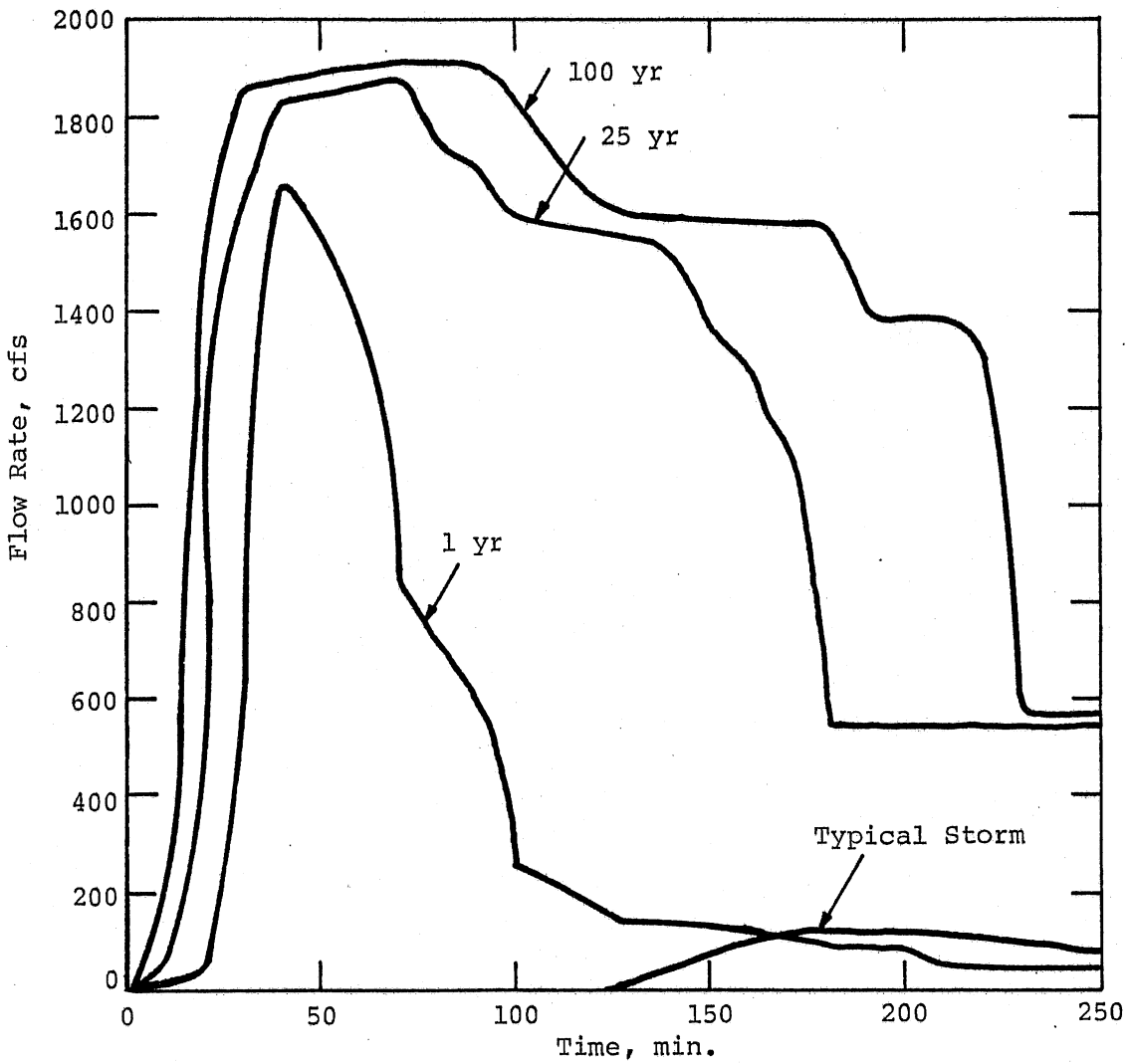

Fig. D-1. Total Inflow into the Cross-Irondequoit Tunnel without Culver-Goodman.

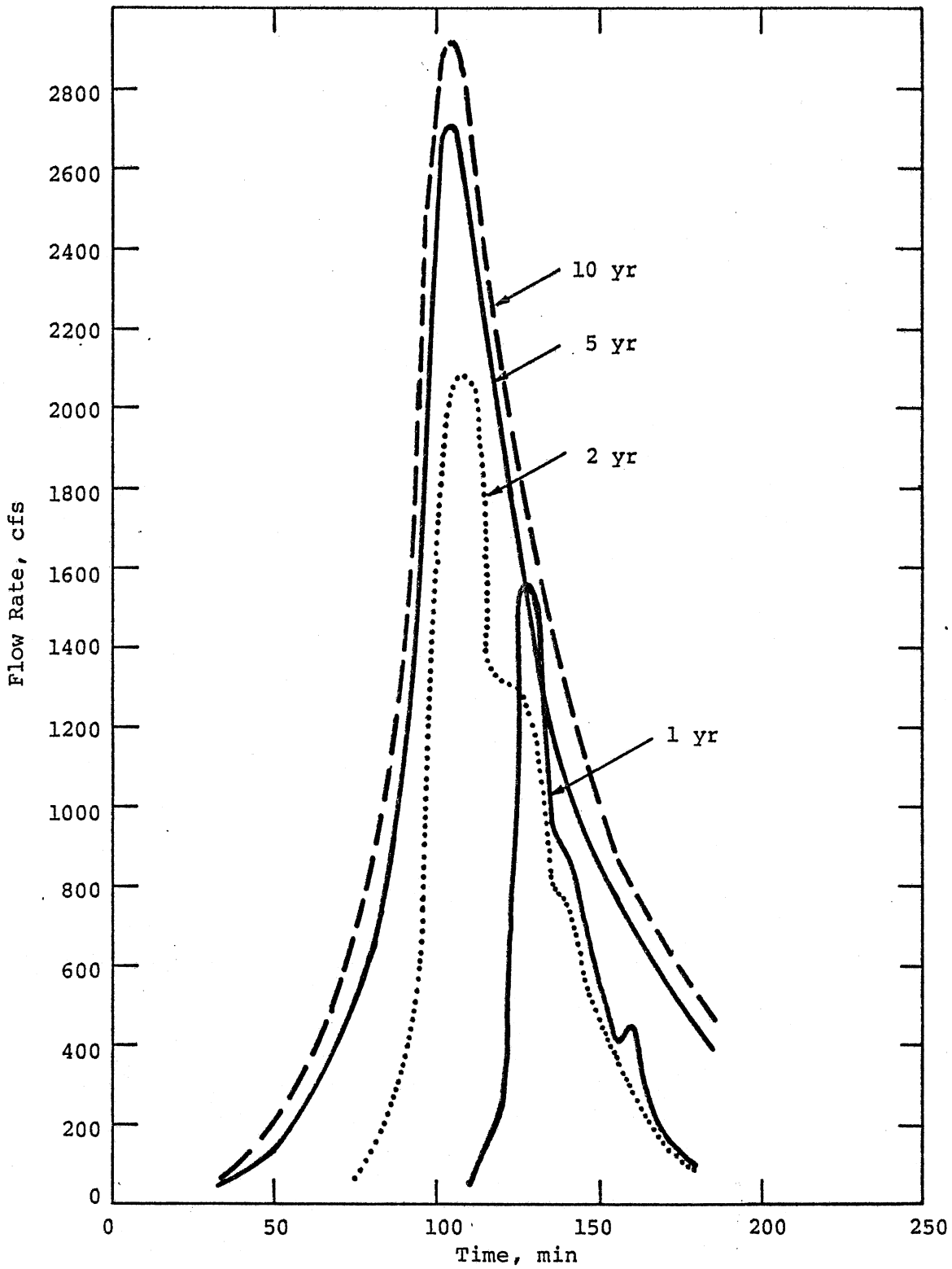

Fig. D-2. Total Inflow into the Culver-Goodman Cross-Irondequoit Tunnel System.